PALACKÝ UNIVERSITY

FACULTY OF MEDICINE AND DENTISTRY

Program DSP: Pediatry

NEW ANTICANCER DRUGS TARGETING CELL CYCLE

Jiří Řehulka, M.Sc.

Supervising department:

Institute of Molecular and Translational Medicine, Faculty of Medicine and Dentistry, Palacký University and University Hospital in Olomouc

Supervisor:

Petr Džubák, M.D., Ph.D.

Olomouc 2017

I declare that this thesis was done by myself and that all the sources used in this thesis are cited and included in the references part. The research was carried out in the Institute of Molecular and Translational Medicine, Faculty of Medicine and Dentistry, Palacký University Olomouc.

Olomouc   ………………………

June, 2017   Jiří Řehulka, M.Sc.

Acknowledgments

Bibliografická identifikace

Jméno a příjmení autora	Jiří Řehulka
Název práce	Nová protinádorová léčiva zasahující do buněčného cyklu
Typ práce	Dizertační
Pracoviště	Ústav molekulární a translační medicíny, Lékařská fakulta, Univerzita Palackého v Olomouci
Vedoucí práce	MUDr. Petr Džubák, Ph.D.
Rok obhajoby práce	2017
Klíčová slova	Buněčný cyklus, apoptóza, mikrotubuly, pelorusid A, kyselina betulinová
Jazyk	Anglický

Abstrakt

Poruchy v regulaci buněčného cyklu spolu s nadměrnou aktivací proliferace jsou hlavními příčinami karcinogeneze. Teoretický úvod práce přibližuje regulační mechanismy buněčného cyklu i nejčastěji používaná klinická a experimentální cytostatika. Předmětem této disertační práce byla charakterizace protinádorové aktivity nízkomolekulárních látek pelorusidu A a semisyntetických derivátů triterpenů. Výsledky této práce prokazují, že aktivita pelorusidu A není na rozdíl od paklitaxelu negativně ovlivněna hypoxií v podmínkách *in vitro*. Přestože pelorusid A stejně jako paklitaxel stabilizuje mikrotubuly, jejich odlišné β-tubulin vazebné místo je zřejmě příčinou rozdílné citlivosti vůči hypoxií indukovaným změnám v buňkách kolorektálního karcinomu. V další části práce byla studována protinádorová aktivita nových triterpenů a jejich modulační vliv na buněčný cyklus linie T-lymfoblastické leukemie. Cytotoxicita derivátů byla závislá na přítomnosti substituentu v poloze 2 a korelovala s elektronegativitou substituentu. Nejúčinější deriváty kyseliny dihydrobetulinové, oleanonové a methyl betulonátu indukovaly akumulaci buněk v S a G2/M fázi buněčného cyklu.

Bibliographical identification:

Author's name and surname Jiří Řehulka

Title New anticancer drugs targeting cell cycle

Type of thesis Dissertation

Department Institute of Molecular and Translational Medicine,

Faculty of Medicine and Dentistry,

Palacký University Olomouc

Supervisor Petr Džubák, MD, PhD

The year of presentation 2017

Keywords Cell cycle, apoptosis, microtubule, peloruside A, betulinic acid

Language English

Abstract

The cell cycle is a complex sequence of events that directs cell growth and division. Importantly, the cell cycle regulation is frequently impaired in human cancer cells. The carcinogenesis relies on the multistep accumulation of genetic alterations that results in deregulated tumor growth. The majority of current chemotherapeutics activate cell cycle checkpoints such as DNA damage checkpoint or spindle assembly checkpoint. Although new targeting strategies are being developed, they still require combination with conventional drugs. The theoretical part of the thesis introduces the regulation of cell cycle and summarizes the most important anticancer agents currently used in clinics as well as novel cell cycle inhibitors. Experimental part evaluates anticancer activity of non-taxoid microtubule stabilizing drug peloruside A and novel semisynthetic triterpene derivatives. The data show, that in contrast to paclitaxel, peloruside A maintains the activity in hypoxia pre-exposed human colorectal carcinoma cells. Study of novel triterpene analogues with unknown mode of action revealed their cell cycle modulatory properties. The most active derivatives of dihydrobetulinic acid, oleanonic acid and methyl betulonate induced cell cycle arrest in S or G2/M phase. The study clearly demonstrated that modification of triterpenes with electronegative substituents such as fluorine or thiocyanate moiety at carbon 2 significantly improve *in vitro* anticancer activity.

Table of contents

Abbreviations

AIF	Apoptosis inducing factor
ANT	Adenine nucleotide transporter
APC/C	Anaphase promoting complex or cyclosome
ATM	Ataxia telangiectasia mutated
ATR	ATM- and Rad3-related
BA	Betulinic acid
BubR1	BUB1-related kinase 1
CAK	CDK activating kinase
CDK	Cyclin dependent protein kinase
CIN	Chromosomal instability
CKI	Cyclin dependent kinases inhibitor
CPC	Chromosomal passenger complex
DSB	Double strand break
FDA	US Food and Drug Administration
FLIP	FLICE-like inhibitory protein
GADD45	DNA damage-inducible 45 protein
GCPs	γ-tubulin complex proteins
GSK3 β	Glykogen synthase kinase 3 β
γTuSC	γ-tubulin small complex
HC	Hypoxia-conditioned
HDAC	Histone deacetylase
IAP	Inhibitor of apoptosis protein
INCENP	Inner centromere protein
KIF2B	Kinesin family member 2B
K-MTs	Kinetochore microtubules
KNL1	Kinetochore null protein 1

MCAK	Mitotic centromere-associated kinesin
MCC	Mitotic checkpoint complex
MCR	Mitotic cell rounding
MDR	Multi-drug resistance
MIS12	Mis-segregation 12
MPF	Mitosis-promoting factor
MTA	Microtubule targeting agent
MTOC	Microtubule organizing center
NDC80	Nuclear division cycle 80
NF-κB	Nuclear factor-κB
NRX	Normoxia
OMM	Outer mitochondrial membrane
ORC	Origin recognition complexes
PARP-1	Poly-(ADP) ribose polymerase
PCM	Pericentriolar matrix
PELA	Peloruside A
PiC	Inorganic phosphate transporter
PLK1	Polo-like kinase 1
Pre-RC	Pre-replicative complexes
PTP	Permeability transition pore
PTX	Paclitaxel
Rb	RB transcriptional corepressor 1
RPA	Replication protein A
SAC	Spindle assembly checkpoint
SP1	Spacer protein1
TSPO	Translocator protein
VCR	Vincristine

| VDAC | Voltage dependent anion channel |
| VEGF | Vascular endothelial growth factor |

I. INTRODUCTION

1. Cell cycle

The cell cycle is the period between two mitotic divisions that results in division into two daughter cells. The cell cycle can be thus divided into mitosis (M phase) and interphase. The most prominent event of interphase is DNA replication (S phase) preceded by G1 phase and followed by G2 phase (Fig. 1). These gap phases enable cellular growth and synthesis of proteins required for next M phase. Cells in differentiated tissues are maintained predominantly in quiescent G0 phase and potential cell cycle entry is strictly regulated [1].
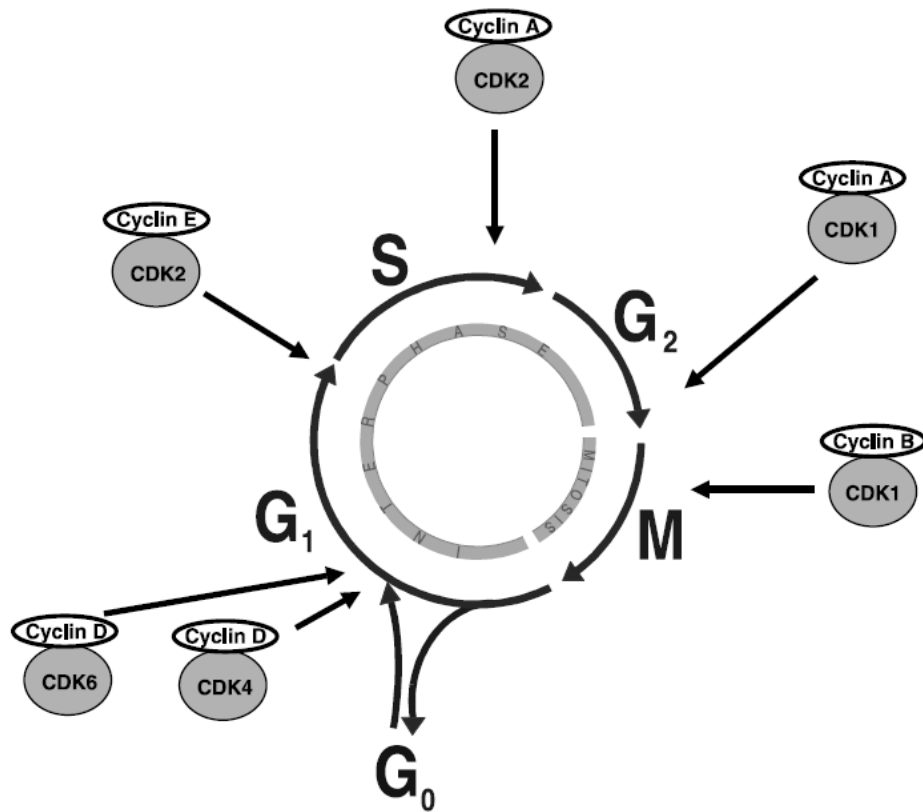
Figure 1. The cell cycle with depicted activities of CDK/cyclin complexes. Adapted from [2]**.**

1.1. Cell cycle regulation

Cell cycle entry can be initiated by numerous stimuli including extracellular signals (activation of pathways such as RAS, MAPK, mTOR by peptide growth factors) or nuclear estrogen receptor activation [1]. The cell cycle is driven by sequential activation of cyclin dependent protein kinases (CDKs), a family of serine/threonine kinases that coordinate timed progression of cellular events. Five members of the protein family contribute to cell cycle regulation. CDK4, CDK6, CDK2 and CDK1 are active during different phases of cell cycle. The CDK7 participates in CDK activating kinase (CAK) complex that activates other CDKs [2]. Its role in cell cycle regulation will be discussed later. Other CDKs have a role in basal transcriptional processes such as transcriptional initiation, transcriptional elongation or RNA processing [3].

Cyclins are proteins cyclically expressed in specific cell cycle phases that bind to and activate appropriate CDKs (Table 1).

Table 1. Overview of CDK/cyclin complexes and their most important substrates. Adapted from [3].

CDK	Cyclin	Function	Processes
CDK4/6	D	G1–S progression	Phosphorylation of Rb stimulates E2F Accumulation of FOXM1
CDK2	E, A	G1–S progression DNA replication	Hyperphosphorylation of Rb Centrosome duplication Induction of histone synthesis Phosphorylation of replication factors
CDK1	B, A	G2–M progression Mitotic entry	Nuclear envelope breakdown Mitotic condensation Spindle assembly
CDK5	p35, p39	Neuronal viability	Phosphorylation of Rb
CDK7	H	Basal transcriptional processes	Transcriptional initiation Transcriptional elongation RNA processing
CDK8	C		
CDK9	T		
CDK11	L		

D-type cyclin expression is dependent on growth factors, whereas levels of other cyclins E, A and B are regulated by periodical transcriptional activation and proteasomal degradation. CDKs required for G1 entry, CDK4 and CDK6, are

activated by cyclin D1, cyclin D2 and D3. Activated CDKs in turn phosphorylate substrate proteins required for cell cycle progression, such as Rb or other protein substrates. CDK2 is activated by cyclin E in G1 phase and cyclin A in S phase. Cyclin A also associates with CDK1 in G2 phase and resulting complex mediate mitotic entry. Finally, mitosis is regulated by CDK1 in complex with cyclin B.

The activity of CDKs is further controlled by diverse mechanisms (Fig. 2) including activating phosphorylations, inhibitory phosphorylations and interactions with cyclin dependent kinases inhibitors (CKIs) [3]. CAK complex of CDK7 and cyclin H activates CDK2 and CDK1 by phosphorylation of Thr160 and Thr161, respectively [4]. In addition, CDK7 is involved in the formation of TFIIH complex required for transcription initiation [5]. Inhibitory phosphorylations at tyrosine-15 and/or threonine-14 of CDK1 are promoted by kinases Wee1 and Myt1. The inhibition is reversed by Cdc25 phosphatase that can dephosphorylate these sites. Moreover, the activity of cyclin B-CDK1 is regulated spatially. Sequestration with 14-3-3 proteins during interphase prevents Cdc25 translocation into the nucleus, whereas cyclin B is exported to cytoplasm based on its nuclear exclusion signal until the beginning of prophase [2].
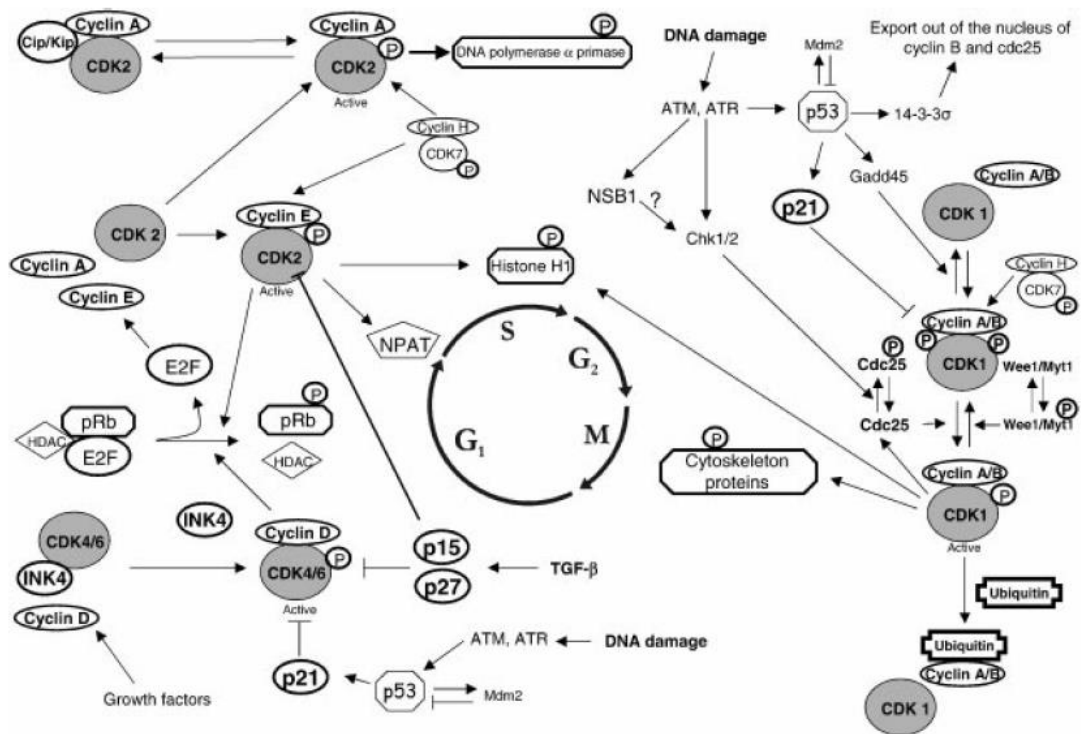

Figure 2. Schematic representation of important cell cycle regulatory mechanisms. Adapted from [2]**.**

CKI inhibit CDKs by interactions with INK4 family and Cip/Kip family members. While INK4 family members p15, p16, p18, and p19(ARF) inhibit CDK4 and CDK6 before cyclin binding, Cip/Kip family p21, p27, p57 inactivate G1 CDK-cyclin complexes or cyclin B-CDK1 complex [6]. Proteins p19(ARF) and p21 are involved in DNA damage response mediated by p53. Upon DNA damage p21 inhibits CDKs and prevent transition into next cell cycle phase [7].

G1 phase

Rb phosphorylation plays a central role in so-called restriction point, from where the cell completes current cell cycle regardless of growth-promoting and growth-inhibitory stimuli. The process is coordinated by cyclin D-CDK4/6 and cyclin E-CDK2 complexes particularly by Rb phosphorylation. Rb hyperphosphorylation releases E2F transcription factor, allowing transcription of cyclin E and CDK-activating Cdc25 phosphatases, which results in further activation of cyclin E-CDK2 complexes by positive feedback mechanism [8]. In addition, cyclin E-CDK2 activity enables degradation of its own inhibitor p27. CDK2 is involved in the initiation of DNA synthesis during S-phase [9]. Cells can activate G1 DNA damage checkpoint pathways to prevent cell cycle progression with incorrectly replicated or damaged DNA [10].

S phase

DNA synthesis is initiated at replication origins, where origin recognition complexes (ORC) form pre-replicative complexes (pre-RC). Pre-RCs conversion into replication forks requires origin unwinding by helicases, stabilization of single-stranded DNA by replication protein A (RPA) and recruitment of polymerases [11], [12]. DNA polymerases are enzymes that copy template DNA into new complementary DNA strands. There are at least three polymerases α, δ and ε involved in DNA replication. DNA polα synthesizes short RNA primers for leading and lagging strand synthesis and is replaced by the following two polymerases with greater processivity and proofreading exonuclease activity [11]. The leading DNA strand is extended continuously in the direction of the fork opening, while the lagging strand is elongated in the opposite direction in short segments, named Okazaki fragments [13]. The nucleosomes are disrupted, as the replication fork passes, and again reassembled from the former and newly synthesized histone proteins [14]. DNA replication is driven by cyclin A/E-CDK2 complexes and tightly controlled to occur only once per cycle [15]. The centriole duplication takes part in

S-phase after phosphorylation of centrosomal substrates by CDK2 [1].

G2 phase

Cyclin A-CDK1 binding promotes cell cycle progression during the G2 phase. Also, it induces transcription of cyclin B, that plays a major role in mitotic entry and during mitosis. Mitotic events are directed by cyclin B-CDK1 complex, also referred as the mitosis-promoting factor (MPF). A complex interplay is regulated by cellular localization of cyclin B-CDK1. During G2, it is imported via importin β into the nucleus to phosphorylate its nuclear substrates [16].

M phase

The most characteristic event of M phase is mitosis comprised of several substages and followed by cytokinesis. Prophase events include chromosomal condensation and nuclear envelope disassembly mediated by phosphorylation of histone H3 and nuclear lamins by active CDK1. Centrosomes with duplicated centrioles start organization of microtubules into the mitotic spindle. In metaphase, kinetochore microtubules align chromosomes at the equatorial plate, whereas radiating microtubules anchore centrosomes to poles. In anaphase, kinetochore microtubules shorten and pull sister chromatids of each chromosome toward the opposite pole. Separation of sister chromatids is facilitated by topoisomerases. During telophase chromosomes decondense and the nuclear lamina is reassembled [1].

Cytokinesis

At the end of mitosis, cytokinesis completes cell division into two daughter cells. The process is conserved among eukaryotic organisms and temporally coordinated to ensure spatial segregation of genetic material and physical separation of cells. Similarly to mitosis, cytokinesis is highly dependent on microtubule cytoskeleton. After chromosome segregation in anaphase, microtubules assemble in midzone and form the midbody. Subsequently, microtubules of the spindle midzone promote ingression of the cleavage furrow by constriction of actomyosin ring that remodels the plasma membrane [17], [18]. The forces of contractile ring are generated mainly by actin filaments and myosin-II motor proteins [19]. In addition, successful cytokinesis requires kinase activity of Polo and ABI complex. The final step in cytokinesis is resolution of the midbody and abscission, which results in physical separation of the daughter cells [20].

1.2. Cell cycle in cancer

Carcinogenesis is a multistep process characterized by the accumulation of genetic alterations that influence key cellular pathways involved in growth and development [21]. Alterations in the genetic control of cell division are frequently responsible for deregulated proliferation. These alterations occur particularly in two classes of genes referred as proto-oncogenes and tumor suppressor genes. While proto-oncogenes in normal cells stimulate cell proliferation, their mutated forms in cancer cells promote uncontrolled growth. In contrast, products of tumor suppressor genes inhibit cell cycle progression. Mutations or deletions of tumor suppressor genes lead to dysfunction of cell cycle regulatory pathways [2].

The most known tumor suppressors are p53, ATM (ataxia telangiectasia mutated), p16, Rb and BRCA1. The loss of checkpoint function imparts substantial growth advantages to cancer cells and contribute to the lowered sensitivity to the growth signals [22]. The proteins encoded by oncogenes usually act as transcription factors, growth factors, growth factors receptors, signal transducers, chromatin remodelers or regulators of apoptosis (Table 2). Oncogenes can be activated by structural alterations such as mutations, gene fusions, amplifications or translocations [23]. Importantly, oncogenic proteins constitute significant therapeutic targets (Table 3).

Table 2. Examples of oncogenes. Adapted from [24]**,** [23]**.**

Class	Gene
Growth factors	*SIS* (PDGF-β)
Growth factors receptors	*EGFR*
	ERBB2
	KIT
Signal transducers	*ABL*
	SRC
	AKT
	RAS
	RAF
	MOS
Transcription factors	*MYC*
	FOS
	JUN
	GLI
Regulators of apoptosis	*Bcl-2*
Chromatin remodelers	*MLL*

Table 3. Small molecules and monoclonal antibodies targeting oncogenic proteins. Adapted from [23]**.**

Anticancer Drug	Target	Disease
Monoclonal antibodies		
Trastuzumab (Herceptin, Genentech)	ERBB2	Breast cancer
Cetuximab (Erbitux, ImClone)	EGFR	Colorectal cancer
Bevacizumab (Avastin, Genentech)	VEGF	Colorectal cancer, non–small-cell lung cancer
Small molecules		
Imatinib (Gleevec, Novartis)	ABL, PDGFR, KIT	Chronic myelogenous leukemia, gastrointes-tinal stromal tumors, chordoma
Gefitinib (Iressa, AstraZeneca)	EGFR	Non–small-cell lung cancer
Erlotinib (Tarceva, Genentech)	EGFR	Non–small-cell lung cancer
Sorafenib (Nexavar, Bayer/Onyx)	VEGFR, PDGFR, FLT3	Renal-cell carcinoma
Sunitinib (Sutent, Pfizer)	VEGFR, PDGFR, FLT3	Gastrointestinal stromal tumors, renal-cell carcinoma

Other factors that contribute to carcinogenesis are often associated with cyclins and cell cycle modulators. Most notably, cyclin D and CDK4 are frequently overexpressed in many cancer types including carcinomas of head and neck, cervical carcinomas, astrocytomas, non-small-cell lung cancers and soft tissue sarcomas. The overexpression is promoted by amplification or rearrangement of genes encoding cyclin D1, D2 and D3 [25]. In contrast, molecular analysis of breast cancer samples revealed that gene encoding cyclin E is rarely amplified, however its overexpression is caused by alterations in its degradation pathway. Although concomitant overexpression of cyclin D1 and E is rare, such alterations contribute to dysregulation of G1/S transition by E2F activation independently of Rb [21].

Another hallmark of cancer is abnormal chromosome number (aneuploidy) and chromosomal instability (CIN). Aneuploidy is a contributing factor in tumorigenesis, that results in segregation errors in mitosis manifested by multipolarity, abnormal centrosome number, defects in spindle assembly checkpoint (SAC) signaling and errors during cytokinesis. Cancer cells exhibiting CIN are incapable of equal chromosome segregation and gain or lose chromosomes or their parts [26].

1.3. Cell cycle checkpoints

Cell cycle checkpoints ensure normal cell cycle progression and tightly control completion of preceding phase before entry into the following phase (Fig. 3). While G1 and S phase checkpoints prevent replication of damaged DNA, G2 checkpoint prevents segregation of damaged DNA into daughter cells [15].
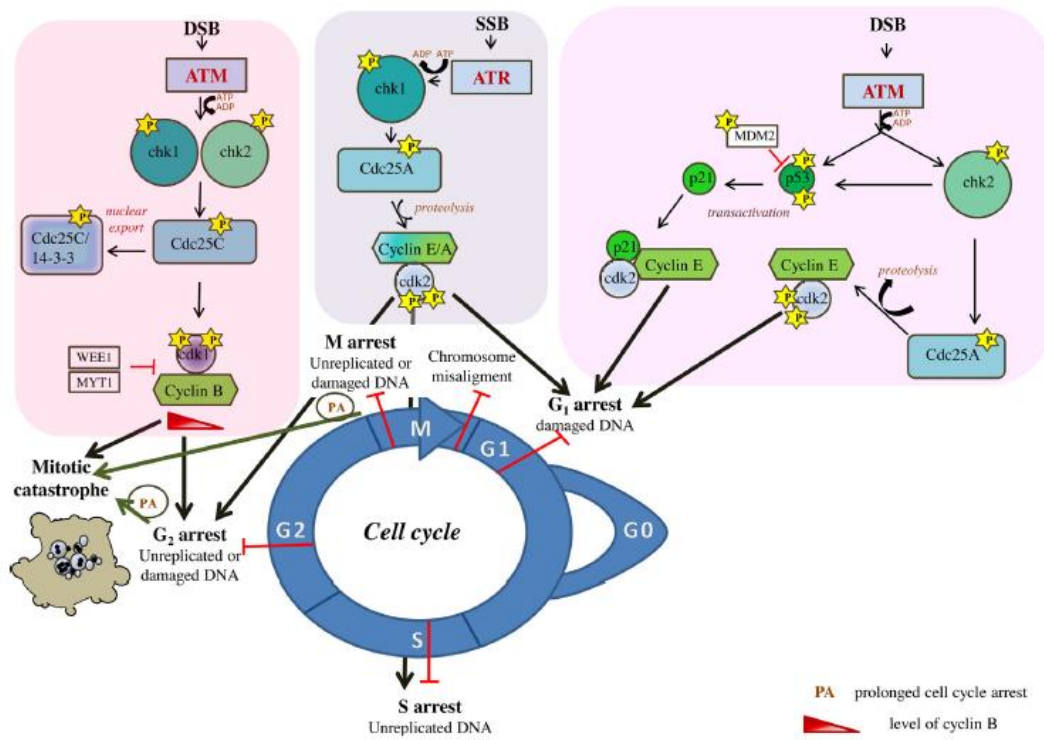
Figure 3. Cell cycle checkpoints induced by DNA damage. Adapted from [27]**.**

The central role in G1 DNA damage checkpoint network play the phosphoinositide 3-kinase related kinases ATM, ATR (ATM- and Rad3-related) and their downstream substrates Chk1 and Chk2 that can mediate G1, S or G2 phase cell cycle arrest in response to DNA lesions [10], [28]. While ATM responds in particular to double-stranded DNA breaks (DSBs), ATR is activated by a variety of DNA lesions [29]. DSBs, induced by a plethora of physiologic and pathologic causes (ionizing radiation, oxidative free radicals, topoisomerase failure or breaks during recombination), are recognized by the Mre11–Rad50–Nbs1(MRN) complex [30], [10]. The signal is transduced by DNA damage sensors and adaptor proteins H2AX, ATRIP, 53BP1, MDC1, and BRCA1 to ATM that stabilize p53 and prevents its degradation by abrogation of p53–MDM-2 interaction [28]. Stabilization of p53 promotes its transcriptional activity and expression of p21, which in turn inhibits

CDK2 activity and results in cell cycle arrest. Moreover, Chk1 or Chk2 mediate G1 arrest through inactivation of Cdc25A [7].

Intra-S-phase checkpoint uses basically the same ATM/ATR–Chk2/Chk1–Cdc25A–CDK2 signaling axis, however, the main consequence is an extension of DNA replication time. The underlying mechanism involves blocking of Cdc45 that is required for initiation of DNA replication. Delayed replication then enables DNA repair.

Similarly to previous checkpoints, the G2/M checkpoint is determined by the type of DNA lesion and results in Cds25A-dependent cell cycle arrest. Also, both Chk1 and Chk2 upregulate Wee1, an inhibitory kinase of cyclin B-CDK1 complex, that prevents entry into mitosis [7], [31]. The checkpoint mechanisms can be either p53-dependent or p53-independent [22]. For example, DNA damage in p53 deficient cells activates p38MAPK/MK2 stress kinase pathway independently of Chk1 [32].

1.4. Role of p53 in cell cycle control

Tumor suppressor protein p53 plays a central role in response to stress factors which can promote cell cycle arrest and apoptosis [33]. The level of the p53 transcription factor is regulated by numerous positive and negative feedback loops. The most known is p53/MDM-2/p19(ARF) autoregulatory loop (Fig. 4) [34]. MDM-2 is an ubiquitin ligase that mediates p53 rapid proteasomal degradation. Thus p53 half-life is approximately 5-30 minutes and its cellular level very low. MDM-2 itself is a product of the p53 inducible gene; thereby these two partners form a negative feedback loop [35]. In addition, p53 turnover is modulated by p19(ARF). It was shown to inhibit nuclear export of MDM-2 and thus stabilize p53 [36]. The p19(ARF) level is negatively regulated by p53 and stimulated by E2F, β-catenin, Ras and MYC proteins [34].
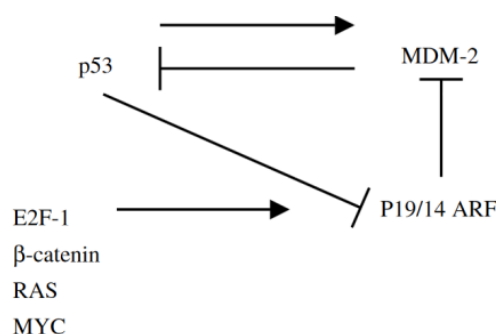

Figure 4. p53/MDM-2/p19/14 ARF loop. Adapted from [34]**.**

Activation of p53 is induced by diverse stress signals and mediated by post-translational modifications such as phosphorylation, acetylation, methylation and ubiquitination (Fig. 5). Interestingly, the response strongly depends on nature and duration of stress signal. While mild stress leads to transient cell cycle arrest and activation of repairing mechanisms, severe stress results in irreversible response such as apoptosis [37]. Activated p53 induces transcription of target genes including p21, 14-3-3, growth arrest and DNA damage-inducible 45 protein (GADD45) and proapoptotic proteins Bax, Puma and Noxa [38], [39]. The induction of apoptosis is not solely dependent on the ratio of pro- and antiapoptotic proteins, because p53 itself can directly interact with Bcl-2 family members. It has been shown that p53 can directly antagonize antiapoptotic Bcl-2 proteins or alternatively, directly bind proapoptotic Bcl-2 family members and induce permeabilization of mitochondria [37], [40].
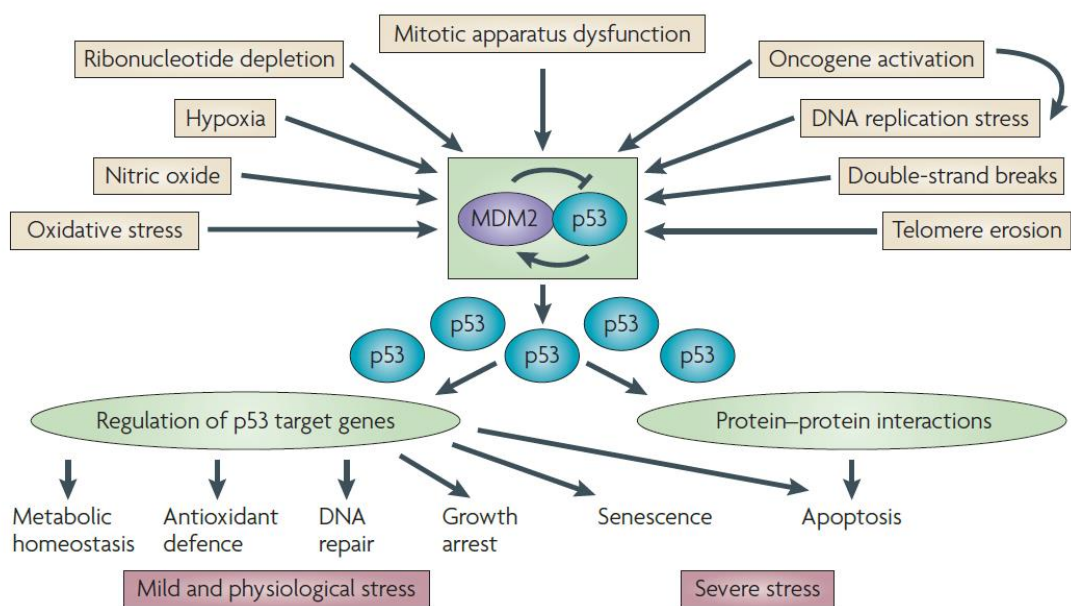
Figure 5. Schematic view of the p53 pathway. Adapted from [33]**.**

p53 also plays an important role in metabolic homeostasis, because it contributes to the metabolic regulation of glycolysis, oxidative phosphorylation and response to oxidative stress [41]. Although wild-type p53 acts as a tumor suppressor, mutant p53 can have an oncogenic activity through its gain-of-function. There is a large body of evidence that mutant p53 reprogrammes cancer cell metabolism. It has been shown that it stimulates Warburg effect by increasing glucose uptake, increases metabolic utilization of pyruvate and alters nucleotide metabolism [42].

1.5. Spindle assembly checkpoint

The metaphase to anaphase transition is regulated by spindle assembly checkpoint (SAC) that control kinetochore attachments to spindle microtubules. Kinetochores are multiprotein complexes at the centromere of each sister chromatid that enable microtubule-chromosome contact. Accurate chromosome segregation during cell division is vital for genome integrity, because chromosome mis-segregation leads to aneuploidy. The kinetochore–microtubule attachments develop during prometaphase trough transient intermediates such as monotelic attachments when only one of the sister kinetochores is bound to microtubules from one spindle pole, and lateral attachments characterized by attachment of kinetochore to the side wall of microtubules (Fig. 6). In the amphitelic attachment, the sister kinetochores are correctly connected to microtubules from opposite poles, resulting in bi-oriented chromosomes. However, there are also erroneous connections such as syntelic and merotelic attachments. While attachment of both sister kinetochores to microtubules from the same spindle pole is referred as syntelic, merotelic attachment binds a single kinetochore to microtubules from both spindle poles [43], [44].
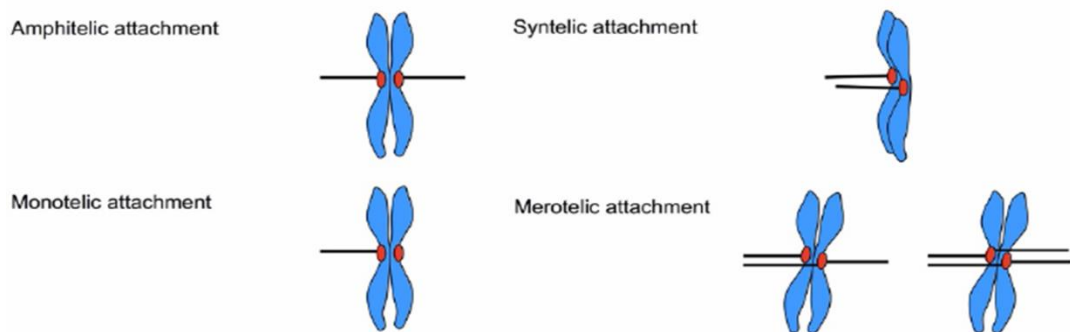
Figure 6. Kinetochore-microtubule attachments. Adapted from [44]**.**

The progression through mitosis critically depends on efficient error correction that is achieved by sensing the tension forces characteristic for bi-oriented kinetochores. Incorrect attachments with low tension are destabilized by Aurora A and Aurora B kinase activity and get another chance for bi-orientation [45]. Although successful attachments are robust enough to promote faithful chromosome segregation, the proteasome-dependent decrease in cyclin A level further stabilizes the attachments in metaphase [46]. Importantly, the regulation of spindle microtubule attachment is often disrupted in cancer cells with CIN. Nevertheless, errors in kinetochore-microtubule attachment are common due to stochastic microtubule

capture in early phases of mitosis. Thus, the precision of attachments is regulated by multiple mechanisms (Fig. 7).
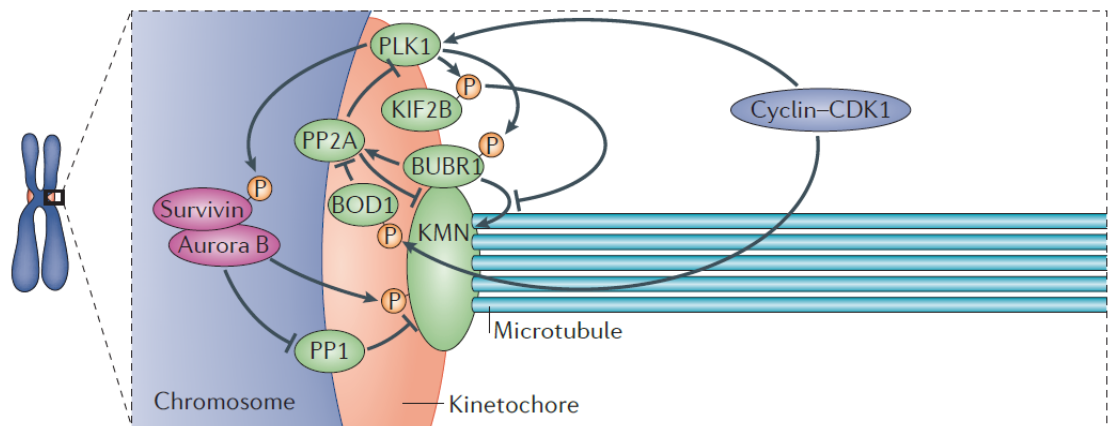
Figure 7. The regulatory networks at kinetochore-microtubule attachment. **Adapted from** [43]**.**

KMN network consists of kinetochore proteins that directly bind to microtubule plus end. It is composed of kinetochore null protein 1 (KNL1), mis-segregation 12 (MIS12) and the nuclear division cycle 80 (NDC80) complexes. The microtubule-binding affinity of KMN is negatively regulated by Aurora B kinase.

Core control network regulates kinetochore-microtubule attachment stability. Core control network is composed of SAC, CDKs, Polo-like kinase 1 (PLK1) and Aurora kinases that receive the signals from KMN network. PLK1 phosphorylates BUB1-related kinase 1 (BubR1) and thus stabilizes kinetochore-microtubule attachments. In contrast, phosphorylation of kinesin family member 2B (KIF2B) by PLK1 destabilizes these attachments and enables repair of kinetochore-microtubule attachment errors. Protein phosphatases PP1 and PP2A form a negative feedback by dephosphorylating PLK1 and Aurora B substrates [43]. BOD1 is a small kinetochore-associated protein required for mitotic chromosome alignment. It regulates PP2A phosphatase activity at the kinetochore to ensure efficient chromosome congression and maintenance of chromatid cohesion [47].

Although survivin belongs to the family of inhibitor of apoptosis proteins (IAPs), the main molecular function of survivin is linked to the control of SAC and cytokinesis. During early mitosis, survivin associates with Aurora B, Borealin and inner centromere protein (INCENP) to form a chromosomal passenger complex

(CPC) that corrects non-bipolar microtubule-kinetochore interactions. By regulating the chromosomal segregation, survivin prevents aneuploidy in a p53 independent manner [48]. Control of mitotic progression by the SAC is active in prometaphase and turns off in metaphase when chromosomes are bi-oriented. SAC proteins Mad1, Mad2, Bub1, Bub3, BubR1, Mps1, and Cdc20 are recruited to kinetochores, where they assemble the mitotic checkpoint complex (MCC), which inhibits the anaphase promoting complex or cyclosome (APC/C) [49]. Checkpoint proteins inhibit APC/C mediated cyclin B ubiquitination and degradation until all kinetochores are attached. Once all kinetochores have proper attachment and the SAC is inactivated, cyclin B is degraded and enables progression to anaphase [50].

The mitotic failure leads to the type of cell death called mitotic catastrophe (Fig. 8).

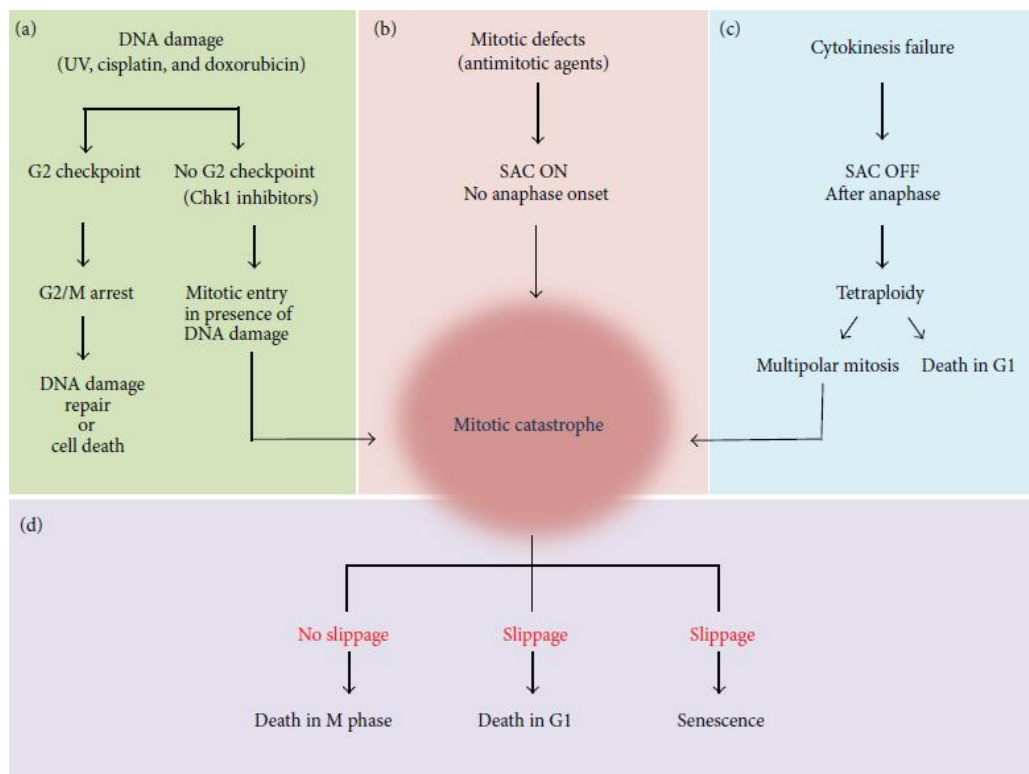**Figure 8. Mitotic catastrophe. Adapted from** [51]**.**

Mitotic catastrophe is by definition an intrinsic oncosuppressive mechanism that senses mitotic failure and responds by driving a cell to an irreversible antiproliferative fate of death or senescence [51]. Mitotic catastrophe can be subdivided into two types. It can occur during metaphase in a p53 independent manner or after failed mitosis in p53 dependent manner.

The exit of cells with activated SAC from metaphase-anaphase arrest is called mitotic slippage [52]. Mitotic slippage is a phenomenon characterized by tetraploid DNA content after mitotic exit without cytokinesis. Although the cell cycle is blocked by SAC checkpoint activity, prolonged arrest still enables slow but continuous proteasomal degradation of cyclin B. Abnormal mitosis results in multinucleated cells that can consequently arrest at G1 and die through p53-dependent apoptosis or do not arrest at G1 and enter S phase and die through necrosis [53]. The G1 arrest in the presence of p53 is promoted by induction of p21 and irreversibly prevents further propagation of errors [52].

1.6. Cell cycle as therapeutic target

Many conventional chemotherapeutics act through activation of cell cycle checkpoints (Fig. 9). Genotoxic agents and ionizing radiation induce G1 or G2 checkpoint arrest, 5-florouracyl and other inhibitors of DNA replication trigger S phase block, whereas microtubule targeting agents (MTAs) activate mitotic arrest [22]. An attractive strategy for cancer treatment is restoring of cell cycle control by CDK inhibitors [54]. The MTAs will be discussed in detail in following chapters together with an overview of the small-molecule inhibitors from other drug classes.
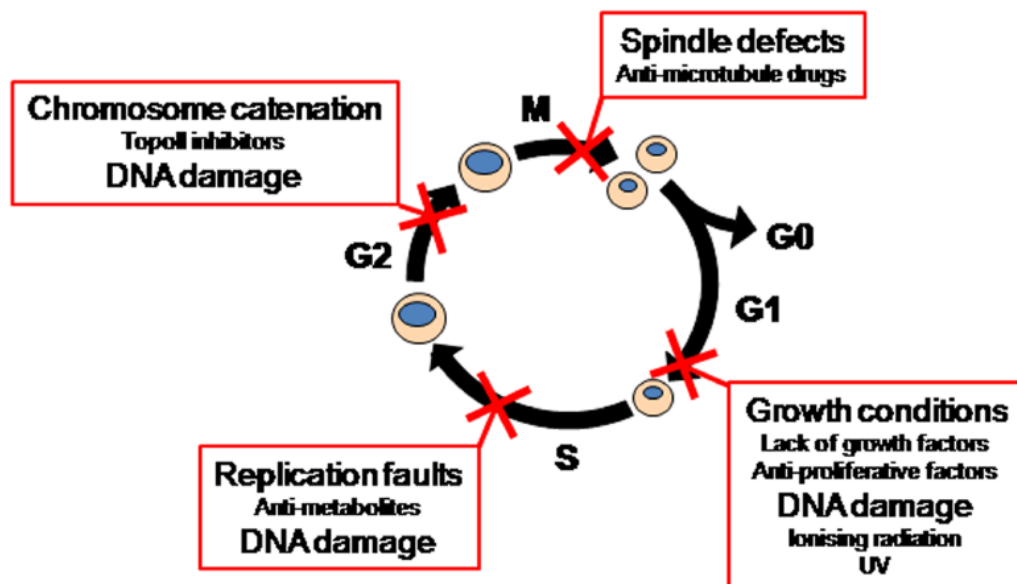
Figure 9. Cell cycle checkpoints activated by internal and external stresses [22]**.**

Irreparable DNA damage ultimately leads to apoptosis or senescence. However, the presence of functional checkpoint pathways and DNA repair mechanisms may to some extent reduce the efficacy of these compounds. For example, the arrest can be reversed once the DNA damage has been repaired and tumor cell can re-enter the cell cycle. On the other hand, checkpoint control in cancer cells is frequently altered. Numerous types of cancers with p53 mutation or deficiency are incapable of G1 checkpoint arrest and following DNA damage depends on compensatory G2 checkpoint promoted by ATR/Chk1 and ATM/Chk2. As a result, these cells are more sensitive to inhibitors of Chk1 and inactivation of the G2 checkpoint [55]. Thus the defects in checkpoint machinery can be exploited for cancer treatment.

This concept referred as synthetic lethality is based on simultaneous inactivation of two genes that results in cell death [56]. In the case of Chk1 inhibition, the loss of p53 sensitizes cancer cells to genotoxic stress (Fig. 10). Another example is the treatment of BRCA1/2 deficient cancer cells with poly-(ADP) ribose polymerase (PARP-1) inhibitors. In this case, PARP-1 mediated base excision repair compensates for defective double-strand DNA break induced DNA repair by homologous recombination [57].
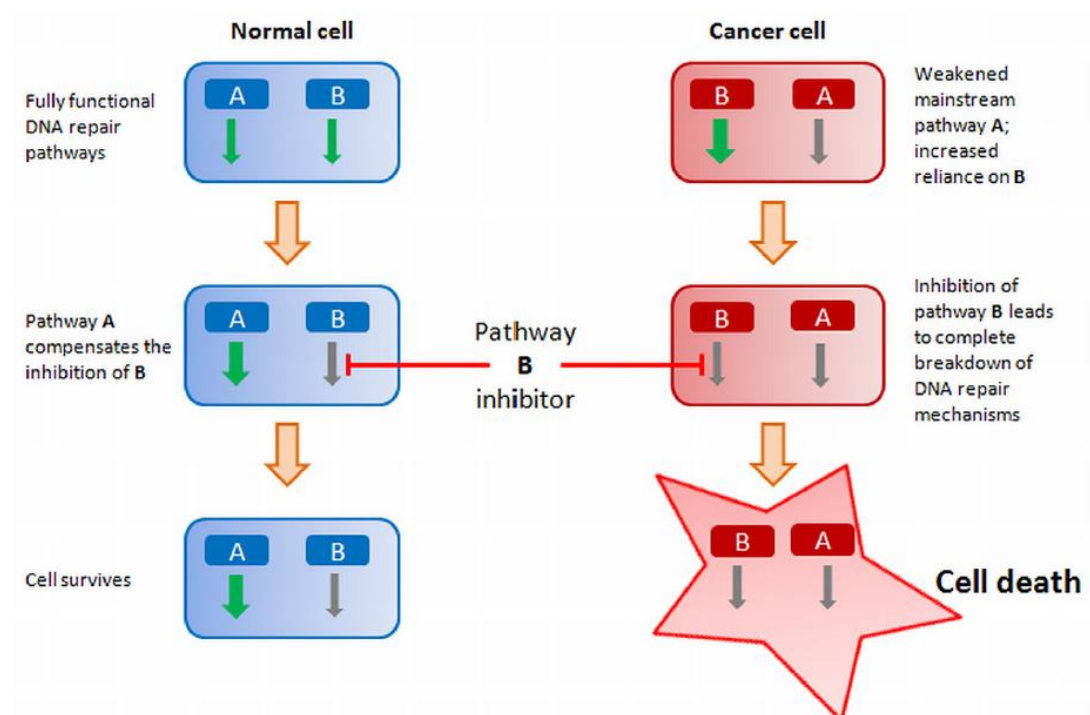
Figure 10. Strategy of synthetic lethality based on inhibition of DNA-damage repair pathways. Adapted from [56]**.**

1.7. Apoptosis induced by chemotherapeutics

Currently used anticancer therapeutics target fundamental cellular processes such as DNA replication and chromosome segregation or induce DNA damage directly. These interventions activate multiple mechanisms in order to protect the genomic integrity and promote survival of the organism. The cell can either employ DNA repairing mechanisms or induce apoptosis [58]. The central event in intrinsic apoptosis is permeabilization of the outer mitochondrial membrane (OMM) and cytochrome c release (Fig. 11). The exact mechanism of OMM is still matter of debate and formally divided into phenomenons of permeability transition pore (PTP) formation and Bcl-2 family members mediated permeabilization [59]. While these two processes have been historically considered as independent, there is evidence of a connection between these events. For example, they ensure rapid and complete cytochrome c release by the mechanism of mitochondrial cristae reorganization [60]. Soluble proapoptotic proteins in turn activate caspases-2, 3 and 6. AIF can also induce caspase-8 cleavage. DNA fragmentation, another hallmark of apoptosis, is induced by caspase mediated PARP cleavage or in caspase-independent manner by AIF [61].
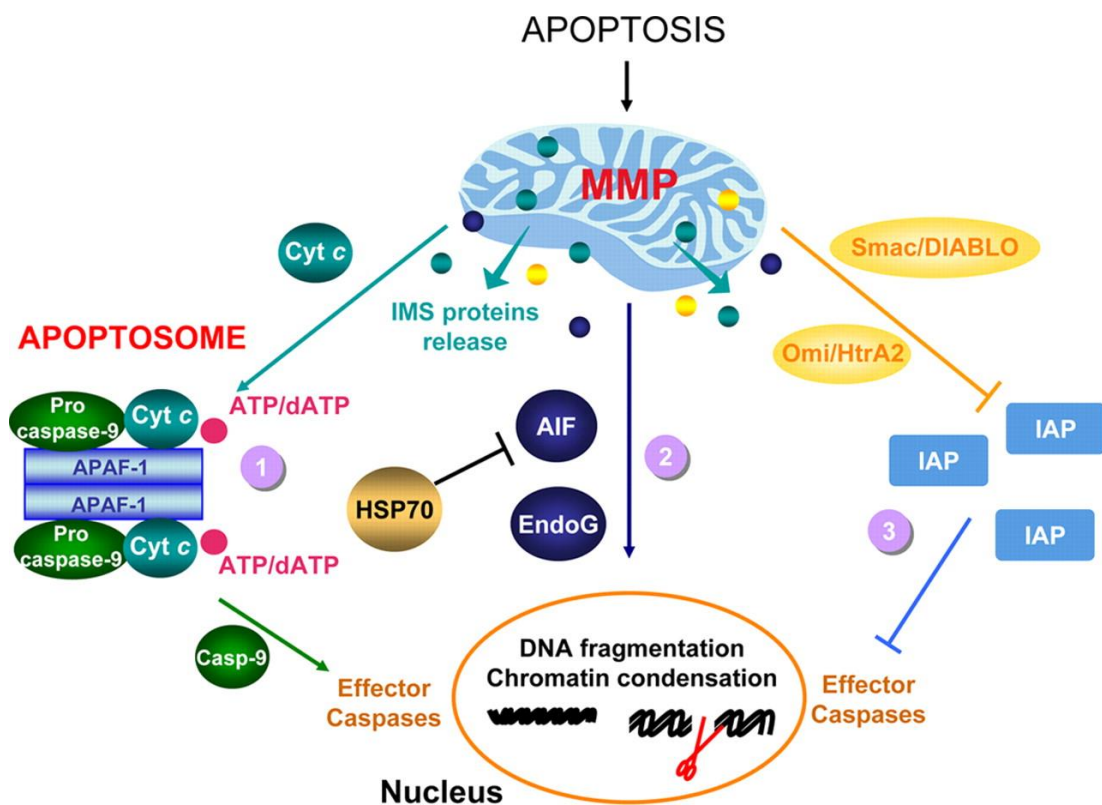
Figure 11. Intrinsic pathway of apoptosis. Adapted from [62]**.**

PTP structure

The initial model of PTP included voltage dependent anion channel (VDAC) located on outer mitochondrial membrane and adenine nucleotide transporter (ANT) on inner membrane surrounded by translocator protein (TSPO), hexokinase II (HKII), cyclophilin D, creatine kinase, glycogen synthase kinase 3 β (GSK3 β) and Bcl-2 family proteins. Revisited model is based on F_1/F_0 ATP synthase organized into super-structures with regulators ANT and inorganic phosphate transporter (PiC), which are modulated by hexokinase II, VDAC, TSPO and creatine kinase. GSK3 β and Bax/Bak facilitate mitochondrial network fragmentation and mitochondrial swelling upon mitochondrial pore transition induction [63]. Cyclophilin D is probably not a structural component of PTP, but plays a regulatory role. It can be modified by several post-translational modifications and interact with Bcl-2, GSK3 β, F_1/F_0 ATP synthase and chaperones HSP60 and HSP90 [64]. The PTP formation is also regulated by Ca^{2+} and metabolites ATP, ADP and inorganic phosphate [65]. The role of lipids, protein-lipid interactions and mitochondrial membrane composition is not clearly elucidated [66].

Bcl-2 family members

Bcl-2 family members regulate apoptotic mitochondrial pathway by mutual interactions on the mitochondrial outer membrane. Diverse stimuli, including chemotherapeutic agents or oncogenic stress, activate BH3-only family members, which enable activation of the pro-apoptotic effectors Bax and Bak by releasing them from inhibition mediated by pro-survival Bcl-2-like proteins. Pro-apoptotic and anti-apoptotic Bcl-2 family members can interact in membranes and set the apoptotic threshold, which may either result in membrane permeabilization and subsequent cytochrome c release or prevent it [67]. Bcl-2 family consist of three functionally and structurally distinct subgroups: BH3 (Bcl-2 homology 3)-only proteins (apoptosis initiators), the pro-survival proteins such as Bcl-2 itself, and the pro-apoptotic proteins Bax (Bcl-2-associated X protein) and Bak (Bcl-2 antagonist/killer) [68]. An anti-apoptotic subgroup consisting of Bcl-2, Bcl-x_L, Bcl-w, A1 and MCL-1 preserve outer mitochondrial membrane (OMM) integrity by directly inhibiting the proapoptotic Bcl-2 proteins.
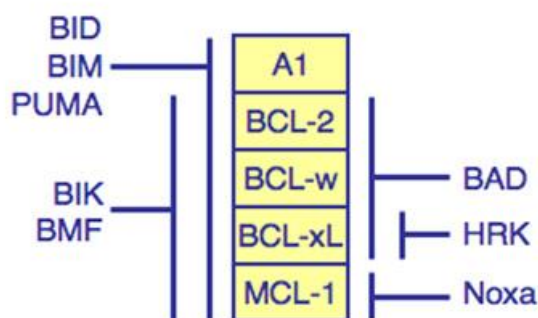
Figure 12.The antiapoptotic BCL-2 protein binding profiles for the BH3-only proteins. Adapted from [69]**.**

The proapoptotic Bcl-2 members are divided into the effector proteins Bax, Bak and the BH3-only proteins. BH3-only proteins Bad, Bik, BMF, bNIP3, HRK, Noxa and Puma are capable to bind and neutralize antiapoptotic Bcl-2 proteins (Fig. 12) [70], but their role in Bax/Bak activation is not completely understood. Bid (tBid), Bim, and Puma, exert an additional activity of directly activating Bax/Bak *in vitro*, however recently was shown, that they are not essential for activating Bax/Bak once the anti-apoptotic Bcl-2 proteins are neutralized [71]. Bax/Bak activation results in mitochondrial outer membrane permeabilization and release of cytochrome c, Smac/DIABLO, Omi/HtrA2, endonuclease G (EndoG) and apoptosis-inducing factor (AIF) and other intermembrane space proteins to the cytosol [70].

Apoptosome formation and DNA fragmentation

Released proteins activate downstream proteins responsible for typical features of apoptosis. Cytochrome c participate with Apaf-1 and dATP in the formation of the apoptosome, caspase-9 activation and triggering caspase cascade [72]. The important consequence of caspase activation is a loss of mitochondrial structural integrity and failure in ATP production [73]. Smac/DIABLO and Omi/HtrA2 derepress caspase activation by binding to and antagonizing inhibitors of apoptosis proteins (IAP) [74]. Moreover, Omi/HtrA2 has the potential to induce apoptosis in cells independently of its IAP binding activity through its function as a serine protease [75]. AIF and endonuclease G translocate from the intermembrane space to the nucleus, where they are involved in chromatin condensation and DNA fragmentation in caspase-independent fashion [76].

Caspases

Caspases are endoproteases involved in cell death or inflammation. They are produced as inactive zymogens, which upon activation acquire specific protease activity and cleave substrates after aspartate residues. Their activation by dimerization or cleavage triggers a cascade of signaling events responsible for controlled degradation of cellular substrates. On the other hand, caspases or other substrates can become also activated by the cleavage and contribute to an amplification of the cascade [77]. In the context of cell death, caspases can be divided into initiator caspases-2, 8, 9, 10 and executioner caspases-3, 6 and 7. Activation of both classes is precisely controlled by posttranslational modifications (phosphorylation, ubiquitylation, nitrosylation) or inhibitory interactions with other proteins such as an inhibitor of apoptosis proteins (IAPs) and FLICE-like inhibitory protein (FLIP) [78].

2. Cell cycle targeting agents
2.1. Microtubule targeting agents

Microtubules

Microtubules form a dynamic cytoskeletal network, which enables movement of vesicles, organelles, chromosomes or other cellular structures inside the cells [79]. Microtubule typically consists of 13 protofilaments assembled from α and β tubulin heterodimers and this organization is responsible for microtubule polarity and its dynamic nature. Microtubule minus end is anchored at centrosome while plus end grows by addition of GTP-bound β-tubulin. GTP-bound tubulin stabilize newly assembled subunit, however GTP is hydrolyzed by tubulin GTPase activity to GDP-tubulin which is more prone to depolymerization. Upon depolymerization, GDP-tubulin is released and requires nucleotide exchange to regenerate into polymerizable GTP-tubulin [80]. Furthermore, MT dynamics is controlled by other proteins such as stathmin or microtubule associated proteins (MAPs), which regulate microtubule stability depending on cell cycle events [81].

α- and β-tubulin structure

α- and β-tubulin monomers share some structural similarities such as nucleotide-binding domain (GTPase domain) at the N-terminus (loops T1–T5), small globular (activation) domain (helixes H8-H10 and a beta sheets S7-S10) and C-terminal domain (H11-H12). On the other hand, the difference in helix H8 has an

impact on GTP hydrolysis during microtubule extension. While GTP bound to α-tubulin is non-exchangeable and is not hydrolyzed, GTP bound to β-tubulin at the plus end of growing microtubule is hydrolyzed upon interaction with α-tubulin subunit of the free dimer. Differences in loop T5 play probably a role in strength and reversibility of longitudinal contacts between tubulins [82], [83]. The longitudinal tubulin interactions between α-tubulin helix H8 and β-tubulin subunit of adjacent dimer formed by loops S3-H3, S5-H5, and H11-H11 implicate microtubule lattice organization [84].

Microtubule nucleation

Centrosomes form the microtubule organizing centers (MTOCs) that nucleate microtubule assembly and establish microtubule polarity (Fig. 13c). Microtubule nucleation is regulated by γTuRC which acts as microtubule template. γ-tubulin complex proteins (GCPs) associate with γ-tubulin to form γ-tubulin small complex (γTuSC), a core of the microtubule nucleating machinery. The γTuSC consists of two γ-tubulin subunits and one GCP2 and GCP3 (Fig. 13a). The γTuSCs then assemble with GCP4, GCP5 and GCP6 into the γTuRC (Fig. 13b). According to the template model, 6 γTuSC subunits present ring of γ-tubulins that make longitudinal contacts with α- and β-tubulin and allow further growth of microtubule plus end [85], [86].
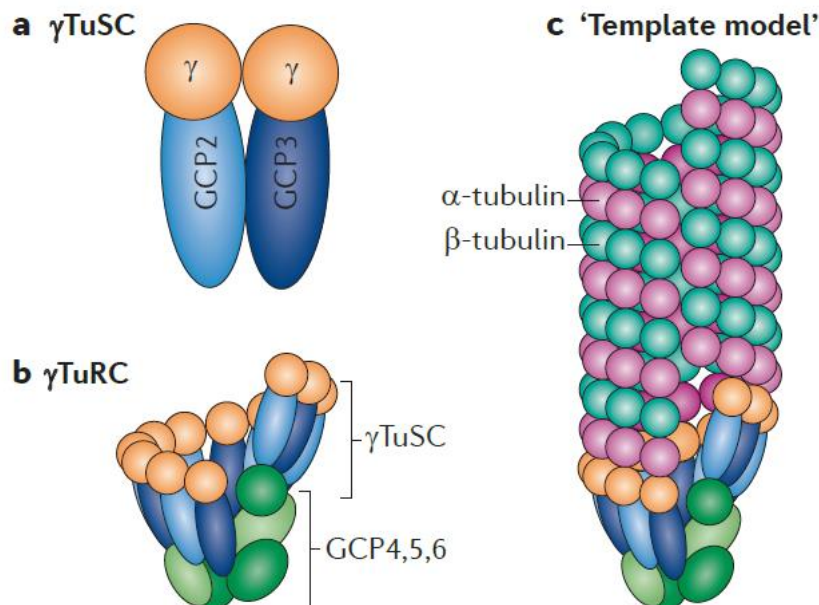
Figure 13. Template model of microtubule nucleation. Adapted from [85]**.**

Centrosomes

During cell cycle the centrosome undergoes duplication in a highly regulated manner (Fig. 14). In addition, it plays a critical role in mitotic spindle organization. Centrosome consists of a pair of centrioles and as a result of cell division, cells begin the cell cycle with exactly one centrosome. Doubling mechanism results in asymmetric duplication of centrioles and as a consequence, the centrosome consists of one original centriole and one newly formed. The original centriole harbours subdistal and distal appendages that play crucial roles in anchoring microtubules. The pair of centrioles is embedded in the pericentriolar matrix (PCM). The PCM contains microtubule nucleating centres γ-TuRCs [87], [88]. Centrosome replication begins at the G1/S transition with nucleation of a procentriole at the proximal end of the mother centriole (Fig. 14). During S and G2 phases, the elongation of centrioles is stimulated by overexpression of centrosomal protein CPAP. In G2 phase, PLK1 and Aurora A kinases induce centrosome maturation characterized by recruitment of PCM proteins and increased the ability to nucleate microtubules. Finally, the connecting linker is detached by Nek2 kinase and a kinesin related motor protein Eg5 and centrosomes are separated [87].
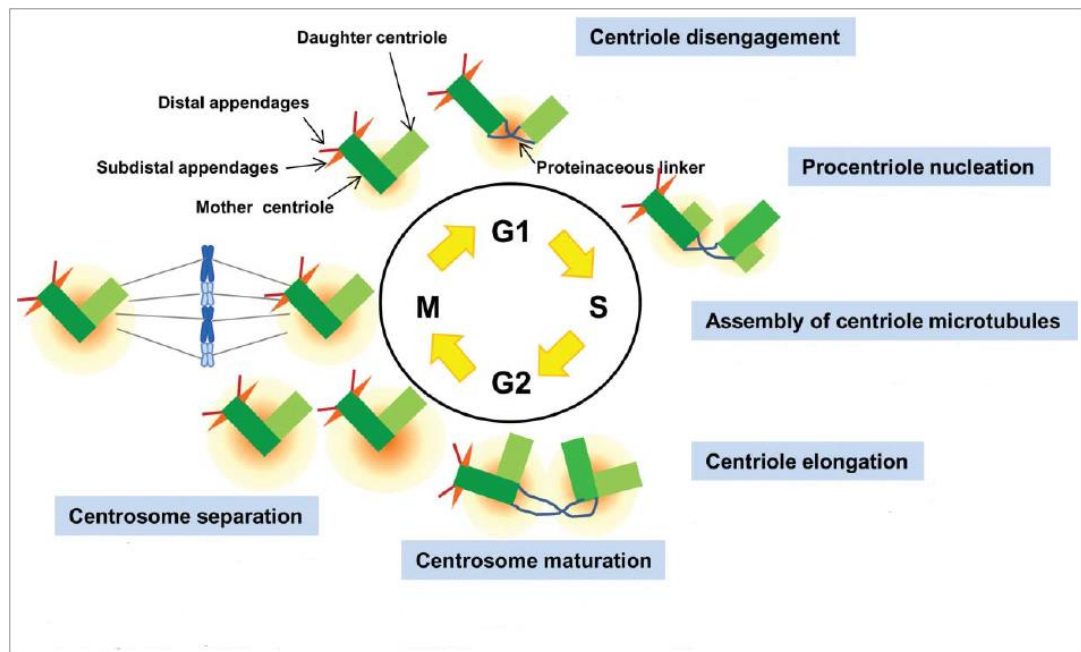
Figure 14. Centrosome cycle. **Adapted from** [87]**.**

Spindle assembly

The mitotic spindle is a bipolar array of microtubules constituted of kinetochore microtubules (K-MTs), non-kinetochore microtubules (nK-MTs) and astral microtubules (Fig. 15). Attachment of a number of K-MTs to a kinetochore leads to their stabilization into a kinetochore fibre (K-fibre), which mediates chromosome movement. The role of astral microtubules resides in positioning spindle through contacts with the cell cortex.
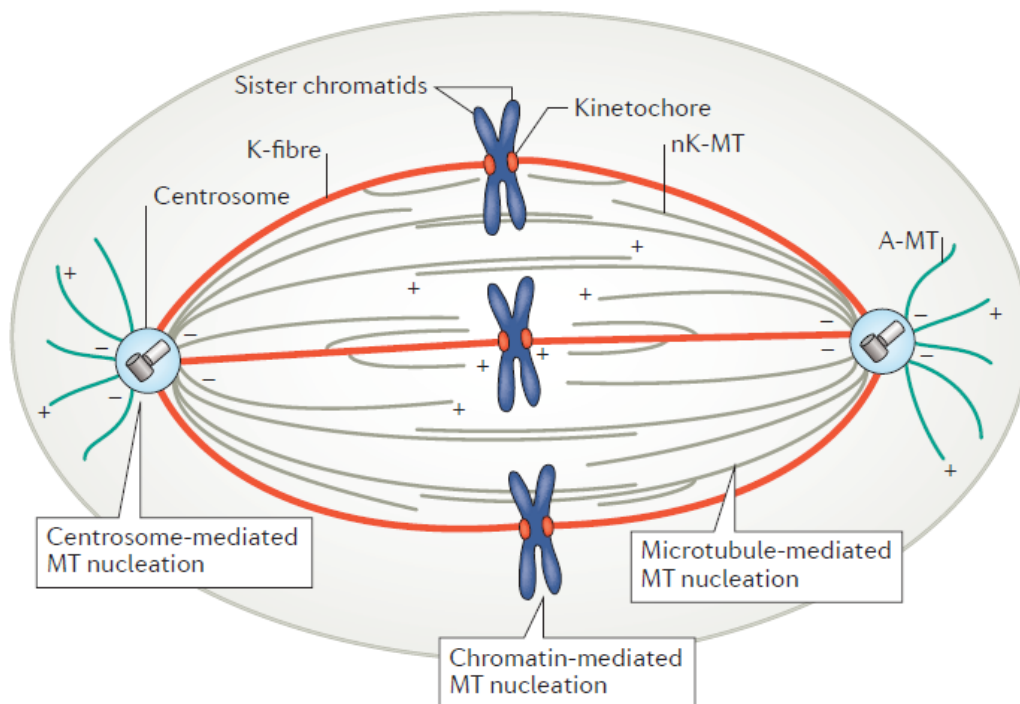
Figure 15. Mitotic spindle assembly. Adapted from [43]**.**

Formation of the mitotic spindle is driven by centrosome-, chromatin- and microtubule-mediated microtubule nucleation pathways. In contrast to the initial "search and capture" model that assumes only stochastic search of microtubules, it is now widely accepted that there are additional factors facilitating spindle assembly. Chromatin mediated nucleation pathway creates a localized biochemical gradient of RanGTP-RanGDP that supports the nucleation and growth of microtubules. The RanGTP gradient is established by the association of its guanine nucleotide exchange factor RCC1 with the chromatin and cytoplasmic localization of GTPase-activating protein RanGAP1 [89]. Another mechanism involves regulation of microtubule nucleation via chromosome passenger complex. It is presumably a RanGTP

independent mechanism that negatively regulates microtubule depolymerizing proteins, such as mitotic centromere-associated kinesin (MCAK) and Op18/Stathmin, thereby facilitating microtubule stabilization. Chromosome movement and precise arrangement of microtubules are controlled by molecular motors. Transport towards plus ends is promoted by the large family of kinesins, whereas only one cytoplasmic dynein is recruited for the minus end transport. Moreover, there were identified more than 200 MAPs essential for spindle assembly. Therefore mechanistic details of microtubule nucleation pathways and their coordination remain to be revealed [90].

Microtubule targeting agents

MTAs usually halt cell cycle in mitosis when mitotic spindle microtubules organize the precise division of chromosomal material (Fig. 16).
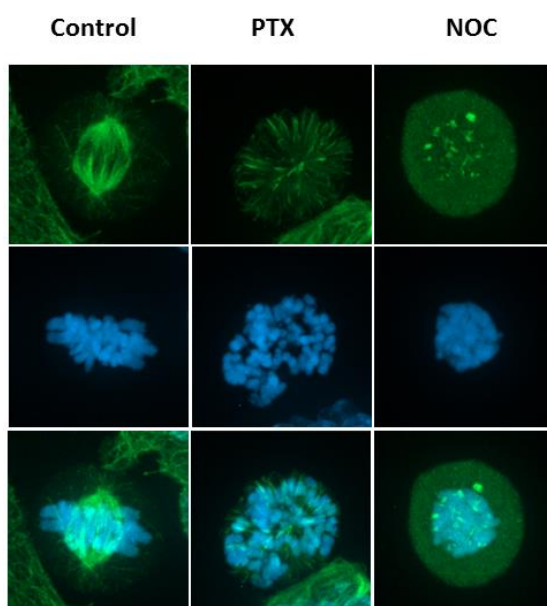
Figure 16. Immunofluorescence images of microtubules in HCT116 cells. Cells were treated with 1 μM nocodazole, 1 μM paclitaxel and DMSO (control) for 24 hours. α tubulin was visualized by FITC and nuclei stained with DAPI, 100x objective.

Thus, interference with mitotic spindle assembly is conventionally considered as a primary cytotoxic mechanism of MTAs [91]. There is, however, a large body of evidence that interphase microtubule network is also significantly affected by MTAs. These effects include axonal transport, transcription, translation, mitochondrial permeability, immune cell function, directional migration and centrosome clustering

[92]. An important target of some MTAs is tumor vasculature since tumor blood vessels display differential sensitivity to MTAs compared with normal vessels [93]. Abnormal organization of endothelial cells is more prone to damage of cytoskeleton and cell junctions and consequent tumor vasculature disruption leads to tumor ischemia and necrosis [94].

MTAs are structurally heterogeneous compounds, which bind to different sites of tubulin protein and stabilize assembled tubulin subunits or prevent their polymerization (Table 4, Fig. 17). The nature of interactions is also diverse, ranging from weak non-covalent to very strong or covalent.

Table 4. Tubulin binding sites with the most important ligands.

Effect on microtubules	Binding site	Ligands
Microtubule-destabilizing agents	Colchicine binding site	Colchicine, Combretastatin, ZD6126, Podophyllotoxin, Steganacin, Nocodazole, Curacin A, 2-Methoxyestradiol, ABT-751, T138067
	Vinca alkaloids	Vincristine, Vinblastine, Vinorelbine, Vinflunine, Phomopsin A, Dolastatin 10, Soblidotin, Cryptophycins, Hemiasterlin
	Maytansine-site	Maytansine, Rhizoxin, PM060184
	Others	Halichondrin B and Eribulin mesylate, Rhazinilam
Microtubule stabilizing agents	Taxoid site	Paclitaxel, Docetaxel, CTX-40, Epothilone
	Non-taxoid site	Peloruside A, Laulimalide
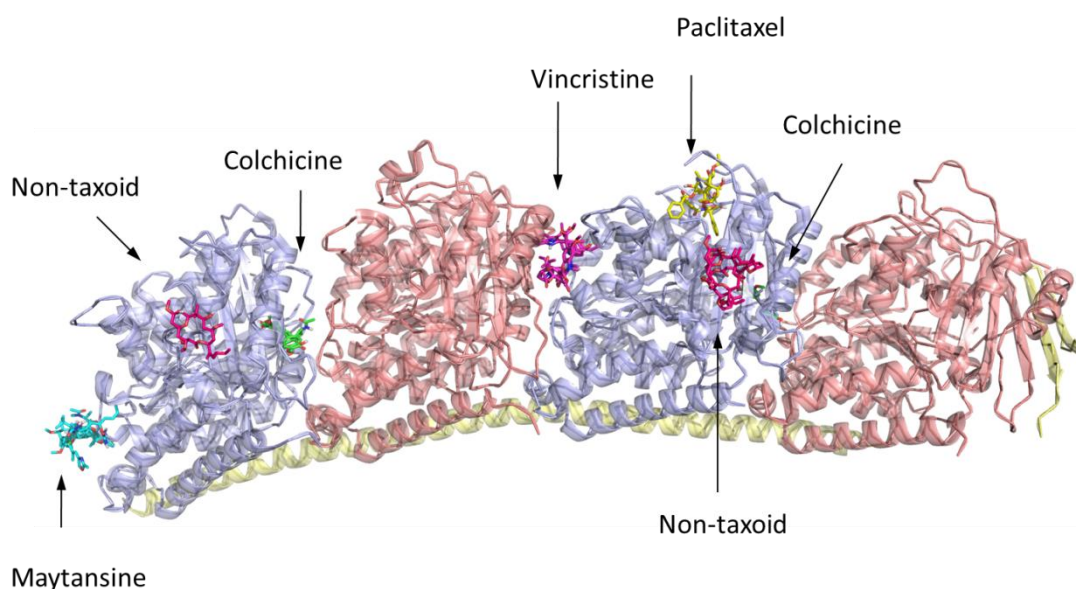
Figure 17. Visualization of MTAs binding sites on tubulin protofilament. The figure was prepared in collaboration with Pavlo Polishchuk Ph.D., M.Sc.; α-tubulin – pink, β-tubulin – blue, RB3/stathmin-yellow.

Colchicine binding site

Colchicine is a plant alkaloid from *Colchicum autumnale* with anticancer and anti-inflammatory properties. Colchicine prevents proper tubulin polymerization by binding to β-tubulin subunit at the interface with α-tubulin. The tubulin assembly can, however, occur with the production of the curved tubulin dimer [95]. In addition to tubulin assembly inhibition, colchicine-site compounds stimulate tubulin-promoted GTP hydrolysis in a reaction uncoupled from polymerization [96].

Vinca alkaloids

The vinca domain is composed of two neighbouring α and β-tubulin heterodimers since structural elements of both partners have been shown to contribute to ligand binding (Fig. 17) [97]. Therefore ligand acts as a wedge between two tubulin dimers and inhibits curved to straight conformational transition required for microtubule growth [84]. The presence of vinca site ligand can, however, lead to the formation of ring-like non-functional aggregates, which also contribute to microtubule destabilization. Affinities of the resulting liganded heterodimers for such polymerized spiral oligomers slightly affect overall affinity, despite the affinities towards tubulin heterodimers are comparable [98]. Vincristine (Fig. 18) and vinblastine are naturally occurring vinca alkaloids isolated from *Catharanthus roseus*, whereas vinorelbine, vinflunine (20,20-difluoro-3,4-dihydrovinorelbine) and vindesine are semi-synthetic analogues [99].
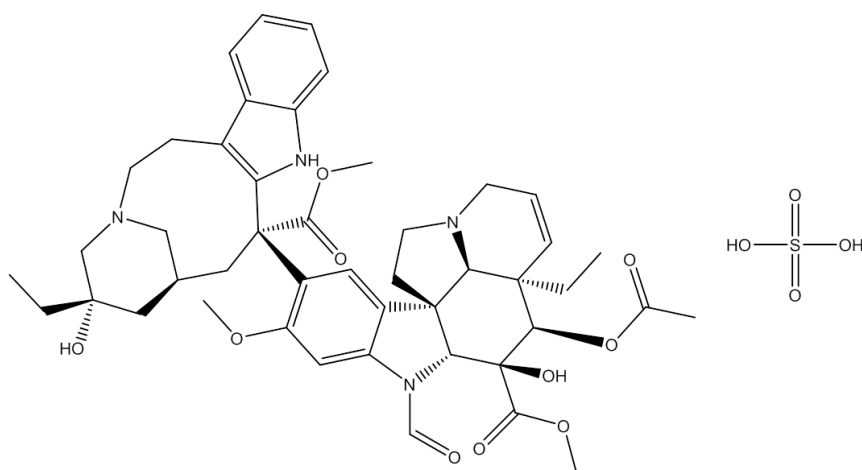
Figure 18. The structure of vincristine sulfate

Maytansine-site

Maytansine-site is a binding site on β-tubulin involved in the formation of longitudinal contacts in microtubules. It is targeted by maytansine, its analogues and other compounds such as rhizoxin and PM060184. Binding of the ligand prevents longitudinal tubulin interactions and also binding of vinca-binding site ligands to vinca domain [100].

Taxoid site

Paclitaxel inhibits tubulin depolymerization by stabilizing longitudinal contacts and lateral interactions between protofilaments [101]. Paclitaxel (Fig. 19) was first isolated from the bark of *Taxus brevifolia*. Despite having a complex structure and poor water solubility, its preparation was solved by a semisynthetic method and aqueous solubility by formulation in Cremofor. The Cremofor-free paclitaxel formulations are designed in order to eliminate hypersensitivity reactions [102]. Novel strategies are being developed to improve efficacy in hypoxic tumors and tumors with MDR phenotype [103]. Paclitaxel derivative docetaxel is used for the treatment of solid tumors including breast, prostate, lung, ovarian and gastric cancer [104]. Cabazitaxel is semisynthetic taxane with antitumor activity regardless innate or acquired resistance. The preclinical study reported that it possess significant activity even in cancers resistant to other taxanes [105].
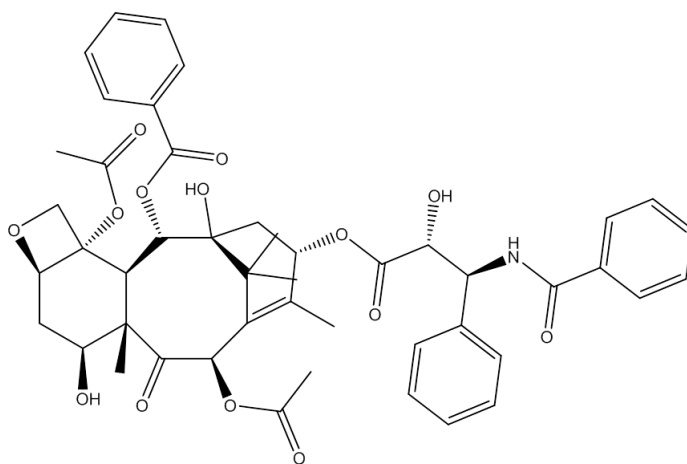
Figure 19. The structure of paclitaxel.

Non-taxoid site ligands

Laulimalide

Marine product laulimalide (Fig. 20) is microtubule stabilizing agent that similarly to peloruside A interacts with β-tubulin site distinct from paclitaxel. Interestingly, the compounds display notable synergy with paclitaxel, epothilone or discodermolide [106]. Moreover, laulimalide is active against cell lines resistant to paclitaxel or epothilones A and B on the basis of mutations in the M40 human β-tubulin gene [107].
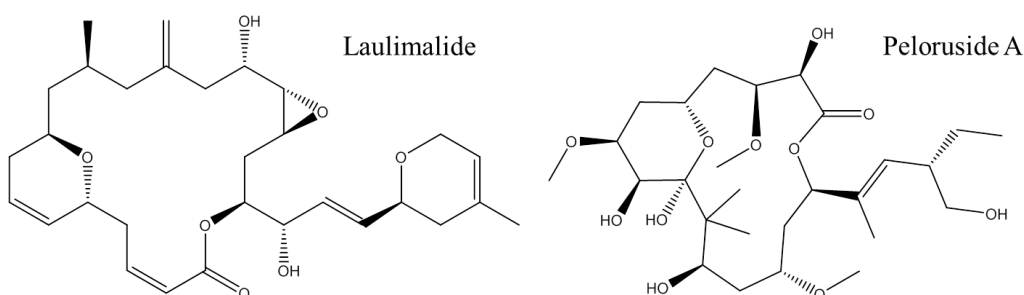
Figure 20. Laulimalide and peloruside A structures. Adapted from [108]**.**

Peloruside A

Peloruside A (Fig. 20) is 16-membered polyketide macrolactone isolated from marine sponge *Mycale hentsheli*. X-ray crystallography study with PELA bound to tubulin showed that PELA binds to a pocket at β-tubulin formed by hydrophobic and polar residues of helices H9 and H10 and loops H9–H90 and H10–S9. PELA probably causes an allosteric stabilization of the M-loop responsible for lateral contacts with adjacent protofilaments [108]. PELA was shown to possess a significant antitumor activity in murine xenograft models. Moreover, it displays anti-angiogenic activity and increases CIN frequency in cancer cells.

Similarly to other MTAs, resistance to PELA is mediated by several mechanisms such as βIII tubulin isotype expression and β-tubulin mutation, that are in detail discussed in next section. Targeting non-taxoid site of β-tubulin has several advantages over taxane site and endorse the future potential use of PELA as a chemotherapeutic. PELA can synergize with other MTAs due to an unique binding site and, unlike paclitaxel, it is a poor substrate of P-gp efflux pump [109]. PELA maintains its efficacy in paclitaxel and epothilone resistant cell lines harbouring β-tubulin mutations at taxoid site as well as in cell lines with multidrug resistance

phenotype [110]. The effect of hypoxia on PELA efficacy has not been evaluated and it is subject of this thesis.

Mechanisms of acquired resistance towards MTAs

Development of drug resistance to MTAs is often associated with the limited clinical outcome of cancer therapy. Tumor susceptibility to paclitaxel, vinblastine and other MTAs can be altered by diverse mechanisms that include tubulin mutations, βIII tubulin isotype expression, altered expression of miRNA, multidrug resistance and hypoxia-induced resistance.

Multidrug resistance

Overexpression of drug efflux pumps from the ATP binding cassette (ABC) family is a factor frequently responsible for tumor chemoresistance. ABC transporters constitute a large family of ATP dependent transmembrane proteins that participate in translocation of numerous substrates [111]. Although blocking P-gp mediated efflux of chemotherapeutics seemed initially as promising, it was shown to be very limited by toxicity [112]. While co-administration of ABC or P-gp competitive inhibitors was ineffective, covalently bound ligands or drugs with high-affinity to microtubules such as paclitaxel analogue CTX-40 could potentially overcome the resistance due to limited access to efflux transporters [113]. The covalent nature of zampanolide binding mode overcame the P-gp-mediated MDR mechanism, since it displayed comparable activity in the sensitive ovarian carcinoma cell line A2780 and its complementary subline with MDR phenotype [114]. Compounds that are less susceptible to P-gp drug efflux may possess novel pharmacokinetic and pharmacodynamic profiles, that may alter oral administration potential [115].

Mutations or binding site alterations

Acquired resistance can be mediated through β-tubulin mutation, which in turn leads to substitution in aminoacid sequence and structural alteration. The substitution can be within specific site required for drug interaction, GTP-binding site or other sites. Despite numerous studies demonstrating the association of β-tubulin mutations with acquired drug resistance in cell lines, their clinical relevance needs to be investigated. While one study identified β -tubulin gene mutations as a strong predictor of response to paclitaxel [116], other studies reported

no contribution of mutations on paclitaxel resistance [117], [118]. Another striking difference was also in the frequency of clinical occurrence, since the latter detected no mutations. The majority of studies were conducted on cell lines with developed resistance to MTAs, although the development of such alterations in tumors remains debatable. Moreover, the sequencing interpretation is complicated by parallel expression of different tubulin isotypes and presence of tubulin pseudogenes. More recently, analysis of 90 breast cancer patient samples revealed mutations in tubulin βI, βIIA or βIVB isotypes, that increase their resemblance to the βIII isotype. These mutations were shown to confer invasiveness, survival advantage and resistance to reactive oxygen species (ROS) [119].

βIII tubulin isotype expression

Tubulin gene family consist of several α and β tubulin isotypes, that can be differentially expressed in tissues or cells. For example, specialized microtubules such as ciliary axonemes, neuronal microtubules or microtubules of platelets and haematopoietic cells are enriched in βII, βIV or βVI-tubulin isotypes [120]. Distinct isotypes and post-translational modifications, in turn, modulate interactions with microtubule-associated proteins and affect the motility of motor proteins [121]. βIII tubulin isotype expression has been linked to drug resistance, especially towards antimitotic drugs [122]. It was shown to reduce the ability of paclitaxel to suppress microtubule dynamics and thus counteract the effect of paclitaxel [123], [124]. βIII tubulin expression was shown to be strong unfavourable prognostic marker in non-small cell lung cancer (NSCLC) patients. Furthermore, it is more frequently expressed in advanced stage NSCLC [125] and its level correlates with lower PTX sensitivity [126]. In addition, similar results were obtained in a study of NSCLC patients receiving vinorelbine-based chemotherapy. High level of βIII tubulin expression in tumor cells is associated with resistance to vinorelbine and a poor prognosis [127].

MicroRNA

A large body of evidence links abnormal expression of miRNAs to resistance against MTAs, however the mechanisms of resistance are largely unknown. These small non-coding RNAs can posttranscriptionally attenuate protein expression by interactions with its mRNA. miRNAs including miR-34, miR-200c and others were shown to modulate sensitivity to paclitaxel or vincristine in many solid cancers. Numerous studies indicate that miRNAs can confer protective effect towards

apoptosis by affecting the expression of Bcl-2 family members, FOXO3A, ALDH1 or caspases [128]. In addition, some miRNAs such as of let-7g, miR-138 modulate expression of drug efflux transporters including MDR1, glutathione-S-transferase-π, and MRP [129].

Hypoxia mediated resistance

  Oxygen homeostasis within cells is tightly controlled by hypoxia inducible factor 1 (HIF-1). HIF-1 is a transcription factor consisting of HIF-1α and HIF-1β subunits, nevertheless HIF-1α plays a key regulatory role. In the presence of oxygen, HIF-1α is hydroxylated by prolyl hydroxylase (PHD) and factor inhibiting HIF-1 (FIH-1), subsequently ubiquitinylated by von Hippel–Lindau E3 ligase tumor suppressor (VHL) and rapidly degraded by the ubiquitin-proteasome pathway (Fig. 21) [130]. Under hypoxic conditions, however, low oxygen levels prevent hydroxylation and degradation of HIF-1α [131]. Stabilized HIF-1α then translocates to the nucleus, forms a heterodimer with HIF-1β subunit and in the presence of p300-CBP transcriptional coactivators induces expression of target genes under hypoxia response element (HRE).
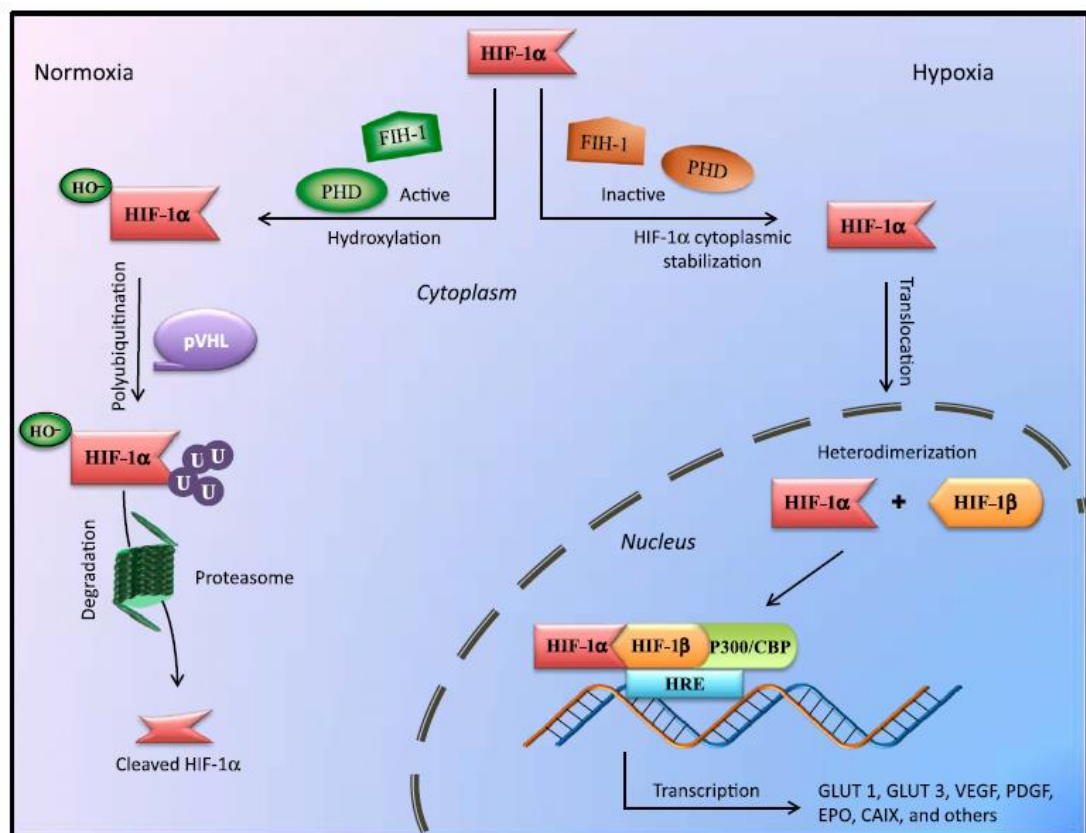
Figure 21. HIF-1α pathway. Adapted from [103]**.**

Hypoxia induces expression of genes involved in cell proliferation, survival, angiogenesis or multidrug resistance such as vascular endothelial growth factor (VEGF), transforming growth factor β3 (TGF-β3), erythropoietin (EPO), glucose transporters (GLUT), C-MYC, P-gp and others [103]. The level of HIF-1α has a significant impact on the sensitivity of cancer cells to paclitaxel both *in vitro* [132] and *in vivo* [133]. In addition, taxotere and other MTAs down-regulate HIF-1α level on the post-transcriptional level and inhibit its transcriptional activity. So there is a complex interplay between microtubules and HIF-1α, because an intact microtubular network is required for HIF-1α accumulation [134]. Thus, oxygen deprivation contributes to resistance of solid tumors to chemotherapy. Moreover, periods of intermittent hypoxia further promote the evolution of more aggressive tumor phenotypes with altered susceptibility to apoptosis and enhanced angiogenesis [135], [136].

2.2. DNA damaging agents

DNA alkylating agents induce DNA damage by directly alkylating purine bases. Monofunctional methylating agents temozolomide and dacarbazine form adducts with N- and O-atoms of DNA bases. Bifunctional alkylating agents melphalan, chlorambucil and cyclophosphamide possess two reactive sites. They crosslink two DNA bases or DNA with proteins. Chloroethylating agents carmustine form adducts at O^6-guanine [137]. The alkylating-like platinum agents cisplatin, carboplatin and oxaliplatin bind guanine and adenine residues and form intrastrand crosslinks. Pyrimidine analogues 5-fluorouracil, gemcitabine and purine analogues fludarabine and cladribine are antimetabolites, which mimics natural nucleotides and interfere with DNA replication and nucleotide metabolism. Inhibitors of dihydrofolate reductase methotrexate, aminopterin and pemetrexed block nucleotide synthesis [138]. An important class of anticancer drugs are antimetabolites based on 5-fluorouracil. They block the conversion of 20-deoxyuridine-5-monophosphate (dUMP) into 2-deoxythymidine-5-monophosphate by inhibiting thymidylate synthase. Interference with deoxynucleotide (dNTP) metabolism results in DNA damage [139].

2.3. Topoisomerase inhibitors

Topoisomerases are enzymes essential for DNA strand separation during replication, transcription and recombination, since these processes generate DNA supercoiling. They are responsible for relaxation of supercoiled DNA and decatenation of interlocked DNA by binding to DNA and attacking DNA phosphodiester backbone. The mechanism includes the formation of an enzyme/DNA covalent intermediate by phosphotyrosine bond, strand passage and re-forming of DNA phosphodiester backbone. Type I topoisomerases make single-stranded cuts in DNA, whereas type II enzymes cut double-stranded DNA [140]. DNA topoisomerases are targets of clinically used anticancer drugs. Camptothecin derivatives topotecan and irinotecan are topoisomerase I inhibitors, whereas etoposide, doxorubicin, daunorubicin, mitoxantrone and amsacrine inhibit topoisomerase IIα [141].

2.4. Inhibitors of mitotic kinases and related targets

The underlying strategy of novel anti-mitotics and SAC inhibitors is the induction of SAC mediated cell cycle arrest or premature mitotic exit resulting in aneuploidy and massive genetic imbalance. These interventions, in turn, lead to apoptosis and suppression of cell proliferation. The targets are represented by Aurora kinase A and B, Polo-like kinase 1 and kinesins Cenp-E and KSP/Eg5 [26].

Barasertib, Alisertib and Danusertib are specific Aurora kinase inhibitors in clinical trials. Although inhibitors of such targets show less adverse effects than MTAs, their efficacy in solid tumors is limited. The reason for unsatisfactory results is apparently long doubling time of cells within the solid tumor. Therefore Aurora kinases inhibitors are currently under clinical investigation for the treatment of rapidly proliferating hematologic malignancies [142]. Rigosertib and Volasertib are dual inhibitors of PLK1 and phosphoinositide 3-kinase signaling pathways. GSK461364A is a selective ATP-competitive inhibitor of PLK1, which already underwent phase I clinical study and shows radiosensitizing effect [143].

Kinesins are microtubule-associated motor proteins that move along the microtubules and contribute to the bipolar spindle assembly. Whereas Eg5 and Cenp-E are plus end kinesins [26], HSET is minus end directed kinesin that acts as an Eg5 antagonist. The kinesins are frequently overexpressed in various tumors, thus mitotic

kinesins such as Eg5 and HSET are targets of novel mitosis-directed inhibitors. Monastrol is the first identified inhibitor of Eg5 that induces mitotic arrest and mono-astral cells. (S)-Trityl-L-Cysteine (STLC) is an ATP-non-competitive reversible inhibitor with higher affinity to Eg5 than monastrol. The potential of HSET inhibitors CW069 and AZ82 remains to be explored [144]. Clinical study of Cenp-E inhibitor GSK923295 showed stable disease in one-third of refractory cancer patients [26].

2.5. Inhibitors of cyclin dependent kinases

Flavopiridol is a pan-CDK inhibitor (CDK1, CDK2, CDK4, CDK6, CDK7 and CDK9) derived from chromone alkaloid. Although it possesses significant *in vitro* activity, achieved *in vivo* was substantially lower. Non-selective inhibitors such as flavopiridol and roscovitine do not allow the rational use of drug due to poor understanding of the mechanism of action. Therefore the second generation of CDKs inhibitors with higher specificity was developed [3]. Olomoucine II is a purine analogue of cytokinin origin. In comparison with other trisubstituted purine analogues such as roscovitine, bohemine, olomoucine and purvalanol A, it exhibits improved ability to inhibit cyclin B-CDK1 complex. It binds to ATP binding pocket of CDK2 [145]. Roscovitine (Seliciclib) is an inhibitor of CDK1, CDK2, CDK5, CDK7 and CDK9. However, its development was terminated during clinical studies. Although successful in preclinical studies, the clinical trials showed the limited efficacy of roscovitine as a single agent [146], [147].

Palbociclib is first specific CDK 4/6 inhibitor in clinics. It is mainly used in combination with other chemotherapeutics as palbociclib alone shows cytostatic activity without inducing apoptosis or senescence. The combination with letrozole was reported to prolong progression-free survival in metastatic hormone receptor (HR)-positive, HER2-negative breast cancer and received FDA approval in HER2-negative luminal breast cancer. The presence of HR remains the only predictor of response. Therefore the research is oriented towards identification and characterization of biomarkers associated with response [8]. Dinaciclib (MK-7965, SCH727965) is second-generation CDK inhibitor specifically developed to inhibit CDK1, CDK2, CDK5 and CDK9 [3].

2.6. Inhibitors of Wee1

The Wee1 kinase is overexpressed in many types of solid carcinomas and leukemias and has been associated with tumor progression. On the other hand, the lack of Wee1 expression in non-small cell lung carcinoma is a negative prognostic factor. Therefore, the efficacy of Wee1 inhibitors is critically dependent on the complex background of genetic alterations. For example, tumors dependent on functional G2/M checkpoint could be sensitized by Wee1 inhibitors to DNA-damaging therapy (Fig. 22). Development of Wee1 inhibitors is complicated by high structural homology of ATP-binding site with other kinases [148]. Nevertheless, data from phase I clinical study of AZD1775 alone or in combination with cisplatin, carboplatin or gemcitabine show promising responses. Interestingly, the response rate in refractory solid tumors was correlated with p53 status. Thus, p53-deficient cells are preferentially sensitized damaging agents [149].
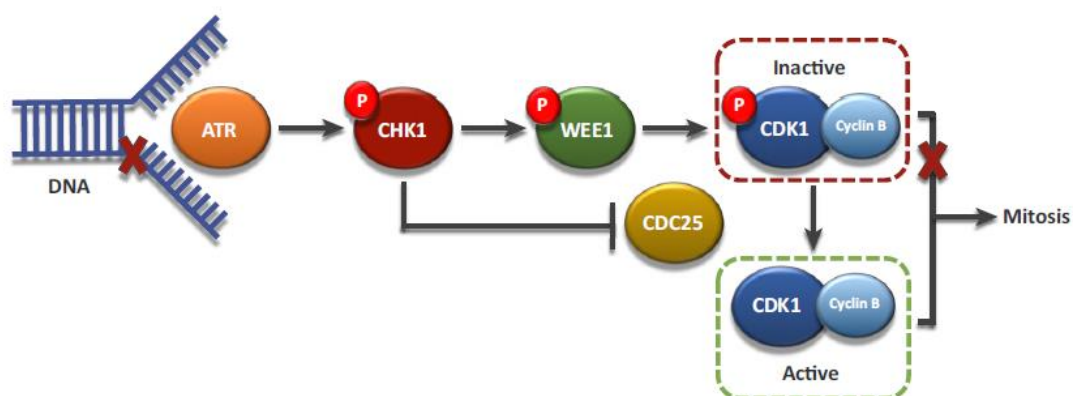
Figure 22. The role of Wee1 in the G2/M checkpoint. Adapted from [148]**.**

2.7. Inhibitors of DNA damage signaling pathway

The preclinical studies of Chk1 inhibitors UCN-01 and ICP-1 showed promising results, particularly in combination with DNA damaging drug cisplatin. UCN-01 failed in clinical trials. However, second-generation Chk1 inhibitors display better outcomes. Currently, SCH900776 is undergoing a phase II trial for the treatment of leukemia in combination with cytarabine [58]. LY2606368 is being evaluated in phase II clinical trial for the treatment of squamous cell carcinoma [150]. AZD6738 is ATR kinase inhibitor, which similarly as Chk1 inhibitors potentiates DNA damaging agents [151]. AZD6738 was shown to sensitize p53- or

ATM-defective primary chronic lymphocytic leukemia cells to chemotherapy [152]. Preclinical study of another ATR inhibitor NU6027 indicates that it sensitize p53 deficient cells to hydroxyurea, cisplatin and temozolomide. In addition, it is synthetically lethal when combined with PARP inhibitor [153].

2.8. Proteasomal inhibitors

Proteasomal degradation of specific cell cycle proteins is an integral part of cell cycle regulation. Thereby interference with ubiquitin/proteasome pathway can be used as a strategy for cancer treatment [154]. Bortezomib is clinically used dipeptide boronic acid derivative with anticancer activity. It reversibly and specifically inhibits the threonine residue of the 26S proteasome [155]. It was shown to abrogate degradation of p21, p27 and cyclins [154]. Disabled degradation machinery then leads to cell cycle arrest induced by multiple factors and endoplasmic reticulum stress caused by the accumulation of misfolded proteins (Fig. 23).
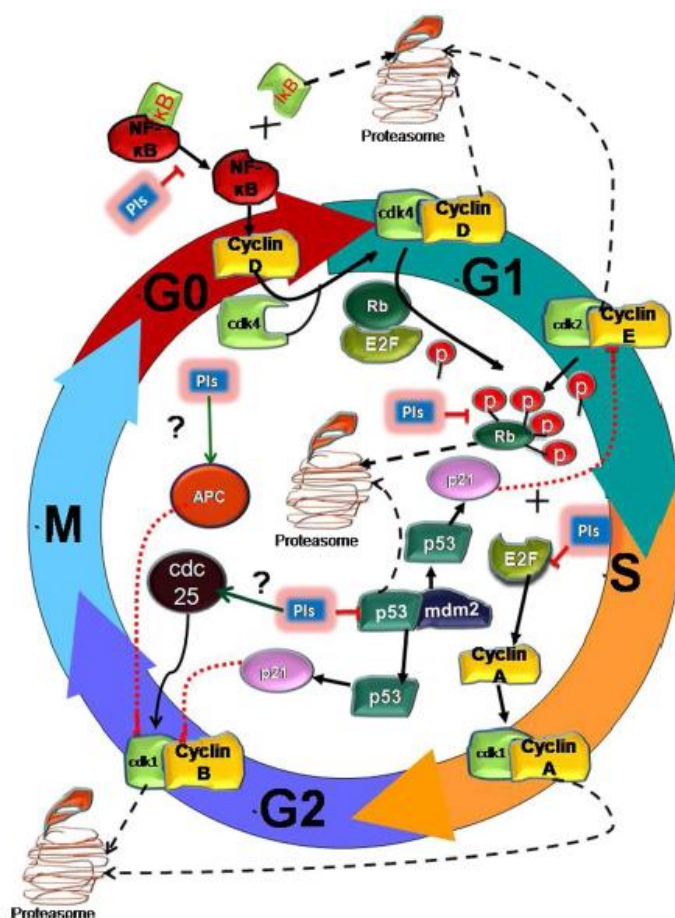
Figure 23. Modulation of cell cycle checkpoints by proteasomal inhibitors. Adapted from [156]**.**

Proteasome inhibition was also reported to increase the endogenous level of reactive oxygen species that in turn causes a higher rate of DNA damage. Moreover, stabilization of p53 induces expression p21, a cyclin dependent kinase inhibitor that inactivates cyclin B-CDK2 complex. In addition, proteasome inhibition modulates numerous other signaling pathways including, but not limited to ATM, ATR, Rb/E2F, NFκB and MAPK. As in the case of other therapeutics, cancer resistance provoked a development of the second generation of proteasome inhibitors such as Carfilzomib, Salinosporamide A and MLN9708 [156].

2.9. Histone deacetylase inhibitors

Posttranslational modifications such as acetylation play a central role in the regulation of gene transcription. Acetylation of histone proteins alters secondary DNA structure and repress gene expression [157]. This regulatory mechanism participates in repression of E2F-dependent genes, since Rb mediate recruitment of histone deacetylase (HDAC) to E2F promoter sites. In addition, HDAC inhibitor depsipeptide was reported to induce p21-dependent G1 and p21-independent G2 arrest with alteration of cyclin D1 and cyclin E expression [154]. HDAC inhibitors modulate acetylation pattern of histones and nonhistone proteins, which in turn results in increased or decreased gene expression. Thereby HDAC inhibitors affect diverse cellular processes including DNA replication, cell cycle arrest and apoptosis. HDAC inhibitors can be divided into several classes such as hydroxamic acids, cyclic peptides, bibenzimides and short-chain fatty acids. Although HDAC inhibitors possess limited clinical efficacy in monotherapy, vorinostat and depsipeptide received FDA approval for treatment of T-cell lymphoma. Currently, there are clinical trials investigating novel HDAC inhibitors as well as combinatorial therapies with conventional drugs [158].

3.   Betulinic acid and its analogues
3.1. Betulinic acid

Betulinic acid is a naturally occurring compound with many biological activities (Fig. 24). The extensive research efforts in this group were supported by evidence that betulinic acid is selectively cytotoxic against tumor cells. Moreover, melanoma cells were shown to be much more sensitive to betulinic acid in comparison with normal melanocytes [159]. The compound selectively induces

apoptosis, however beside apoptosis, it is also known to modulate multiple pathways involved in angiogenesis, survival or stress response.
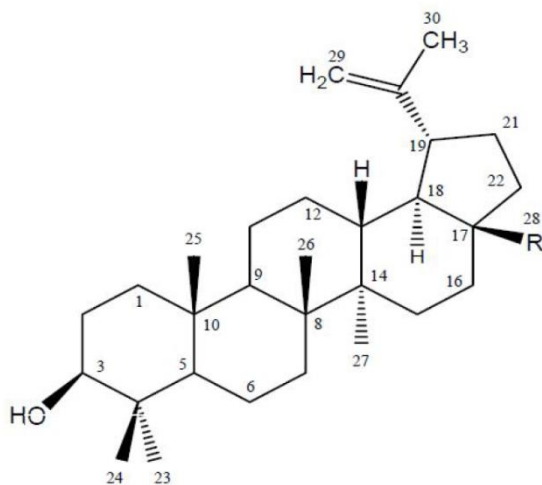
Figure 24. Chemical structure of betulinic acid. Adapted from [160]**.**

Topoisomerase inhibition

Betulinic acid has been shown to inhibit eukaryotic topoisomerase I and IIα by preventing topoisomerase-DNA interaction and formation of topoisomerase I–DNA cleavable complex both *in vitro* and *in vivo*. The process does not involve intercalation in DNA and requires carboxylic group C-28 at C-17 [161], [162], [163].

Induction of intrinsic apoptosis

Betulinic acid antitumor activity is associated with the production of reactive oxygen species (ROS), mitochondrial membrane potential perturbation, permeabilization of mitochondrial outer membrane release of apoptogenic factors cytochrome c and AIF to the cytosol and intrinsic apoptosis. Generation of ROS was monitored within 15 minutes after treatment and ROS are considered as key signaling molecules responsible for apoptosis induction, as the apoptosis was prevented by pretreatment with antioxidants such as reduced glutathione or vitamin E [164].

Bcl-2 family members

The effect of betulinic acid on proapoptotic and antiapoptotic Bcl-2 family members have not been clearly elucidated. Betulinic acid was reported to downregulate Bcl-2 gene expression in human lung carcinoma and human colon adenocarcinoma cells [165]. However, the data are in contradiction with previously published literature, where the level of Bcl-2 protein was not affected [166]. A study

in neck squamous cellular carcinoma cells showed no changes in Bcl-2 and Mcl-1 levels following betulinic treatment, whereas proapoptotic family member Bax was downregulated [167]. There is also evidence of Mcl-1 induction by betulinic acid in human melanoma [168]. The contradictory data can be to some extent explained by aberrant Bcl-2 family members expression in particular tumor cells or by cell line specific effects. Experiments with cells overexpressing antiapoptotic Bcl-2 family members showed that Bcl-2 and Bcl-x_L can only temporarily protect against betulinic acid-induced apoptosis and the effect is independent on proapoptotic proteins Bax/Bak [169].

Inhibition of angiogenesis

Betulinic acid has been shown to inhibit angiogenesis and reduce vascular endothelial growth factor (VEGF) levels in the tumor [170], [171]. Importantly, betulinic acid inhibits constitutive activation of STAT3, which is a crucial mediator of angiogenesis and direct transcriptional activator VEGF [172]. BA treatment suppressed the binding of STAT3 and HIF-1α to VEGF promoter in hypoxic condition [171]. In addition, STAT3 transcriptional targets include Bcl-x_L, Bcl-2, cyclin D1 or survivin and betulinic acid treatment resulted in their downregulation [173]. It was also proposed, that modulation of mitochondrial reducing potential by betulinic can contribute to the antiangiogenic activity of betulinic acid [174].

3.2. Bardoxolone methyl

Bardoxolone methyl is orally-available semi-synthetic triterpenoid derived from oleanolic acid. It is an activator of the Nrf2 pathway and an inhibitor of the nuclear factor-κB (NF-κB) and JAK/STAT pathways with anti-inflammatory and chemoprotective effect (Fig. 25). Keap1/Nrf2 and NF-κB pathways are modulated through reversible adducts between cysteine residues in target proteins Keap1 or IκB kinase and α,β-unsaturated carbonyl groups on rings A and C. The bardoxolone methyl mode of action is dependent on concentration. While low nanomolar doses have a protective effect against reactive oxygen species, micromolar concentrations induce apoptosis accompanied by reduced glutathione levels and elevated ROS levels [175], [176]. Bardoxolone methyl has been shown to possess antiproliferative activity *in vitro* and antitumorigenic effect *in vivo*. The inhibition of cell proliferation is mediated by inhibition Akt, NF-κB, MAPK (Erk1/2) and mTOR signaling pathways and results in apoptosis. The preclinical study in pancreatic ductal

adenocarcinoma indicates possible destruction of residual disease and prevention of relapse. In addition, bardoxolone methyl treatment prolonged the survival of mice MiaPaCa-2 xenografts [177].
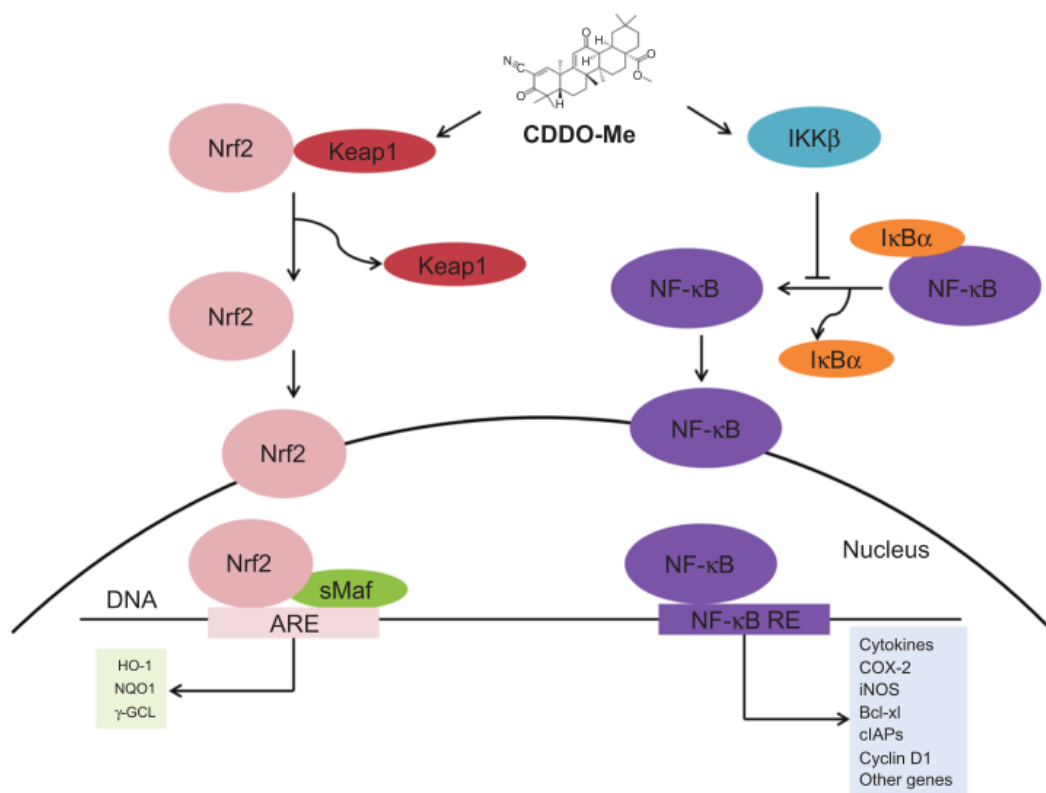
Figure 25. Bardoxolone methyl (CDDO-Me) induced activation of antioxidant response pathway and suppression of NF-κB pathway. Adapted from [175]**.**

The data from the first clinical trial indicated objective antitumor activity against mantle cell lymphoma and anaplastic thyroid carcinoma. Surprisingly, it has been found to improve glomerular filtration. Therefore another clinical trials evaluated bardoxolone methyl for the treatment of chronic kidney disease. However, the clinical trial was terminated phase III because of cardiotoxicity [176]. Other clinical investigations were conducted for the treatment of pulmonary hypertension and chronic kidney disease associated with type 2 diabetes [175]. Bardoxolone methyl is well tolerated with relatively long terminal phase half-life (39 hours at 900mg/day) following oral absorption [176].
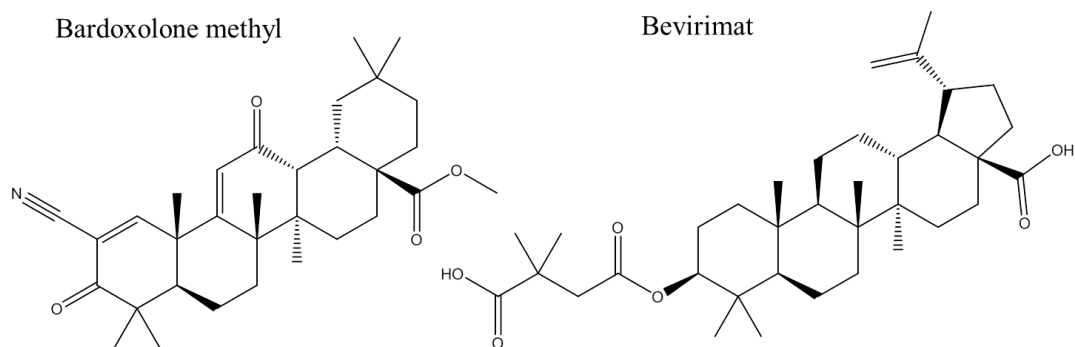
Figure 26. Chemical structures of bardoxolone methyl and bevirimat.

3.3. Bevirimat

Bevirimat is first in class HIV maturation inhibitor (Fig. 26). Unlike other anti-HIV drugs which inhibit reverse transcriptase, integrase or protease, it targets Gag precursor maturation and interferes with HIV replication. Bevirimat specifically inhibits cleavage of the Ca-spacer protein1 (SP1) intermediate, which is a late event in the HIV-1 Gag processing cascade, and results in the release of non-infectious virus particles. Thus, the progression of infection from host cells to new cells is efficiently blocked. However, antiviral response to bevirimat was not uniform among the patients in phase II and the clinical trial was terminated in 2010, because of the natural polymorphism of the target Ca-SP1 junction, which confers a natural resistance of the virus to bevirimat. Further analysis identified V7 polymorphism in SP1 as a primary determinant of naturally occurring resistance to bevirimat [178].

3.4. Semi-synthetic triterpenes

Triterpenes display low aqueous solubility and limited bioavailability due to their lipophilic nature [179]. This limitations can by solved by appropriate derivatization and formulation. New compounds are designed with respect to available chemistry approaches that are employed in order to improve pharmacological properties of the active compound. In addition, new structures must be developed with special attention to patentability. Therefore an accent is put on unexplored modifications of triterpene scaffolds.

Lupane skeleton can be modified by core modification on rings A, D and E. For example by ring cleavage or condensation of different heterocyclic rings. The another possibility is a modification on three accessible positions at carbon 3, 28 and

30 [180]. The introduction of side chain can alter, increase or abolish biological activity, but also affects hydrophobicity of the whole molecule, which in turn significantly influences overall activity. Compounds modified with suitable side chain and ester bond can be developed as prodrugs. A prodrug is a compound that is administered in its inactive or less active form with appropriate pharmacological properties and transformed into an active form in the target cells or tissue. These esterase-activated prodrugs are usually converted into an active form in the blood. Most commonly used prodrug groups are esters, amides, ethers, hemiesters and glycosides [181].

II.   AIMS OF THE STUDY

The aim of the thesis is to evaluate antiproliferative properties of small-molecule compounds *in vitro*. According to the origin of compounds and their drug development status, the specific aims can be further subdivided:

I. Peloruside A efficacy in hypoxia pre-exposed human colorectal carcinoma cells   and comparison with clinically used microtubule targeting drugs paclitaxel and vincristine

- Assess efficacy of peloruside A and model microtubule targeting compounds in hypoxic conditions
- Discover alterations induced by drugs or hypoxia exposure
- Find the underlying mechanisms responsible for differential efficacy of peloruside A and paclitaxel in hypoxia pre-exposed colorectal carcinoma cells

II. Cell cycle modulatory properties of novel triterpene analogues with yet unknown mode of action

- Determine cytotoxic/cytostatic activity
- Analyze cell cycle modulation by flow cytometry methods
- Find relationship between structure and activity with respect to unpublished results of G2/M arrest induced by triterpenes

III.   MATERIALS AND METHODS

Compounds and reagents

Peloruside A (PELA) was kindly provided by Dr Peter Northcote of the School of Chemical and Physical Sciences, Victoria University of Wellington. Taxol® (PTX) was purchased from Bristol-Myers Squibb Company (New York City, NY) and vincristine sulphate (VCR) from Teva Czech Industries s.r.o. (Komarov, Czech Republic). Unless otherwise mentioned, all reagents were purchased from Sigma-Aldrich (Prague, Czech Republic). The studied triterpene analogues are listed below (Table 5, Fig. 27).

Table 5.

Structure	Compound	Reference
2,2-Dibromodihydrobetulonic acid	I	[195], [182]
Betulin	II	[182]
Dihydrobetulin-3β-acetate	III	[182]
Acetyldihydrobetulinic acid	IV	[182]
Dihydrobetulinic acid	V	[182]
Benzyl dihydrobetulinate	VI	[182]
Benzyl dihydrobetulonate	VII	[182]
Benzyl 2α-hydroxydihydrobetulonate	VIII	[182]
Benzyl 2,2-difluorodihydrobetulonate	IX	[182]
2,2-Difluorodihydrobetulonic acid	X	[182]
Benzyl-2,2-difluorodihydrobetulinate	XI	[182]
2,2-Difluorodihydrobetulinic acid	XII	[182]
2-Hydroxyallobetulon	XIII	[182]
Difluoroallobetulone	XIV	[182]
Difluoroallobetulin	XV	[182]
3β-O-hemiglutaryl-2,2-difluorodihydrobetulinic acid	XVI	[182]
3β-O-hemisuccinyl-2,2-difluorodihydrobetulinic acid	XVII	[182]
3β-O-3′,3′-dimethylhemiglutaryl-2,2-difluorodihydrobetulinic acid	XVIII	[182]
3β-O-3′,3′-dimethylhemisuccinyl-2,2-difluorodihydrobetulinic acid	XIX	[182]
2,2-Difluoro-19β,28-epoxy-18α-oleanane-3β-yl hemiglutarate	XX	[182]
2,2-Difluoro-19β,28-epoxy-18α-oleanane-3β-yl hemisuccinate	XXI	[182]

2,2-Difluoro-19β,28-epoxy-18α-oleanane-3β-yl 3´,3´-dimethylhemiglutarate	XXII	[182]
Allobetulon	XXIIIa	[183]
2-Bromoallobetulon	XXIIIb	[183]
2-Thiocyanatoallobetulon	XXIIIc	[183]
Methyl betulonate	XXIVa	[183]
2-Bromomethyl betulonate	XXIVb	[183]
2-Thiocyanatomethyl betulonate	XXIVc	[183]
Methyl oleanonate	XXVa	[183]
2-Bromomethyl oleanonate	XXVb	[183]
2-Thiocyanatomethyl oleanonate	XXVc	[183]
Oleanonic acid	XXVIa	[183]
2-Bromooleanonic acid	XXVIb	[183]
Oleanonic acid	XXVIc	[183]
30-Oxobetulinic acid	XXVII	[184], [185]
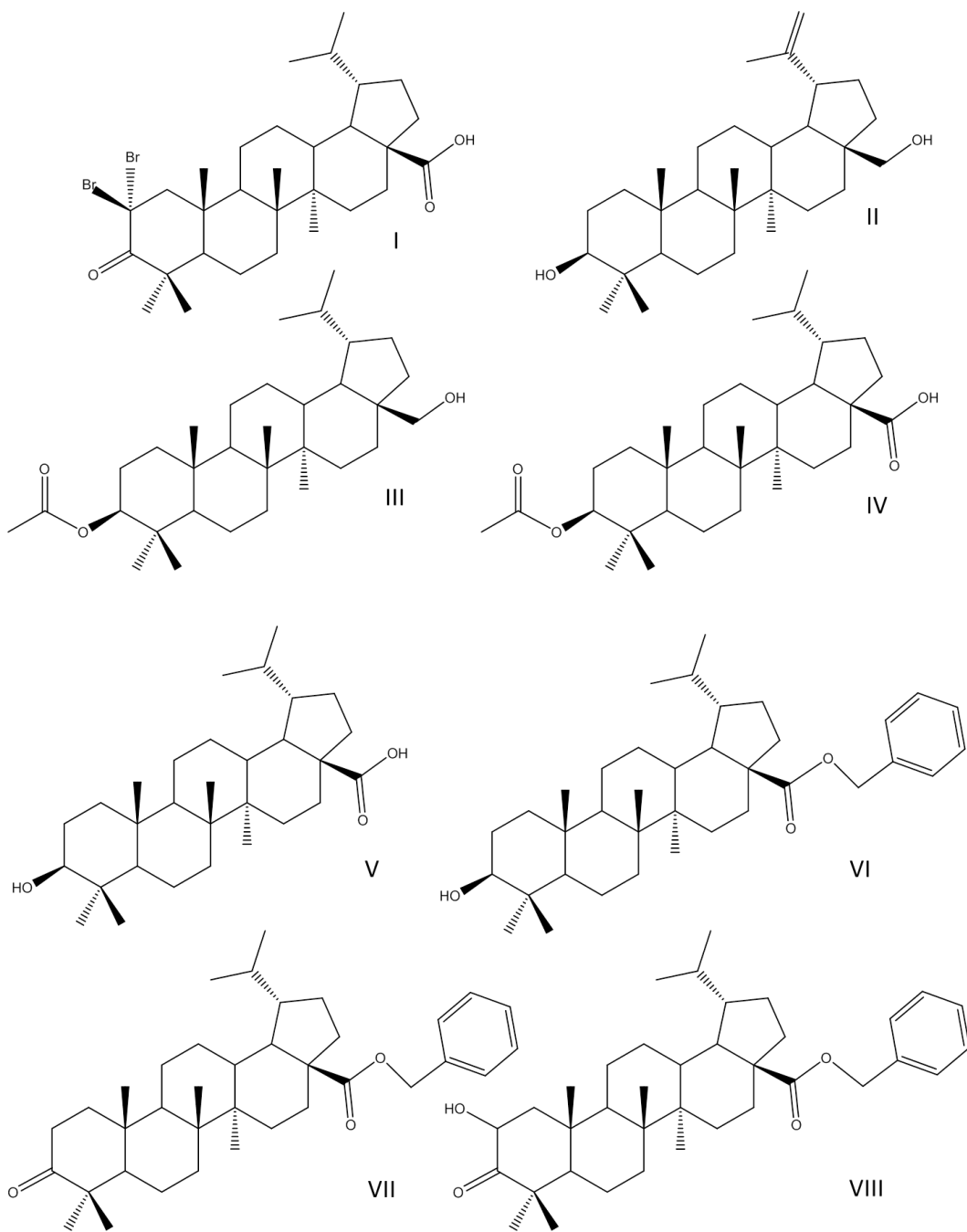
Figure 27. Chemical structures of triterpenoids in the study (continues on the next pages)**.**

IX

X

XI

XII

XIII

XIV

XV

XVI

XVII

XVIII

XIX

XX

XXI

XXII

XXIIIa

XXIIIb

XXIIIc

XXIVa

XXIVb

XXIVc

XXVa

XXVb

XXVc

XXVIa

58

XXVIb

XXVIc

XXVII
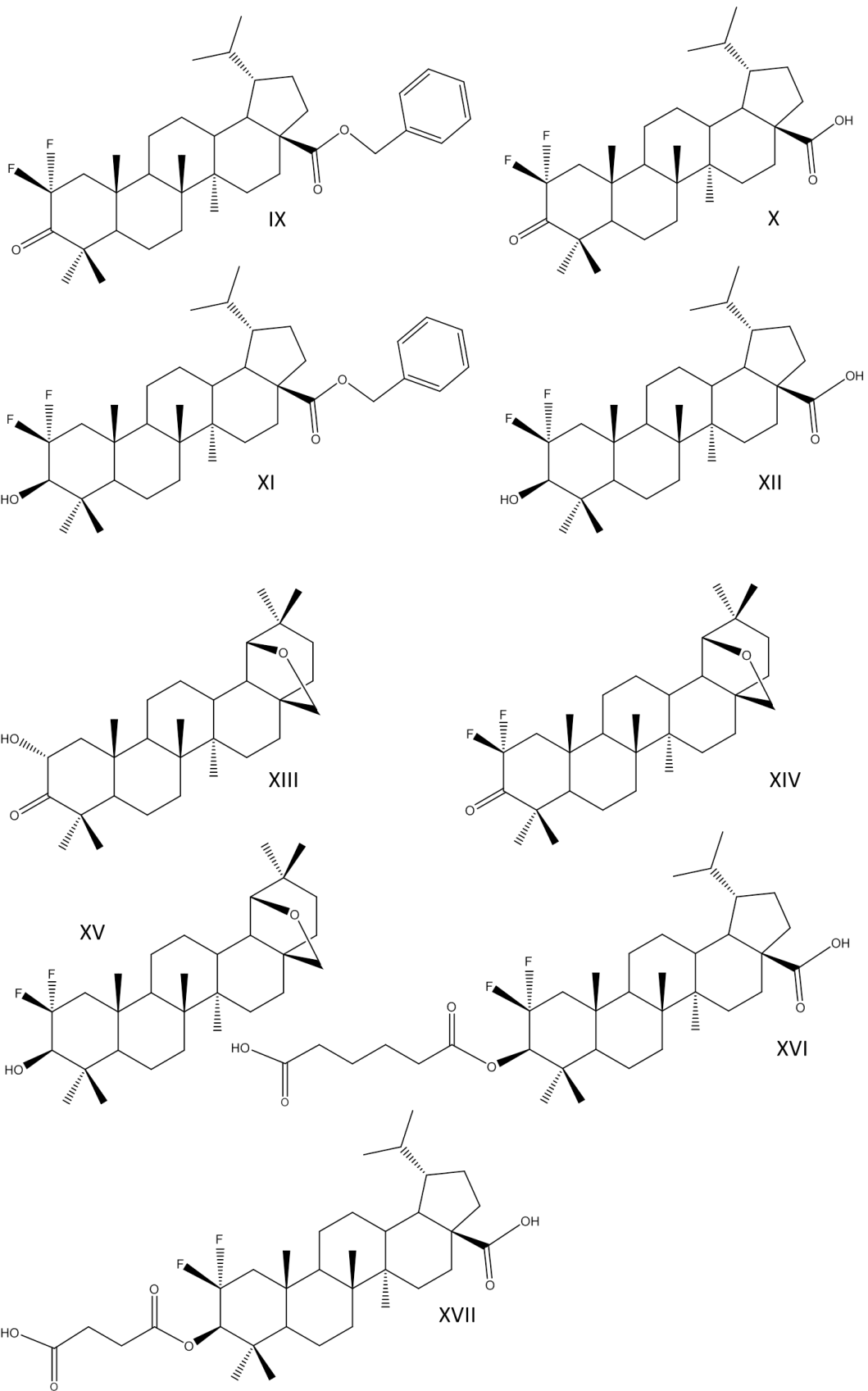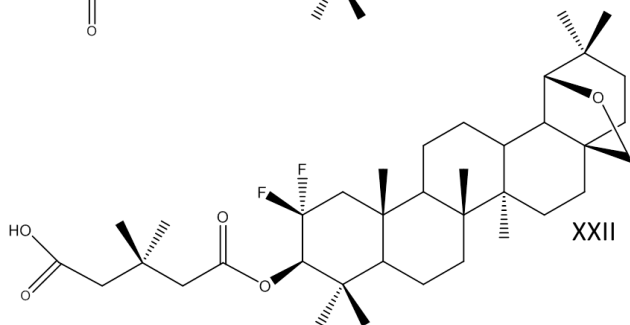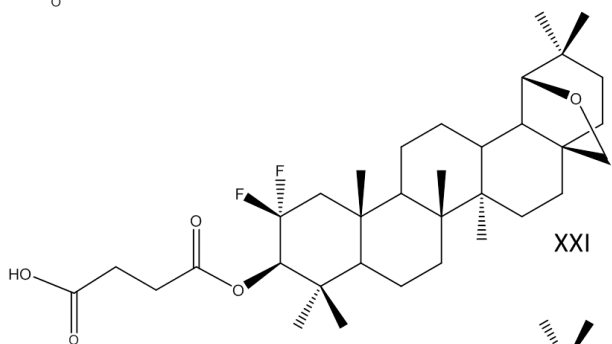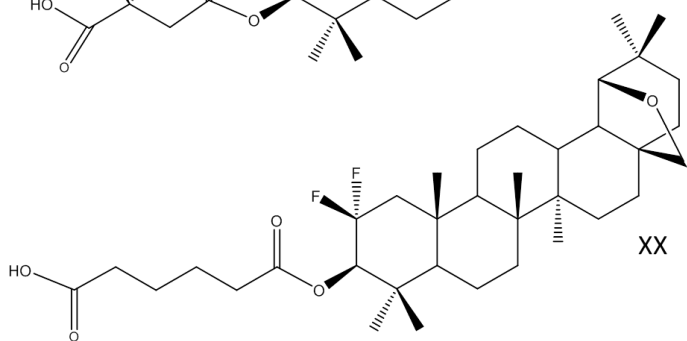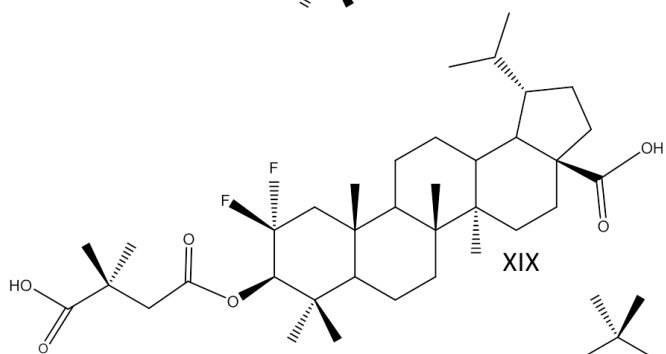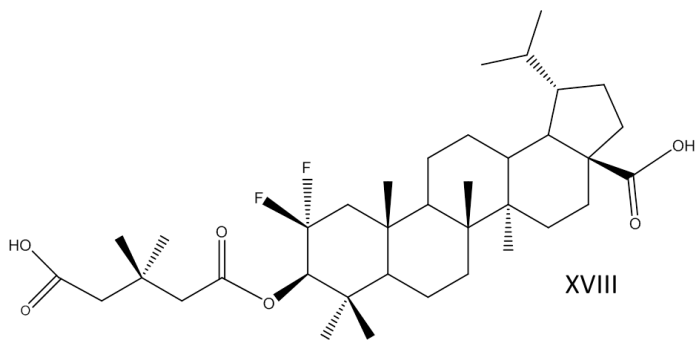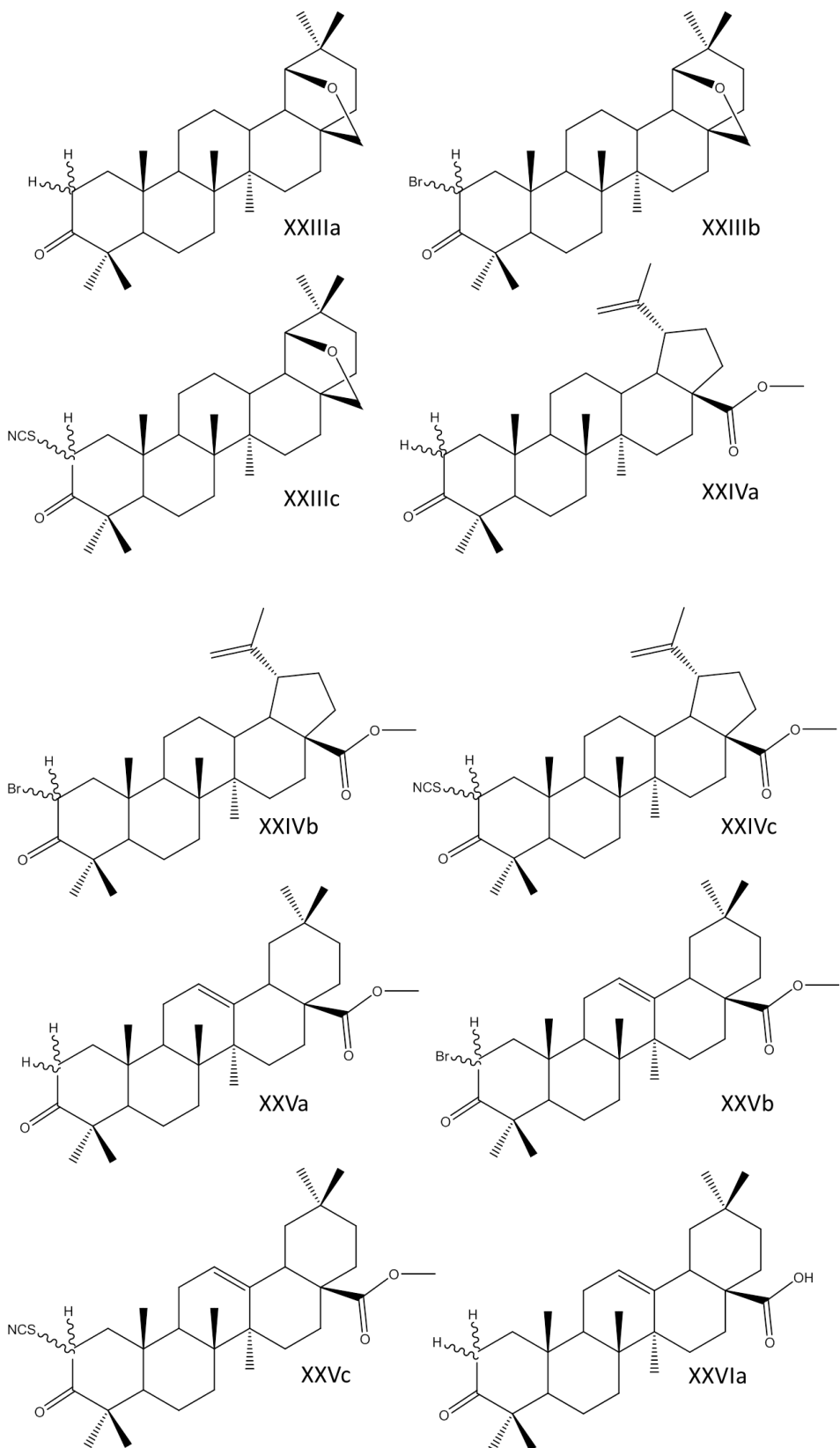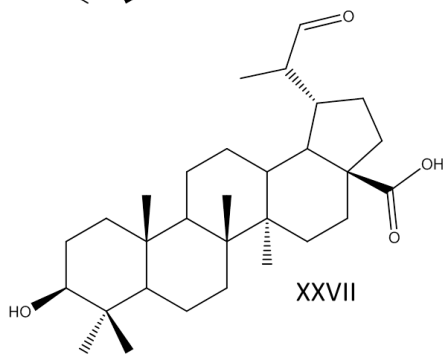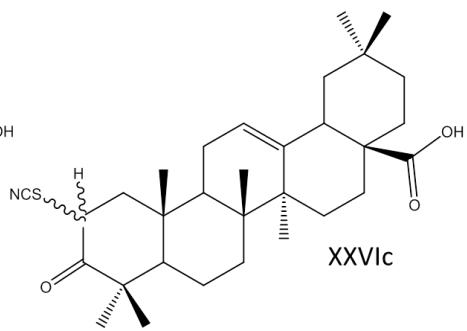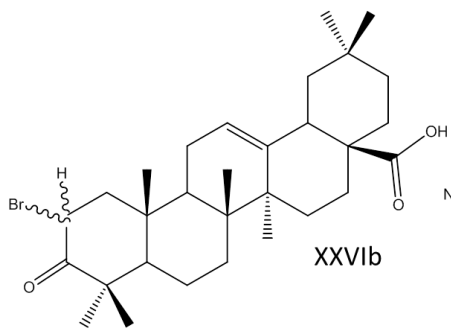
Cell Culture

T-lymphoblastic leukemia cell line CCRF-CEM, chronic myelogenous leukemia cell line K562, lung carcinoma cell line A549, colorectal carcinoma cell line HCT116 and non-tumor skin fibroblasts BJ and MRC-5 cell lines were purchased from the American Tissue Culture Collection (ATCC). HCT116p53-/- deficient in p53 were purchased from Horizon Discovery. The daunorubicin-resistant CCRF-CEM cell line CEM-DNR bulk and paclitaxel-resistant K562-Tax sublines were selected in our laboratory by the cultivation of maternal cell lines in increasing concentrations of daunorubicin and paclitaxel, respectively. The CEM-DNR bulk cells overexpress the P-gp and LRP protein, while K562-Tax cells overexpress only P-glycoprotein [186]. Human cervical cancer HeLa cells expressing the Fluorescence Ubiquitination Cell-Cycle Indicator (FUCCI) were obtained from RIKEN (Japan). Cells were cultured in appropriate medium (Sigma-Aldrich) supplemented with 10 % fetal calf serum 100 U/mL penicillin and 100μg/mL streptomycin in humidified incubator under atmosphere of 95 % air and 5 % CO_2 at 37 °C. For specific experiments evaluating the effect of hypoxic conditions the cells were cultivated in Heracell 150i humidified incubator (Thermo Fisher Scientific, Waltham, MA) at 37ºC/1% O_2, 94% N_2 and 5% CO_2 levels. These hypoxia conditioned cells are labeled as HC and control cells cultivated parallelly in normoxia as NRX. Unless mentioned otherwise, all drug treatments following hypoxia preconditioning of cells were performed under normoxic conditions of 5% CO_2/atmospheric air at 37ºC in a standard humidified incubator.

Plasmids, transfections and transductions

HCT116 were transduced with ready-to-use HIF-1α lentiviral particles (AMS Biotechnology, Oxfordshire, UK) following the manufacturer's instructions. All infections were performed in the presence of 8 µg/mL polybrene infection/transfection reagent (Merck Millipore, Billerica, MA) in bio-safety II cabinets and HIF-1α overexpressing cells were selected by blasticidin. The Proteasome Sensor Vector (pZsProSensor-1) for protein degradation monitoring was purchased from Clontech. It encodes green fluorescent protein (ZsGreen) fused to the mouse ornithine decarboxylase (MODC) degradation domain (amino acids 410–461). Ubiquitin-GFP encoding plasmid with G418 selection marker was a kind gift

from Dr. Martin Mistrík. Transfections were performed using jetPRIME (Polyplus) according to manufacturer´s instructions. Stably transfected cells were selected using G-418 (Sigma-Aldrich).

Cell viability and cytotoxicity assays

MTS assay in 384-well plates used for IC50 value determination of triterpenes.

MTS assay was performed at Institute of Molecular and Translational Medicine by robotic platform (HighResBiosolutions). Cell suspensions were prepared and diluted according to the particular cell type and the expected target cell density (27 000−33 000 cells/mL based on cell growth characteristics). Cells were added by automatic pipetor (30 μL) into 384-well microtiter plates. All tested compounds were dissolved in 100% DMSO and 4-fold dilutions of the intended test concentration were added in 0.15 μL aliquots at time zero to the microtiter plate wells by the echo-acoustic noncontact dispensor Echo550 (Labcyte). The experiments were performed in technical duplicates and three biological replicates. The cells were incubated with the tested compounds for 72 h at 37 °C, in a 5% CO_2 atmosphere at 100% humidity. At the end of the incubation period, the cells were assayed by using the MTS test. Aliquots (5 μL) of the MTS stock solution were pipetted into each well and incubated for an additional 1−4 h. After this incubation period, the optical density (OD) was measured at 490 nm with an Envision reader (PerkinElmer). The IC50 value, the drug concentration that is lethal to 50% of the tumor cells, was calculated from the appropriate dose−response curves in Dotmatics software.

MTT assay used for IC50 value determination in PELA study.

5000 cells were seeded in 96-well plates and after overnight incubation treated with compounds in 3-fold dilutions. Cells were incubated for 72 h at 37°C and 5% CO_2 atmosphere. 10 μL of MTT solution was then added to each well and incubated for 3 hours. Formazan crystals were dissolved in 100 μL of 10% SDS (w/v, pH 5,5) and absorbances measured using plate reader at 540 nm. Three independent experiments were performed in triplicates and IC_{50} values were determined from appropriate curves using GraphPad Prism (GraphPad Software, San Diego, CA).

FACS Analysis

Treated cells were harvested, washed with cold PBS and fixed in cold 70% ethanol and stored at -20°C. Fixed cells were permeabilized 15 min with 0,25% Triton X-100 in phosphate buffered saline (PBS), blocked in 1% bovine serum and incubated with anti-phospho-Histone H3 (Ser10) antibody (Merck Millipore). Subsequently, the samples were treated with 50 μg/mL RNase, stained with propidium iodide and analyzed by FACSCalibur (Becton Dickinson) flow cytometer at 488 nm. Distribution of cells in G1, S and G2/M phases of the cell cycle was analyzed using ModFitLT (Verity) and reflects viable population prior the fixing procedure. The particles with propidium iodide content lower than G1 cells were considered as fragmented DNA of apoptotic cells.

BrdU Incorporation analysis

30 min before harvesting, the cells were pulse-labelled with 10 μM 5-bromo-2-deoxyuridine (BrdU). The cells were fixed overnight with ice-cold 70% ethanol, resuspended in 2 M HCl and following 30 min incubation at RT washed with 0.1 M $Na_2B_4O_7$ and blocked with PBS containing 0.5% Tween-20 and 1% BSA. BrdU incorporation was analysed using Anti-BrdU antibody clone MoBu-1 (Exbio) and secondary antimouse-FITC antibody (Sigma-Aldrich). The cells were then washed with 1×PBS and incubated with 0.1 mg/mL propidium iodide and 0.5 mg/mL RNase A for 1 h at room temperature and analyzed by flow cytometry using a 488 nm single beam laser (FACSCalibur, Becton Dickinson). Percentage of cells with incorporated BrdU was analysed using CellQuest software.

BrU Incorporation analysis

Prior the trypsinization the cells were treated with 1 mM 5-bromouridine (BrU) for 30 min. Subsequently, the cells were fixed 15 min in 1% paraformaldehyde with 0.05% of NP-40 at room temperature and stored overnight at 4 °C. Fixed cells were washed with 1% glycine in PBS and stained with primary anti-BrdU antibody clone MoBu-1 crossreacting to BrU (Exbio) for 30 min at RT, washed with 1×PBS and labelled with secondary antimouse-FITC antibody (Sigma-Aldrich). Following

1-hour incubation in 1% paraformaldehyde with 0.05% NP-40 the samples were stained with propidium iodide (0.1 mg/mL) and treated with RNase A (0.5 mg/mL) for 1 h at room temperature. The percentage of positive cells was analysed using CellQuest software.

Immunofluorescence

HCT116 cells grown on coverslips were washed in PBS and fixed in 3% paraformaldehyde and 10 mM MES, 150 mM NaCl, 5 mM EGTA, 5 mM MgCl2, 5 mM glucose, pH 6.1. Following the blocking with 5% goat serum in PBS (SpinChem) for 60 min samples were incubated 60 min with α-tubulin (DM1A) mouse monoclonal antibody (Cell Signaling) and for purpose of dual staining also with rabbit anti-HIF-1α antibody from (Santa Cruz) in PBS containing 1% BSA and 0.3% Triton X-100. For visualization were used Alexa Fluor-568, Alexa Fluor-488 and Alexa Fluor-647 conjugated anti-mouse or anti-rabbit antibodies (Life Technologies). After each step the samples were washed three times with 1x PBS for 5 min. The samples were mounted with Vectashield Mounting Medium with DAPI. Images were captured using a spinning disk confocal microscope (Zeiss) with CSU-X1 unit (Yokogawa).

Western blot analysis

Cultured cells were lysed in RIPA buffer or, in case of HIF-1α detection, in sodium dodecyl sulfate (SDS) buffer. The protein concentration in RIPA lysates was determined using the Bicinchoninic acid kit (Sigma-Aldrich). 20 µg of total protein was separated on a 10% or 12% SDS-containing polyacrylamide gel. Proteins were transferred to nitrocellulose membrane (Bio-Rad). Membrane was blocked with 5% non-fat dry milk in TRIS buffered saline with 0,1% Tween 20 (TBST) for 60 min and subsequently incubated with primary antibody in TBST with 5% bovine serum albumin overnight at 4°C. Primary antibodies against human β-actin, cyclin B1 and p53 were purchased from Sigma-Aldrich, cyclin D1 antibody was obtained from Merck Millipore. Rb, phospho-Rb (Ser795), acetyl-α-tubulin (Lys40) and p21 antibodies were from Cell Signaling, HIF-1α was purchased from Santa Cruz, caspase 8 and caspase 3 antibodies were from Bio-Techne Corporation. Following three washing steps with TBST for 5 min, the membrane was incubated in TBST with 5% non-fat dry milk and secondary Alexa Fluor-488 conjugated anti-mouse or

anti-rabbit antibodies (Life Technologies). Images were acquired after three washing steps with TBST for 5 min using ChemiDoc Imaging system (Bio-Rad).

Intracellular tubulin polymerization assay

Cells were harvested, washed twice with PBS (37 °C) and lysed in 100 µL hypotonic buffer (1 mM $MgCl_2$, 2 mM EGTA, 0.5% Nonidet P-40, cOmplete Protease Inhibitor Cocktail Roche, 20 mM Tris-HCl, pH 6.8). Soluble and polymerized tubulin fractions were separated by centrifugation at 14000 rpm for 10 minutes at RT. Pellet was resuspended in 100 µL hypotonic buffer, incubated 10 minutes on ice and disrupted by sonication. After addition of 25 µL of 5x SDS sample buffer, the samples were denaturated 5 minutes at 95 °C, processed according to the western blot protocol and probed against α-tubulin as described above. The solubilized and polymerized tubulin fractions were analyzed densitometrically using ImageJ. The percentage of polymerized tubulin was calculated as the ratio of polymerized tubulin and total tubulin from both fractions.

HeLa-FUCCI and time-lapse imaging

HeLa-FUCCI cells in 384-well plates CellCarrier (PerkinElmer, Waltham, MA) were first subjected to 4 h and 24 h hypoxia. Immediately following hypoxia, but before drug treatment, cells were imaged in a CellVoyager™ CV7000 High-throughput Cytological Discovery System (Yokogawa Electric Corporation, Musashino, Tokyo, Japan) using a 20× objective. NRX and HC cells were then treated with MTAs using an automatic liquid handler (Echo 555; Labcyte, Sunnyvale, CA), and the imaging was continued for 24 h at an interval of 2 h in an atmosphere of 5% CO2/air/37ºC. Geminin-mAG (green) and Cdt1-mKO2 (red) fluorescent proteins were excited by 488 nm and 561 nm laser lines, and their emission signals were collected using 515/30 nm and 595/40 nm band pass filters, respectively. The exposure time for both channels was set to 500 ms. Captured images were exported to Columbus™ Image Analysis Software for analysis (version 2.7.1; PerkinElmer). The red and green channels were merged to create a third temporary channel, which was used in the next analysis step for determination of the segmentation of nuclei and measurement of mean fluorescence intensity of each channel separately within a selected object. To analyse the distribution of cell-cycle

phases, a scatter plot of mean fluorescent intensities of Cdt1-mKO2 (Red) was plotted against Gem-mAG (Green). The plot was then divided into three different areas, and the percentage of cells in each area was calculated. Following cell-cycle recording, phase selection criteria were applied: cells with mean fluorescent intensities in the red channel > 320 and green channel < 320 were assessed as G1-phase cells, G1/S-phase cells (red > 320 and green > 320) and S/G2/M-phase cells (red < 450 and green > 320). Cell roundness was calculated using the formula: $R = [area \times \pi \times (perimeter)2]/4$. Round cells were presumed to have an R = 1. Threshold compactness (TrCom), a measure of the multinucleation of cells, was calculated following the method described by P. Kask [187]. A low TrCom value indicates a multinucleated cell [187]. Phase contrast images were acquired by Zeiss Axio Observer 6.1 microscope.

Statistical analysis

All statistical analyses were carried out in GraphPad Prism, and results were considered significant at $p \leq 0.05$. Unless otherwise stated, data were analyzed by one-way ANOVA with Tukey's multiple comparison test, and are presented as the mean ± SEM.

Chemical Structures

The structures were created using ChemBioDraw v. 12 (Perkin-Elmer).

IV. RESULTS AND DISCUSSION

IV.a Peloruside A efficacy in hypoxia pre-exposed human colorectal carcinoma cells and comparison with clinically used microtubule targeting drugs paclitaxel and vincristine

Insufficient tumor vasculature and oxygen deprivation contribute to differential sensitivity of solid tumors to chemotherapy. Hypoxia alters cancer cell response to taxane-site-binding drugs (see chapter 2.1 Microtubule targeting agents above). However, the susceptibility of non-taxoid site ligands such as peloruside A (PELA) to hypoxia mediated alterations is unknown. In the present study, we compared the cytotoxic effects of PELA to the effects of paclitaxel (PTX) and vincristine (VCR) in colorectal HCT116 cancer cells under normoxic and hypoxic conditions.

Results

The initial experiments on HCT116 and HCT116 HIF-1α cells were conducted to assess response to hypoxia exposure. In normoxia, HCT116 HIF-1α cells show higher expression of HIF-1α subunit than HCT116 (Fig. 28A). Hypoxia exposure for 4 and 24 hours resulted in higher HIF-1α levels in both cell lines. Nevertheless HIF-1α total level was still higher in HCT116 HIF-1α. An immunofluorescence staining also revealed a higher accumulation of HIF-1α in the nucleus in hypoxia conditioned cells (Fig. 28B). Thus, 4 hour and 24 hour hypoxia exposure is capable of inducing cellular response to low oxygen condition. In addition, flow cytometry analysis indicated a slight increase in G1 phase population following 24 hour exposure to hypoxia (Fig. 28C).
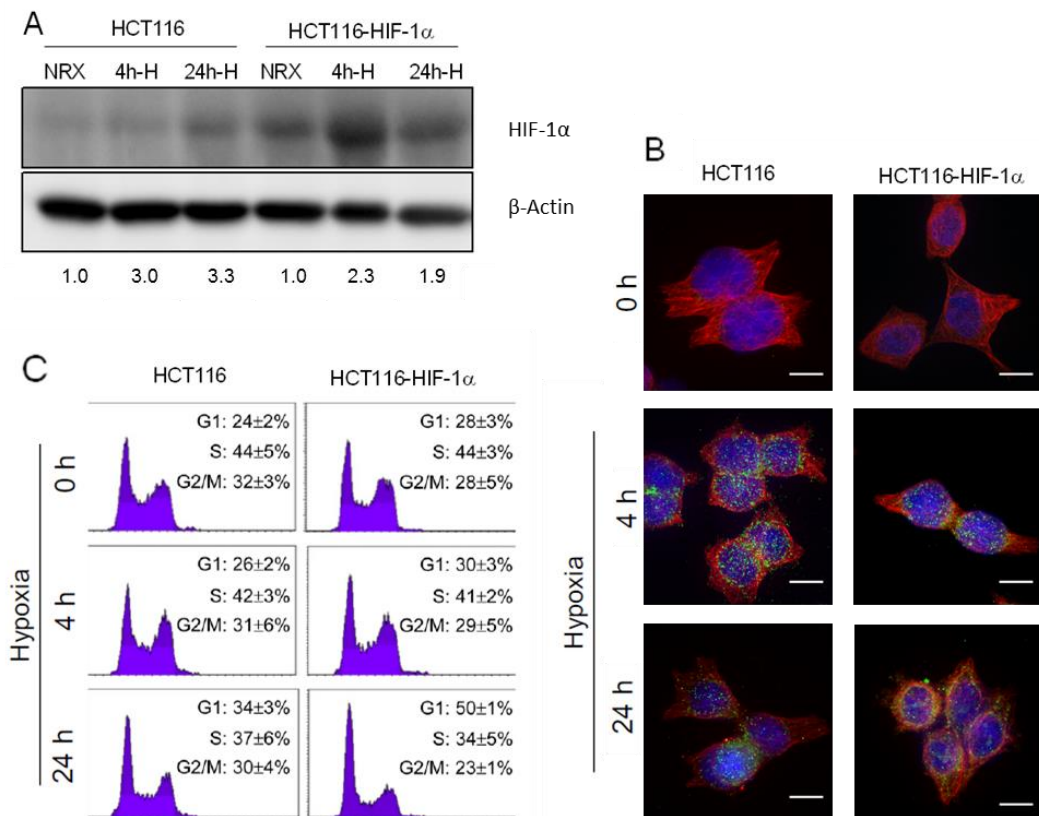
Figure 28. Induction of HIF-1α in cells exposed to hypoxic insult. Western blot showing the expression of HIF-1α in HCT116 cells and HCT116 transfected with HIF-1α following 4 h and 24 h hypoxia exposure. The calculated densities are relative to expression of normoxic cells (B) Cells were exposed to 4 h and 24 h and stained with DAPI (blue), and antibodies for HIF-1α (green) and α-tubulin (red). An increase in the accumulation of HIF-1α is seen in cells exposed to hypoxia for 4 h and 24 h. 100x objective, Scale bar – 10 μm. (C) Flow cytometry analysis of cells immediately following hypoxia show an increase in G1, and a decrease in S and G2/M cells in 24h-H-exposed cells.

To determine whether hypoxia affects sensitivity to PELA or clinically used MTAs, both cell lines were first exposed to hypoxia for 4 or 24 h and then treated with PELA, PTX or VCR in normoxia for 72 h. The MTT assay dose response curves showed that there was no difference in the cytotoxicity of PELA and VCR in hypoxia-preexposed cells (Fig. 29A, 29B). In contrast, 24-hour hypoxia pre-exposure significantly increased the resistance of HCT116 and HCT116 HIF-1α cells to PTX. Comparison of calculated IC_{50} values confirmed that PELA exerted an uniform cytotoxic effect, whereas hypoxia pre-conditioned HCT116 and HCT116 HIF-1α cells were less sensitive to PTX. The susceptibility to VCR was also significantly altered in 24-hour hypoxia conditioned HCT116 HIF-1α (Fig. 29C).
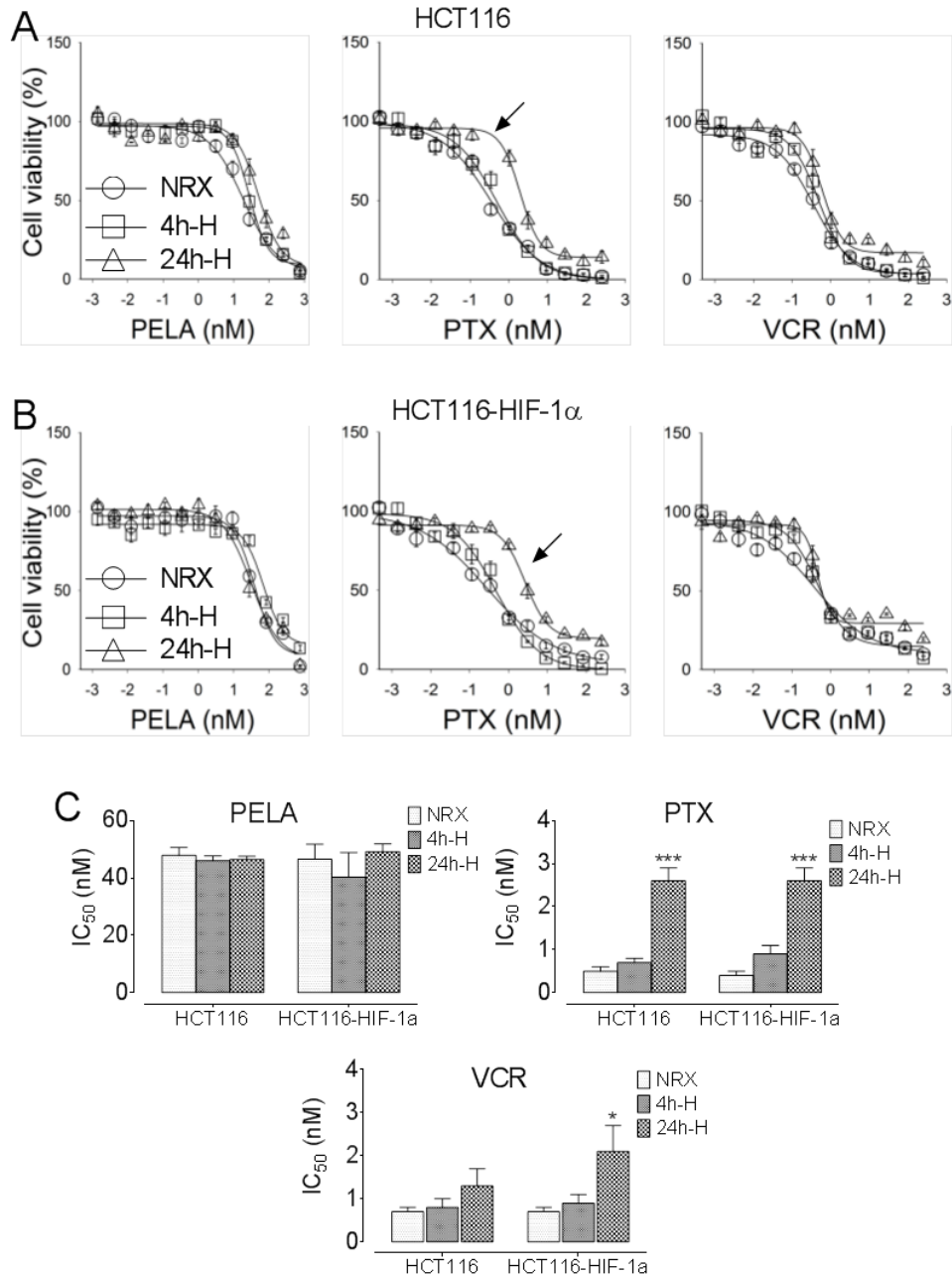
Figure 29. The effect of hypoxia pretreatment on cytotoxicity of PELA, PTX and VCR. (A, B) Dose-response curves of PELA, PTX and VCR in HCT116 (A) and HCT116-HIF-1α (B). Cells were treated with drugs in normoxia for 72 h, or first exposed to hypoxia for 4 h and 24 h, and then treated with MTAs in normoxia for 72 h. Arrows indicate a significant right-shift in dose-response curves of paclitaxel in cells exposed to 24 h hypoxia. (C) Bar graphs showing the averaged IC_{50} values of PELA, PTX and VCR in normoxic and hypoxia-pretreated cells are presented. Pre-exposing HCT116 and HCT116-HIF-1α cells to 24 h hypoxia increases their resistance to PTX compared to normoxic cells. VCR is significantly less cytotoxic only in HCT116-HIF-1α cells following 24 h hypoxia. *** $p < 0.001$, ** $p < 0.01$, * $p < 0.05$, n = 4-5, one-way ANOVA with Tukey's multiple comparison test.

69

Next, flow cytometry analysis was performed to examine if the reduced cytotoxicity is accompanied with lowered capability to promote mitotic arrest (Fig. 30).
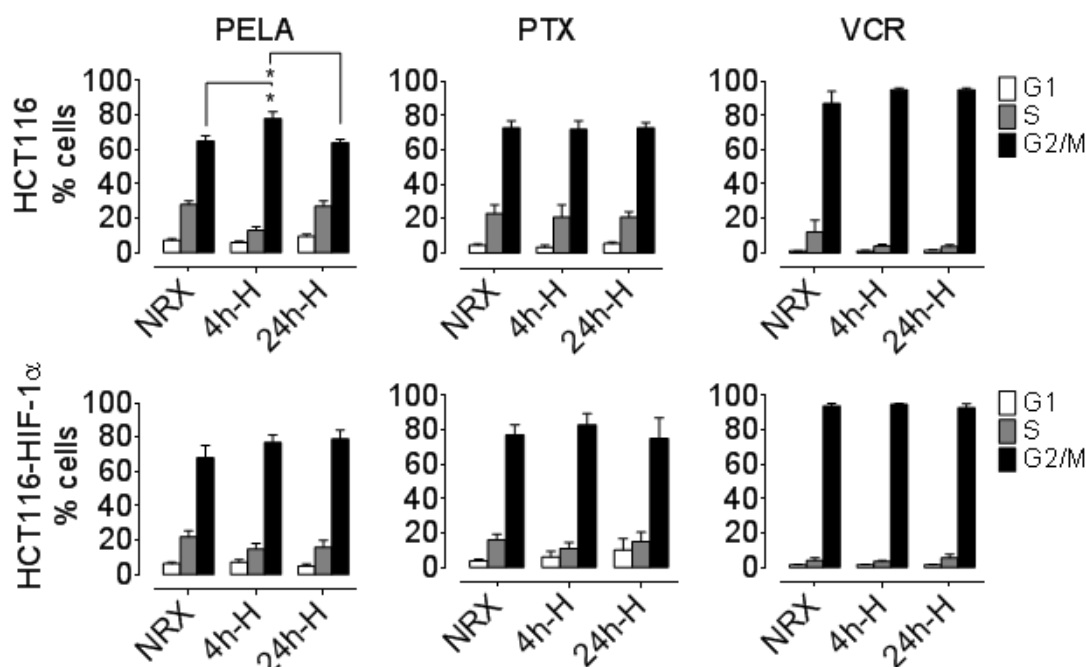
Figure 30. Modulation of the cell cycle by MTAs. Treatment with 200 nM PELA for 16 in normoxia results in significant increase in G2/M block in HCT116 pre-exposed to 4h-H. * $p < 0.05$, $n = 4$, one-way ANOVA with Tukey's multiple comparison test.

HCT116 and HCT116 HIF-1α were pre-conditioned and treated 16 hours with MTAs. Notably, 200 nM PELA, 20 nM PTX and 20 nM VCR caused more or less equal percentage of G2/M arrested cells. Therefore these concentrations were also used for following experiments. The potencies of PTX and VCR to induce G2/M phase block remained unaffected by hypoxic pre-exposure. 200 nM concentration of PELA induced G2/M arrest more potently in 4 hour pre-conditioned HCT116 cells than in cells without hypoxia pretreatment.

To gain further insight into PELA-induced G2M arrest in hypoxia-conditioned cells, changes in cell-cycle-associated proteins following drug treatment were examined. Hypoxia preconditioning resulted in downregulation of cyclin D1 and hypophosphorylation of retinoblastoma protein (Rb) in both parental and HIF-1α

cells (Fig.31).
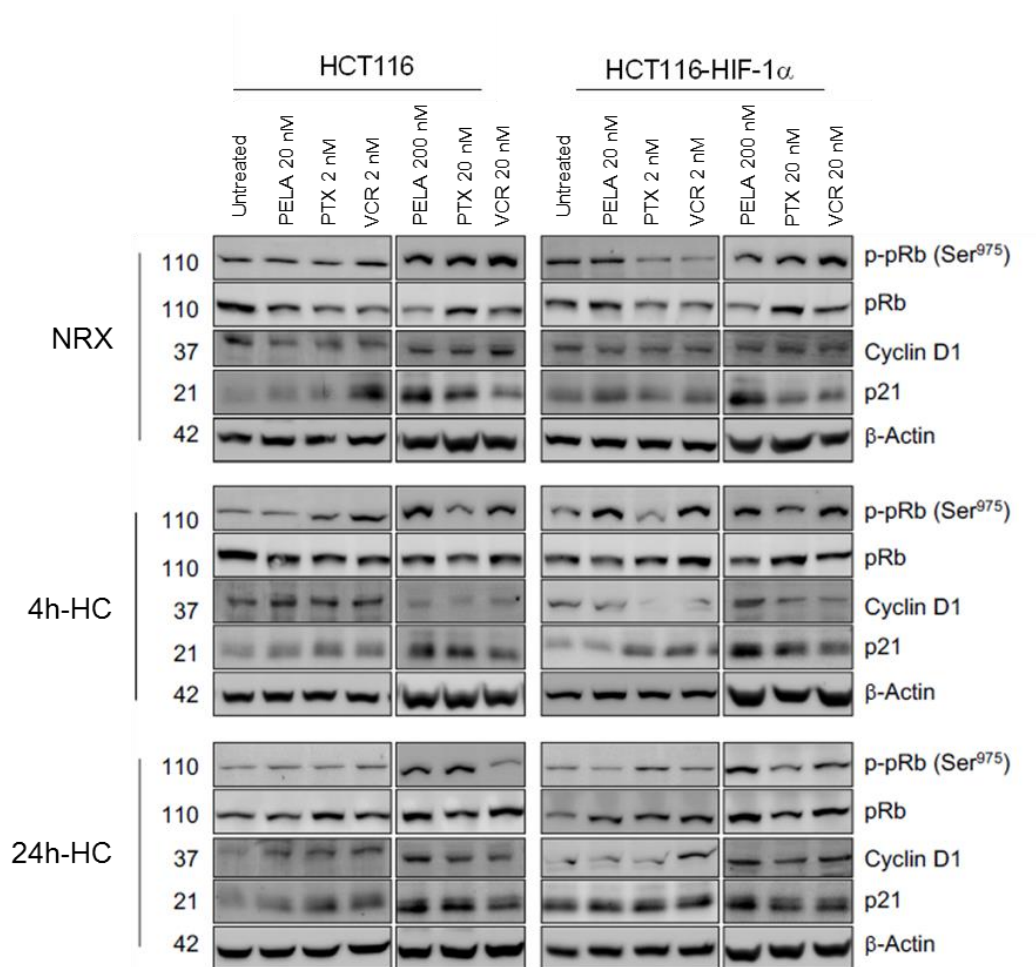
Figure 31. PELA effects expression of cell cycle-associated proteins in HCT116 and HCT116-HIF-1α cells.

Hypoxia pre-exposure for 4 h and 24 h resulted in hypophosphorylation of Rb at Ser795 in HCT116 and HCT116-HIF-1α cells. On the other hand, cyclin D1 expression was not modulated by overexpression of HIF-1α in normoxic conditions. PELA and PTX at 200 nM reversed Rb hypophosphorylation in hypoxia conditioned cells. VCR treatment did not affect Rb phosphorylation.

Treatment with MTAs resulted in an increase in cyclin B1 levels, which reflects the higher number of G2/M arrested cells. 24 hour hypoxia preconditioning reduced cyclin B1 expression, but PELA and other MTAs clearly abrogated this trend (Fig. 32). Hypoxia and MTAs induced expression of cyclin dependent kinase inhibitor p21, the effect was particularly apparent HIF-1α overexpressing cells.
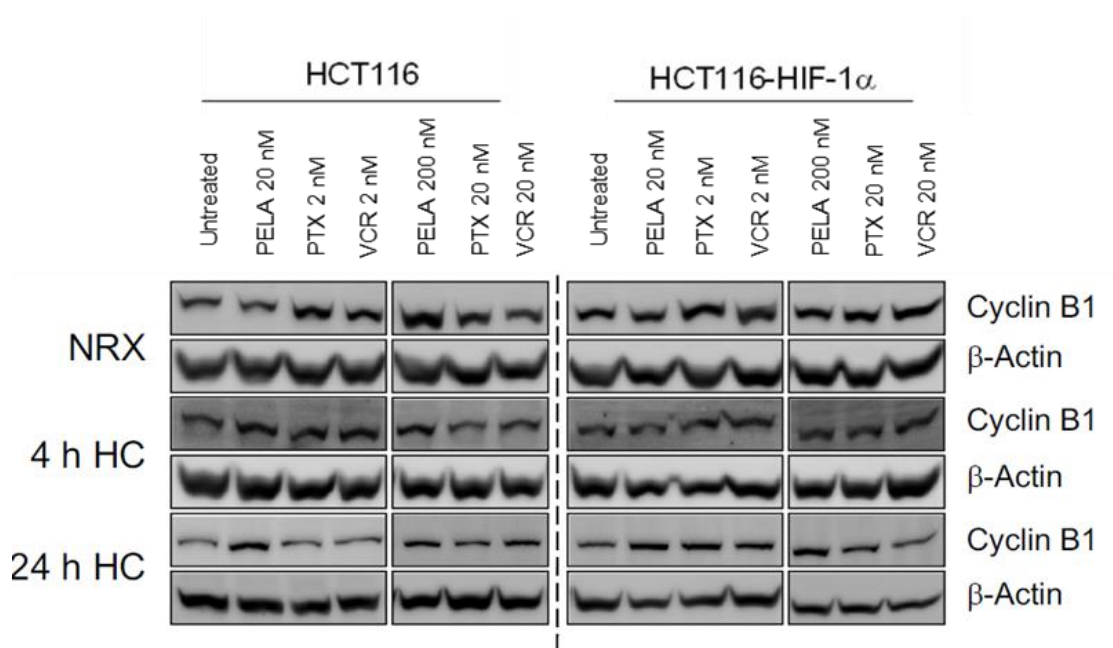
Figure 32. Cyclin B1 expression in HCT116 and HCT116-HIF-1α cells.

Next, to better understand the effects of PELA on cell cycle of hypoxia-pretreated cells at single cell level we utilized the HeLa-FUCCI model system. The system enables monitoring the cell cycle phases in real time. However, evidences indicate that certain MTAs induce abnormal fluorescence in HeLa-FUCCI cells, making it difficult to precisely distinguish cell-cycle changes [188]. We noticed a similar abnormal fluorescence and therefore, employed image analysis of cell rounding and TrCom to classify mitotic and multinucleated cells. PELA at 200 nM resulted in a significant increase in mitotic cell rounding in HeLa-FUCCI preincubated in hypoxia for 24 hours (Fig. 33A). Similarly to the flow cytometry data, PELA at 200 nM caused an increased MCR in 24 h hypoxia preconditioned HeLa-FUCCI cells (Fig. 33B). In contrast, pre-exposure negatively affected MCR after 2 nM PTX treatment when compared to NRX cells. There was no difference in the effect of VCR on MCR in NRX and HC cells.
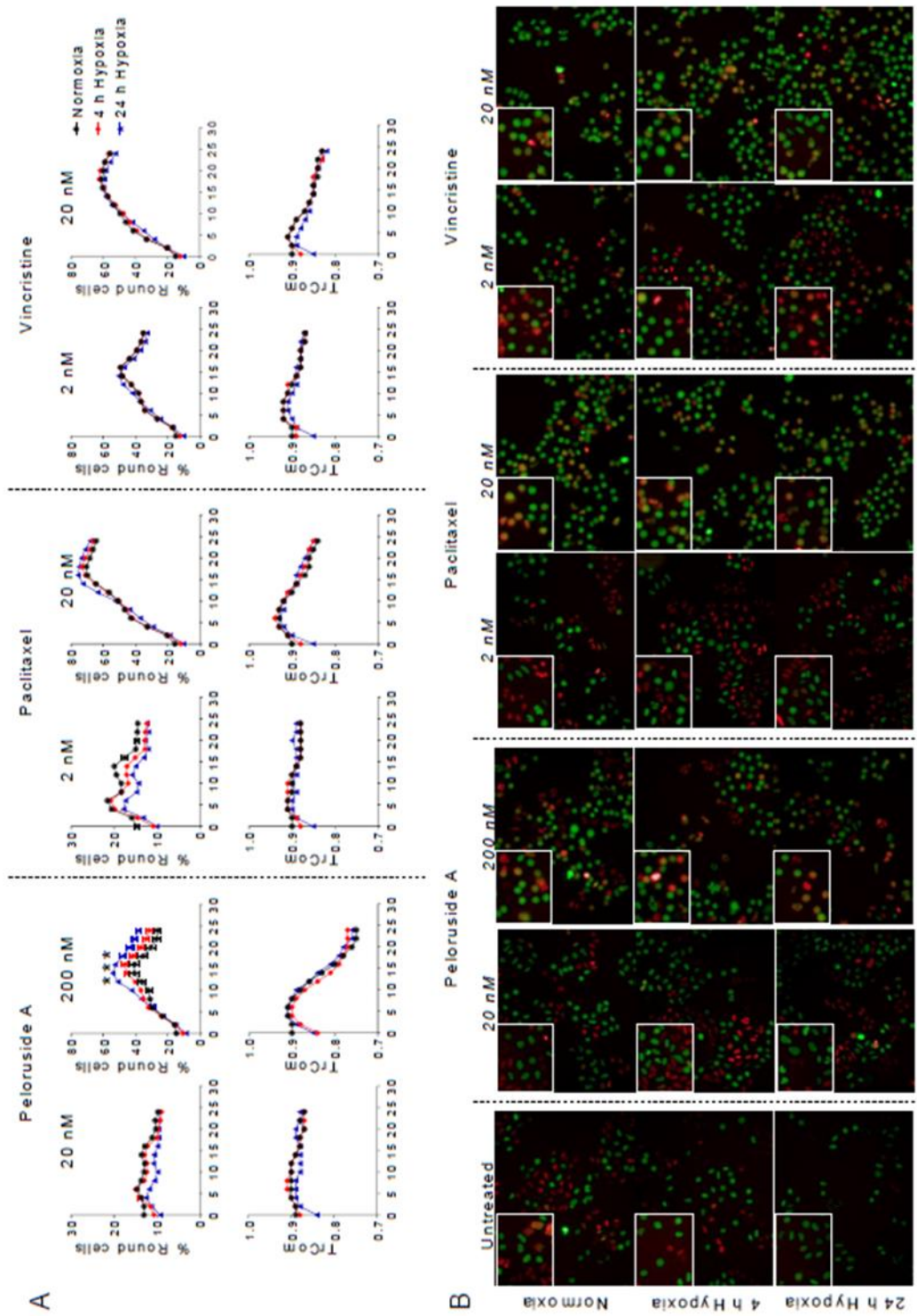
Figure 33. PELA alters the cell cycle of hypoxic cells. (A) Graphs showing mitotic cell rounding and TrCom following live-cell imaging of hypoxia-exposed HeLa-Fucci cells treated with MTA show an increase in cell rounding following 200 nM PELA treatment in 24h-H cells. There is no major difference in TrCom following PELA treatment of NRX and hypoxic cells. Each value represents mean ± SEM of 500-4000 analyzed cells. (B) Representative images of HeLa-Fucci cells after 16 h incubation with indicated concentrations of PELA, PTX and VCR are shown.

To exclude the contribution of apoptosis to observed cell rounding, HeLa-FUCCI cells were subjected to simultaneous treatment with MTAs and a pan-caspase inhibitor Z-VAD-FMK with 2-hour preincubation (Fig. 34). PELA and other MTAs induced cell rounding even in the presence of caspase inhibitor, indicating specificty of mitotic rounding.
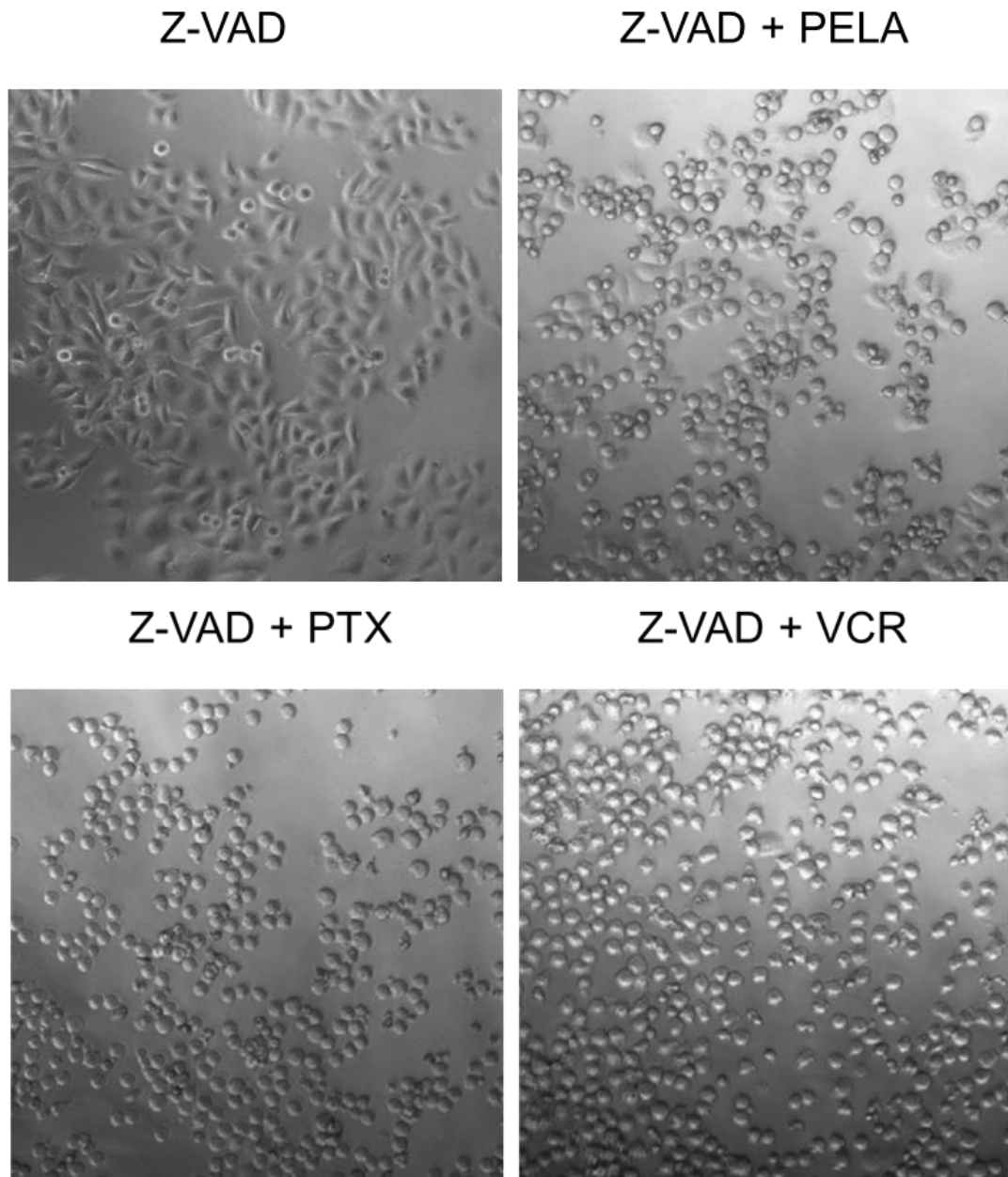
Figure 34. Pre-treatment of HeLa-FUCCI cells with 50 μM Z-VAD-FMK for 2 h and 16 hour simultaneous treatment with Z-VAD-FMK and 200 nM PELA, 20 nM PTX or 20 nM VCR did not inhibit MTA-mediated MCR. 10× objective.

To examine the effects of PELA-induced stabilization of MTs, cells after 4h-H and 24h-H were analyzed for changes in the expression of acetylated α-tubulin following treatment for 16 h (Fig. 35). There was a dose-dependent increase of tubulin acetylation following PELA and PTX treatment. Whereas PELA and PTX at 20 nM induced a comparable level of acetylation in HCT116 cells, 4 hour hypoxia prevented PTX-mediated tubulin acetylation. Acetylated tubulin level remained unaffected by vincristine treatment.
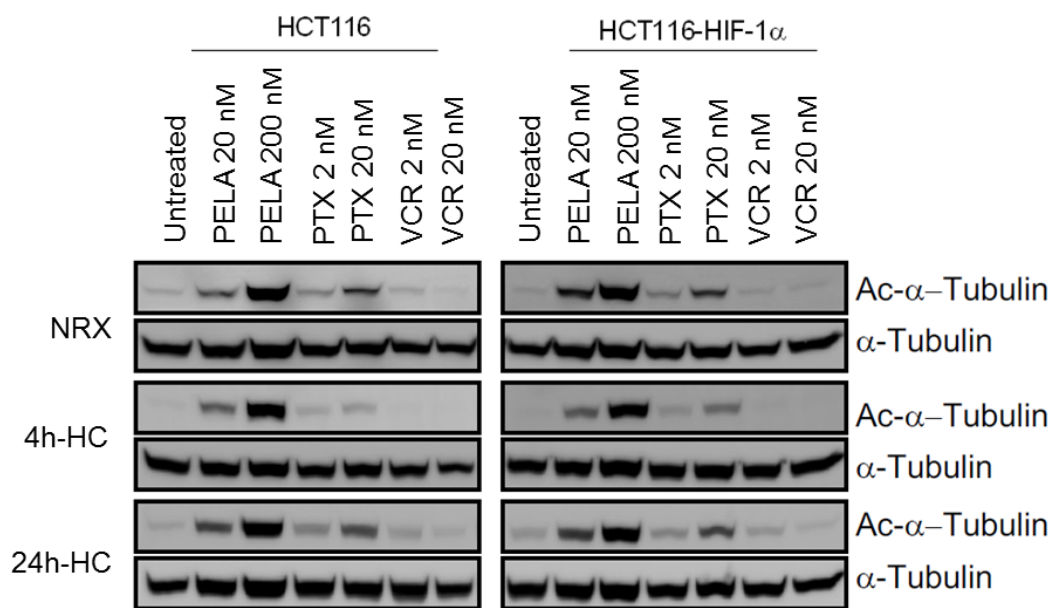
Figure 35. PELA-induced stabilization and polymerization of tubulin remains unaffected in hypoxia-exposed cells. Representative blots of Ac-tubulin in normoxia and hypoxia-subjected HCT116 and HCT116-HIF-1α cells following PELA, PTX and VCR treatment are shown.

Because hypoxia is known to modulate intracellular tubulin polymerization, it was of particular interest to determine the level of PELA-stabilized microtubules. Incubation of cells for 4 and 24 hours in hypoxia led to a lower level of polymerized tubulin, the effect was even more significant in HCT116 HIF-1α cells. While 200 nM PELA and 20 nM PTX polymerized comparable amounts of tubulin in NRX cells, the same concentration of PTX was less efficient in cells exposed to 4h-H (Fig. 36). Furthermore, PELA ability to promote tubulin polymerization in normoxia was unaffected by HIF-1α overexpression. On the contrary, HIF-1α overexpression significantly reduced the sensitivity of HIF-1α cells to PTX. VCR-treated cells

showed consistently high level of soluble tubulin of approximately 90% (data not shown).
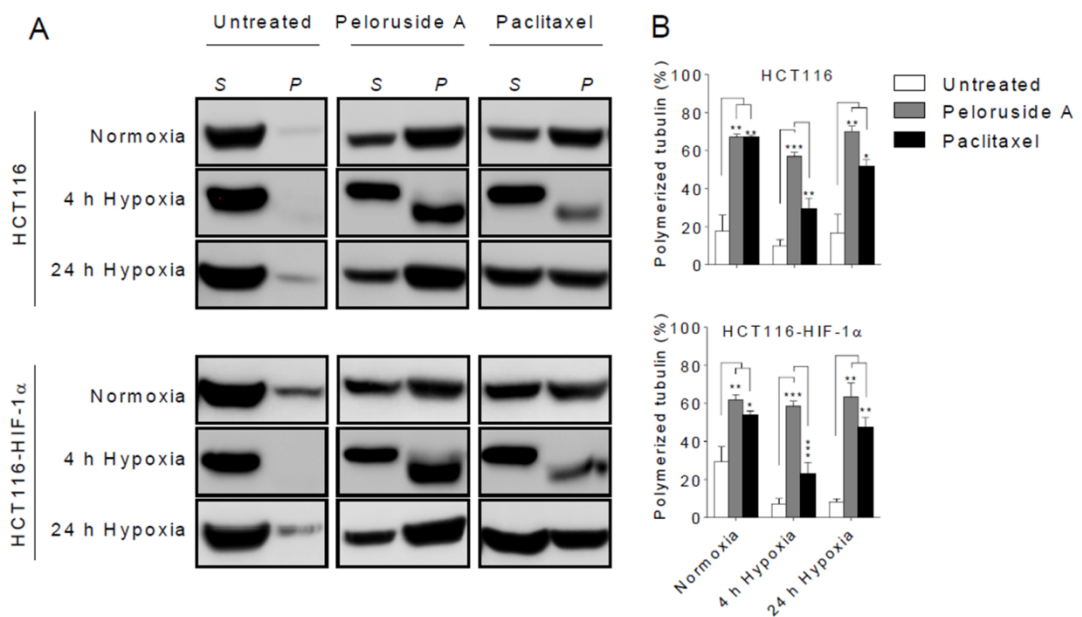
Figure 36. PELA-induced stabilization and polymerization of tubulin remains unaffected in hypoxia-exposed cells. (A) Representative blots of soluble (S) and polymerized (P) tubulin following treatment with PELA and PTX in NRX and hypoxia-exposed are presented. (B) There is no effect of hypoxia on PELA-induced polymerization of tubulin; however, 4h-H significantly affected tubulin polymerization in HCT116 and HCT116-HIF-1α cells following PTX treatment. *** $p < 0.001$, ** $p < 0.01$, * $p < 0.05$, one-way ANOVA with Tukey's multiple comparison test, n = 4-5. (E) Under NRX conditions, HCT116-HIF-1α cells are significantly more resistant to PTX-induced polymerization than HCT116 cells. **$p < 0.01$, n = 3-4, Student t-test, unpaired.

Analysis of DNA fragmentation indicated no cytotoxic effect on cells cultivated in hypoxia for 4 and 24 hours (Fig. 37). On the other hand, hypoxia affected cytotoxic activity of PTX. There was significantly less apoptosis following PTX treatment of hypoxia-conditioned parental and HIF-1α cells. There was no effect of hypoxia on PELA- and VCR-induced apoptosis.
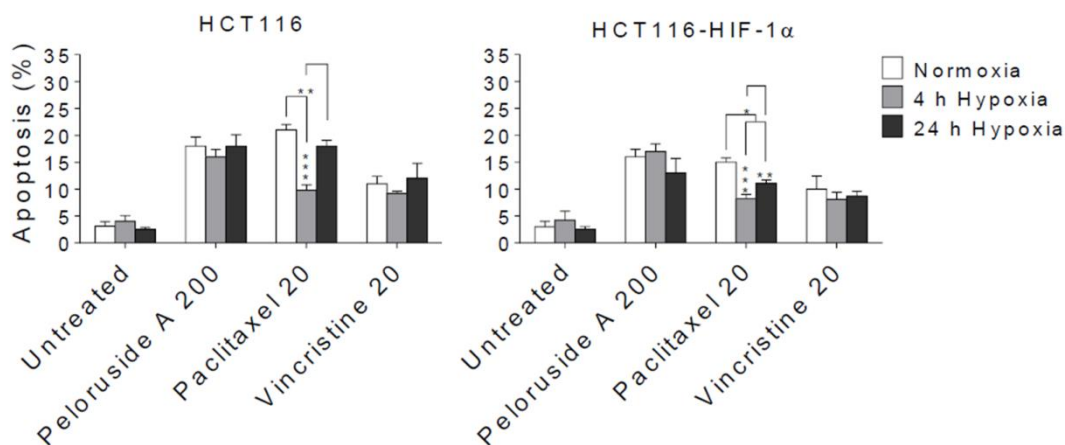
Figure 37. Apoptosis in hypoxia preconditioned cells following treatment with MTAs. Flow cytometry analysis indicates a significant decrease in PTX- but not PELA- and VCR-mediated apoptosis of parental and HIF-1α cells pre-exposed to hypoxia. * p < 0.05 compared to NRX cells, *n* = 3-4.

To determine if hypoxia altered apoptosis of cells following PELA treatment, we examined the changes in the activation of apoptosis-associated caspase 3 and 8 proteins by western blot. PELA at 200 nM resulted in the cleavage of caspase 3 and 8 both in NRX and hypoxia pretreated cells, indicating that hypoxia did not alter PELA-induced cell apoptosis (Fig. 38). However, hypoxia affected the activation of caspase 3 following PTX but not VCR treatment. Lower concentrations of MTAs did not result in the activation of caspases both in NRX and hypoxic cells. Hypoxia by itself did not induce apoptosis in the untreated cells.
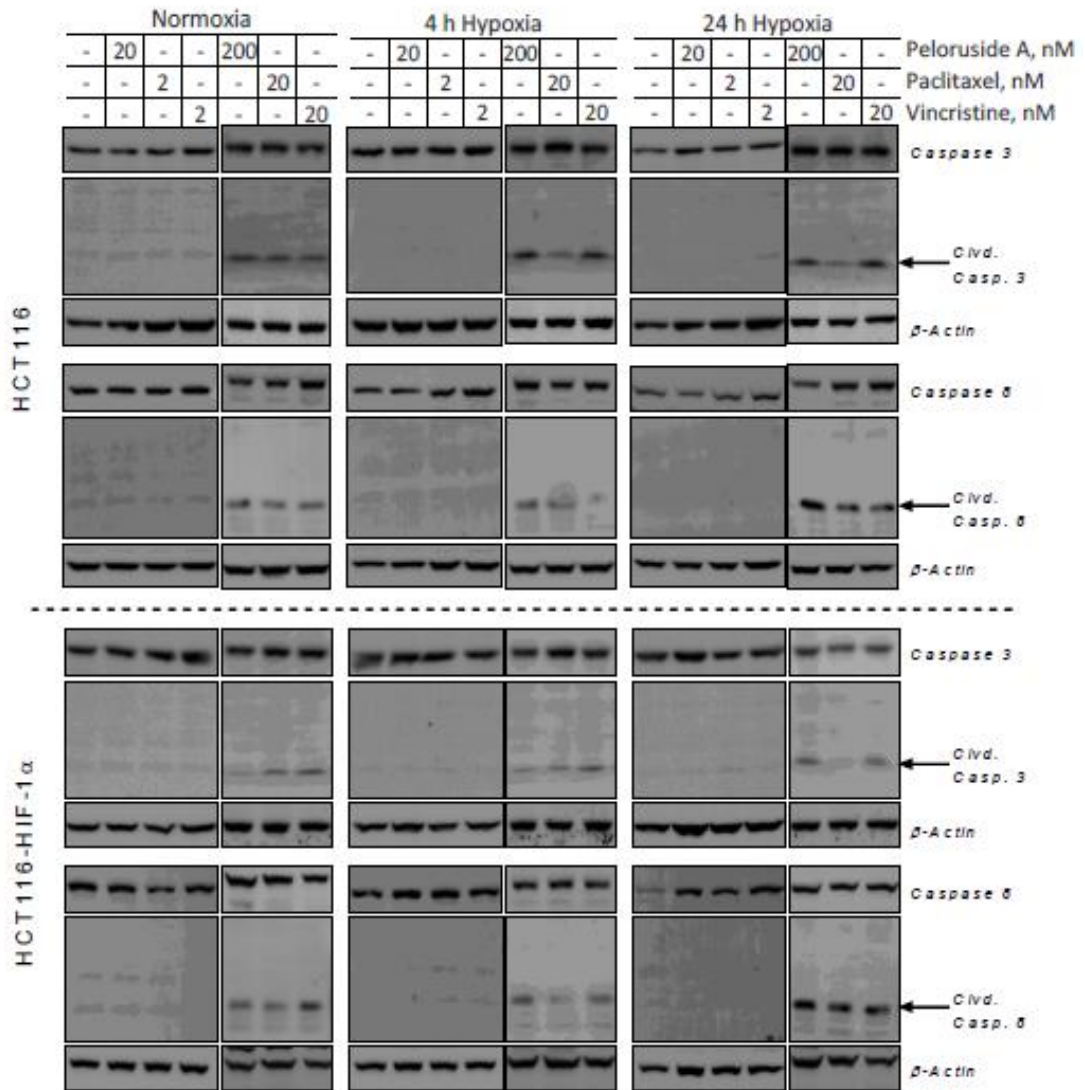
Figure 38. Caspase cleavage in HCT116 HC cells following PELA treatment.
NRX and HC cells were treated with PELA, PTX and VCR for 16 h and cleavage of caspase-8 and -3 were analyzed by western blot. Arrows indicate the cleaved caspase bands. Caspase 8 and 3 blots are from different gels. n = 3.

Discussion

Microtubule targeting agents constitute an important class of drugs widely used in cancer therapy. Microtubule stabilizing drugs such as paclitaxel and other taxanes have a critical role in cancer treatment and management. However, their activity is often lowered by hypoxia-associated alterations in solid tumors [103]. Recently, several studies demonstrated extraordinary properties of peloruside A (PELA), a non-taxoid-site microtubule-stabilizing agent isolated from marine sponge *Mycale hentscheli* [109], [189]. Nevertheless, the impact of hypoxia on PELA efficacy has not yet been revealed. Although complex rearrangements induced by hypoxia *in vivo* cannot be perfectly simulated in 2D culture, hypoxia-conditioning is often used to provide evidence for differential sensitivity in conditions more resembling the situation in solid tumors [135]. The level of HIF-1α have significant impact on the sensitivity of cancer cells to paclitaxel [133]. Therefore we compared the cytotoxic effects of PELA to the known effects of PTX in colorectal HCT116 cancer cells under normoxic and hypoxic conditions. Our data show that hypoxia pre-exposure does not alter the susceptibility of parental and HIF-1α-expressing HCT116 cells to PELA. In agreement with previous studies, hypoxia significantly decreases cytotoxicity of PTX [132,190,191]. Therefore, hypoxia abrogates PTX-mediated stabilization of microtubules, most likely by alterations in the expression of microtubule associated proteins, which could also contribute to MTA resistance [192]. The differential effect of PELA and PTX on cell cycle could be caused by the different concentration of each drug. However, PELA at 200 nM and PTX at 20 nM induce the comparable amount of polymerized tubulin in normoxia. On the other hand, treatment with 20 nM PELA and 20 nM PTX resulted in equal level of tubulin acetylation. In contrast to previously published study [193], we did not observe a significant effect of hypoxia on the G2/M arrest of hypoxia-conditioned cells following PTX treatment. This difference is probably caused by the different method of cell pretreatment. We first exposed the cells to hypoxia and then treated them with MTAs in normoxia for an additional 16 h which apparently resulted in the degradation of the majority of HIF-1α in untreated cells. However, preconditioned cells display prolonged response to hypoxia, which is demonstrated by hypophosphorylated Rb and decreased levels of cyclin D1 in cells transferred to normoxia for 16 hours. Therefore, hypoxia has long-lasting effects on molecular

signaling in cancer cells. The downregulation of cyclin D1 and Rb hypophosphorylation is probably result of p21 activation in hypoxic condition. Unsurprisingly, PELA treatment led to the mitotic arrest and a high percentage of cells in G2/M phase. Low concentration 40 nM PELA was reported to interfere with the formation of kinetochore-microtubule attachment and induce aneuploidy. Interestingly, low PELA doses increase the frequency of pseudo-metaphase cells, which are not detected by the spindle assembly checkpoint [189]. Abnormal mitosis and mitotic slippage have been reported to enhance the cytotoxicity of PTX through p53-mediated apoptosis in different cancer cell types. The induction of apoptosis upon multinucleation and post-slippage DNA damage significantly contributes to PTX cytotoxicity [194]. Our data demonstrate that PELA induces caspase-dependent apoptosis accompanied by DNA fragmentation in both parental and HIF-1α-expressing cells. The obtained results indicate that PELA-induced alterations in microtubule dynamics promote cell cycle arrest and apoptosis regardless of hypoxia pretreatment *in vitro*. Thus, PELA activity is worthy of further investigation in a physiologically relevant model of a solid tumor.

IV.b Cell cycle modulatory properties of novel betulinic acid analogues with unknown mode of action

The aim of the study was biological characterization of novel fluoroderivatives synthesized at colaborating chemistry departments. A set of dihydrobetulinic acid derivatives containing highly electronegative 2,2-difluoro moiety or their intermediates was tested against cancer cell lines to prove the hypothesis, that electronegative moiety at C2 position increases anticancer activity. This tendency was observed in previous study of dihydrobetulonic acid with bromine substituents [195]. The impact of novel fluorderivatives on cancer cell cycle was of particular interest, because fluorine introduction is known to alter molecular recognition and may completely change the mode of action. The collected data from chemistry and biological part were published [182]. Study on triterpenoid thiazoles [183] provided oportunity to prove, if the electronegative substituent increases cytotoxicity of other triterpenoid scaffolds such as oleanonic acid, methyl oleanonate and methyl betulonate. In addition, the potential mode of action of novel oleanonic acid thiocyanate will be discussed with respect to original unpublished data of G2/M arrest inducing triterpene XXVII. Therefore the data indicative of XXVII inhibitory effect on proteasome are shown in results. Synthesis and anticancer activity of XXVII were described previously [184], [185].

Results

In vitro cytotoxic activity of triterpenoid derivatives was tested against CCRF-CEM T-lymphoblastic leukemia cells (Table 6). The most active compounds of the tested set were 2,2-difluorodihydrobetulonic acid X, that is structurally related to 2,2-dibromodihydrobetulonic acid I, and methyl betulonate derivative XXIVb. Other active compounds with an IC_{50} value up to 10 micromolar concentration were almost exclusively acids with a free carboxyl group in C-28 position. With the exception of XXIVb, methylesters showed generally lower cytotoxic activity in comparison with free acids. Dihydrobetulinic acid derivatives modified with acetyl or benzyl group at C-28 IV, VI were less active than unsubstituted dihydrobetulinic acid V. Introduction of fluorine atoms to position 2 significantly increased the cytotoxicity as apparent from comparison of corresponding pairs of dihydrobetulinic acid V (IC_{50} = 9.2 μM) and 2,2-difluorodihydrobetulinic acid XII (IC_{50} = 4.0 μM) or benzyl dihydrobetulinate VI (IC_{50} = 69.4 μM) and 2,2-difluorodihydrobetulinate XI (IC_{50} = 13.4 μM) (Fig. 39, Table 6). Interestingly, the data indicate that difluoro moiety can counteract the unfavourable effect of benzyl moiety. 2-bromo moiety of XXIIIb, XXIVb and XXVIb imparts cytotoxic activity in a similar manner as 2,2-difluoro substitution and significantly improved the activity of previously inactive allobetulon XXIIIa, methyl betulonate XXIVa and less active oleanonic acid XXVIa. Thus bromine introduction had a striking impact since allobetulon analogues are frequently inactive. 2-thiocyanate substituted compounds XXIVc and XXVIc followed the same trend, however they were less cytotoxic than bromine containing derivatives. The general trend of slightly higher cytotoxicity of 3-oxoderivatives than 3-hydroxyderivatives is evidenced by comparison of X with XII (Fig. 39). Hemiesters XVI, XVII, XVIII and XIX (Fig. 40) show comparable activity with 3-hydroxylated 2,2-difluorodihydrobetulinic acid XII (Fig. 39). Difluoroallobetulin hemiesters XX, XXI and XXII were much less active than those made from 2,2-difluorobetulinic acid, however, they were more active than 2,2-difluoroallobetulins XIV and XV (Table. 6).

Table 6. Cytotoxic activity against CCRF-CEM lymphoblastic leukemia cell line presented as IC$_{50}$ concentrations. The standard deviation is typically up to 10% of the average value.

Compound	IC$_{50}$ (µM)
I	1.0
II	250.0
III	250.0
IV	14.1
V	5.2
VI	69.4
VII	68.3
VIII	15.6
IX	69.8
X	2.4
XI	13.4
XII	4.0
XIII	250.0
XIV	250.0
XV	250.0
XVI	4.2
XVII	8.3
XVIII	4.9
XIX	4.5
XX	23.5
XXI	102.0
XXII	127.0
XXIIIa	>50.0
XXIIIb	5.2
XXIIIc	43
XXIVa	>50.0
XXIVb	2.9
XXIVc	10.8
XXVa	>50.0
XXVb	14.0
XXVc	29.0
XXVIa	15.1
XXVIb	4.5
XXVIc	6.4
XXVII	7.2
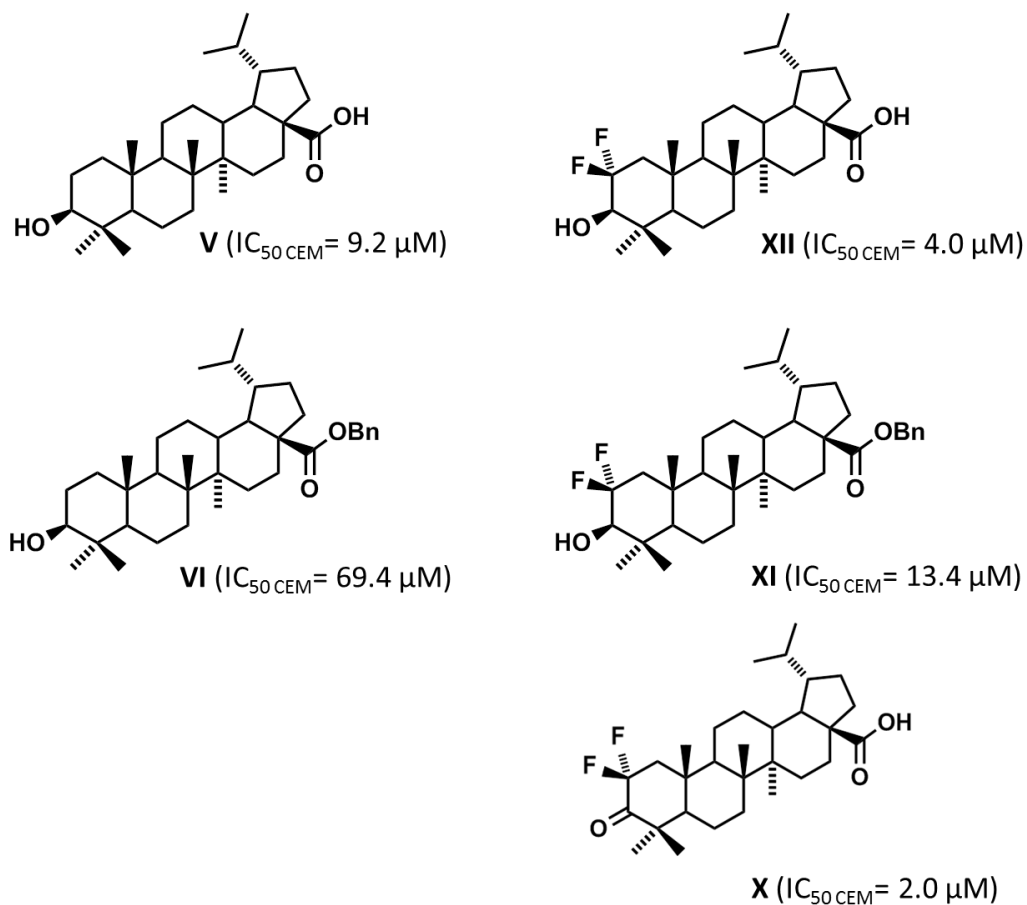
Figure 39. Effect of fluorine substituents on cytotoxicity. CCRF-CEM IC_{50} values are shown to demonstrate improved cytotoxicity.
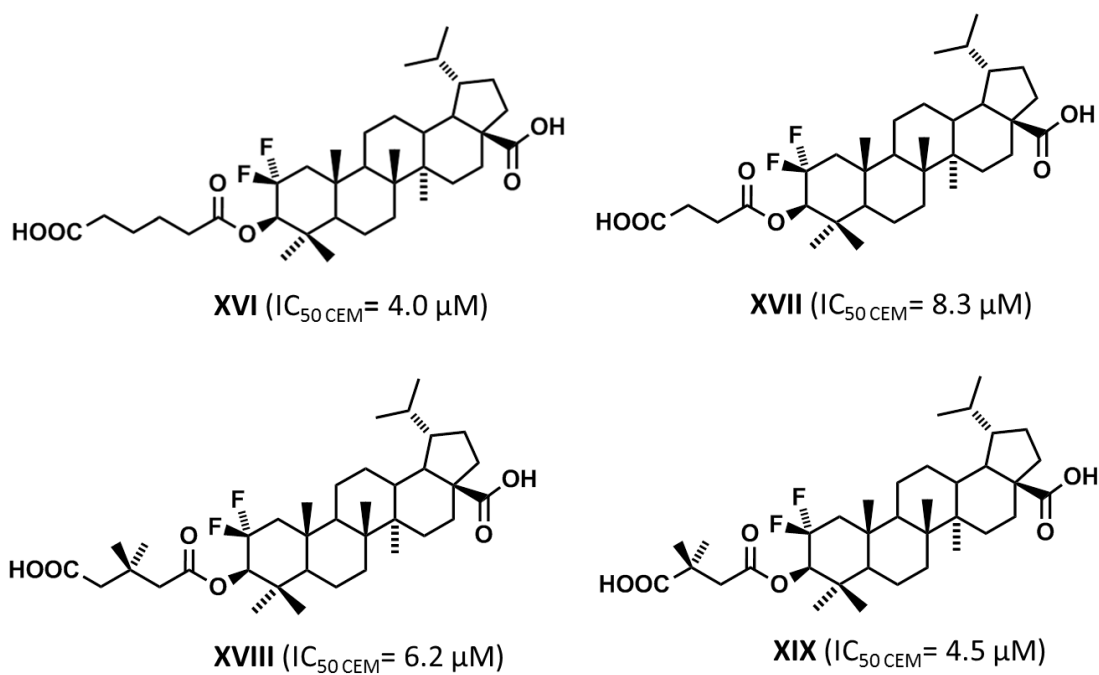
Figure 40. Effect of hemiester side chain on cytotoxicity.

The cytotoxic activity of the most active derivatives were further tested on six cancer cell lines of different histogenetic origin and on two types of normal human fibroblasts BJ and MRC-5 (Table 7). The cancer cell lines were derived from T-lymphoblastic leukemia CCRF-CEM, chronic myelogenous leukemia K562 and colon carcinoma (HCT116, HCT116p53-/-). Sublines with multi-drug resistance (MDR) phenotype CCRF-CEM-DNR-bulk and K562-Tax (in the table CEM-DNR, K562-TAX) were employed to predict possible effect of MDR. The IC_{50} value of tested compounds was in low micromolar range at most of the cancer cell lines. Compounds I and X showed the highest cytotoxicity, however they displayed toxicity against normal human fibroblasts as well as other compounds. HCT116 p53 status had low or no impact on the susceptibility of HCT116 to tested compounds.

With the exception of V and X, the compounds show slightly lower activity against daunorubicin resistant CCRF-CEM-DNR-bulk cell line. On the other hand, compounds show highly comparable activity in K562 and K562-Tax.

Table 7. Cytotoxic activities of selected compounds on tumor and normal cell lines. CCRF-CEM IC_{50} values are shown for comparison with its resistant subline.

Compound	Cell line							
	CEM	CEM-DNR	K562	K562-TAX	HCT116	HCT116p53$^{-/-}$	BJ	MRC-5
I	1.0	7.0	0.9	1.1	2.4	2.6	13.3	8.0
V	5.2	5.5	3.7	4.8	15.1	4.6	24.7	12.8
X	2.4	6.2	2.6	2.3	4.4	4.7	15.4	9.1
XII	4	10.9	5.5	4.1	7.3	5.8	18.7	14.7
XVI	4.1	14.7	6.5	5.8	6.1	5.9	34.7	29.2
XVII	8.3	24.4	18.3	19.8	14.8	8.6	76.6	27.9
XVIII	6.2	15.7	12.9	16	14.2	7.1	39.6	14.7
XIX	4.5	11.4	11.8	11.5	8.5	3.7	26	12.8
XXIIIb	5.2	>50.0	11.7	7.5	21.5	22.8	>50.0	>50.0
XXIVb	2.9	15	9	11	14.9	12.4	22.9	26.3
XXIVc	10.8	>50.0	15.5	>50.0	34.6	29.9	32.3	36.1
XXVIb	4.5	14.8	2.1	13.5	4.1	8.2	27.7	20.0
XXVIc	6.4	31.1	28.6	>50.0	23.6	16.3	>50.0	48.0

Next, flow cytometry methods were employed to further characterize the anti-tumor properties of the active compounds. The influence on the cell cycle of CCRF-CEM cells was analyzed after the 24 hour treatment with $1\times$ and $5\times IC_{50}$ concentration (Table 8).

Table 8. Cell cycle phase distribution in the entire cell population(%). Cell cycle data of XXVII with $IC_{50\ CEM}$ value 7.2 µM are adapted from [185].

Used concentration (IC_50)		Sub G1 (%)	G0/G1 (%)	S (%)	G2/M (%)	pH3^Ser10 (%)	BrdU positive cells (%)	BrU positive cells (%)
Control	0	3.4	41.6	44.2	14.2	1.6	58.8	48.8
I	1x	4.8	37.6	51.0	11.4	NA	64.4	52.5
	5x	26.2	33.2	52.9	13.9	NA	45.1	39.6
V	1x	5.3	34.4	51.4	14.2	NA	64.5	46.7
	5x	5.3	28.8	62.3	9.0	NA	55.6	33.0
X	1x	2.9	39.4	47.6	13.1	NA	NA	NA
	5x	1.3	39.1	39.7	21.2	NA	NA	NA
XII	1x	2.5	39.7	50.2	10.2	NA	61.4	35.6
	5x	8.5	31.6	57.5	11.0	NA	34.8	1.7
XVI	1x	3.0	45.6	43.9	10.5	NA	60.0	39.4
	5x	2.3	44.2	39.4	16.4	NA	41.3	30.1
XVII	1x	3.0	46.2	44.2	9.6	NA	NA	NA
	5x	3.3	43.2	36.9	20.0	NA	NA	NA
XVIII	1x	1.9	42.8	46.8	10.4	NA	NA	NA
	5x	2.7	42.6	41.6	15.8	NA	NA	NA
XIX	1x	2.8	44.4	44.6	11.1	NA	NA	NA
	5x	3.7	40.1	40.0	19.9	NA	NA	NA
XXIIIb	1x	5.8	44.8	41.0	14.3	1.0	52.2	41.4
	5x	43.6	44.3	37.9	17.8	1.7	37.2	31.8
XXIVb	1x	7.8	40.2	38.2	21.5	2.8	26.0	49.3
	5x	32.5	45.6	31.1	23.4	2.4	13.3	1.4
XXIVc	1x	3.4	36.1	47.9	15.9	2.1	41.1	47.5
	5x	58.5	30.9	41.3	27.8	1.0	13.8	1.0
XXVIb	1x	6.0	42.7	42.5	14.8	1.1	61.7	53.5
	5x	57.7	45.4	39.9	14.7	1.6	36.2	24.6
XXVIc	1x	41.6	56.9	22.8	20.4	1.1	10.5	5.4
	5x	83.1	34.9	25.3	39.8	0.3	2.9	0.6
XXVII	1x	8.0	10.7	49.0	40.3	4.9	NA	NA
	5x	40.4	13.4	59.6	27.0	3.7	NA	NA

Treatment with compounds I, V and XII at $5\times IC_{50}$ caused a shift in cell cycle from G1 to S phase. A lower percentage of G1 cells can be associated with lower proliferation rate as apparent from reduced level of BrdU incorporating cells. In addition, an increase in S phase indicates that compounds disturb S phase progression, most likely by the non-specific mechanism. Compound XII completely inhibited synthesis of cellular RNA transcripts, which suggest massive interference with cellular processes. The level of BrU incorporation was less affected by $5\times IC_{50}$

concentrations of other compounds. Compound XVI had no direct impact on cell cycle with the exception of reduced BrdU and BrU incorporation into DNA and RNA, respectively.

Cell cycle profile analysis revealed G2/M arrest after treatment of CCRF-CEM cells with XXIVb, XXIVc and XXVIc that was most pronounced effect among tested derivatives, compounds X, XVII and XIX displayed weaker effect. The results could be in some cases of $5 \times IC_{50}$ dose, however, affected by high DNA fragmentation. Nevertheless, the sub-G1 population in the majority of analyzed cells was below 10 %. Phosphorylation of histone H3 at Ser10 as a mitotic marker did not indicate cell cycle arrest in M-phase after treatment with XXIVb, XXIVc and XXVIc. Thus XXIVb, XXIVc and XXVIc arrest cell cycle progression most probably in G2 or during the transition to M phase by an unknown mechanism that remains to be solved.

According to our experience, triterpene derivatives induce G2/M phase block rather rarely. The analogous question was resolved during the previous original unpublished study of C-30 modified betulinic acid analogue XXVII that induced G2/M phase block of the cell cycle (40.3 %). The level of phospho H3 at Ser10 induced by XXVII was, however, higher (4-5 %) than of XXVIc (1.1 %).

A detailed study revealed interference with ubiquitin-proteasome system as visible from Proteasome Sensor accumulation (Fig. 41A). The inhibition is, however, in much higher concentrations in comparison with specific proteasome inhibitor bortezomib. Ubiquitin is predominantly bound to histones and upon treatment with betulinic acid derivative, ubiquitin bound proteins were translocated from the nucleus and accumulated in the cytoplasm in a similar manner as after treatment with specific proteasomal inhibitor bortezomib (Fig. 41B). Western blot of ubiquitinylated proteins showed dose-dependent accumulation of ubiquitin-bound proteins (Fig. 41C, D). Nevertheless, the concentration of bortezomib sufficient to promote the same effect was more than 2 orders of magnitude lower.
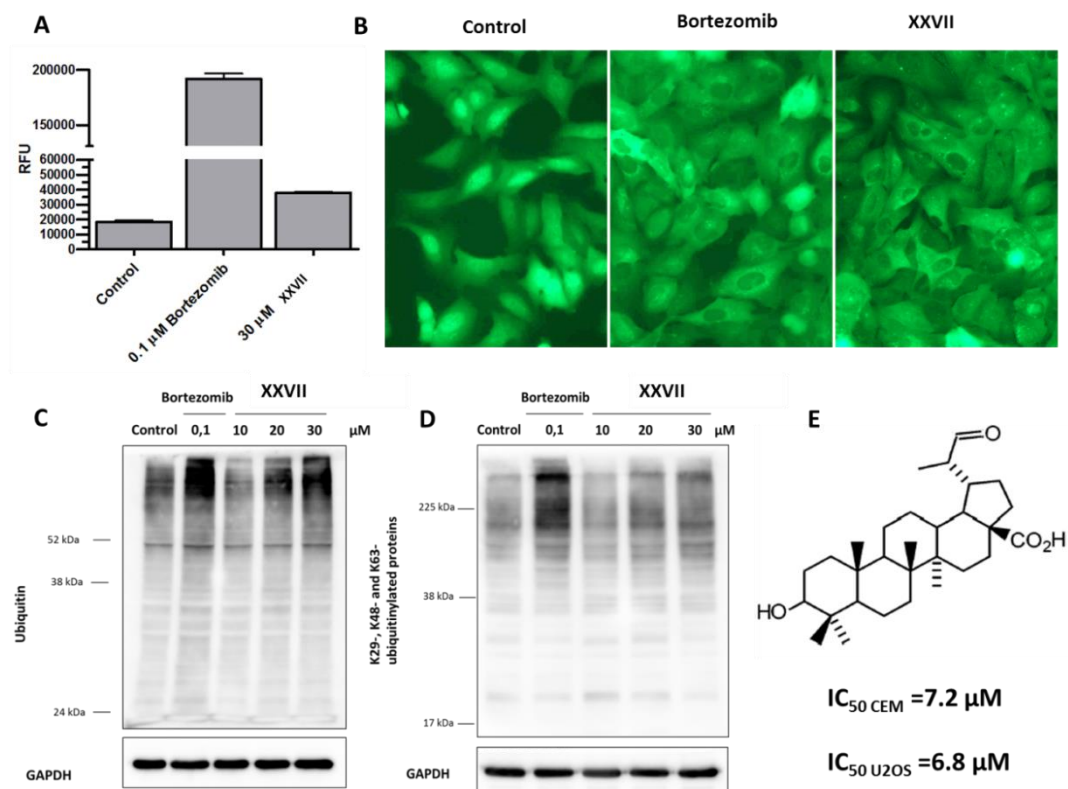
Figure 41. XXVII inhibits proteasome-mediated degradation of ubiquitinylated proteins. (A) Accumulation of fluorescent proteasomal substrate Proteasome Sensor in U2OS cells after 20-hour treatment with indicated compounds. (B) Nucleus to cytosol translocation of ubiquitin-GFP in U2OS cells after 4 h treatment with 0.1 µM Bortezomib and 30 µM XXVII. (C and D) The dose-dependent level of ubiquitin and K29-, K48- and K63-ubiquitinylted proteins in U2OS cells following 4 h treatment. (E) XXVII structure and IC_{50} values obtained for CCRF-CEM and U2OS cell lines. $IC_{50\ CEM}$ value adapted from [185].

Discussion

The aim of the study was a biological characterization of novel triterpene fluoroderivatives. A set of dihydrobetulinic acid derivatives containing highly electronegative 2,2-difluoro moiety or their intermediates was tested against cancer cell lines to prove the hypothesis, that electronegative moiety at C2 position increases anticancer activity. This tendency is indicated by cytotoxic activity of 2-bromo dihydrobetulonic and 2,2-dibromo dihydrobetulonic acid [195]. Fluorine atoms were introduced to the position 2 of dihydrobetulinic acid since other possibilities (alkyl-flouro and aryl-fluoro moieties) would probably further increase its hydrophobicity. To decrease overall hydrophobicity, various hemiester groups were introduced at position 3. The impact of novel fluorderivatives on cancer cell cycle was of particular interest because fluorine introduction is known to alter molecular recognition and may completely change the mode of action. Organofluorine compounds represent a significant group of drugs in the pharmaceutical industry, although fluorine is very rarely found as part of natural organic compounds. Due to high electronegativity of fluorine and other chemical properties of fluorine, the C-F bond is extremely polar and its presence increases lipophilicity (logP) and absorption, which affects the pharmacological properties in general. It also shows higher thermal and chemical stability in comparison with C-H bond [196], [197], [198], [199]. The comparison of 2,2-difluoro with unsubstituted counterparts confirms the hypothesis that a strong electron withdrawing group in position 2 increases the cytotoxicity of triterpene derivatives. The cytotoxic activity of bromine and fluorine containing derivatives was highly comparable. However, fluorine is potentially more preferred since organofluorine compounds are widely used in clinics. Although 2-thiocyanate substitution enhanced the activity of inactive compounds, the effect was not as convincing as the case of 2,2-difluoro substituent. In addition, recent report showed also cytotoxic activity of 2-amino allobetulin [200]. Another finding is that these difluoroderivatives had high cytotoxic activity, when they contained a free carboxylic group or methylester. The absence of carboxyl group is therefore presumably responsible for the low activity of allobetulin derivatives. The results indicate that tested compounds display generally low selectivity. Therefore future research must be focused on the improvement of the potential therapeutic window between cancer and normal cells. Activities of all

lupane hemiesters were comparable with the activity of structures without long side chains. Nevertheless, hemiester groups most likely affect water solubility and can provide an advantage in terms of possible formulations with cyclodextrins. In contrast to bevirimat, hemiester group is not an important part of the pharmacophore for anticancer activity. This finding is not surprising when we consider the molecular basis of inhibition of virus maturation through the interaction of bevirimat with viral GAG protein. Flow cytometry analysis revealed accumulation in S phase after the treatment of CCR-CEM cells with I, V and XII and G2/M arrest of the cell cycle induced by XXIVb, XXIVc and XXVIc. The effect is mediated by an unknown mechanism, however, with respect to original unpublished data of G2/M arrest inducing betulinic acid derivative XXVII (synthesis and basic anticancer activity were described previously [184], [185]), the proteasomal inhibitory activity is rather unlikely. Although oleanonic acid thiocyanate XXVIc induced G2/M arrest of the cell cycle, it did not elevate phospho H3 at Ser10 in contrast to XXVII. A different mode of action is also evidenced by high structural diversity between XXVIc and XXVII. While XXVIc is oleanonic acid derivative with modified position C-2 and C-3, XXVII is betulinic acid analogue with substitution at opposite C-30. XXVII induced G2/M arrest might be, as in the case of proteasomal inhibitor bortezomib, a result of ATM mediated checkpoint arrest [201]. In addition, a higher level of mitotic cells can be caused by poor degradation of proteasomal substrates such as cyclin B1, whose degradation is required for further progression from mitosis [50].

The observed proteasomal inhibition by XXVII is in concordance with literature, since the C-3 and C-30 positions of betulinic acid with larger side chains were reported to increase the inhibition of the chymotrypsin-like activity of 20S proteasome [202]. Nevertheless, a more detailed study employing proteasome activity assay is needed for the *in vitro* validation of proteasome inhibitors derived from betulinic acid. On the other hand, these advanced tests are reasonable only for highly active compounds.

The study provides evidence for future design of new structures. Because it can not be further directed towards more electronegative substituents at C-2, the possibility of the side chain in another position should be considered to increase activity and specificity.

V.SUMMARY

The cell cycle is a sequence of events necessary for successful DNA replication and subsequent cell division into two daughter cells. Cell cycle dysregulation and abnormal activation of pathways that stimulate cell cycle progression are the underlying factors in cancer development. Although the key players in cell cycle regulation have been identified, the complexity of signaling pathways complicates specific targeting of cancer cells. In addition, cancer cells possess great ability to counterbalance the interventions by various compensatory mechanisms. Therefore, novel targets and strategies, as well as small molecule inhibitors, are being developed. However, new drugs such as kinase inhibitors targeting cyclin dependent kinases, Aurora kinases, Chk1 and Chk2 and Wee 1 show limited activity in monotherapy. On the other hand, combined therapy with conventional chemotherapy may improve cytotoxic activity or overcome drug resistance [203]. Moreover, the therapeutic effect of novel drugs is also affected by therapeutic indication. For example, Aurora kinases inhibitors did not meet the expected outcomes in clinical studies for the treatment of solid tumors, whereas higher response rates were achieved in hematologic malignancies. Nevertheless, the vast majority of clinically used chemotherapies relies on activation of cell cycle checkpoints that mediate cell cycle arrest upon DNA damage or incorrect mitosis. The most important class of antimitotic drugs are microtubule targeting agents (MTAs) that interfere with mitotic spindle formation, although they were also shown to upset cellular functions of interphase cells.

This PhD thesis integrates two studies dedicated to cancer cell cycle targeting by small molecule compounds. The first study is focused on inhibition of microtubule dynamics, a known molecular target of peloruside A (PELA). The efficacy of MTAs such as paclitaxel is often limited by hypoxia-associated alterations in solid tumors, however, the susceptibility of PELA to such alterations has not been determined. Therefore, the study compared the effects of hypoxia-mediated cellular changes on microtubule stabilization promoted by peloruside A and paclitaxel or microtubule assembly inhibition induced by vincristine. The study showed that hypoxia pre-exposure has no effect on the susceptibility of HCT116 cells to PELA. In contrast, hypoxia significantly reduced the cytotoxicity of PTX and prevented PTX-induced apoptosis. The data demonstrate that the ability of PELA to

induce G2/M arrest is not modulated by hypoxia conditioning of HCT116 cells in contrast to PTX. Hypoxia pretreatment also significantly reduced level of PTX-stabilized microtubules and level of PTX-induced tubulin acetylation. Thereby hypoxia pre-exposure reverses the PTX-induced changes in microtubule structure and probably affects the binding of microtubule-associated proteins (MAPs).

These findings indicate that oxygen deficiency in solid tumors has a striking impact on response to MTAs. In addition to direct effects of HIF-1α on microtubules, HIF-1α-mediated altered expression of the cell cycle, multidrug resistance-associated and apoptosis-regulating proteins also results in a poor response of tumor cells to MTAs in hypoxia. In contrast to PTX, PELA is a poor substrate of P-glycoprotein (P-gp), a downstream target of HIF-1α. Thus PELA is potentially less sensitive to HIF-1α mediated P-glycoprotein expression than PTX and it was shown to have favourable outcomes in a number of cancer cell lines resistant to PTX. The obtained results suggest that MTAs that bind to an alternative site than the taxane site, can potently inhibit the growth of hypoxic cancer cells with altered microtubule sensitivity. Nevertheless, further validation in more sophisticated pre-clinical models is needed to assess PELA potential for treatment of solid tumors.

The second study is focused on characterization of antiproliferative activity of novel triterpene derivatives with the yet unexplored molecular target. Despite betulinic and oleanonic acid analogues have been extensively studied for more than two decades, a broad spectrum of their biological activities and low target specificity limit their clinical potential. However, recent systematic bioinformatic analysis of drug discovery data revealed that low-affinity drugs with multiple targets could be in complex disease more effective than high-affinity binders [204]. The triterpenes bardoxolone methyl and bevirimat failed in clinical trials due to side effect or development of drug resistance. On the other hand, these compounds inspire the design of novel triterpenoid analogues with improved activity and bioavailability. One of these approaches employs introduction of fluorine atoms to enhance bioavailability and molecular recognition. Therefore, the study evaluated the potential of fluorinated dihydrobetulinic acid analogues. The set of 2,2-difluoroderivatives, derivatives with electronegative substituents in the same position and their intermediates were tested against cancer and non-cancerous cell lines. An electronegative moiety such as difluoro-, bromo- or thiocyano- substituents enhanced the cytotoxic activity of triterpenoid scaffolds. However, the comparison of activities

towards cancer cell lines and normal fibroblasts indicates low selectivity of tested compounds. The most active compounds induced S phase or G2/M arrest in CCRF-CEM. The exact mechanism of G2/M arrest induced by XXIVb, XXIVc and XXVIc is unknown, but unlike previously studied betulinic acid derivative and proteasomal inhibitor XXVII, the treatment did not induced H3 phosphorylation at Ser10. Thereby novel compounds probably do not act as modulators of the ubiquitin-proteasome system. In conclusion, this thesis summarises the progress in targeting of the cell cycle in cancer and shows the importance of novel small-molecule agents in cancer treatment.

In conclusion, the studies revealed promising anticancer activities of peloruside A and semisynthetic triterpenes and form the basis for further research.

Souhrn

Buněčný cyklus je ohraničen dvěma po sobě následujícími buněčnými děleními a sestává ze série kroků nezbytných pro rozdělení buňky. Nádorové buňky často vykazují deregulaci buněčného cyklu a nadměrnou aktivaci signalizačních drah stimulujících růst. Přestože hlavní regulační dráhy buněčného cyklu jsou známy, specifické cílení na nádorové buňky zůstává obtížné. I přes významné pokroky v biomedicínském výzkumu zůstávají základem pro léčbu používaná cytostatika interferující s biosyntézou DNA nebo dynamikou mikrotubulů. Předložená disertační práce integruje různé přístupy k vývoji nových protinádorových látek interferujících s průběhem buněčného cyklu.

Pelorusid A inhibuje dynamiku mikrotubulů stabilizací jejich podjednotek, avšak na rozdíl od paklitaxelu se pelorusid A váže na odlišné místo podjednotky β-tubulinu. Nedostatečné zásobení kyslíkem je zodpovědné za sniženou účinnost paklitaxelu při léčbě solidních nádorů, studie byla tedy zaměřena na dosud neznámé účinky pelorusidu A v hypoxických podmínkách. Pro srovnání byly experimenty provedeny i s klinicky používaným inhibitorem polymerizace mikrotubulů vinkristinem. Studie ukázala, že preinkubace buněk kolorektálního karcinomu HCT116 v hypoxii indukovala HIF-1α dráhu, avšak citlivost nádorových buněk k pelorusidu A a vinkristinu se nezměnila. V souladu s literaturou, hypoxické podmínky významně snížily účinnost paklitaxelu. Hypoxie také snížila schopnost paklitaxelu indukovat blok v G2/M fázi buněčného cyklu a stabilizovat mikrotubuly. Naopak pelorusid A si zachoval vysokou účinnost, stabilizoval mikrotubuly a stimuloval jejich acetylaci bez ohledu na preinkubaci. Stejný trend snížené cytotoxicity paklitaxelu byl patrný i v aktivaci kaspáz a indukci apoptózy. V hypoxických podmínkách solidního nádoru vzniká stres, který je příčinou alterací v homeostáze i v odpovědi k protinádorové léčbě. Navíc hypoxií indukovaná aktivace transkripčních faktorů HIF-1α vede k expresi proteinů regulujících metabolismus, angiogenezi i apoptózu. Transkripčním cílem HIF-1α je i P-glykoprotein zodpovědný za mnohočetnou lékovou rezistenci. To může mít i další navazující efekt na rozdílnou citlivost k paklitaxelu a pelorusidu A, protože pelorusid A na rozdíl od paklitaxelu není substrátem pro P-glykoprotein. Z dat předložených v této práci vyplývá, že pelorusid A má silný protinádorový účinek, který není negativně ovlivněn stimulací drah odpovědi na hypoxické podmínky.

Studie prokázala významný potenciál nových látek, které interagují s jiným vazebným místem β-tubulinu než taxany.

Cílem druhé studie byla charakterizace protinádorové aktivity triterpenů s neznámým mechanismem účinku. Přestože deriváty kyseliny betulinové a oleanonové jsou intenzivně studovány, jejich široká biologická aktivita komplikuje jejich klinické využití i určení vazebných partnerů na molekulární úrovni. Nicméně i léčiva s více cíli mohou být ve výsledku efektivní proti komplexním onemocněním [204]. Některá analoga triterpenů jako bevirimat nebo bardoxolon methyl již byla testována v preklinických a klinických zkouškách pro léčbu AIDS nebo chronického selhání ledvin, bardoxolon methyl má navíc také silné protinádorové účinky. V souvislosti s protinádorovou aktivitou je nejvíce prostudovaným triterpenem kyselina betulinová, která selektivně indukuje vnitřní dráhu apoptózy nádorových buněk. Navíc bylo prokázáno, že inhibuje topoizomerázu eukaryot i angiogenezi v solidních nádorech. Vhodnými modifikacemi kyseliny betulinové může být také ovlivněna její schopnost indukovat blok v různých fázích buněčného cyklu. Zavedení fluoru je v medicinální chemii často používanou strategií ke zlepšení biodostupnosti a účinku léčiv, a proto byla studie zaměřena na 2,2-difluoro deriváty kyseliny dehydrobetulinové. Soubor derivátů s 2,2-difluoro a dalšími elektronegativními skupinami (Br, SCN) i jejich meziprodukty byly testovány na panelu nádorových i nenádorových linií. Elektronegativní substituent v poloze 2 významně zvyšoval cytotoxickou aktivitu triterpenů, tento trend byl patrný i u původně neaktivních allobetulinů. V porovnání substituentů vykazovaly thiokyanáty slabší účinnost než fluorderiváty. Z výsledků cytotoxicity proti nádorovými buněčným liniím a nenádorovým fibroblastům však vyplývá nedostatečná selektivita proti nádorovým buňkám. Analýza buněčného cyklu CCRF-CEM metodami průtokové cytometrie prokázala blok v S fázi indukovaný deriváty I, V a XII. Deriváty XXIVb, XXIVc and XXVIc způsobovaly akumulaci buněk v G2/M fázi, avšak analýza fosforylace histonu H3 na Ser10 jako mitotického markeru vyloučila mitotický blok. Mechanismus jakým tyto látky interferují s buněčným cyklem je předmětem dalšího výzkumu. Nicméně ve srovnání s dalším derivátem kyseliny betulinové XXVII uvedené látky zřejmě nepatří do skupiny triterpenů inhibujících ubiquitin-proteazomový systém. Studie přispěly k hlubšímu pochopení protinádorové aktivity pelorusidu A a semisyntetických triterpenů.

VI. REFERENCES

[1]   A. Kierszenbaum, Histology and Cell Biology: Introduction to Pathology, 2nd ed., 2007.

[2]   K. Vermeulen, D.R. Van Bockstaele, Z.N. Berneman, The cell cycle: a review of regulation, deregulation and therapeutic targets in cancer, Cell Prolif. 36 (2003) 131–149. doi:10.1046/j.1365-2184.2003.00266.x.

[3]   U. Asghar, A.K. Witkiewicz, N.C. Turner, E.S. Knudsen, The history and future of targeting cyclin-dependent kinases in cancer therapy, Nat. Rev. Drug Discov. 14 (2015) 130–146. doi:10.1038/nrd4504.

[4]   M.E. Law, P.E. Corsino, S. Narayan, B.K. Law, Cyclin-Dependent Kinase Inhibitors as Anticancer Therapeutics, Mol. Pharmacol. 88 (2015) 846–852. doi:10.1124/mol.115.099325.

[5]   S.R. Whittaker, A. Mallinger, P. Workman, P.A. Clarke, Inhibitors of cyclin-dependent kinases as cancer therapeutics, Pharmacol. Ther. (2017). doi:10.1016/j.pharmthera.2017.02.008.

[6]   E.T. Cánepa, M.E. Scassa, J.M. Ceruti, M.C. Marazita, A.L. Carcagno, P.F. Sirkin, M.F. Ogara, INK4 proteins, a family of mammalian CDK inhibitors with novel biological functions., IUBMB Life. 59 (2007) 419–426. doi:10.1080/15216540701488358.

[7]   J.H. Houtgraaf, J. Versmissen, W.J. van der Giessen, A concise review of DNA damage checkpoints and repair in mammalian cells, Cardiovasc. Revascularization Med. 7 (2006) 165–172. doi:10.1016/j.carrev.2006.02.002.

[8]   A. Rocca, A. Schirone, R. Maltoni, S. Bravaccini, L. Cecconetto, A. Farolfi, G. Bronte, D. Andreis, Progress with palbociclib in breast cancer: latest evidence and clinical considerations, Ther. Adv. Med. Oncol. 9 (2017) 83–105. doi:10.1177/1758834016677961.

[9]   J. Slingerland, M. Pagano, Regulation of the Cdk inhibitor p 27 and its deregulation in cancer, J. Cell. Physiol. 183 (2000) 10–17. doi:10.1002/(SICI)1097-4652(200004)183:1<10::AID-JCP2>3.0.CO;2-I.

[10] J. Bartek, J. Lukas, DNA damage checkpoints: from initiation to recovery or adaptation, Curr. Opin. Cell Biol. 19 (2007) 238–245. doi:10.1016/j.ceb.2007.02.009.

[11] David O. Morgan, Cell Cycle: Principles of Control, New Science Press, London, 2006.

[12] P. Ruff, R.A. Donnianni, E. Glancy, J. Oh, L.S. Symington, RPA Stabilization of Single-Stranded DNA Is Critical for Break-Induced Replication, Cell Rep. 17 (2016) 3359–3368. doi:10.1016/j.celrep.2016.12.003.

[13] L. Balakrishnan, R.A. Bambara, Okazaki Fragment Metabolism, Cold Spring Harb. Perspect. Biol. 5 (2013) a010173–a010173.

doi:10.1101/cshperspect.a010173.

[14] S. Ramachandran, S. Henikoff, Replicating nucleosomes, Sci. Adv. 1 (2015) e1500587–e1500587. doi:10.1126/sciadv.1500587.

[15] R. a Woo, R.Y.C. Poon, Cyclin-dependent kinases and S phase control in mammalian cells., Cell Cycle. 2 (2003) 316–324. doi:10.4161/cc.2.4.468.

[16] A. Kousholt, T. Menzel, C. Sørensen, Pathways for Genome Integrity in G2 Phase of the Cell Cycle, Biomolecules. 2 (2012) 579–607. doi:10.3390/biom2040579.

[17] F.A. Barr, U. Gruneberg, Cytokinesis: Placing and Making the Final Cut, Cell. 131 (2007) 847–860. doi:10.1016/j.cell.2007.11.011.

[18] A.F. Straight, C.M. Field, Microtubules, membranes and cytokinesis, Curr. Biol. 10 (2000) 760–770. doi:10.1016/S0960-9822(00)00746-6.

[19] I. Mendes Pinto, B. Rubinstein, A. Kucharavy, J.R. Unruh, R. Li, Actin Depolymerization Drives Actomyosin Ring Contraction during Budding Yeast Cytokinesis, Dev. Cell. 22 (2012) 1247–1260. doi:10.1016/j.devcel.2012.04.015.

[20] M. Glotzer, Animal cell cytokinesis., Annu. Rev. Cell Dev. Biol. 17 (2001) 351–86. doi:10.1146/annurev.cellbio.17.1.351.

[21] C. Osborne, Oncogenes and Tumor Suppressor Genes in Breast Cancer: Potential Diagnostic and Therapeutic Applications, Oncologist. 9 (2004) 361–377. doi:10.1634/theoncologist.9-4-361.

[22] B. Gabrielli, K. Brooks, S. Pavey, Defective cell cycle checkpoints as targets for anti-cancer therapies, Front. Pharmacol. 3 FEB (2012) 1–6. doi:10.3389/fphar.2012.00009.

[23] C.M. Croce, Oncogenes and Cancer, N. Engl. J. Med. 358 (2008) 502–511. doi:10.1056/NEJMra072367.

[24] P. Klener, Klinická onkologie, Galén, 2002.

[25] A. Deshpande, P. Sicinski, P.W. Hinds, Cyclins and cdks in development and cancer: a perspective., Oncogene. 24 (2005) 2909–2915. doi:10.1038/sj.onc.1208618.

[26] A.-L. Salmela, M.J. Kallio, Mitosis as an anti-cancer drug target, Chromosoma. 122 (2013) 431–449. doi:10.1007/s00412-013-0419-8.

[27] T. V. Denisenko, I. V. Sorokina, V. Gogvadze, B. Zhivotovsky, Mitotic catastrophe and cancer drug resistance: A link that must to be broken, Drug Resist. Updat. 24 (2016) 1–12. doi:10.1016/j.drup.2015.11.002.

[28] N. Motoyama, K. Naka, DNA damage tumor suppressor genes and genomic instability, Curr. Opin. Genet. Dev. 14 (2004) 11–16. doi:10.1016/j.gde.2003.12.003.

[29] A. Marechal, L. Zou, DNA Damage Sensing by the ATM and ATR Kinases,

Cold Spring Harb. Perspect. Biol. 5 (2013) a012716–a012716. doi:10.1101/cshperspect.a012716.

[30]   M.R. Lieber, The Mechanism of Double-Strand DNA Break Repair by the Nonhomologous DNA End-Joining Pathway, Annu. Rev. Biochem. 79 (2010) 181–211. doi:10.1146/annurev.biochem.052308.093131.

[31]   K. Okamoto, N. Sagata, Mechanism for inactivation of the mitotic inhibitory kinase Wee1 at M phase., Proc. Natl. Acad. Sci. USA. 104 (2007) 3753–3758. doi:10.1073/pnas.0607357104.

[32]   H.C. Reinhardt, A.S. Aslanian, J.A. Lees, M.B. Yaffe, p53-Deficient Cells Rely on ATM- and ATR-Mediated Checkpoint Signaling through the p38MAPK/MK2 Pathway for Survival after DNA Damage, Cancer Cell. 11 (2007) 175–189. doi:10.1016/j.ccr.2006.11.024.

[33]   A.J. Levine, M. Oren, The first 30 years of p53: growing ever more complex., Nat. Rev. Cancer. 9 (2009) 749–58. doi:10.1038/nrc2723.

[34]   S.L. Harris, A.J. Levine, The p53 pathway: positive and negative feedback loops, Oncogene; Oncogene. 24 (2005) 2899–2908. doi:10.1038/sj.onc.1208615.

[35]   U.M. Moll, O. Petrenko, The MDM2-p53 Interaction, Mol. Cancer Res. 1 (2004) 1001–1008. doi:10.1016/s0092-8674(00)81871-1.

[36]   W. Tao, A.J. Levine, P19(ARF) stabilizes p53 by blocking nucleo-cytoplasmic shuttling of Mdm2., Proc. Natl. Acad. Sci. U. S. A. 96 (1999) 6937–41. doi:10.1073/pnas.96.12.6937.

[37]   M.T. Hemann, S.W. Lowe, The p53–Bcl-2 connection, Cell Death Differ. 13 (2006) 1256–1259. doi:10.1038/sj.cdd.4401962.

[38]   T. Tokino, Y. Nakamura, The role of p53-target genes in human cancer, Crit. Rev. Oncol. Hematol. 33 (2000) 1–6. doi:10.1016/S1040-8428(99)00051-7.

[39]   K. Nakano, K.H. Vousden, PUMA, a novel proapoptotic gene, is induced by p53., Mol. Cell. 7 (2001) 683–94. http://www.ncbi.nlm.nih.gov/pubmed/11463392.

[40]   S. Erster, U.M. Moll, Stress-induced p53 runs a transcription-independent death program, Biochem. Biophys. Res. Commun. 331 (2005) 843–850. doi:10.1016/j.bbrc.2005.03.187.

[41]   K.H. Vousden, K.M. Ryan, P53 and Metabolism., Nat. Rev. Cancer. 9 (2009) 691–700. doi:10.1038/nrc2715.

[42]   M. Kollareddy, E. Dimitrova, K.C. Vallabhaneni, A. Chan, T. Le, K.M. Chauhan, Z.I. Carrero, G. Ramakrishnan, K. Watabe, Y. Haupt, S. Haupt, R. Pochampally, G.R. Boss, D.G. Romero, C.G. Radu, L. a. Martinez, Regulation of nucleotide metabolism by mutant p53 contributes to its gain-of-function activities., Nat. Commun. 6 (2015) 7389. doi:10.1038/ncomms8389.

[43]   K.M. Godek, L. Kabeche, D.A. Compton, Regulation of kinetochore-

microtubule attachments through homeostatic control during mitosis., Nat. Rev. Mol. Cell Biol. 16 (2015) 57–64. doi:10.1038/nrm3916.

[44]   A.A. Guerrero, C. Martínez-A, K.H. van Wely, Merotelic attachments and non-homologous end joining are the basis of chromosomal instability., Cell Div. 5 (2010) 13. doi:10.1186/1747-1028-5-13.

[45]   K.K. Sarangapani, C.L. Asbury, Catch and release: how do kinetochores hook the right microtubules during mitosis?, Trends Genet. 30 (2014) 150–159. doi:10.1016/j.tig.2014.02.004.

[46]   L. Kabeche, D.A. Compton, Cyclin A regulates kinetochore microtubules to promote faithful chromosome segregation, Nature. 502 (2013) 110–113. doi:10.1038/nature12507.

[47]   I.M. Porter, K. Schleicher, M. Porter, J.R. Swedlow, Bod1 regulates protein phosphatase 2A at mitotic kinetochores, Nat Commun. 4 (2013) 2677. doi:10.1038/ncomms3677.

[48]   R. Wiedemuth, B. Klink, K. Töpfer, E. Schröck, G. Schackert, M. Tatsuka, A. Temme, Survivin safeguards chromosome numbers and protects from aneuploidy independently from p53., Mol. Cancer. 13 (2014) 107. doi:10.1186/1476-4598-13-107.

[49]   K. Overlack, V. Krenn, A. Musacchio, When Mad met Bub, EMBO Rep. 15 (2014) 326–328. doi:10.1002/embr.201438574.

[50]   D.R. Matson, P.T. Stukenberg, Spindle poisons and cell fate: a tale of two pathways., Mol. Interv. 11 (2011) 141–50. doi:10.1124/mi.11.2.12.

[51]   M.M.M. Gee, Targeting the Mitotic Catastrophe Signaling Pathway in Cancer, 2015 (2015).

[52]   M. Castedo, J.-L. Perfettini, T. Roumier, K. Andreau, R. Medema, G. Kroemer, Cell death by mitotic catastrophe: a molecular definition, (n.d.). doi:10.1038/sj.onc.1207528.

[53]   H. Vakifahmetoglu, M. Olsson, B. Zhivotovsky, Death through a tragedy: mitotic catastrophe., Cell Death Differ. 15 (2008) 1153–62. doi:10.1038/cdd.2008.47.

[54]   E.L. Mayer, Targeting Breast Cancer with CDK Inhibitors, Curr. Oncol. Rep. 17 (2015) 15–19. doi:10.1007/s11912-015-0443-3.

[55]   R.H. Medema, L. Macůrek, Checkpoint control and cancer., Oncogene. 31 (2012) 2601–13. doi:10.1038/onc.2011.451.

[56]   C. Liu, S. Srihari, K.A.L. Cao, G. Chenevix-Trench, P.T. Simpson, M.A. Ragan, K.K. Khanna, A fine-scale dissection of the DNA double-strand break repair machinery and its implications for breast cancer therapy, Nucleic Acids Res. 42 (2014) 6106–6127. doi:10.1093/nar/gku284.

[57]   A. Ashworth, A synthetic lethal therapeutic approach: Poly(ADP) ribose polymerase inhibitors for the treatment of cancers deficient in DNA double-

strand break repair, J. Clin. Oncol. 26 (2008) 3785–3790. doi:10.1200/JCO.2008.16.0812.

[58]   R. Visconti, R. Della Monica, D. Grieco, Cell cycle checkpoint in cancer: a therapeutically targetable double-edged sword., J. Exp. Clin. Cancer Res. 35 (2016) 153. doi:10.1186/s13046-016-0433-9.

[59]   M. Forte, P. Bernardi, The permeability transition and BCL-2 family proteins in apoptosis: co-conspirators or independent agents?, Cell Death Differ. 13 (2006) 1287–1290. doi:10.1038/sj.cdd.4401957.

[60]   L. Scorrano, M. Ashiya, K. Buttle, S. Weiler, S.A. Oakes, C.A. Mannella, S.J. Korsmeyer, A distinct pathway remodels mitochondrial cristae and mobilizes cytochrome c during apoptosis, Dev. Cell. (2002). doi:10.1016/S1534-5807(01)00116-2.

[61]   S. Fulda, S.A. Susin, G. Kroemer, K.M. Debatin, Molecular ordering of apoptosis induced by anticancer drugs in neuroblastoma cells, Cancer Res. 58 (1998) 4453–4460.

[62]   G. Kroemer, L. Galluzzi, C. Brenner, Mitochondrial Membrane Permeabilization in Cell Death, Physiol. Reveiw. (2007) 99–163. doi:10.1152/physrev.00013.2006.

[63]   M. Bonora, P. Pinton, G.P. Mcstay, The mitochondrial permeability transition pore and cancer: molecular mechanisms involved in cell death, (1970). doi:10.3389/fonc.2014.00302.

[64]   A. Rasola, P. Bernardi, The mitochondrial permeability transition pore and its adaptive responses in tumor cells, Cell Calcium. (2014). doi:10.1016/j.ceca.2014.10.003.

[65]   G. Kroemer, L. Galluzzi, C. Brenner, Mitochondrial Membrane Permeabilization in Cell Death, (n.d.).

[66]   V. Izzo, J. Manuel Bravo-San Pedro, V. Sica, G. Kroemer, L. Galluzzi, Mitochondrial Permeability Transition: New Findings and Persisting Uncertainties, (2016). doi:10.1016/j.tcb.2016.04.006.

[67]   A.R. D Delbridge, S. Grabow, A. Strasser, D.L. Vaux, Thirty years of BCL-2: translating cell death discoveries into novel cancer therapies, Nat. Publ. Gr. 16 (2016). doi:10.1038/nrc.2015.17.

[68]   P.E. Czabotar, G. Lessene, A. Strasser, J.M. Adams, Control of apoptosis by the BCL-2 protein family: implications for physiology and therapy, Nat. Publ. Gr. 15 (2014). doi:10.1038/nrm3722.

[69]   J.E. Chipuk, T. Moldoveanu, F. Llambi, M.J. Parsons, D.R. Green, The BCL-2 Family Reunion, Mol. Cell. (2010). doi:10.1016/j.molcel.2010.01.025.

[70]   J.E. Chipuk, D.R. Green, How do BCL-2 proteins induce mitochondrial outer membrane permeabilization?, Trends Cell Biol. (2008). doi:10.1016/j.tcb.2008.01.007.

[71] J. Zhang, K. Huang, K.O.' Neill, X. Pang, X. Luo, Bax/Bak activation in the absence of Bid, Bim, Puma, and p53, Nat. Publ. Gr. 7167 (2016). doi:10.1038/cddis.2016.167.

[72] P. Li, D. Nijhawan, I. Budihardjo, S.M. Srinivasula, M. Ahmad, E.S. Alnemri, X. Wang, Cytochrome c and dATP-Dependent Formation of Apaf-1/Caspase-9 Complex Initiates an Apoptotic Protease Cascade, Cell. 91 (1997) 479–489. doi:10.1016/S0092-8674(00)80434-1.

[73] J.-E. Ricci, C. Muñoz-Pinedo, P. Fitzgerald, B. Bailly-Maitre, G.A. Perkins, N. Yadava, I.E. Scheffler, M.H. Ellisman, D.R. Green, Disruption of mitochondrial function during apoptosis is mediated by caspase cleavage of the p75 subunit of complex I of the electron transport chain., Cell. 117 (2004) 773–86. doi:10.1016/j.cell.2004.05.008.

[74] L. Yang, T. Mashima, S. Sato, M. Mochizuki, H. Sakamoto, T. Yamori, T. Oh-Hara, T. Tsuruo, Predominant suppression of apoptosome by inhibitor of apoptosis protein in non-small cell lung cancer H460 cells: therapeutic effect of a novel polyarginine-conjugated Smac peptide., Cancer Res. 63 (2003) 831–7. http://www.ncbi.nlm.nih.gov/pubmed/12591734.

[75] A.M. Verhagen, J. Silke, P.G. Ekert, M. Pakusch, H. Kaufmann, L.M. Connolly, C.L. Day, A. Tikoo, R. Burke, C. Wrobel, R.L. Moritz, R.J. Simpson, D.L. Vaux, HtrA2 promotes cell death through its serine protease activity and its ability to antagonize inhibitor of apoptosis proteins., J. Biol. Chem. 277 (2002) 445–54. doi:10.1074/jbc.M109891200.

[76] N. Joza, S. a Susin, E. Daugas, W.L. Stanford, S.K. Cho, C.Y. Li, T. Sasaki, a J. Elia, H.Y. Cheng, L. Ravagnan, K.F. Ferri, N. Zamzami, a Wakeham, R. Hakem, H. Yoshida, Y.Y. Kong, T.W. Mak, J.C. Zúñiga-Pflücker, G. Kroemer, J.M. Penninger, Essential role of the mitochondrial apoptosis-inducing factor in programmed cell death., Nature. 410 (2001) 549–554. doi:10.1038/35069004.

[77] D.R. McIlwain, T. Berger, T.W. Mak, Caspase functions in cell death and disease., Cold Spring Harb. Perspect. Biol. (2013). doi:10.1101/cshperspect.a008656.

[78] A.B. Parrish, C.D. Freel, S. Kornbluth, Cellular mechanisms controlling caspase activation and function, Cold Spring Harb. Perspect. Biol. (2013). doi:10.1101/cshperspect.a008672.

[79] J. Howard, A.A. Hyman, Dynamics and mechanics of the microtubule plus end, Nature. 422 (2003) 753–758. doi:10.1038/nature01600.

[80] A. Cormier, M. Marchand, R.B.G. Ravelli, M. Knossow, B. Gigant, Structural insight into the inhibition of tubulin by vinca domain peptide ligands, EMBO Rep. 9 (2008) 1101–1106. doi:10.1038/embor.2008.171.

[81] M.T. Baquero, J.A. Hanna, V. Neumeister, H. Cheng, A.M. Molinaro, L.N. Harris, D.L. Rimm, Stathmin expression and its relationship to microtubule-associated protein tau and outcome in breast cancer, Cancer. 118 (2012) 4660–4669. doi:10.1002/cncr.27453.

[82] J. Löwe, H. Li, K.. Downing, E. Nogales, Refined structure of αβ-tubulin at 3.5 Å resolution, J. Mol. Biol. 313 (2001) 1045–1057. doi:10.1006/jmbi.2001.5077.

[83] L.A. Amos, What tubulin drugs tell us about microtubule structure and dynamics, Semin. Cell Dev. Biol. 22 (2011) 916–926. doi:10.1016/j.semcdb.2011.09.014.

[84] A.E. Prota, K. Bargsten, J.F. Diaz, M. Marsh, C. Cuevas, M. Liniger, C. Neuhaus, J.M. Andreu, K.-H. Altmann, M.O. Steinmetz, A new tubulin-binding site and pharmacophore for microtubule-destabilizing anticancer drugs, Proc. Natl. Acad. Sci. 111 (2014) 13817–13821. doi:10.1073/pnas.1408124111.

[85] J.M. Kollman, A. Merdes, L. Mourey, D.A. Agard, Microtubule nucleation by γ-tubulin complexes., Nat. Rev. Mol. Cell Biol. 12 (2011) 709–21. doi:10.1038/nrm3209.

[86] B.R. Oakley, V. Paolillo, Y. Zheng, γ-Tubulin complexes in microtubule nucleation and beyond, Mol. Biol. Cell. 26 (2015) 2957–2962. doi:10.1091/mbc.E14-11-1514.

[87] H. Fujita, Y. Yoshino, N. Chiba, Regulation of the centrosome cycle., Mol. Cell. Oncol. 3 (2016) e1075643. doi:10.1080/23723556.2015.1075643.

[88] T. Stearns, NIH Public Access, 13 (2014) 1154–1160. doi:10.1038/ncb2345.The.

[89] S.L. Prosser, L. Pelletier, Mitotic spindle assembly in animal cells: a fine balancing act, Nat. Rev. Mol. Cell Biol. 18 (2017) 187–201. doi:10.1038/nrm.2016.162.

[90] S. Petry, Mechanisms of Mitotic Spindle Assembly, Annu. Rev. Biochem. 85 (2016) 659–683. doi:10.1146/annurev-biochem-060815-014528.

[91] B.H. Long, C.R. Fairchild, Paclitaxel Inhibits Progression of Mitotic Cells to G1 Phase by Interference with Spindle Formation without Affecting Other Microtubule Functions during Anaphase and Telephase, Cancer Res. 54 (1994) 4355–4361.

[92] A. Ogden, P.C.G. Rida, M.D. Reid, R. Aneja, Interphase microtubules: Chief casualties in the war on cancer?, Drug Discov. Today. 19 (2014) 824–829. doi:10.1016/j.drudis.2013.10.022.

[93] G.M. Tozer, C. Kanthou, B.C. Baguley, Disrupting tumour blood vessels, Nat. Rev. Cancer. 5 (2005) 423–435. doi:10.1038/nrc1628.

[94] C. Gridelli, A. Rossi, P. Maione, E. Rossi, V. Castaldo, P.C. Sacco, G. Colantuoni, Vascular Disrupting Agents: A Novel Mechanism of Action in the Battle Against Non-Small Cell Lung Cancer, Oncologist. 14 (2009) 612–620. doi:10.1634/theoncologist.2008-0287.

[95] A. Dorléans, B. Gigant, R.B.G. Ravelli, P. Mailliet, V. Mikol, M. Knossow, Variations in the colchicine-binding domain provide insight into the structural

switch of tubulin., Proc. Natl. Acad. Sci. U. S. A. 106 (2009) 13775–9. doi:10.1073/pnas.0904223106.

[96]   A. V Blokhin, H.D. Yoo, R.S. Geralds, D.G. Nagle, W.H. Gerwick, E. Hamel, Characterization of the interaction of the marine cyanobacterial natural product curacin A with the colchicine site of tubulin and initial structure-activity studies with analogues., Mol. Pharmacol. 48 (1995) 523–31. http://www.ncbi.nlm.nih.gov/pubmed/7565634.

[97]   M. Botta, S. Forli, M. Magnani, F. Manetti, Molecular Modeling Approaches to Study the Binding Mode on Tubulin of Microtubule Destabilizing and Stabilizing Agents, in: 2008: pp. 279–328. doi:10.1007/128_2008_20.

[98]   C. Coderch, Tubulin-based Structure-affinity Relationships for Antimitotic Vinca Alkaloids, Anticancer. Agents Med. Chem. 12 (2012) 219–225. doi:10.2174/187152012800228841.

[99]   J. Fahy, A. Duflos, J.P. Ribet, J.C. Jacquesy, C. Berrier, M.P. Jouannetaud, F. Zunino, Vinca alkaloids in superacidic media: A method for creating a new family of antitumor derivatives, J. Am. Chem. Soc. 119 (1997) 8576–8577. doi:10.1021/ja971864w.

[100] M. Takahashi, S. Iwasaki, H. Kobayashi, S. Okuda, T. Murai, Y. Sato, Rhizoxin binding to tubulin at the maytansine-binding site., Biochim. Biophys. Acta. 926 (1987) 215–23. http://www.ncbi.nlm.nih.gov/pubmed/3120782.

[101] E. Nogales, M. Whittaker, R.A. Milligan, K.H. Downing, High-resolution model of the microtubule, Cell. 96 (1999) 79–88. doi:10.1016/S0092-8674(00)80961-7.

[102] C. Nehate, S. Jain, A. Saneja, V. Khare, N. Alam, R.D. Dubey, P.N. Gupta, Paclitaxel formulations: challenges and novel delivery options., Curr. Drug Deliv. 11 (2014) 666–86. http://www.ncbi.nlm.nih.gov/pubmed/24909147.

[103] V. Das, J. Štěpánková, M. Hajdúch, J.H. Miller, Role of tumor hypoxia in acquisition of resistance to microtubule-stabilizing drugs, Biochim. Biophys. Acta - Rev. Cancer. 1855 (2015) 172–182. doi:10.1016/j.bbcan.2015.02.001.

[104] A. Montero, F. Fossella, G. Hortobagyi, V. Valero, Docetaxel for treatment of solid tumours: a systematic review of clinical data., Lancet. Oncol. 6 (2005) 229–39. doi:10.1016/S1470-2045(05)70094-2.

[105] P. Vrignaud, D. Sémiond, P. Lejeune, H. Bouchard, L. Calvet, C. Combeau, J.F. Riou, A. Commerçon, F. Lavelle, M.C. Bissery, Preclinical antitumor activity of cabazitaxel, a semisynthetic taxane active in taxane-resistant tumors, Clin. Cancer Res. 19 (2013) 2973–2983. doi:10.1158/1078-0432.CCR-12-3146.

[106] E. Hamel, B.W. Day, J.H. Miller, M.K. Jung, P.T. Northcote, A.K. Ghosh, D.P. Curran, M. Cushman, K.C. Nicolaou, I. Paterson, E.J. Sorensen, Synergistic effects of peloruside A and laulimalide with taxoid site drugs, but not with each other, on tubulin assembly., Mol. Pharmacol. 70 (2006) 1555–

1564. doi:10.1124/mol.106.027847.

[107] D.E. Pryor, A. O'Brate, G. Bilcer, J.F. Díaz, Y. Wang, Y. Wang, M. Kabaki, M.K. Jung, J.M. Andreu, A.K. Ghosh, P. Giannakakou, E. Hamel, The microtubule stabilizing agent laulimalide does not bind in the taxoid site, kills cells resistant to paclitaxel and epothilones, and may not require its epoxide moiety for activity, Biochemistry. 41 (2002) 9109–9115. doi:10.1021/bi020211b.

[108] A.E. Prota, K. Bargsten, P.T. Northcote, M. Marsh, K.H. Altmann, J.H. Miller, J.F. Díaz, M.O. Steinmetz, Structural basis of microtubule stabilization by laulimalide and peloruside A, Angew. Chemie - Int. Ed. 53 (2014) 1621–1625. doi:10.1002/anie.201307749.

[109] A. Kanakkanthara, Peloruside A: a lead non-taxoid-site microtubule-stabilizing agent with potential activity against cancer, neurodegeneration, and autoimmune disease, Nat. Prod. Rep. 33 (2016) 549–561. doi:10.1039/C5NP00146C.

[110] T.N. Gaitanos, R.M. Buey, J. Fernando Díaz, P.T. Northcote, P. Teesdale-Spittle, J.M. Andreu, J.H. Miller, Peloruside A does not bind to the taxoid site on β-tubulin and retains its activity in multidrug-resistant cell lines, Cancer Res. 64 (2004) 5063–5067. doi:10.1158/0008-5472.CAN-04-0771.

[111] M. Dean, Y. Hamon, G. Chimini, The human ATP-binding cassette (ABC) transporter superfamily., J. Lipid Res. 42 (2001) 1007–17. http://www.ncbi.nlm.nih.gov/pubmed/11441126.

[112] S.L. Chan, J. Thiessen, E. Kingston, M.O. Brien, L. Hungerford, L. Gallie, Combining Retinoblastoma Cyclosporin without with Chemotherapy Radiation ' Controls Intraocular Requiring, Clin. Cancer Res. 2 (1996) 1499–1508.

[113] B. Pera, M.N. Calvo-Vidal, S. Ambati, M. Jordi, A. Kahn, J.F. Díaz, W. Fang, K. Altmann, L. Cerchietti, M.A.S. Moore, High affinity and covalent-binding microtubule stabilizing agents show activity in chemotherapy-resistant acute myeloid leukemia cells, Cancer Lett. 368 (2015) 97–104. doi:10.1016/j.canlet.2015.07.038.

[114] J.J. Field, A. Kanakkanthara, J.H. Miller, Microtubule-targeting agents are clinically successful due to both mitotic and interphase impairment of microtubule function, Bioorganic Med. Chem. 22 (2015) 5050–5059. doi:10.1016/j.bmc.2014.02.035.

[115] C. Dumontet, M.A. Jordan, Microtubule-binding agents: a dynamic field of cancer therapeutics, Nat. Rev. Drug Discov. 9 (2010) 790–803. doi:10.1038/nrd3253.

[116] M. Monzó, R. Rosell, J.J. Sánchez, J.S. Lee, A. O'Brate, J.L. González-Larriba, V. Alberola, J.C. Lorenzo, L. Núñez, J.Y. Ro, C. Martín, Paclitaxel resistance in non-small-cell lung cancer associated with beta-tubulin gene mutations., J. Clin. Oncol. 17 (1999) 1786–93. doi:10.1200/JCO.1999.17.6.1786.

[117] K. Maeno, K. Ito, Y. Hama, K. Shingu, M. Kimura, M. Sano, H. Nakagomi, S. Tsuchiya, M. Fujimori, Mutation of the class I β-tubulin gene does not predict response to paclitaxel for breast cancer, Cancer Lett. 198 (2003) 89–97. doi:10.1016/S0304-3835(03)00279-9.

[118] N. Urano, Y. Fujiwara, S. Hasegawa, Y. Miyoshi, S. Noguchi, S. Takiguchi, T. Yasuda, M. Yano, M. Monden, Absence of beta-tubulin gene mutation in gastric carcinoma., Gastric Cancer. 6 (2003) 108–12. doi:10.1007/s10120-003-0235-6.

[119] W. Wang, H. Zhang, X. Wang, J. Patterson, P. Winter, K. Graham, S. Ghosh, J.C. Lee, C.D. Katsetos, J.R. Mackey, J.A. Tuszynski, G.K.-S. Wong, R.F. Ludueña, Novel mutations involving βI-, βIIA-, or βIVB-tubulin isotypes with functional resemblance to βIII-tubulin in breast cancer, Protoplasma. 254 (2017) 1163–1173. doi:10.1007/s00709-016-1060-1.

[120] C. Janke, The tubulin code: Molecular components, readout mechanisms, and functions, J. Cell Biol. 206 (2014) 461–472. doi:10.1083/jcb.201406055.

[121] M. Sirajuddin, L.M. Rice, R.D. Vale, Regulation of microtubule motors by tubulin isotypes and post-translational modifications., Nat. Cell Biol. 16 (2014) 335–44. doi:10.1038/ncb2920.

[122] C.A. Burkhart, M. Kavallaris, S.B. Horwitz, The role of ??-tubulin isotypes in resistance to antimitotic drugs, Biochim. Biophys. Acta - Rev. Cancer. 1471 (2001) 1–9. doi:10.1016/S0304-419X(00)00022-6.

[123] M. Kavallaris, C. a Burkhart, S.B. Horwitz, Antisense oligonucleotides to class III beta-tubulin sensitize drug-resistant cells to Taxol., Br. J. Cancer. 80 (1999) 1020–1025. doi:10.1038/sj.bjc.6690507.

[124] K. Kamath, L. Wilson, F. Cabral, M.A. Jordan, βIII-tubulin induces paclitaxel resistance in association with reduced effects on microtubule dynamic instability, J. Biol. Chem. 280 (2005) 12902–12907. doi:10.1074/jbc.M414477200.

[125] Y. Koh, B. Jang, S.-W. Han, T.-M. Kim, D.-Y. Oh, S.-H. Lee, C.H. Kang, D.-W. Kim, S.-A. Im, D.H. Chung, Y.T. Kim, T.-Y. Kim, Y.-W. Kim, J.H. Kim, D.S. Heo, Y.-J. Bang, Expression of class III beta-tubulin correlates with unfavorable survival outcome in patients with resected non-small cell lung cancer., J. Thorac. Oncol. 5 (2010) 320–325. doi:10.1097/JTO.0b013e3181ce684f.

[126] A. Ohashi, Different cell fates after mitotic slippage: From aneuploidy to polyploidy, Mol. Cell. Oncol. 3 (2016) e1088503. doi:10.1080/23723556.2015.1088503.

[127] P. Sève, S. Isaac, O. Trédan, P.-J. Souquet, Y. Pachéco, M. Pérol, L. Lafanéchère, A. Penet, E.-L. Peiller, C. Dumontet, Expression of class III {beta}-tubulin is predictive of patient outcome in patients with non-small cell lung cancer receiving vinorelbine-based chemotherapy., Clin. Cancer Res. 11 (2005) 5481–6. doi:10.1158/1078-0432.CCR-05-0285.

[128] P. Magee, L. Shi, M. Garofalo, Role of microRNAs in chemoresistance., Ann. Transl. Med. 3 (2015) 332. doi:10.3978/j.issn.2305-5839.2015.11.32.

[129] A. Kanakkanthara, J.H. Miller, MicroRNAs: Novel mediators of resistance to microtubule-targeting agents, Cancer Treat. Rev. 39 (2013) 161–170. doi:10.1016/j.ctrv.2012.07.005.

[130] S.S. Karuppagounder, R.R. Ratan, Hypoxia-inducible factor prolyl hydroxylase inhibition: robust new target or another big bust for stroke therapeutics?, J. Cereb. Blood Flow Metab. 32 (2012) 1347–1361. doi:10.1038/jcbfm.2012.28.

[131] A. Patel, S. Sant, Hypoxic tumor microenvironment: Opportunities to develop targeted therapies, Biotechnol. Adv. 34 (2016) 803–812. doi:10.1016/j.biotechadv.2016.04.005.

[132] L. Huang, Q. Ao, Q. Zhang, X. Yang, H. Xing, F. Li, G. Chen, J. Zhou, S. Wang, G. Xu, L. Meng, Y. Lu, D. Ma, Hypoxia induced paclitaxel resistance in human ovarian cancers via hypoxia-inducible factor 1α, J. Cancer Res. Clin. Oncol. 136 (2010) 447–456. doi:10.1007/s00432-009-0675-4.

[133] L. Zeng, S. Kizaka-Kondoh, S. Itasaka, X. Xie, M. Inoue, K. Tanimoto, K. Shibuya, M. Hiraoka, Hypoxia inducible factor-1 influences sensitivity to paclitaxel of human lung cancer cell lines under normoxic conditions, Cancer Sci. 98 (2007) 1394–1401. doi:10.1111/j.1349-7006.2007.00537.x.

[134] D. Escuin, E.R. Kline, P. Giannakakou, Both microtubule-stabilizing and microtubule-destabilizing drugs inhibit hypoxia-inducible factor-1alpha accumulation and activity by disrupting microtubule function., Cancer Res. 65 (2005) 9021–8. doi:10.1158/0008-5472.CAN-04-4095.

[135] K. Yao, J.A. Gietema, S. Shida, M. Selvakumaran, X. Fonrose, N.B. Haas, J. Testa, P.J. O'Dwyer, In vitro hypoxia-conditioned colon cancer cell lines derived from HCT116 and HT29 exhibit altered apoptosis susceptibility and a more angiogenic profile in vivo., Br. J. Cancer. 93 (2005) 1356–63. doi:10.1038/sj.bjc.6602864.

[136] P. Martinive, F. Defresne, C. Bouzin, J. Saliez, F. Lair, V. Grégoire, C. Michiels, C. Dessy, O. Feron, Preconditioning of the tumor vasculature and tumor cells by intermittent hypoxia: implications for anticancer therapies., Cancer Res. 66 (2006) 11736–44. doi:10.1158/0008-5472.CAN-06-2056.

[137] N. Kondo, A. Takahashi, K. Ono, T. Ohnishi, DNA Damage Induced by Alkylating Agents and Repair Pathways, J. Nucleic Acids. 2010 (2010) 1–7. doi:10.4061/2010/543531.

[138] K. Cheung-Ong, G. Giaever, C. Nislow, DNA-Damaging Agents in Cancer Chemotherapy: Serendipity and Chemical Biology, Chem. Biol. 20 (2013) 648–659. doi:10.1016/j.chembiol.2013.04.007.

[139] D.B. Longley, D.P. Harkin, P.G. Johnston, 5-fluorouracil: mechanisms of action and clinical strategies., Nat. Rev. Cancer. 3 (2003) 330–8. doi:10.1038/nrc1074.

[140] J.L. Nitiss, E. Soans, A. Rogojina, A. Seth, M. Mishina, Topoisomerase assays., Curr. Protoc. Pharmacol. Chapter 3 (2012) Unit 3.3. doi:10.1002/0471141755.ph0303s57.

[141] Y. Pommier, E. Leo, H. Zhang, C. Marchand, DNA topoisomerases and their poisoning by anticancer and antibacterial drugs., Chem. Biol. 17 (2010) 421–33. doi:10.1016/j.chembiol.2010.04.012.

[142] V. Bavetsias, S. Linardopoulos, Aurora Kinase Inhibitors: Current Status and Outlook., Front. Oncol. 5 (2015) 278. doi:10.3389/fonc.2015.00278.

[143] X. Liu, Targeting Polo-Like Kinases: A Promising Therapeutic Approach for Cancer Treatment, Transl. Oncol. 8 (2015) 185–195. doi:10.1016/j.tranon.2015.03.010.

[144] S.M. Myers, I. Collins, Recent findings and future directions for interpolar mitotic kinesin inhibitors in cancer therapy., Future Med. Chem. 8 (2016) 463–89. doi:10.4155/fmc.16.5.

[145] V. Kryštof, R. Lenobel, L. Havlíček, M. Kuzma, M. Strnad, Synthesis and biological activity of Olomoucine II, Bioorganic Med. Chem. Lett. 12 (2002) 3283–3286. doi:10.1016/S0960-894X(02)00693-5.

[146] L. Meijer, A. Borgne, O. Mulner, J.P. Chong, J.J. Blow, N. Inagaki, M. Inagaki, J.G. Delcros, J.P. Moulinoux, Biochemical and cellular effects of roscovitine, a potent and selective inhibitor of the cyclin-dependent kinases cdc2, cdk2 and cdk5, Eur. J. Biochem. 243 (1997) 527–536. doi:10.1111/j.1432-1033.1997.t01-2-00527.x.

[147] J. Cicenas, K. Kalyan, A. Sorokinas, E. Stankunas, J. Levy, I. Meskinyte, V. Stankevicius, A. Kaupinis, M. Valius, Roscovitine in cancer and other diseases., Ann. Transl. Med. 3 (2015) 135. doi:10.3978/j.issn.2305-5839.2015.03.61.

[148] C.J. Matheson, D.S. Backos, P. Reigan, Targeting WEE1 Kinase in Cancer, Trends Pharmacol. Sci. 37 (2016) 872–881. doi:10.1016/j.tips.2016.06.006.

[149] S. Leijen, R.M.J.M. van Geel, A.C. Pavlick, R. Tibes, L. Rosen, A.R.A. Razak, R. Lam, T. Demuth, S. Rose, M.A. Lee, T. Freshwater, S. Shumway, L.W. Liang, A.M. Oza, J.H.M. Schellens, G.I. Shapiro, Phase I Study Evaluating WEE1 Inhibitor AZD1775 As Monotherapy and in Combination With Gemcitabine, Cisplatin, or Carboplatin in Patients With Advanced Solid Tumors, J. Clin. Oncol. 34 (2016). doi:10.1200/JCO.2016.67.5991.

[150] D. Hong, J. Infante, F. Janku, S. Jones, L.M. Nguyen, H. Burris, A. Naing, T.M. Bauer, S. Piha-Paul, F.M. Johnson, R. Kurzrock, L. Golden, S. Hynes, J. Lin, A.B. Lin, J. Bendell, Phase i study of LY2606368, a checkpoint kinase 1 inhibitor, in patients with advanced cancer, J. Clin. Oncol. 34 (2016) 1764–1771. doi:10.1200/JCO.2015.64.5788.

[151] F.P. Vendetti, A. Lau, S. Schamus, T.P. Conrads, M.J. O'Connor, C.J. Bakkenist, The orally active and bioavailable ATR kinase inhibitor AZD6738 potentiates the anti-tumor effects of cisplatin to resolve ATM-deficient non-

small cell lung cancer in vivo., Oncotarget. 6 (2015) 44289–305. doi:10.18632/oncotarget.6247.

[152] M. Kwok, N. Davies, A. Agathanggelou, E. Smith, C. Oldreive, E. Petermann, G. Stewart, J. Brown, A. Lau, G. Pratt, H. Parry, M. Taylor, P. Moss, P. Hillmen, T. Stankovic, ATR inhibition induces synthetic lethality and overcomes chemoresistance in TP53 or ATM defective chronic lymphocytic leukemia cells., Blood. 127 (2016) 582–95. doi:10.1182/blood-2015-05-644872.

[153] A. Peasland, L.-Z. Wang, E. Rowling, S. Kyle, T. Chen, A. Hopkins, W.A. Cliby, J. Sarkaria, G. Beale, R.J. Edmondson, N.J. Curtin, Identification and evaluation of a potent novel ATR inhibitor, NU6027, in breast and ovarian cancer cell lines, Br. J. Cancer. 105 (2011) 372–381. doi:10.1038/bjc.2011.243.

[154] C. Swanton, Cell-cycle targeted therapies, Lancet Oncol. 5 (2004) 27–36. doi:10.1016/S1470-2045(03)01321-4.

[155] B.C. Das, P. Thapa, R. Karki, C. Schinke, S. Das, S. Kambhampati, S.K. Banerjee, P. Van Veldhuizen, A. Verma, L.M. Weiss, T. Evans, Boron chemicals in diagnosis and therapeutics., Future Med. Chem. 5 (2013) 653–76. doi:10.4155/fmc.13.38.

[156] N. Rastogi, D.P. Mishra, Therapeutic targeting of cancer cell cycle using proteasome inhibitors., Cell Div. 7 (2012) 26. doi:10.1186/1747-1028-7-26.

[157] C. Damaskos, S. Valsami, M. Kontos, E. Spartalis, T. Kalampokas, E. Kalampokas, A. Athanasiou, D. Moris, A. Daskalopoulou, S. Davakis, G. Tsourouflis, K. Kontzoglou, D. Perrea, N. Nikiteas, D. Dimitroulis, Histone Deacetylase Inhibitors: An Attractive Therapeutic Strategy Against Breast Cancer., Anticancer Res. 37 (2017) 35–46. doi:10.21873/anticanres.11286.

[158] K. Ververis, A. Hiong, T.C. Karagiannis, P. V. Licciardi, Histone deacetylase inhibitors (HDACIS): Multitargeted anticancer agents, Biol. Targets Ther. 7 (2013) 47–60. doi:10.2147/BTT.S29965.

[159] V. Zuco, R. Supino, S.C. Righetti, L. Cleris, E. Marchesi, C. Gambacorti-Passerini, F. Formelli, Selective cytotoxicity of betulinic acid on tumor cell lines, but not on normal cells., Cancer Lett. 175 (2002) 17–25. http://www.ncbi.nlm.nih.gov/pubmed/11734332.

[160] M.E.H. Shumaia Parvin, Md. Abdul Kader, Md. Abdul Muhit, M.A. Mosaddik, And, M.I.I. Wahed, Triterpenoids and phytosteroids from stem bark of Crataeva nurvala buch ham., J. Appl. Pharm. Sci. 1 (2011) 47–50.

[161] T. Syrovets, B. Büchele, E. Gedig, J.R. Slupsky, T. Simmet, Acetyl-boswellic acids are novel catalytic inhibitors of human topoisomerases I and IIalpha., Mol. Pharmacol. 58 (2000) 71–81. http://www.ncbi.nlm.nih.gov/pubmed/10860928.

[162] A.R. Chowdhury, S. Mandal, B. Mittra, S. Sharma, S. Mukhopadhyay, H.K. Majumder, Betulinic acid, a potent inhibitor of eukaryotic topoisomerase I:

identification of the inhibitory step, the major functional group responsible and development of more potent derivatives., Med. Sci. Monit. 8 (2002) BR254-65. http://www.ncbi.nlm.nih.gov/pubmed/12118187.

[163] A. Ganguly, B. Das, A. Roy, N. Sen, S.B. Dasgupta, S. Mukhopadhayay, H.K. Majumder, Betulinic acid, a catalytic inhibitor of topoisomerase I, inhibits reactive oxygen species-mediated apoptotic topoisomerase I-DNA cleavable complex formation in prostate cancer cells but does not affect the process of cell death, Cancer Res. 67 (2007) 11848–11858. doi:10.1158/0008-5472.CAN-07-1615.

[164] Y. Tan, R. Yu, J.M. Pezzuto, Betulinic acid-induced programmed cell death in human melanoma cells involves mitogen-activated protein kinase activation., Clin. Cancer Res. 9 (2003) 2866–75. http://www.ncbi.nlm.nih.gov/pubmed/12855667.

[165] W. Rzeski, A. Stepulak, M. Szymañski, M. Sifringer, J. Kaczor, K. Wejksza, B. Zdzisiñska, M. Kandefer-Szerszeñ, Betulinic acid decreases expression of bcl-2 and cyclin D1, inhibits proliferation, migration and induces apoptosis in cancer cells, Naunyn. Schmiedebergs. Arch. Pharmacol. 374 (2006) 11–20. doi:10.1007/s00210-006-0090-1.

[166] S. Fulda, C. Friesen, M. Los, C. Scaffidi, W. Mier, M. Benedict, G. Nuñez, P.H. Krammer, M.E. Peter, K.M. Debatin, Betulinic acid triggers CD95 (APO-1/Fas)- and p53-independent apoptosis via activation of caspases in neuroectodermal tumors., Cancer Res. 57 (1997) 4956–64. http://www.ncbi.nlm.nih.gov/pubmed/9354463.

[167] D. Thurnher, D. Turhani, M. Pelzmann, B. Wannemacher, B. Knerer, M. Formanek, V. Wacheck, E. Selzer, Betulinic acid: A new cytotoxic compound against malignant head and neck cancer cells, Head Neck. 25 (2003) 732–740. doi:10.1002/hed.10231.

[168] E. Selzer, E. Pimentel, V. Wacheck, W. Schlegel, H. Pehamberger, B. Jansen, R. Kodym, Effects of betulinic acid alone and in combination with irradiation in human melanoma cells., J. Invest. Dermatol. 114 (2000) 935–40. doi:10.1046/j.1523-1747.2000.00972.x.

[169] F.B. Mullauer, J.H. Kessler, J.P. Medema, Betulinic acid induces cytochrome c release and apoptosis in a Bax/Bak-independent, permeability transition pore dependent fashion, Apoptosis. 14 (2009) 191–202. doi:10.1007/s10495-008-0290-x.

[170] W. Ren, L. Qin, Y. Xu, N. Cheng, Inhibition of betulinic acid to growth and angiogenesis of human colorectal cancer cell in nude mice, Chinese-German J. Clin. Oncol. 9 (2010) 153–157. doi:10.1007/s10330-010-0002-1.

[171] J. Shin, H.J. Lee, D.B. Jung, J.H. Jung, H.J. Lee, E.O. Lee, S.G. Lee, B.S. Shim, S.H. Choi, S.G. Ko, K.S. Ahn, S.J. Jeong, S.H. Kim, Suppression of STAT3 and HIF-1 Alpha mediates Anti-Angiogenic activity of Betulinic acid in Hypoxic PC-3 prostate cancer cells, PLoS One. 6 (2011). doi:10.1371/journal.pone.0021492.

[172] R. Carpenter, H.-W. Lo, STAT3 Target Genes Relevant to Human Cancers, Cancers (Basel). 6 (2014) 897–925. doi:10.3390/cancers6020897.

[173] M.K. Pandey, B. Sung, B.B. Aggarwal, Betulinic acid suppresses STAT3 activation pathway through induction of protein tyrosine phosphatase SHP-1 in human multiple myeloma cells, Int. J. Cancer. (2010) NA-NA. doi:10.1002/ijc.25059.

[174] H.J. Kwon, J.S. Shim, J.H. Kim, H.Y. Cho, Y.N. Yum, S.H. Kim, J. Yu, Betulinic acid inhibits growth factor-induced in vitro angiogenesis via the modulation of mitochondrial function in endothelial cells., Jpn. J. Cancer Res. 93 (2002) 417–25. http://www.ncbi.nlm.nih.gov/pubmed/11985792.

[175] S.-F. Zhou, Y.-Y. Wang, H. Zhe, Y. Yang, Z. He, Bardoxolone methyl (CDDO-Me) as a therapeutic agent: an update on its pharmacokinetic and pharmacodynamic properties, Drug Des. Devel. Ther. (2014) 2075. doi:10.2147/DDDT.S68872.

[176] D.S. Hong, R. Kurzrock, J.G. Supko, X. He, A. Naing, J. Wheler, D. Lawrence, J.P. Eder, C.J. Meyer, D.A. Ferguson, J. Mier, M. Konopleva, S. Konoplev, M. Andreeff, D. Kufe, H. Lazarus, G.I. Shapiro, B.J. Dezube, A phase I first-in-human trial of bardoxolone methyl in patients with advanced solid tumors and lymphomas, Clin. Cancer Res. 18 (2012) 3396–3406. doi:10.1158/1078-0432.CCR-11-2703.

[177] X. Gao, D. Deeb, Y. Liu, P. Liu, Y. Zhang, J. Shaw, S.C. Gautam, CDDO-Me inhibits tumor growth and prevents recurrence of pancreatic ductal adenocarcinoma, Int. J. Oncol. 47 (2015) 2100–2106. doi:10.3892/ijo.2015.3212.

[178] D. Wang, W. Lu, F. Li, Pharmacological intervention of HIV-1 maturation, Acta Pharm. Sin. B. 5 (2015) 493–499. doi:10.1016/j.apsb.2015.05.004.

[179] S. Safe, R. Kasiappan, Natural Products as Mechanism-based Anticancer Agents: Sp Transcription Factors as Targets, Phyther. Res. 30 (2016) 1723–1732. doi:10.1002/ptr.5669.

[180] D. Sarek, J., Kvasnica, M., Vlk, M., Biedermann, Semisynthetic Lupane Triterpenes with Cytotoxic Activity, in: Pentacyclic Triterpenes as Promis. Agents Cancer Ther., Nova Science Publishers, Inc., 2010.

[181] J. Urban, M., Kvasnica, M., Dickinson, N.J., Sarek, Biologically active triterpenoids usable as prodrugs, in: Terpenoids Squalene Biosynthesis, Funct. Heal. Implic., Nova Science Pub. Inc, 2015.

[182] L. Borkova, L. Jasikova, J. Rehulka, K. Frisonsova, M. Urban, I. Frydrych, I. Popa, M. Hajduch, N.J. Dickinson, M. Vlk, P. Dzubak, J. Sarek, Synthesis of cytotoxic 2,2-difluoroderivatives of dihydrobetulinic acid and allobetulin and study of their impact on cancer cells, Eur. J. Med. Chem. 96 (2015) 482–490. doi:10.1016/j.ejmech.2015.03.068.

[183] L. Borkova, R. Adamek, P. Kalina, P. Dra?ar, P. Dzubak, S. Gurska, J. Rehulka, M. Hajduch, M. Urban, J. Sarek, Synthesis and Cytotoxic Activity of

Triterpenoid Thiazoles Derived from Allobetulin, Methyl Betulonate, Methyl Oleanonate, and Oleanonic Acid, ChemMedChem. 12 (2017) 390–398. doi:10.1002/cmdc.201600626.

[184] M. Urban, J. Klinot, I. Tislerova, D. Biedermann, M. Hajduch, I. Cisarova, J. Sarek, Reactions of Activated Lupane Oxo-Compounds with Diazomethane: An Approach to New Derivatives of Cytotoxic Triterpenes, Synthesis (Stuttg). 2006 (2006) 3979–3986. doi:10.1055/s-2006-950327.

[185] Kameníčková Alžběta, Screening of potential antitumor drugs inducing changing in the cell cycle. Bachelor thesis, Palacký University in Olomouc, 2008.

[186] V. Noskova, P. Dzubak, G. Kuzmina, A. Ludkova, D. Stehlik, R. Trojanec, A. Janostakova, G. Korinkova, V. Mihal, M. Hajduch, In vitro chemoresistance profile and expression/function of MDR associated proteins in resistant cell lines derived from CCRF-CEM, K562, A549 and MDA MB 231 parental cells., Neoplasma. 49 (2002) 418–25. http://www.ncbi.nlm.nih.gov/pubmed/12584592.

[187] P. Kask, H. Maakond, Methods and apparatus for image analysis using threshold compactness features, US 2013/0114874 A1, 2013.

[188] A. Sakaue-Sawano, T. Kobayashi, K. Ohtawa, A. Miyawaki, Drug-induced cell cycle modulation leading to cell-cycle arrest, nuclear mis-segregation, or endoreplication, BMC Cell Biol. 12 (2011) 2. doi:10.1186/1471-2121-12-2.

[189] A. Chan, A.J. Singh, P.T. Northcote, J.H. Miller, Peloruside A, a microtubule-stabilizing agent, induces aneuploidy in ovarian cancer cells, Invest. New Drugs. 34 (2016) 424–438. doi:10.1007/s10637-016-0355-6.

[190] A. Notte, N. Ninane, T. Arnould, C. Michiels, Hypoxia counteracts taxol-induced apoptosis in MDA-MB-231 breast cancer cells: role of autophagy and JNK activation, Cell Death Dis. 4 (2013) e638.

[191] A. Sermeus, M. Genin, A. Maincent, M. Fransolet, A. Notte, L. Leclere, H. Riquier, T. Arnould,, C. Michiels, Hypoxia-induced modulation of apoptosis and BCL-2 family proteins in different cancer cell types., PLoS One. 7 (2012) e47519.

[192] S. Xie, A. Ogden, R. Aneja, J. Zhou, Microtubule-Binding Proteins as Promising Biomarkers of Paclitaxel Sensitivity in Cancer Chemotherapy, Med. Res. Rev. 36 (2016) 300–312. doi:10.1002/med.21378.

[193] X.L. Dong, P.F. Xu, C. Miao, Z.Y. Fu, Q.P. Li, P.Y. Tang, T. Wang, Hypoxia decreased chemosensitivity of breast cancer cell line MCF-7 to paclitaxel through cyclin B1, Biomed. Pharmacother. 66 (2012) 70–75. doi:10.1016/j.biopha.2011.11.016.

[194] Y. Zhu, Y. Zhou, J. Shi, Post-slippage multinucleation renders cytotoxic variation in anti-mitotic drugs that target the microtubules or mitotic spindle, Cell Cycle. 13 (2014) 1756–1764. doi:10.4161/cc.28672.

[195] M. Urban, M. Vlk, P. Dzubak, M. Hajduch, J. Sarek, Cytotoxic heterocyclic

triterpenoids derived from betulin and betulinic acid, Bioorg. Med. Chem. 20 (2012) 3666–3674. doi:10.1016/j.bmc.2012.03.066.

[196] F. Menaa, B. Menaa, O.N. Sharts, Importance of Fluorine and Fluorocarbons in Medicinal Chemistry and Oncology, J. Mol. Pharm. Org. Process Res. 1 (2013) 1–6. doi:10.4172/jmpopr.1000104.

[197] J. Wang, M. Sánchez-Roselló, J.L. Aceña, C. Del Pozo, A.E. Sorochinsky, S. Fustero, V.A. Soloshonok, H. Liu, Fluorine in pharmaceutical industry: Fluorine-containing drugs introduced to the market in the last decade (2001-2011), Chem. Rev. 114 (2014) 2432–2506. doi:10.1021/cr4002879.

[198] E.P. Gillis, K.J. Eastman, M.D. Hill, D.J. Donnelly, N.A. Meanwell, Applications of Fluorine in Medicinal Chemistry, J. Med. Chem. 58 (2015) 8315–8359. doi:10.1021/acs.jmedchem.5b00258.

[199] D. O'Hagan, Fluorine in health care: Organofluorine containing blockbuster drugs, J. Fluor. Chem. 131 (2010) 1071–1081. doi:10.1016/j.jfluchem.2010.03.003.

[200] L. Borkova, S. Gurska, P. Dzubak, R. Burianova, M. Hajduch, J. Sarek, I. Popa, M. Urban, Lupane and 18-oleanane derivatives substituted in the position 2, their cytotoxicity and influence on cancer cells, Eur. J. Med. Chem. 121 (2016) 120–131. doi:10.1016/j.ejmech.2016.05.029.

[201] Y.S. Hong, S.-W. Hong, S.-M. Kim, D.-H. Jin, J.-S. Shin, D.H. Yoon, K.-P. Kim, J.-L. Lee, D.S. Heo, J.S. Lee, T.W. Kim, Bortezomib induces G2-M arrest in human colon cancer cells through ROS-inducible phosphorylation of ATM-CHK1., Int. J. Oncol. 41 (2012) 76–82. doi:10.3892/ijo.2012.1448.

[202] K. Qian, S.-Y. Kim, H.-Y. Hung, L. Huang, C.-H. Chen, K.-H. Lee, New betulinic acid derivatives as potent proteasome inhibitors., Bioorg. Med. Chem. Lett. 21 (2011) 5944–7. doi:10.1016/j.bmcl.2011.07.072.

[203] M.A. Dickson, G.K. Schwartz, Development of cell-cycle inhibitors for cancer therapy, Curr. Oncol. 16 (2009) 36–43. doi:10.1111/j.1582-4934.2009.00876.x.

[204] J. Wang, Z. Guo, Y. Fu, Z. Wu, C. Huang, C. Zheng, P.A. Shar, Z. Wang, W. Xiao, Y. Wang, Weak-binding molecules are not drugs?—toward a systematic strategy for finding effective weak-binding drugs, Brief. Bioinform. 18 (2016) bbw018. doi:10.1093/bib/bbw018.

VII.   PUBLICATION LIST

Original research articles

J. Rehulka, N. Annadurai, I. Frydrych, P. Znojek, P. Dzubak, P. Northcote, J.H. Miller, M. Hajduch, V. Das, Cellular effects of the microtubule-targeting agent peloruside A in hypoxia-conditioned colorectal carcinoma cells, Biochim. Biophys. Acta - Gen. Subj. (2017). doi:10.1016/j.bbagen.2017.03.023. IF: 5.083

L. Borkova, R. Adamek, P. Kalina, P. Drasar, P. Dzubak, S. Gurska, **J. Rehulka**, M. Hajduch, M. Urban, J. Sarek, Synthesis and cytotoxic activity of triterpenoid thiazoles derived from allobetulin, methyl betulonate, methyl oleanonate, and oleanonic acid, ChemMedChem. 12 (2017) 390–398. doi:10.1002/cmdc.201600626. IF: 2.980

L. Borkova, L. Jasikova, **J. Rehulka**, K. Frisonsova, M. Urban, I. Frydrych, I. Popa, M. Hajduch, N.J. Dickinson, M. Vlk, P. Dzubak, J. Sarek, Synthesis of cytotoxic 2,2-difluoroderivatives of dihydrobetulinic acid and allobetulin and study of their impact on cancer cells, Eur. J. Med. Chem. (2015). doi:10.1016/j.ejmech.2015.03.068. IF: 3.432

T. Ozdian, D. Holub, Z. Maceckova, L. Varanasi, G. Rylova, **J. Rehulka**, J. Vaclavkova, H. Slavik, P. Moudry, P. Znojek, J. Stankova, J.B. de Sanctis, M. Hajduch, P. Dzubak, Proteomic profiling reveals DNA damage, nucleolar and ribosomal stress are the main responses to oxaliplatin treatment in cancer cells. J Proteomics. (2017) doi: 10.1016/j.jprot.2017.05.005. IF: 3.867

Poster presentations

J. Řehulka, M. Urban, P. Džubák, M. Hajdúch, Derivatives of betulinic acid inducing the mitotic arrest in cancer cells. CIMST Summer School of Bio-medical Imaging, 5.-16. 9. 2011 , ETH Curych, Switzerland.

Oral presentations

J. Řehulka, M. Urban, P. Džubák, M. Hajdúch, Multifaceted properties of betulinic acid derivatives. In: *XII. Diagnostic, Predictive and Experimetnal Oncology Days: Abstract Book*. 30.11.-.12. 2016, Olomouc.

J. Řehulka, J. Hlaváč, I. Frydrych , P. Džubák, M. Hajdúch, New quinolone fluoroderivatives with specific antitumour effect. In: *XI. Diagnostic, Predictive and Experimetnal Oncology Days: Abstract Book*. 2.12.-3.12. 2015, Olomouc.

J. Řehulka, L. Borková, M. Urban, I. Frydrych, J. Šarek, P. Džubák, M. Hajdúch, Novel triterpenoid fluoroderivatives with anticancer activity. In: *X. Diagnostic, Predictive and Experimetnal Oncology Days: Abstract Book*. 2.12.-3.12. 2014, Olomouc.

J. Řehulka, M. Urban, N.J. Dickinson, D. Holub, P. Džubák, M. Hajdúch, Identifikace molekulárního cíle pomocí metabolického značení SILAC. In: *IX. Diagnostic, Predictive and Experimetnal Oncology Days: Abstract Book*. 21.11.-22.11.2013, hotel NH Congress, Olomouc, 2013, A36-A37.

J. Řehulka, M. Urban, I. Frydrych, J. Šarek, P. Džubák, M. Hajdúch, Deriváty kyseliny betulinové inhibují aktivitu transkripčních faktorů GLI a proliferaci nádorové linie glioblastomu. In: *Chemické listy: XIII Mezioborové setkání mladých biologů, biochemiků a chemiků*. 14.5.-17.5.2013, Źďár nad Sázavou, 2013, 107, 435. ISSN 0009-2770.

J. Řehulka, P. Džubák, I. Frydrych, P. Krejčí, M. Soural, M. Hajdúch, Novel fluoroquinolone-derived compounds inhibits tubulin polymerization. In: *Biomedical Papers of the Medical Faculty of the University Palacký, Olomouc, Czech Republic*, 2012, **156**(Supplement 3), 118. ISSN 1213-8118.

J. Řehulka, I. Frydrych, P. Džubák, A. Benedíková, V. Menšíková, S. Purová, M. Urban, J. Šarek, M. Hajdúch, Deriváty kyseliny betulinové inhibují Gli1/2 zprostředkovanou proliferaci glioblastomu. In: *VIII. dny diagnostické, prediktivní a experimentální onkologie. Onkologie.* 2012, **6**, Suppl. B, B25. ISSN 1802-4475.

J. Řehulka, P. Džubák, I. Frydrych, P. Krejčí, M. Soural, M. Hajdúch, Selekce účinných 4-chinolonů s protinádorovou aktivitou a studium mechanizmu jejich účinku. In: *VII. dny diagnostické, prediktivní a experimentální onkologie. Onkologie*. 2011, **5**, Suppl. B, B17. ISSN 1802-4475.

J. Řehulka, P. Džubák, I. Frydrych, J. Šarek, M. Hajdúch, Induction of Mitotic Arrest and Apoptosis by Betulinic Acid Derivatives. In: *Biomedical papers of the Medical Faculty of the University Palacký, Olomouc, Czechoslovakia*. 2011, **155**(4),S6. ISSN 1213-8118. Vyškov, 26.11. 2011.

J. Řehulka, P. Džubák, D. Holub, T. Oždian, A. Kameníčková, P. Konečný, M. Urban, I. Frydrych, S. Šálková, J. Šarek, M. Kvasnica, M. Vlk, M. Hajdúch, Diverse groups of triterpenoid compounds derived from betulinic acid rapidly inducing apoptosis and G2/M block. In: *VI. dny diagnostické, prediktivní a experimentální onkologie. Onkologie*. 2010, **4**, Suppl.A., 24. ISSN 1803-5922.

VIII. SUPPLEMENT

Cellular effects of the microtubule-targeting agent peloruside A in hypoxia-conditioned colorectal carcinoma cells

Cellular effects of the microtubule-targeting agent peloruside A in hypoxia-conditioned colorectal carcinoma cells

Jiří Řehulka[a], Narendran Annadurai[a], Ivo Frydrych[a], Pawel Znojek[a], Petr Džubák[a], Peter Northcote[b], John H. Miller[c], Marián Hajdúch[a], Viswanath Das[a,*]

[a] Institute of Molecular and Translational Medicine, Faculty of Medicine and Dentistry, Palacký University, Hněvotínská 5, 77900 Olomouc, Czech Republic
[b] Schools of Chemical and Physical Sciences, Victoria University of Wellington, Wellington, New Zealand
[c] Biological Sciences, Victoria University of Wellington, Wellington, New Zealand

A R T I C L E   I N F O

A B S T R A C T

Background: Hypoxia is a prominent feature of solid tumors, dramatically remodeling microtubule structures and cellular pathways and contributing to paclitaxel resistance. Peloruside A (PLA), a microtubule-targeting agent, has shown promising anti-tumor effects in preclinical studies. Although it has a similar mode of action to paclitaxel, it binds to a distinct site on β-tubulin that differs from the classical taxane site. In this study, we examined the unexplored effects of PLA in hypoxia-conditioned colorectal HCT116 cancer cells.
Methods: Cytotoxicity of PLA was determined by cell proliferation assay. The effects of a pre-exposure to hypoxia on PLA-induced cell cycle alterations and apoptosis were examined by flow cytometry, time-lapse imaging, and western blot analysis of selected markers. The hypoxia effect on stabilization of microtubules by PLA was monitored by an intracellular tubulin polymerization assay.
Results: Our findings show that the cytotoxicity of PLA is not altered in hypoxia-conditioned cells compared to paclitaxel and vincristine. Furthermore, hypoxia does not alter PLA-induced microtubule stabilization nor the multinucleation of cells. PLA causes cyclin B1 and G2/M accumulation followed by apoptosis.
Conclusions: The cellular and molecular effects of PLA have been determined in normoxic conditions, but there are no reports of PLA effects in hypoxic cells. Our findings reveal that hypoxia preconditioning does not alter the sensitivity of HCT116 to PLA.
General significance: These data report on the cellular and molecular effects of PLA in hypoxia-conditioned cells for the first time, and will encourage further exploration of PLA as a promising anti-tumor agent.

1. Introduction

Microtubules (MTs) play a critical role in mitotic and non-mitotic functions of a cell, making them an attractive target for cancer therapy. Paclitaxel (PTX) and vincristine (VCR) are two classical MT-targeting agents (MTAs) extensively used in the clinic for the treatment of different solid tumor types. MTAs alter the dynamics of MTs and cause mitotic arrest followed by apoptosis and cell death in actively dividing cells [1]. In solid tumors, however, MTA-induced cytotoxicity is presumed to result from the alteration of non-mitotic functions of MTs [2–4].

Hypoxia in solid tumors is caused by high interstitial pressure and a poor blood supply that then initiates angiogenesis and the formation of abnormal blood vessels [5]. These changes ultimately lead to low nutrient and oxygen levels in the distal regions of tumors. Oxygen homeostasis in cells is tightly controlled by hypoxia-inducible factor-1 (HIF-1), a key transcriptional regulator of hypoxia. Under normoxic conditions, HIF-1α, one of the subunits of HIF-1, is rapidly degraded in the proteasome. However, in hypoxic conditions, translocation of HIF-1α into the nucleus, followed by dimerization with HIF-1β, results in the activation and alteration of a number of pathways that assist in cell survival [6]. Reprogramming of cellular metabolic pathways by HIF-1 is one of the other typical adaptive hallmarks of malignant cells in solid tumors in response to altered oxygen tension [7,8]. Moreover, the interplay between HIF-1 and p53, which is frequently mutated in cancers, further ameliorates the effect of hypoxia-induced metabolic changes [9]. Recent studies further reveal the role of metabolic enzymes and their substrates in reciprocal regulation of HIF activity

in solid tumors, indicating the complexity of HIF-1 activity in the progression of the disease [7,10].

Hypoxia also promotes the emergence of more aggressive tumor phenotypes with enhanced metastatic potential and altered susceptibility to anti-mitotic drugs [11]. Upregulation of HIF-1α has been shown to significantly impact the sensitivity of tumor cells to PTX under different experimental conditions [12–15]. Interestingly, not all MTAs are prone to HIF-1α-mediated resistance, as docetaxel has been reported to retain its cytotoxic effects in prostate cancer cells under hypoxia [16]. This ability of docetaxel and other MTAs, such as epothilone B and discodermolide, to retain cytotoxicity in hypoxic tumor cells results from their ability to disrupt MT-mediated nuclear translocation of HIF-1α [16,17]. Although several studies have linked hypoxia to MTA resistance, the role of the complex network of pathways activated and/or altered in hypoxia in the development of resistance to MTAs remains debatable [6].

Recent studies have shown significant anti-tumor effects of peloruside A (PLA), a marine sponge-derived MTA, in mitotic and non-mitotic cells [reviewed in 18]. Although PLA has a similar mode of action of MT stabilization to PTX, it binds to a distinct site on β-tubulin that differs from the PTX binding site [18]. Given the fact that hypoxia dramatically remodels MTs [19,20], we speculated that there might be differences in the effects of PLA and PTX on hypoxia-conditioned (HC) MTs. Moreover, PLA is not a good substrate of P-glycoprotein [21,22], a downstream target of HIF-1, making it a potential candidate for the treatment of hypoxic tumors alone or in combination with other MTAs that are susceptible to drug efflux pumps. While mechanisms that contribute to PLA resistance under normoxic conditions are known [18], no information exists on the activity of PLA in hypoxic and/or HC tumor cell lines. Therefore, in this study, we investigated the cellular effects of PLA in HC colorectal HCT116 cells, and show improved effects of PLA in HC cells over the classical MT targeting drug, PTX.

2. Materials and methods

2.1. Compounds and reagents

PLA was isolated and purified as described previously [23]. PTX (Taxol®) was purchased from Bristol-Myers Squibb Company (New York City, NY), and VCR sulphate from Teva Czech Industries s.r.o. (Komarov, Czech Republic). Unless otherwise mentioned, all reagents were purchased from Sigma-Aldrich (Prague, Czech Republic).

2.2. Cell lines, hypoxic induction and drug treatment

The human colon cancer cells HCT116 and HT-29 were purchased and maintained as described elsewhere [24]. Human cervical cancer HeLa cells expressing the *Fluorescence Ubiquitination Cell-Cycle Indicator* (FUCCI) were obtained from RIKEN (Japan), and maintained as described previously [25,26].

Hypoxic conditions were established by culturing cells in a Heracell 150i humidified incubator (Thermo Fisher Scientific, Waltham, MA) at 37 °C/1% O_2, 94% N_2 and 5% CO_2 levels. Unless mentioned specifically, all drug treatments following hypoxia preconditioning of cells were performed under normoxic conditions of 5% CO_2/atmospheric air at 37 °C in a standard humidified incubator.

2.3. HIF-1α lentiviral infection

HCT116 were transduced with ready-to-use HIF-1α lentiviral particles (AMS Biotechnology, Oxfordshire, UK) following the manufacturer's instructions. Transduction was performed at a multiplicity of infection of 25. RFP-fluorescent-transduced cells were sorted via flow cytometry and selected for 3 weeks in medium containing 5 μg/mL blasticidin. All infections were performed in the presence of 8 μg/mL Polybrene Infection/Transfection Reagent (Merck Millipore, Billerica,

MA), and carried out in Bio-safety II cabinets.

HCT116 cells not transfected with HIF-1α will hereafter be referred to as parental cells, whereas those transduced with HIF-1α lentiviral particles will be referred to as HIF-1α cells.

2.4. Cell viability assay

Cells were seeded in 96-well plates and cultured overnight in a standard CO_2 incubator. The next day, the cells were subjected to hypoxia for 0 h, 4 h, or 24 h. Following hypoxia exposure, cells were treated with drugs for 72 h in normoxia. Cell viability was then determined by an MTT cell viability assay as described elsewhere [27]. The IC_{50} values of MTAs were determined from their respective concentration-response curves using GraphPad Prism (GraphPad Software, San Diego, CA).

2.5. Intracellular tubulin polymerization assay

Normoxic (NRX) cells, and 4 h and 24 h HC cells were treated with MTAs for 16 h and processed for soluble and polymerized tubulin extraction as described previously [28].

2.6. Flow cytometry and western blot analysis

Cells were harvested, fixed in ice-cold 70% ethanol, and processed for flow cytometry as described previously [29]. Western blot analysis was performed as described elsewhere [27]. All antibodies used in the study are listed in Table 1.

2.7. HeLa-FUCCI and time-lapse imaging

HeLa-FUCCI cells in 384-well plates (Plate type: CellCarrier; PerkinElmer, Waltham, MA) were first subjected to 4 h and 24 h hypoxia. Immediately following hypoxia, but before drug treatment, cells were imaged in a CellVoyager™ CV7000 High-throughput Cytological Discovery System (Yokogawa Electric Corporation, Musashino, Tokyo, Japan) using a 20 × objective. NRX and HC cells were then treated with MTAs using an automatic liquid handler (Echo 555; Labcyte, Sunnyvale, CA), and the imaging was continued for 24 h at an interval of 2 h in a humidified atmosphere of 5% CO_2/air/37 °C. Geminin-mAG (green) and Cdt1-mKO2 (red) fluorescent proteins were excited by 488 nm and 561 nm laser lines, and their emission signals

Table 1
List of antibodies used.

Antibody name	Supplier	Cat. Num.
Acetylated-α-tubulin	Cell Signaling Technologies, Danvers, MA	5335
p21$^{Waf1/Cip1}$	Cell Signaling Technologies, Danvers, MA	2947
Total pRb	Cell Signaling Technologies, Danvers, MA	9309
Phospho. pRb (Ser795)	Cell Signaling Technologies, Danvers, MA	9301
Caspase-3	Bio-Techne Corporation, Minneapolis, MN	NB100-56708SS
Caspase-8	Bio-Techne Corporation, Minneapolis, MN	NB100-56527SS
Cyclin D1	Merck Millipore, Billerica, MA	CC12
p53	Abcam, Cambridge, UK	ab131442
HIF-1α	Abcam, Cambridge, UK	ab16066
β-actin	Sigma-Aldrich	A2228
α-tubulin	Sigma-Aldrich	T5168
Cyclin B1	Sigma-Aldrich	C8831
Anti-mouse Alexa Fluor 488	Thermo Fisher Scientific, Waltham, MA	A-21202
Anti-rabbit Alexa Fluor 488	Thermo Fisher Scientific, Waltham, MA	A-21206

2

were collected using 515/30 nm and 595/40 nm band pass filters, respectively. The exposure time for both channels was set to 500 ms.

Captured images were exported to Columbus™ Image Analysis Software for analysis (version 2.7.1; PerkinElmer). The red and green channels were merged to create a third temporary channel, which was used in the next analysis step for determination of the segmentation of nuclei and measurement of mean fluorescence intensity of each channel separately for a selected cell. To assess the distribution of cell-cycle phases, a scatter plot of mean fluorescent intensities of Cdt1-mKO2 (red) was plotted against Gem-mAG (green). The plot was then divided into three different areas, and the percentage of cells in each area was calculated. Following cell-cycle recording, phase selection criteria were applied: cells with mean fluorescent intensities in the red channel > 320 and green channel < 320 were assessed as G1-phase cells, G1/S-phase cells (red > 320 and green > 320) and S/G2/M-phase cells (red < 450 and green > 320). Cell roundness was calculated using the formula: R = [area × π × (perimeter)^2]/4. Perfectly round cells were presumed to have an R = 1. Threshold compactness (TrCom), a measure of the multinucleation of cells, was calculated following the method described by P. Kask [30]. A low TrCom value indicates a multinucleated cell [30].

2.8. Statistical analysis

All statistical analyses were carried out in GraphPad Prism, and results were considered significant at $p \leq 0.05$. Unless otherwise stated, data were analyzed by one-way Anova with Tukey's multiple comparison test, and are presented as the mean ± SEM.

3. Results

3.1. Hypoxia modulates sensitivity of HCT116 cells to PTX, but not PLA and VCR

To determine whether hypoxia preconditioning affects the sensitivity to PLA, parental cells were first exposed to hypoxia for 4–24 h and then treated with PLA in normoxia for 72 h. Cell proliferation assay data showed that there was no difference in the cytotoxicity of PLA in HC cells (Fig. 1A, C). To confirm the above findings, we performed a similar cytotoxicity assay in HC HIF-1α cells following PLA treatment. Similar to parental cells, there was no difference in the cytotoxicity of PLA in HIF-1α cells (Fig. 1B, C). In contrast to PLA, the IC$_{50}$ of PTX significantly increased in 24 h HC parental and HIF-1α cells (Fig. 1A–C). Although hypoxia did not alter the cytotoxicity of VCR in the parental cells, 24 h HC HIF-1α cells were less sensitive to VCR than NRX cells (Fig. 1C). It is interesting to note that the cytotoxic efficacy of PTX and VCR is greater than PLA in both cell lines, whether hypoxic-conditioned or not. Similar to HCT116 cells, hypoxia preconditioning did not alter the cytotoxicity of PLA or VCR in HT-29 cells but decreased their sensitivity to PTX (Fig. 1D).

To confirm that the above alterations were distinct to hypoxia, we examined the expression of HIF-1α in both HCT116 cell types immediately following 4 h and 24 h hypoxia exposure. Fig. 1E shows a significant upregulation of HIF-1α protein in parental and HIF-1α cells (Fig. 1E). Furthermore, flow cytometry analysis showed that 35–50% of cells were in G1 cell cycle phase following 24 h hypoxia (Fig. 1F). Extended culture of these cells for 16 h in normoxia reversed the G1 block to normal (see below).

3.2. Increase in G2/M cell cycle arrest of HC cells following PLA exposure

To examine if hypoxia preconditioning altered the PLA effect on the cell cycle, NRX and HC cells treated with PLA, PTX, and VCR for 16 h were analyzed by flow cytometry. Unlike cells immediately following hypoxia (Fig. 1F), untreated HC cells returned to a normal cell cycle distribution similar to NRX cells following 16 h incubation in normoxia

(Fig. 2A). Compared to untreated cells in either NRX or HC cultures, PLA, PTX (at 2 nM only in NRX HIF1α cells), and VCR significantly increased the percentage of G2/M cells (Fig. 2B). Interestingly, however, PLA at 200 nM resulted in the accumulation of 65% of parental cells in G2/M; however, this accumulation significantly increased to 78%, with a corresponding decrease in S cells in 4 h HC cells (Fig. 2C). Likewise, there was an increase in G2/M accumulation of HC HIF-1α cells following treatment with 200 nM PLA. However, there was no difference in the effect of PLA at a high 2 μM concentration on the percentage of G2/M cells in HC cells compared to NRX (Fig. 2C). Unlike PLA, there was no difference in the effect of PTX and VCR at any of the tested concentrations between NRX and HC cells (Fig. 2D, E).

3.3. Cell sensitivity to PLA is unaffected by hypoxia-induced changes in cell cycle regulatory proteins

Cyclin B1, a key regulator of the G2/M transition is downregulated by hypoxia [12]. A decreased expression level of cyclin B1 has been associated with reduced sensitivity of MCF-7 breast cancer cells to PTX [12,31]. Therefore, we next examined the alteration in cyclin B1 levels in HC cells to determine their potential role in sensitivity to PLA in HC cells. Hypoxia preconditioning resulted in downregulation of cyclin B1 in untreated cells as reported previously [12]. In accordance with mitotic accumulation, there was an increase in cyclin B1 levels in NRX cells (Fig. 3A) and a decreased accumulation of cyclin B1 in HC cells at each concentration of the MTAs following 16 h of treatment. However, in HC cells, this level was relatively high following PLA treatment when compared to cyclin B1 levels in PTX- and VCR-treated HC cells.

In addition to cyclin B1, hypoxia-induced alteration of other cell cycle regulatory proteins is linked to decreased sensitivity of cancer cells to taxanes [Reviewed in 6,32]. Hypoxia preconditioning resulted in a p21$^{WAF1/CIP1}$ (p21)-independent downregulation of cyclin D1 and hypophosphorylation of retinoblastoma protein (pRb) in both parental and HIF-1α cells (Fig. 3B). In addition to hypophosphorylation of pRb, there was a decrease in the level of total pRb. Overexpression of HIF-1α on its own did not affect cyclin D1 expression in untreated HIF-1α cells under NRX conditions. However, subjecting these cells to hypoxia before drug treatment affected cyclin D1 levels, consistent with a previous report that showed negative regulation of cyclin D1 by HIF-1 in hypoxia [33].

Interestingly, PLA (200 nM) reversed hypoxia preconditioning-induced hypophosphorylation of pRb in HC cells, presumably by preventing the downregulation of cyclin D1 (Fig. 3B). A similar effect was seen following 20 nM PTX treatment in 24 h HC parental cells. Although VCR increased cyclin D1 levels in 24 h HC HIF-1α cells, VCR had no effect on pRb phosphorylation. Although p21 upregulation is known to effect cyclin D1 expression [34], there was no effect of MTA-mediated upregulation of p21 on cyclin D1 levels in HC HIF-1α cells. Moreover, this induction of p21 was also independent of p53 (see Fig. 4).

3.4. PLA results in mitotic cell rounding and an increase in the number of multinucleated of cells

To understand the effects of PLA at single cell level in real time, we performed time-lapse imaging of HeLa-FUCCI cells over 24 h of MTA treatment following hypoxia preconditioning for 0–24 h. MTAs have been reported to induce abnormal fluorescence in HeLa-FUCCI [35], and we noticed a similar abnormal fluorescence that affected the precise characterization of cell cycle phase distribution (data not shown). To overcome this limitation, we determined mitotic cell rounding (MCR) and TrCom as a measure of the number of mitotic cells and multinucleation, respectively, following MTA treatment [30,36]. Similar to the cell cycle data, PLA at 200 nM caused an increased MCR in 24 h HC HeLa-FUCCI cells, consistent with the accumulation of cells in G2/M of the cell cycle following PLA treatment

3
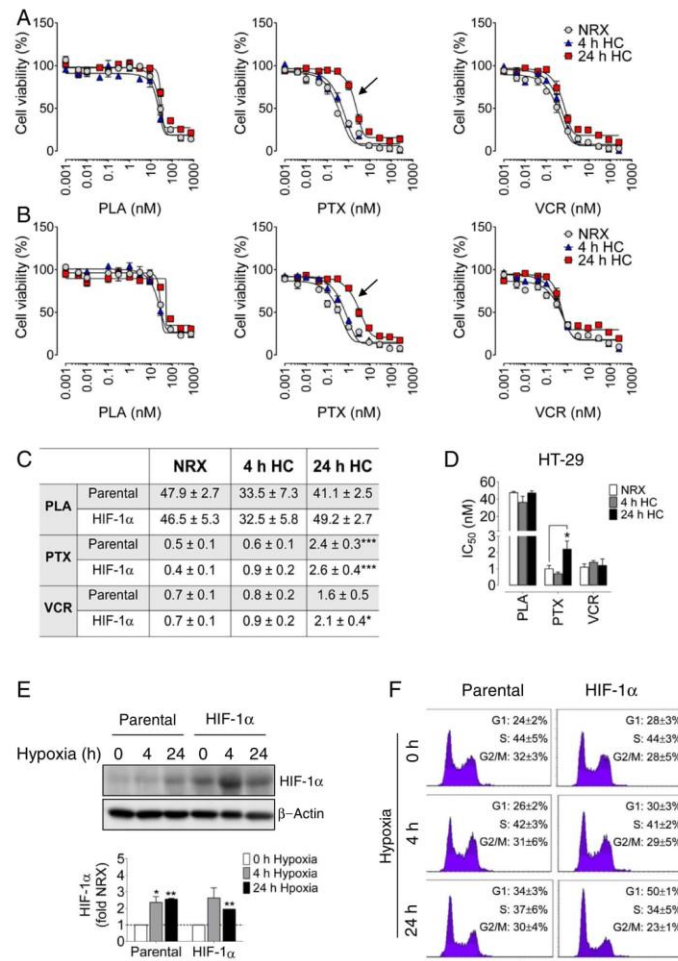
Fig. 1. Cytotoxicity of PLA is not affected by hypoxia. Representative concentration-response curves of PLA, PTX, and VCR in NRX and 4 h and 24 h HC parental (A) and HIF-1α (B) HCT116 cells are shown. Arrows show a significant right-shift in the concentration-response curves of PTX in parental and HIF-1α cells pre-exposed to 24 h hypoxia. (C) Averaged IC$_{50}$ concentrations (nM) of PLA, PTX, and VCR in HCT116 parental and HIF-1α cells are presented. Sensitivity to PTX is significantly decreased in 24 h HC cells compared to NRX cells. VCR is less cytotoxic only in 24 h HC HIF-1α cells. ***$p < 0.001$, *$p < 0.05$ comparing 4 h and 24 h HC to NRX, $n = 4$–5. (D) Averaged IC$_{50}$ values in HT-29 cells following hypoxia pre-exposure of cells. *$p < 0.05$, $n = 3$. (E) HIF-1α protein levels in parental and HIF-1α cells following 4 h and 24 h hypoxia. Bar graph showing the change in HIF1α level relative to NRX. **$p < 0.01$, *$p < 0.05$ compared to NRX set to 1, $n = 2$, one-sample t-test. (F) Flow cytometry analysis of cells in (E) showed an increase in G1 cells following 24 h hypoxia. Data are from 2 to 3 independent experiments.Note that cells in (E) and (F) were analyzed immediately following hypoxia exposure without any additional incubation in normoxia.

(Fig. 4A). In contrast, hypoxia preconditioning significantly affected MCR following PTX (6.25 nM) treatment in 4 h and 24 h HC cells compared to NRX cells. There was no difference in the effect of VCR on MCR in NRX and HC cells. It is also interesting to note that HC cells treated with PTX and VCR appeared to spend a longer time in a 'rounded' state than PLA-treated HC cells (see less steep slope at 16 h and 24 h in Fig. 4A indicated by arrowheads).

Although there was no difference in the effect of PLA on multi-

nucleation of HC and NRX cells, the multinucleation effect was more pronounced in PLA- than PTX- and VCR-treated cells (Fig. 4A, B). Hypoxia preconditioning, however, significantly affected PTX-induced multinucleated cell formation (Fig. 4A, left panel). Hypoxia on its own resulted in a decrease in MCR (Fig. 4C). In addition to an MCR reducing effect, hypoxia preconditioning also resulted in an increase in multi-nucleation of HeLa-FUCCI cells (Fig. 4C).

Since both mitosis and apoptosis are associated with rounding of

4

Fig. 2. PLA alters the cell cycle of hypoxia preconditioned HCT116 cells. (A) NRX and HC untreated cells after 16 h in normoxia. $n = 4$. (B) Table showing p-values of statistical comparisons between drug-treated and untreated cells in NRX, 4 h HC and 24 h HC cultures of parental and HIF-1α cells. ns – not significant. (C-E) Significant G2/M accumulation of HC cells fo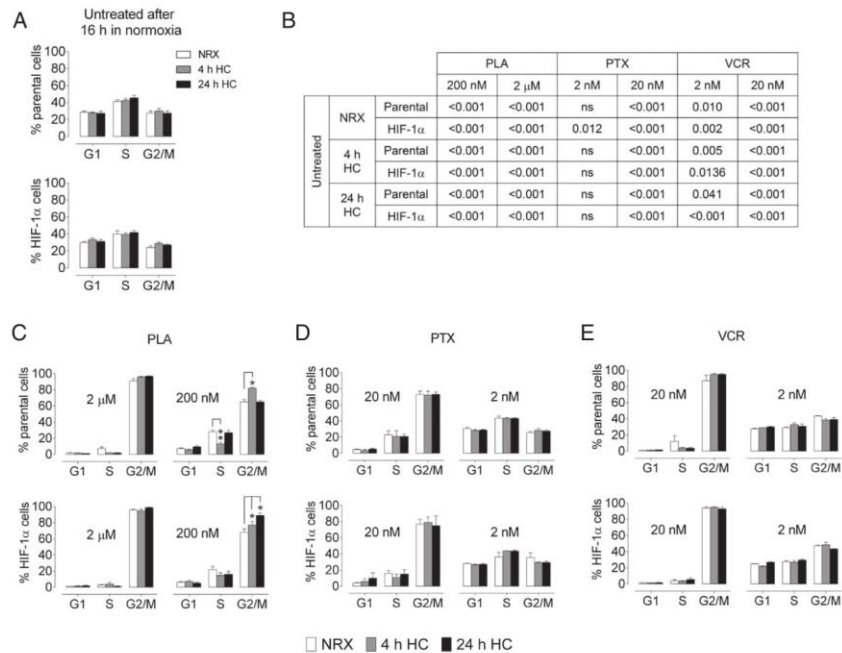llowing 200 nM PLA (B), but not PTX (C) or VCR (D) treatment. Cells were treated with the indicated concentrations of drugs for 16 h in normoxia. $^{**}p < 0.051$, $^*p < 0.05$ compared to NRX cells, $n = 2$–4.

cells [37], we next determined whether rounding of HeLa-FUCCI cells following MTA treatment was specific to mitotic accumulation and not apoptosis-associated. NRX cells were pretreated for 2 h with 50 μM Z-VAD-FMK, a pan-caspase inhibitor, which is reported to prevent apoptosis in HeLa and other cancer cells [38,39]. Following Z-VAD-FMK treatment, cells were treated with 200 nM PLA, 20 nM PTX, and 20 nM VCR for 24 h in normoxia. Fig. 4D shows that pretreatment with Z-VAD-FMK did not affect rounding of HeLa-FUCCI cells following MTA treatment, indicating that the observed cell rounding was specific to the anti-mitotic effects of MTAs. A similar effect was observed in HCT116 cells (data not shown).

Studies indicate that multinucleation induces a p53-mediated DNA damage response to trigger apoptosis in cells that slip out of MTA-induced mitotic arrest [40,41]. To examine this, we analyzed p53 levels following MTA treatment in HCT116 parental and HIF-1α cells. Although there was no induction of p53 following PLA and PTX treatment in NRX cells, a slight increase in p53 was evident in 24 h HC HIF-1α cells treated with MTA in comparison to untreated cells (Fig. 4E).

3.5. Hypoxia preconditioning does not alter sensitivity of MTs towards PLA

Yoon et al. [42] report that hypoxia stimulates cancer cell invasion by stabilization of MTs. To determine how PLA affected stabilization of MTs in HC cells, changes in acetylated-α-tubulin (Ac-α-tubulin) levels were analyzed following 16 h of PLA treatment (Fig. 5A). There was a non-significant upregulation of Ac-α-tubulin levels in HC parental cells

following PLA treatment (Fig. 5B). However, and in contrast, hypoxia preconditioning significantly abrogated PTX-induced tubulin acetylation in parental (at 20 nM only) and HIF-1α cells. As expected, VCR, a destabilizing agent, did not increase the percentage of Ac-α-tubulin in NRX or HC cells.

Hypoxia-induced alteration of MT conformation has been reported to decrease polymerization of tubulin in conditions of 0–1% O_2 [reviewed in 43]. Therefore, we tested whether hypoxia preconditioning could prevent PLA-induced intracellular polymerization of tubulin in parental and HIF-1α cells (Fig. 5C). Similar to previous reports, hypoxia preconditioning significantly reduced polymerized tubulin levels in untreated cells (Fig. 5D). Although PLA and PTX had comparable levels of polymerized tubulin in NRX parental cells, hypoxia preconditioning significantly affected PTX-mediated tubulin polymerization in both parental and HIF-1α cells (Fig. 5D). HIF-1α overexpression on its own without hypoxia preconditioning did not alter PLA polymerization of tubulin. However, in normoxic conditions, polymerized tubulin fractions were slightly, but significantly, reduced in HIF-1α cells compared to parental cells following PTX treatment (Fig. 5E). Soluble tubulin levels in VCR-treated cells were unaffected by hypoxia (data not shown).

Next, we treated cells with PLA and PTX for 16 h in continuous hypoxia to determine the sensitivity of cells to drugs in a hypoxic environment. In contrast to PTX, there was significant increase in the level of polymerized tubulin following PLA treatment, further confirming that PLA activity is not altered in hypoxic conditions (Fig. 5F).
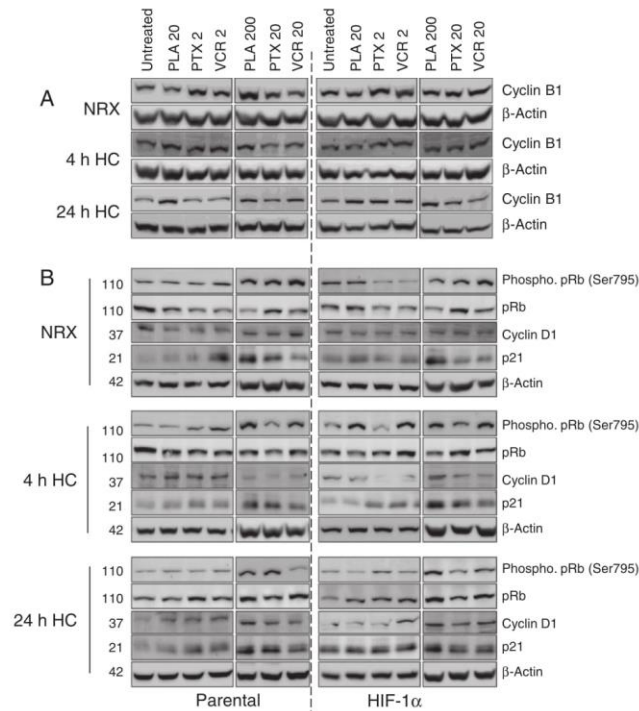
Fig. 3. Alterations in cell cycle-specific markers in HC cells following PLA treatment. (A) Hypoxia preconditioning-induced decrease in cyclin B1 levels is partially restored in cells treated with PLA for 16 h. (B) Immunoblots showing altered expression of other cell cycle-associated proteins in NRX and HC cells following treatment with the indicated concentrations of MTAs. Parental and HIF-1α blots are from different gels. Rb and phosphorylated pRB [Phospho. pRb (Ser795)] were stained in separate blots. Molecular weights of proteins in kDa are indicated next to their respective blots on the left. Western blots in A and B are representative of 3–4 independent experiments.

3.6. PLA induces apoptosis in HC cells

One of the biological roles of HIF-1α in a hostile environment is to activate survival mechanisms by altering cell apoptotic pathways that have been well-reported to abrogate apoptosis induced by PTX and other anticancer drugs [14,44,45]. To determine hypoxia effects on apoptosis of cells following PLA treatment, we examined the cleavage of caspase-8 and -3 proteins by western blot (Fig. 6A, B). Hypoxia on its own and lower concentrations of MTAs did not result in the activation of caspases in NRX and HC cells. However, 200 nM PLA resulted in the activation of apoptosis in HC cells, as can be seen by the cleavage of caspase-3 and -8 in Fig. 6A and B, indicating that hypoxia does not alter PLA-triggered cell apoptosis. In contrast, hypoxia affected the activation of caspases following PTX treatment, which was consistent with previous studies. There was no effect of hypoxia on VCR-mediated caspase activation. Although there were only faint caspase-8 cleaved bands in 4 h HC VCR-treated cells, the activation was presumably sufficient to induce full downstream activation of capase-3 (Fig. 6A, B, middle panel).

To quantify the percentage of HC cells undergoing apoptosis, we performed flow cytometry analysis of PLA-treated cells. Cells were treated with the higher concentrations of MTAs for these flow cytometry studies (Fig. 6C). Similar to the western blot results, we noticed no significant difference in the ability of PLA to induce apoptosis in HC cells compared to NRX cells. However, 4 h hypoxia preconditioning significantly affected the PTX-induced apoptosis in both cell lines. As above, hypoxia preconditioning had no effect on the number of cells undergoing VCR-induced apoptosis.

4. Discussion

MTAs are important therapeutic interventions in cancer therapy; however, their efficacy is often limited by hypoxia and hypoxia-associated alterations in solid tumors [6]. In the last 15 years, PLA has generated significant interest due to its potential therapeutic activity against cancer, tauopathy, and multiple sclerosis [18]. Furthermore, recent studies have shown that PLA inhibits endothelial cell migration at a concentration that is significantly less than the concentration required for antimitotic effects [2,46]. The pioneering work of Northcote and Miller et al. [18] over the last 5 years have significantly contributed to the rational development of PLA as a promising anti-tumor drug [22]. However, given the vast implications of hypoxia in MTA-directed therapy, understanding the effects of PLA in hypoxia will immensely contribute to its progression from bench to bedside. Our data show that pre-exposure to hypoxia has no effect on the suscept-ibility of parental and HIF-1α-expressing HCT116 cells to PLA. In
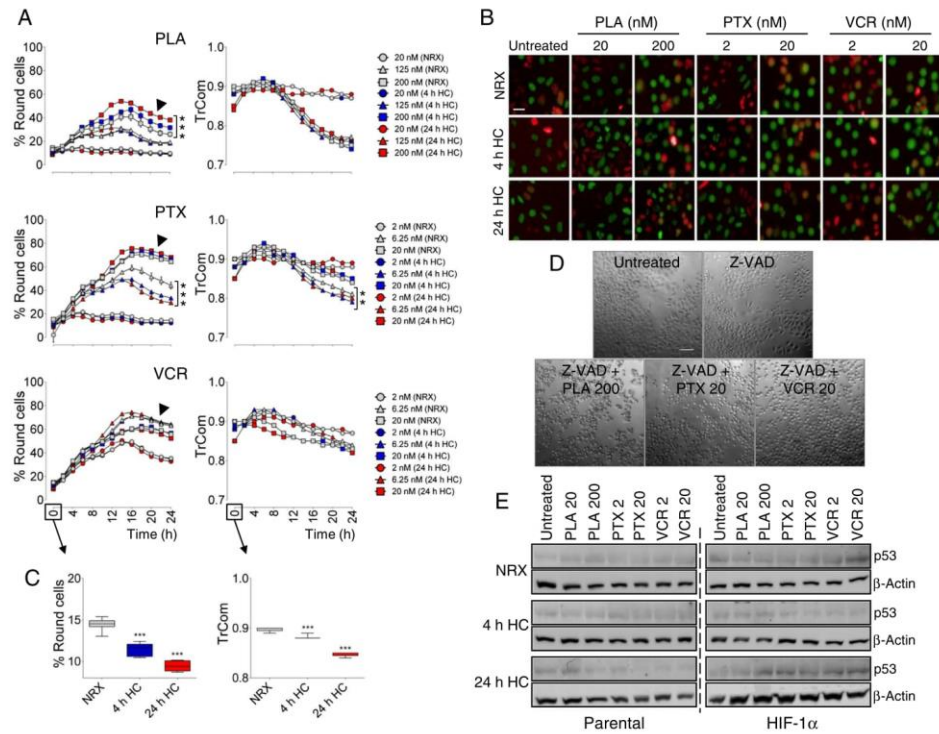
Fig. 4. PLA-induced increased rounding of HeLa-FUCCI cells. Analysis of percent rounded cells, a measure of mitotic cell rounding (MCR), and TrCom, a measure of cell multinucleation, in NRX and hypoxia-conditioned HeLa-FUCCI cells following MTA treatment. (A, right panel) PLA treatment increased MCR in HC cells; however, hypoxic preconditioning significantly reduced PTX-induced MCR. Arrowheads point to the longer duration of arrest of cells in a 'rounded shape' following PTX and VCR. (A, left panel) Graphs showing the MTA-induced changes in TrCom of NRX and HC cells. ***$p < 0.001$, **$p < 0.01$ compared to NRX cells (grey), $n = 500$–4000 cells per culture condition. (B) Representative images of HeLa-FUCCI cells after 16 h of treatment with the indicated concentrations of drugs are shown. Green and red fluorescence represent Cdt1-mKO2 and Gem-mAG, respectively ($20 \times$ objective, scale bar - 20 μm). (C) Boxplots of MCR and multinucleation of cells immediately after hypoxia, but before the start of drug treatment are presented. ***$p < 0.001$ compared to NRX cells, $n = 500$–4000 cells. The boxes and horizontal bar within the boxes in the boxplots represent the 25th and 75th percentiles and median, respectively. The whiskers represent the 5th and 95th percentiles. (D) Pre-treatment of HeLa-FUCCI cells with 50 μM Z-VAD-FMK for 2 h did not inhibit MTA-mediated MCR. $10 \times$ objective, scale bar - 100 μm. (E) Western blots present the expression of p53 in HCT116 parental and HIF-1α-expressing cells following drug treatment. NRX and HC cell p53 blots are from different gels. Western blots are representative of 3 independent experiments. (For interpretation of the references to colour in this figure legend, the reader is referred to the web version of this article.)

contrast, hypoxia preconditioning significantly abrogated the cytotoxicity of PTX in accordance with previous studies on other tumor cell lines [13,45,47].

The high, presumably, saturating concentrations of PTX and VCR used may explain the lack of a difference in cell cycle effects between NRX and HC cells ($20 \times IC_{50}$ of PTX and VCR). This is also evident from the absence of a difference in the effect of 2 μM PLA ($20 \times IC_{50}$) on the cell cycle of HC cells compared to NRX cells. However, even though at a low $4 \times IC_{50}$ concentration, 2 nM VCR increased the percentage of NRX cells in G2/M, whereas the same low concentration did not induce any major change in HC cells.

Hypoxia has been reported to alter MT behavior and result in reduced PTX cytotoxicity, presumably due to perturbation of drug-tubulin interactions and/or changes in MT stability [15,48]. Our data, however, indicate that hypoxia does not alter PLA-tubulin interactions in HC cells, as evidenced by increased acetylation of tubulin and intracellular tubulin polymerization in PLA-treated HC cells. On the

other hand, hypoxia-preconditioning counteracted MT stabilization by PTX. Hypoxia has been reported to alter the expression of MT-associating proteins, which could also contribute to MTA resistance [49,50]; however, and unlike PTX, PLA is not sensitive to altered expression of tau [27].

Upregulation of βIII-tubulin following hypoxia is another known contributor of resistance to PTX [51], and altered expression of tubulin isotypes has also been associated with PLA resistance [52]. Although hypoxia-induced upregulation of βIII-tubulin is known, there are no studies to indicate that hypoxia upregulates other tubulin isotypes. Moreover, a single hypoxia exposure for 4 or 24 h is highly unlikely to establish a stable resistance phenotype by modulating the expression levels of βIII-tubulin. The difference in the proteomic profiles of apoptotic proteins in PLA-treated versus PTX-treated cells suggest these MTAs may activate different apoptotic pathways that are differentially affected by tubulin isotype levels [52,53].

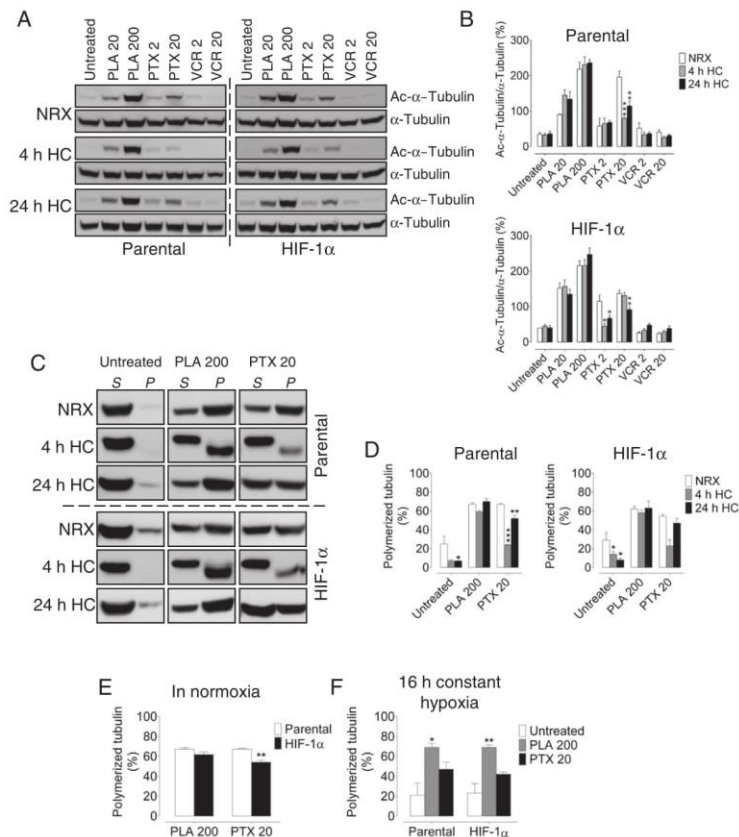Poor chemosensitivity of cancer cells to PTX and other anticancer

Fig. 5. Hypoxia does not alter PLA-induced MT stabilization or polymerization of tubulin in HCT116 cells. (A) Representative western blots of Ac-α-tubulin in NRX and HC cells following drug treatment. $n = 3$. (B) Hypoxic preconditioning inhibited PTX-induced tubulin acetylation but not that of PLA. ***$p < 0.001$, **$p < 0.01$, *$p < 0.05$ compared to NRX cells, $n = 3$. (C) Western blot analysis of cytosolic (soluble, S) and cytoskeletal (polymerized, P) α-tubulin fractions in NRX and HC cells. $n = 4$. (D) Bar graphs reveal that there is no significant effect of hypoxic preconditioning on PLA-induced polymerization of tubulin. ***$p < 0.001$, **$p < 0.01$, *$p < 0.05$ compared to NRX cells, $n = 4$. (E) Overexpression of HIF-1α significantly affected tubulin polymerization by PTX under NRX conditions in HIF-1α cells. **$p < 0.01$ compared to parental cells, $n = 3–4$, Student's t-test, unpaired. (F) Treating cells with PLA for 16 h in hypoxia does not alter the ability of PLA to polymerize tubulin in both parental and HIF-1α cells. **$p < 0.01$, *$p < 0.05$ compared to untreated, $n = 3$.

drugs has been attributed to hypoxia-mediated deregulation of cell cycle-associated proteins [12,33,54]. However, and unlike Dong et al. [12], we did not see a significant effect of hypoxia on G2/M arrest of HC cells following PTX treatment. This difference presumably resulted from a difference in the method of treatment of the cells. Unlike Dong et al., we first exposed the cells to hypoxia and then treated with MTAs in normoxic conditions for an additional 16 h which also resulted in the degradation of the majority of overexpressed HIF-1α in untreated cells (data not shown). However, despite the degradation of the hypoxia-induced HIF-1α, untreated HC cells exposed to normoxia continued to show hypophosphorylated pRb and decreased levels of cyclin D1, indicating that hypoxia has long-lasting effects on cellular and molecular components in cancer cells.

A hypoxia-induced decrease in expression of cyclin D1, presumably via activation of p21, results in hypophosphorylation of pRb and cell cycle alterations [34]. In our study, PLA-treated HC cells showed an increase in cyclin D1 and pRb phosphorylation, suggesting that PLA affects the pRb pathways in HC cells, driving them to G2/M, where the effect of PLA on MTs in mitosis is prominent.

In addition to accumulation of cells in G2/M, other downstream events that may result as a response of cancer cells to MTAs include aberrant mitoses and cell death. Moreover, abnormal mitosis and mitotic slippage have been reported to enhance the cytotoxicity of PTX through p53-mediated apoptosis in different cancer cell types [41,55,56]. Furthermore, this apoptosis strongly correlates with the degree of multinucleation [41]. In contrast to PTX, hypoxic preconditioning in our study did not affect PLA-mediated multinucleation of HC cells, a key trigger of post-slippage apoptosis [41]. Although there was no major change in p53 levels, a recent study reports that once cells have undergone mitotic slippage, proliferative cell death occurs irre-
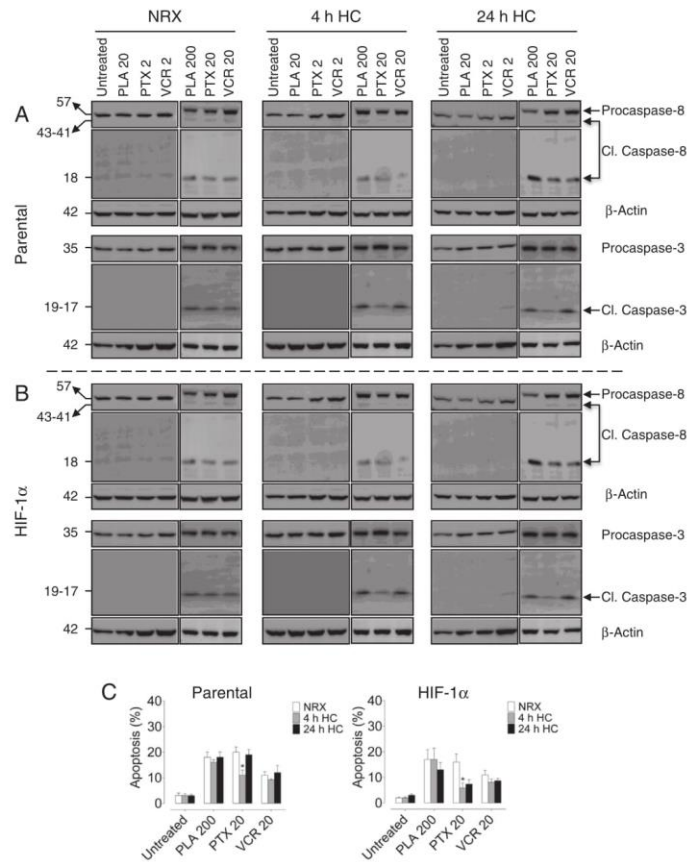
Fig. 6. Apoptosis in HCT116 HC cells following PLA treatment. (A) NRX and HC cells were treated with PLA, PTX, and VCR for 16 h, and cleavage of caspase-8 and -3 was analyzed by western blot. Arrows indicate the cleaved caspase bands. Caspase 8 and 3 blots are from different gels. $n = 3$. (B) Flow cytometry analysis indicates a significant decrease in PTX- but not PLA- and VCR-mediated apoptosis of parental and HIF-1α cells pre-exposed to hypoxia. * $p < 0.05$ compared to NRX cells, $n = 3$–4.

spective of apoptosis or p53 induction [56]. However, our data suggest that PLA-induced post slippage cell death occurs via apoptosis, as evident from caspase-3 activation and DNA fragmentation in HC parental and HIF-1α-expressing cells.

5. Conclusions

Responses to MTAs vary between different cell types and depend on the concentrations of the MTAs. Moreover, hypoxia in solid tumors is a complex process and results in multifactorial alterations [7] that cannot be reproduced effectively and in their entirety in an *in vitro* cell-based study. Nevertheless, our promising findings suggest that underlying factors responsible for an improved response to PLA relative to PTX results from the ability of PLA to alter MT dynamics and induce apoptosis more effectively than PTX in HC cells.

Conflict of interest

The authors declare that they have no conflicts of interest.

Transparency Document

The Transparency document associated with this article can be found, in online version.

Acknowledgment

9

References

[1] M. Kavallaris, Microtubules and resistance to tubulin-binding agents, Nat. Rev. Cancer 10 (2010) 194–204, http://dx.doi.org/10.1038/nrc2803.

[2] A. Chan, A.J. Singh, P.T. Northcote, J.H. Miller, Inhibition of human vascular endothelial cell migration and capillary-like tube formation by the microtubule-stabilizing agent peloruside A, Investig. New Drugs 33 (2015) 564–574, http://dx.doi.org/10.1007/s10637-015-0232-8.

[3] J.J. Field, A. Kanakkanthara, J.H. Miller, Microtubule-targeting agents are clinically successful due to both mitotic and interphase impairment of microtubule function, Cytoskelet. Its Interact. Small Mol. 22 (2014) 5050–5059, http://dx.doi.org/10.1016/j.bmc.2014.02.035.

[4] E. Komlodi-Pasztor, D. Sackett, J. Wilkerson, T. Fojo, Mitosis is not a key target of microtubule agents in patient tumors, Nat. Rev. Clin. Oncol. 8 (2011) 244–250, http://dx.doi.org/10.1038/nrclinonc.2010.228.

[5] A.B. Ariffin, P.F. Forde, S. Jahangeer, D.M. Soden, J. Hinchion, Releasing pressure in tumors: what do we know so far and where do we go from here? A Review, Cancer Res. 74 (2014) 2655, http://dx.doi.org/10.1158/0008-5472.CAN-13-3696.

[6] V. Das, J. Štěpánková, M. Hajdúch, J.H. Miller, Role of tumor hypoxia in acquisition of resistance to microtubule-stabilizing drugs, Biochim. Biophys. Acta Rev. Cancer 1855 (2015) 172–182, http://dx.doi.org/10.1016/j.bbcan.2015.02.001.

[7] M.S. Nakazawa, B. Keith, M.C. Simon, Oxygen availability and metabolic adaptations, Nat. Rev. Cancer 16 (2016) 663–673.

[8] G.L. Semenza, Hypoxia-inducible factors: coupling glucose metabolism and redox regulation with induction of the breast cancer stem cell phenotype, EMBO J. (2016), http://dx.doi.org/10.15252/embj.201695204.

[9] K.L. Eales, K.E.R. Hollinshead, D.A. Tennant, Hypoxia and metabolic adaptation of cancer cells, Oncogene 5 (2016) e190.

[10] F. Yang, H. Zhang, Y. Mei, M. Wu, Reciprocal regulation of HIF-1α and LincRNA-p21 modulates the Warburg effect, Mol. Cell 53 (2014) 88–100, http://dx.doi.org/10.1016/j.molcel.2013.11.004.

[11] P. Martinive, F. Defresne, C. Bouzin, J. Saliez, F. Lair, V. Grégoire, C. Michiels, C. Dessy, O. Feron, Preconditioning of the tumor vasculature and tumor cells by intermittent hypoxia: implications for anticancer therapies, Cancer Res. 66 (2006) 11736, http://dx.doi.org/10.1158/0008-5472.CAN-06-2056.

[12] X.L. Dong, P.F. Xu, C. Miao, Z.Y. Fu, Q.P. Li, P.Y. Tang, T. Wang, Hypoxia decreased chemosensitivity of breast cancer cell line MCF-7 to paclitaxel through cyclin B1, Biomed. Pharmacother. 66 (2012) 70–75, http://dx.doi.org/10.1016/j.biopha.2011.11.016.

[13] L. Huang, Q. Ao, Q. Zhang, X. Yang, H. Xing, F. Li, G. Chen, J. Zhou, S. Wang, G. Xu, L. Meng, Y. Lu, D. Ma, Hypoxia induced paclitaxel resistance in human ovarian cancers via hypoxia-inducible factor 1α, J. Cancer Res. Clin. Oncol. 136 (2010) 447–456, http://dx.doi.org/10.1007/s00432-009-0675-4.

[14] S. Merighi, A. Benini, P. Mirandola, S. Gessi, K. Varani, E. Leung, S. Maclennan, P.G. Baraldi, P.A. Borea, Hypoxia inhibits paclitaxel-induced apoptosis through adenosine-mediated phosphorylation of Bad in glioblastoma cells, Mol. Pharmacol. 72 (2007) 162–172, http://dx.doi.org/10.1124/mol.106.031849.

[15] L. Zeng, S. Kizaka-Kondoh, S. Itasaka, X. Xie, M. Inoue, K. Tanimoto, K. Shibuya, M. Hiraoka, Hypoxia inducible factor-1 influences sensitivity to paclitaxel of human lung cancer cell lines under normoxic conditions, Cancer Sci. 98 (2007) 1394–1401, http://dx.doi.org/10.1111/j.1349-7006.2007.00537.x.

[16] J.C. Forde, A.S. Perry, K. Brennan, L.M. Martin, M.P. Lawler, T.H. Lynch, D. Hollywood, L. Marignol, Docetaxel maintains its cytotoxic activity under hypoxic conditions in prostate cancer cells, Urol. Oncol. 30 (2012) 912–919, http://dx.doi.org/10.1016/j.urolonc.2010.08.015.

[17] D. Escuín, E.R. Kline, P. Giannakakou, Both microtubule-stabilizing and micro-tubule-destabilizing drugs inhibit hypoxia-inducible factor-1α accumulation and activity by disrupting microtubule function, Cancer Res. 65 (2005) 9021–9028, http://dx.doi.org/10.1158/0008-5472.CAN-04-4095.

[18] A. Kanakkanthara, P.T. Northcote, J.H. Miller, Peloruside A: a lead non-taxoid-site microtubule-stabilizing agent with potential activity against cancer, neurodegeneration, and autoimmune disease, Nat. Prod. Rep. 33 (2016) 549–561, http://dx.doi.org/10.1039/C5NP00146C.

[19] Y. Fang, X. Wu, Y. Dang, Y. Zhang, J. Zhang, J. Hu, Q. Zhang, X. Dai, M. Teng, D. Zhang, Y. Huang, MAP4 mechanism that stabilizes mitochondrial permeability transition in hypoxia: microtubule enhancement and DYNLT1 interaction with VDAC1, PLoS One 6 (2011) e28052, , http://dx.doi.org/10.1371/journal.pone.0028052.

[20] J.Y. Hu, Z.G. Chu, J. Han, Y. Dang, H. Yan, Q. Zhang, G. Liang, Y.-S. Huang, The p38/MAPK pathway regulates microtubule polymerization through phosphorylation of MAP4 and Op18 in hypoxic cells, Cell. Mol. Life Sci. 67 (2010) 321–333, http://dx.doi.org/10.1007/s00018-009-0187-z.

[21] T.N. Gaitanos, R.M. Buey, J.F. Díaz, P.T. Northcote, P. Teesdale-Spittle, J.M. Andreu, J.H. Miller, Peloruside A does not bind to the taxoid site on β-tubulin and retains its activity in multidrug-resistant cell lines, Cancer Res. 64 (2004) 5063–5067, http://dx.doi.org/10.1158/0008-5472.can-04-0771.

[22] C.J. Meyer, M. Krauth, M.J. Wick, J.W. Shay, G. Gellert, J.K. De Brabander, P.T. Northcote, J.H. Miller, Peloruside A inhibits growth of human lung and breast tumor xenografts in an athymic nu/nu mouse model, Mol. Cancer Ther. 14 (2015) 1816, http://dx.doi.org/10.1158/1535-7163.MCT-15-0167.

[23] L.M. West, P.T. Northcote, C.N. Battershill, Peloruside A: a potent cytotoxic macrolide isolated from the New Zealand marine sponge Mycale sp, J. Org. Chem. 65 (2000) 445–449, http://dx.doi.org/10.1021/jo991296y.

[24] V. Das, T. Fürst, S. Gurská, P. Džubák, M. Hajdúch, Reproducibility of uniform spheroid formation in 384-well plates: the effect of medium evaporation, J. Biomol.

[25] Screen. (2016), http://dx.doi.org/10.1177/1087057116651867.

[25] A. Sakaue-Sawano, T. Kobayashi, K. Ohtawa, A. Miyawaki, Drug-induced cell cycle modulation leading to cell-cycle arrest, nuclear mis-segregation, or endoreplication, BMC Cell Biol. 12 (2011) 2, http://dx.doi.org/10.1186/1471-2121-12-2.

[26] A. Sakaue-Sawano, H. Kurokawa, T. Morimura, A. Hanyu, H. Hama, H. Osawa, S. Kashiwagi, K. Fukami, T. Miyata, H. Miyoshi, T. Imamura, M. Ogawa, H. Masai, A. Miyawaki, Visualizing spatiotemporal dynamics of multicellular cell-cycle progression, Cell 132 (2008), http://dx.doi.org/10.1016/j.cell.2007.12.033.

[27] V. Das, J.H. Miller, Non-taxoid site microtubule-stabilizing drugs work independently of tau overexpression in mouse N2a neuroblastoma cells, Brain Res. 1489 (2012) 121–132, http://dx.doi.org/10.1016/j.brainres.2012.10.022.

[28] P. Giannakakou, D.L. Sackett, Y.-K. Kang, Z. Zhan, J.T.M. Buters, T. Fojo, M.S. Poruchynsky, Paclitaxel-resistant human ovarian cancer cells have mutant β-tubulins that exhibit impaired paclitaxel-driven polymerization, J. Biol. Chem. 272 (1997) 17118–17125, http://dx.doi.org/10.1074/jbc.272.27.17118.

[29] A. Bourderioux, P. Nauš, P. Perlíková, R. Pohl, I. Pichová, I. Votruba, P. Džubák, P. Konečný, M. Hajdúch, K.M. Stray, T. Wang, A.S. Ray, J.Y. Feng, G. Birkus, T. Cihlar, M. Hocek, Synthesis and significant cytostatic activity of 7-Hetaryl-7-deazaadenosines, J. Med. Chem. 54 (2011) 5498–5507, http://dx.doi.org/10.1021/jm2005173.

[30] P. Kask, H. Maakond, Methods and apparatus for image analysis using threshold compactness features, US 2013/0114874 A1. https://www.google.com/patents/US8705834, (2013).

[31] T. Wang, J.H. Lv, X.F. Zhang, C.J. Li, X. Han, Y.J. Sun, Tissue inhibitor of metalloproteinase-1 protects MCF-7 breast cancer cells from paclitaxel-induced apoptosis by decreasing the stability of cyclin B1, Int. J. Cancer 126 (2010) 362–370, http://dx.doi.org/10.1002/ijc.24753.

[32] S.Y. Cui, R. Wang, L.-B. Chen, MicroRNAs: key players of taxane resistance and their therapeutic potential in human cancers, J. Cell. Mol. Med. 17 (2013) 1207–1217, http://dx.doi.org/10.1111/jcmm.12131.

[33] W. Wen, J. Ding, W. Sun, K. Wu, B. Ning, W. Gong, G. He, S. Huang, X. Ding, P. Yin, L. Chen, Q. Liu, W. Xie, H. Wang, Suppression of cyclin D1 by hypoxia-inducible factor-1 via direct mechanism inhibits the proliferation and 5-fluorouracil-induced apoptosis of A549 cells, Cancer Res. 70 (2010) 2010, http://dx.doi.org/10.1158/0008-5472.CAN-08-4910.

[34] N. Goda, H.E. Ryan, B. Khadivi, W. McNulty, R.C. Rickert, R.S. Johnson, Hypoxia-inducible factor 1α is essential for cell cycle arrest during hypoxia, Mol. Cell. Biol. 23 (2003) 359–369, http://dx.doi.org/10.1128/MCB.23.1.359-369.2003.

[35] A. Kaida, M. Miura, Visualizing the effect of hypoxia on fluorescence kinetics in living HeLa cells using the fluorescent ubiquitination-based cell cycle indicator (Fucci), Exp. Cell Res. 318 (2012) 288–297, http://dx.doi.org/10.1016/j.yexcr.2011.10.016.

[36] C. Cadart, E. Zlotek-Zlotkiewicz, M. Le Berre, M. Piel, H.K. Matthews, Exploring the function of cell shape and size during mitosis, Dev. Cell 29 (2014) 159–169, http://dx.doi.org/10.1016/j.devcel.2014.04.009.

[37] G.M. O'Neill, E.A. Golemis, Proteolysis of the docking protein HEF1 and implications for focal adhesion dynamics, Mol. Cell. Biol. 21 (2001) 5094–5108, http://dx.doi.org/10.1128/MCB.21.15.5094-5108.2001.

[38] B. Gabrielli, Y.Q. Chau, N. Giles, A. Harding, F. Stevens, H. Beamish, Caffeine promotes apoptosis in mitotic spindle checkpoint-arrested cells, J. Biol. Chem. 282 (2007) 6954–6964, http://dx.doi.org/10.1074/jbc.M610104200.

[39] M. Oliver Metzig, D. Fuchs, K.E. Tagscherer, H.-J. Grone, P. Schirmacher, W. Roth, Inhibition of caspases primes colon cancer cells for 5-fluorouracil-induced TNF-[alpha]-dependent necroptosis driven by RIP1 kinase and NF-[kappa]B, Oncogene 35 (2016) 3399–3409.

[40] J. Shi, J.D. Orth, T. Mitchison, Cell type variation in responses to antimitotic drugs that target microtubules and kinesin-5, Cancer Res. 68 (2008) 3269, http://dx.doi.org/10.1158/0008-5472.CAN-07-6699.

[41] Y. Zhu, Y. Zhou, J. Shi, Post-slippage multinucleation renders cytotoxic variation in anti-mitotic drugs that target the microtubules or mitotic spindle, Cell Cycle 13 (2014) 1756–1764, http://dx.doi.org/10.4161/cc.28672.

[42] S.O. Yoon, S. Shin, A.M. Mercurio, hypoxia stimulates carcinoma invasion by stabilizing microtubules and promoting the Rab11 trafficking of the α6β4 integrin, Cancer Res. 65 (2005) 2761, http://dx.doi.org/10.1158/0008-5472.CAN-04-4122.

[43] A.L. Parker, M. Kavallaris, J.A. McCarroll, Microtubules and their role in cellular stress in cancer, Front. Oncol. 4 (2014) 153, http://dx.doi.org/10.3389/fonc.2014.00153.

[44] L. Flamant, A. Notte, N. Ninane, M. Raes, C. Michiels, Anti-apoptotic role of HIF-1 and AP-1 in paclitaxel exposed breast cancer cells under hypoxia, Mol. Cancer 9 (2010) 191, http://dx.doi.org/10.1186/1476-4598-9-191.

[45] A. Notte, N. Ninane, T. Arnould, C. Michiels, Hypoxia counteracts Taxol-induced apoptosis in MDA-MB-231 breast cancer cells: role of autophagy and JNK activation, Cell Death Dis. 4 (2013) e638.

[46] A. Ganguly, F. Cabral, H. Yang, K.D. Patel, Peloruside A is a microtubule-stabilizing agent with exceptional anti-migratory properties in human endothelial cells, Oncoscience 2 (2015) 585–595.

[47] A. Sermeus, M. Genin, A. Maincent, M. Fransolet, A. Notte, L. Leclere, H. Riquier, T. Arnould, C. Michiels, Hypoxia-induced modulation of apoptosis and BCL-2 family proteins in different cancer cell types, PLoS One 7 (2012) e47519.

[48] J.E. Hwang, J.-H. Lee, M.-R. Park, D.-E. Kim, W.-K. Bae, H.-J. Shim, S.-H. Cho, I.-J. Chung, Blockade of VEGFR-1 and VEGFR-2 enhances paclitaxel sensitivity in gastric cancer cells, Yonsei Med. J. 54 (2013) 374–380.

[49] S.H. Moussavi Nik, K. Croft, T.A. Mori, M. Lardelli, The comparison of methods for measuring oxidative stress in zebrafish brains, Zebrafish 11 (2014), http://dx.doi.org/10.1089/zeb.2013.0958.

[50] S. Xie, A. Ogden, R. Aneja, J. Zhou, Microtubule-binding proteins as promising

biomarkers of paclitaxel sensitivity in cancer chemotherapy, Med. Res. Rev. 36 (2016) 300–312, http://dx.doi.org/10.1002/med.21378.

[51] G. Raspaglio, F. Filippetti, S. Prislei, R. Penci, I. De Maria, L. Cicchillitti, S. Mozzetti, G. Scambia, C. Ferlini, Hypoxia induces class III beta-tubulin gene expression by HIF-1α binding to its 3′ flanking region, Gene 409 (2008) 100–108, http://dx.doi.org/10.1016/j.gene.2007.11.015.

[52] A. Kanakkanthara, P.T. Northcote, J.H. Miller, βII- and βIII-tubulin mediate sensitivity to peloruside A and laulimalide, but not paclitaxel or vinblastine, in human ovarian carcinoma cells, Mol. Cancer Ther. 11 (2011) 393–404, http://dx.doi.org/10.1158/1535-7163.mct-11-0614.

[53] A. Wilmes, A. Chan, P. Rawson, T. William Jordan, J. Miller, Paclitaxel effects on the proteome of HL-60 promyelocytic leukemic cells: comparison to peloruside A, Investig. New Drugs 30 (2012) 121–129, http://dx.doi.org/10.1007/s10637-010-

9540-1.

[54] G. Hasvold, C. Lund-Andersen, M. Lando, S. Patzke, S. Hauge, Z. Suo, H. Lyng, R.G. Syljuåsen, Hypoxia-induced alterations of G2 checkpoint regulators, Mol. Oncol. 10 (2016) 764–773, http://dx.doi.org/10.1016/j.molonc.2015.12.015.

[55] L.E. Klein, S.B. Horwitz, Contributions of apoptosis and senescence to cytotoxicity produced by microtubule-stabilizing agents, in: D.A. Gewirtz, S.E. Holt, S. Grant (Eds.), Apoptosis Senescence Cancer, Humana Press, Totowa, NJ, 2007, pp. 465–476, , http://dx.doi.org/10.1007/978-1-59745-221-2_23.

[56] S. Yasuhira, M. Shibazaki, M. Nishiya, C. Maesawa, Paclitaxel-induced aberrant mitosis and mitotic slippage efficiently lead to proliferative death irrespective of canonical apoptosis and p53, Cell Cycle 15 (2016) 3268–3277, http://dx.doi.org/10.1080/15384101.2016.1242537.

11

126

Synthesis of cytotoxic 2,2-difluoroderivatives of dihydrobetulinic acid and allobetulin and study of their impact on cancer cells

Original article

Synthesis of cytotoxic 2,2-difluoroderivatives of dihydrobetulinic acid and allobetulin and study of their impact on cancer cells

Lucie Borkova [a, 1], Lucie Jasikova [b, 1], Jiri Rehulka [c, 1], Katerina Frisonsova [b], Milan Urban [a, c], Ivo Frydrych [c], Igor Popa [a], Marian Hajduch [c], Niall J. Dickinson [a], Martin Vlk [d], Petr Dzubak [c], Jan Sarek [a, c, *]

[a] Department of Organic Chemistry, Faculty of Science, Palacky University Olomouc, 17. listopadu 1192/12, 771 46 Olomouc, Czech Republic
[b] Department of Organic and Nuclear Chemistry, Faculty of Science, Charles University in Prague, Hlavova 8, 128 43 Prague 2, Czech Republic
[c] Institute of Molecular and Translational Medicine, Faculty of Medicine and Dentistry, Palacky University Olomouc, Hnevotinska 5, 779 00 Olomouc, Czech Republic
[d] Faculty of Nuclear Sciences and Physical Engineering, Czech Technical University in Prague, Brehova 7, 115 19 Prague 1, Czech Republic

ARTICLE INFO

ABSTRACT

In this article, we describe the preparation and cytotoxic properties of a small focused library of lupane and 18α-oleanane triterpenoids that contain a combination of two structural motifs known to enhance the biological activities. First, we introduced two fluorine atoms to position 2 of the skeleton. Second, we synthesized a set of hemiester prodrugs, which were intended to increase the solubility and activity. Starting from betulin, we obtained two hydroxyketones (derivatives of dihydrobetulinic acid and allobetulin) and their fluorination using DAST provided 2,2-difluoro-3-oxo-compounds as the main products. Then the 3-oxo group in each derivative was reduced by $NaBH_4$ to obtain 3β-hydroxy compounds suitable for modifying by various hemiesters. We prepared 21 compounds, 11 of them new, their cytotoxicity was tested on T lymphoblastic leukemia CCRF-CEM cells first and the most active derivatives were selected for screening on another six tumor and two non-tumor cell lines. All of them showed selectivity against cancer lines with therapeutic index between 2 and 8. All hemiesters had activity in the same range as the free hydroxyl derivatives and they would be suitable prodrugs for future in vivo experiments. Interestingly, all hemiesters of 2,2-difluorodihydrobetulonic acid had higher activity against p53 knock-out p53−/− cancer cell line than against the non-mutated analog. In active derivatives, the cell cycle was analyzed by flow cytometry and several compounds slowed down cell cycle progression through G0/G1 or S-phase.

© 2015 Elsevier Masson SAS. All rights reserved.

1. Introduction

Triterpenoids belong to a large family of natural compounds with a wide range of biological activities [1,2]. Pentacyclic triterpenoids have anticancer [3], chemopreventive [4], immunosuppressive [5], anti-inflammatory [6], anti-HIV [7,8], antitrypanosomal [9], and antimicrobial properties [6]. The promising anticancer and anti-HIV activities led to an increased research

activity in this field. Commonly, however, the pharmacological properties (such as low solubility in water based media and low bioavailability) of those active compounds are not suitable for their use in medicine. Also, the IC_{50} values are often insufficient. Many research groups have tried to improve the properties of the most promising terpenoids, which would make them useful candidates for HIV and cancer treatment. These studies have either explored new plant species or modified the structures of known active compounds. Among hundreds of new compounds, we have synthesized many derivatives of lupane that are highly cytotoxic on a variety of cancer cell lines in vitro, including those that are resistant to current cytostatics [10–16]. This allowed us to make simplified structure-activity relationship assumptions and to find some trends of how the chemical structure may affect the anti-tumor activity. We found that in general, increasing hydrophobicity leads to less

active compounds while introducing an electronegative substituent to the position 2 of lupane derivatives increases the cytotoxicity.

Previously, we studied a general possibility of introducing one or two atoms of fluorine into the terpenic structures using DAST, and as expected, the result was a group of hydrophobic triterpenes where fluorine replaced carboxyl, carbonyl or hydroxy groups [17]. In agreement with the general trend, there was no cytotoxic activity within this group of hydrophobic fluoroderivatives. However, there is a literature precedent of addition of dichloro- and dibromo-carbene to 20(29)-double bonds of some terpenic structures. Resulting products had very high inhibitory activity on human melanoma cells Colo 38 and Bro.92 [18]. This motivated us to synthesize triterpenic difluorocyclopropanes, analogous adducts of difluorocarbene to the activated double bonds of several triterpenes that we prepared earlier. The resulting compounds, however, were inactive [19].

Based on all our previous work with cytotoxic triterpenes, knowing that an electronegative substituent (EWG) in the position 2 always improved the cytotoxicity [11,14,17,19], we expected the only way to increase the cytotoxicity by adding fluorine to a triterpene is to add the fluorine atoms to the position 2 of the triterpenoid skeleton (preferably dihydrobetulinic acid). Therefore in this work, we used and further optimized the previously [17] developed method of fluorination of 2-hydroxyallobetulone (**12**) with DAST and introduced two fluorine atoms to C-2. It was expected, that the resulting compounds may be highly hydrophobic which can cause associated problems, such as low solubility and bioavailability. Therefore we decided to prepare hemiester prodrugs from the resulting difluoroderivatives in order to decrease the overall hydrophobicity. Hemiesters are well known from Bevirimat (3β-O-3',3'-dimethylsuccinylbetulinic acid), a compound that inhibits the maturation of the HIV particles by interacting with the GAG protein [20]. Solubility of Bevirimat in water-based media was increased significantly by using cyclodextrines and we expected that it would be possible to use similar method in our new fluoroderivatives.

2. Results and discussion

2.1. Chemistry

A three-step process was used to transform betulin (**1**) to dihydrobetulin-3β-O-acetate (**2**), which was further transformed to acetyldihydrobetulinic acid (**3**), dihydrobetulinic acid (**4**), and benzyl dihydrobetulinate (**5**), consecutive oxidation of **5** gave benzyl-dihydrobetulonate (**6**) — **64 % over all 4 steps** [21,22]. Derivative **6** was oxidized by MCPBA to give benzyl-2α-hydroxydihydrobetulonate (**7**) (Scheme 1), which was then treated with DAST in chloroform in presence one equivalent of pyridine [17] to give difluoroderivative **8** at 68% yield (without pyridine, this reaction only gives yield of 40%). Benzyl-esters were deprotected using a catalytic hydrogenolysis on Pd/C catalyst at room temperature under 0.5 MPa of hydrogen. 3-oxoderivatives **8** and **9** were reduced by NaBH$_4$ in THF/MeOH yielding 3β-hydroxyderivatives **10** and **11**. In theory both, α and β-epimers may form by a reduction of 3-oxocompounds to the corresponding alcohols. However, it is well known [23,24] that in triterpenes, the sterical arrangement of the skeleton directs the reaction towards beta alcohols predominantly; and in this case, we did not isolate any α-epimers. We used the original procedure [17] to transform hydroxyketone **12** to 2,2-difluorollobetulone **13** from which 2,2-difluoroallobetulin **14** was accessible by reduction with NaBH$_4$. As a result, we obtained a set of 2,2-difluoroderivatives **8–11**, **13**, and **14**.

Knowing that the hemiester type may play significant role in the biological activity (for example see anti HIV activity of bevirimat analogs), we also prepared small sets of various hemiesters from both **11** and **14** and obtained compounds **15–21**. While the derivatives of lupane **9**, **11**, **15–18** had always interesting IC$_{50}$, the allobetulin analogs **13**, **14**, **19–21** were always inactive, therefore we only synthesized three hemiesters (**19–21**) allobetulin analogs (Scheme 2).

All acylations were performed using the corresponding anhydride in a presence of DMAP in refluxing *sym*-collidine (2,4,6-trimethylpyridine) under argon atmosphere to give desired products **15–21**. Yields of hemiesters were generally low due to harsh reaction conditions (about 180 °C), which caused side reactions. Also, during the general work up procedure a portion of the organic material was not extracted from the aqueous phase because of the ambivalent characters of the products. The biological part of this study was extended by a known [16] 2,2-dibromodihydrobetulonic acid (**22**) because we wanted to compare the activities of the compound **22** with our new 2,2-difluoroderivatives.

2.2. Biological assay

2.2.1. Cytotoxicity

Cytotoxic activity of all synthesized compounds and intermediates was investigated. All prepared compounds were tested for their *in vitro* cytotoxic activity against human T-lymphoblastic leukemia cell line CCRF-CEM using the standard MTT test (Table 1).

All 18α-oleanane derivatives had cytotoxicity in high micromolar ranges. New 2,2-difluoroderivatives of dihydrobetulinic acid had high cytotoxic activity (IC$_{50}$ < 10 μmol/L) when they contained a free 28-COOH group. The most active derivative of the presented set of compounds was 2,2-difluorodihydrobetulonic acid (**9**) and its analog 2,2-dibromodihydrobetulonic acid (**22**), which is in agreement with our previous results, that lupane 3-oxoderivatives are generally more cytotoxic than 3-hydroxyderivatives. Introduction of halogen atoms to position 2 increased the cytotoxicity from IC$_{50}$ = 4 μM (dihydrobetulonic acid, see Ref. [16]) to 2.4 μM (2,2-difluorodihydrobetulonic acid **9**) or to 1.0 μM (2,2-dibromodihydrobetulonic acid **22**). A greater improvement was found in 3-hydroxyderivatives, where the activity went from IC$_{50}$ = 9 μM (dihydrobetulinic acid **4**) to 4.0 μM (2,2-difluorodihydrobetulinic acid **11**), although the cytotoxicity was worse than in 3-oxoderivatives. This confirmed our original hypothesis that a strong electron withdrawing group(s) in the position 2 of a triterpenic skeleton increases the cytotoxicity of lupane derivatives. The activity of all lupane hemiesters was in the same range and it was the same or slightly worse than the activity of a free 2,2-difluorodihydrobetulinic acid (**11**). We concluded that the hemiester group is not an important part of the pharmacophore, which is in sharp contrast to the role of the dimethylhemisuccinate group in bevirimat in which the hemiester is essential to improve the strong non covalent interaction between betulinic acid and the viral GAG protein which results in blocking of the HIV protease and maturation of the virus particles as found in lit [20]. Although not important for the activity, the introduction of a hemiester improved the solubility in water-based media and in combination with additives such as cyclodextrines, compounds fully soluble in water may be obtained. These will be a major focus of our future *in vivo* tests. Hemiesters made from 2,2-difluoroallobetulin (**14**), compounds **19–21** were much less active than those made from 2,2-difluorobetulinic acid (**11**), compounds **15–18**, however, they were more active than 2,2-difluoroallobetulin (**14**). This corresponds with the fact that allobetulin derivatives are almost always less active than analogous lupane derivatives and even the presence of a hemisuccinate is not sufficient to decrease the IC$_{50}$ to low micromolar ranges. Hemiesters though are suitable prodrugs for 2,2-difluoroderivatives of triterpenes, as they possibly improve the
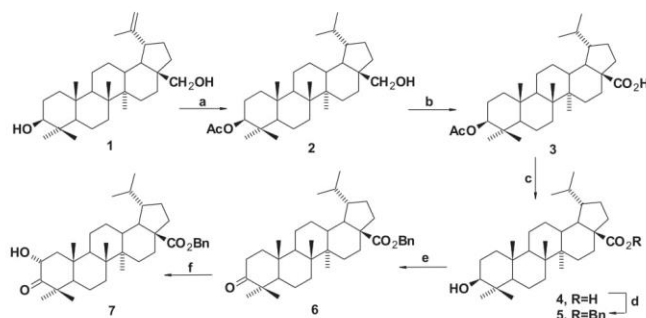
Scheme 1. Reagents and conditions: (a) i: Ac$_2$O, pyridine, r.t., 14 h; ii: H$_2$/Ra–Ni, methoxyethanol, THF, 48 h, 1 MPa, r.t.; iii: KOH (1 equiv), toluene, EtOH, r.t.; (b) RuO$_2$, NaIO$_4$, EtOAc, MeCN, H$_2$O, 55 °C, 140 min; (c) excess KOH, toluene, EtOH, reflux; (d) BnBr, K$_2$CO$_3$, DMF, MeCN; (e) Na$_2$Cr$_2$O$_7$, NaOAc, AcOH, Ac$_2$O, toluene, 22 h, r.t.; (f) MCPBA (added in several portions), H$_2$SO$_4$, CH$_2$Cl$_2$, MeOH, 17 h, r.t.

pharmacological properties including their bioavailability. Since the activities of the hemiesters prepared in this study are in the same range of IC$_{50}$, we may conclude that the simplest hemiester – hemisuccinate is fully acceptable.

The most active derivatives (**9**, **11**, **15**–**18**) were further tested on six cancer cell lines (Table 2) of different histogenetic origin and on two types of normal human fibroblasts. All active derivatives showed selective cytotoxicity in low micromolar range on most of the cancer cell lines, compound **9** proved to be the best. Hemiesters **15**–**18** showed interesting selectivity against p53 knock-out HCT116p53–/– cancer cell line. On the other hand, they were less active against daunorubicin resistant CEM cell line than against nonresistant. Although selective, the calculated therapeutic index is between 2 and 8, therefore our future research must be oriented towards the improvement of the selectivity.

2.2.2. Cell cycle analysis

As a part of the study into the mechanism of action of these compounds, and to further characterize the anti-tumor properties, we used flow cytometry to analyze the influence of the most active compounds on the cell cycle in most sensitive CCRF-CEM cells (Table 3). After the 24 h treatment with 1×, 2× and 5× IC$_{50}$ concentration, the sub-G1 population was below 10% of total cells (with two exceptions, derivatives **19** and **22**), which indicates the use of reasonable dosing range and timing of the cell death. In derivative **19**, rapid induction of apoptosis demonstrated by high percentage of apoptotic cells within 24 h was observed with dependency on concentration. This can be caused either by the pro-drug activity or by a different mechanism of action in this compound. There was no dominant interference with the cell cycle regulation caused by any of the derivatives, however compounds **4**,
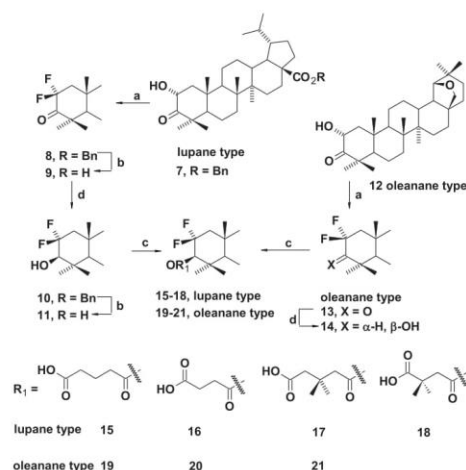
Scheme 2. Reagents and conditions: (a) DAST, pyridine, CHCl$_3$, r.t 11 h; (b) H$_2$, Pd/C (10%), THF, MeOH, r.t., 0.5 MPa; (c) anhydride of each diacid, DMAP, *sym*-collidine, reflux under Ar; (d) NaBH$_4$, MeOH, THF, 0 °C.

Table 1
Cytotoxic activities of all compounds from this work on reference cell line CCRF-CEM. The MTT assays were performed in doublets.

Compound	IC$_{50}$ (μmol/L[a])	Compound	IC$_{50}$ (μmol/L[a])
	CEM		CEM
1	250	12	250
2	250	13	250
3	14	14	250
4	9	15	4
5	69	16	8
6	68	17	5
7	16	18	5
8	70	19	24
9	2	20	102
10	13	21	127
11	4	22	1[b]

The standard deviation in cytotoxicity assays is typically up to 10% of the average value.

[a] 50% inhibiton concentration.
[b] Published in Ref. [16].

Table 2
Cytotoxic activities of selected compounds on 7 tumor (including resistant) and two normal fibroblast cell lines.

Compound	IC_{50} (μmol/L)									
	CEM	CEM-DNR	A549	K562	K562-TAX	HCT116	HCT116p53$^{-/-}$	BJ	MRC-5	TI[a]
9	2.4	6.2	5.8	2.6	2.3	4.4	4.7	15.4	9.1	5.1
11	4.0	10.9	6.7	5.5	4.1	7.3	5.8	18.7	14.7	4.2
15	4.1	14.7	10.7	6.5	5.8	6.1	5.9	34.7	29.2	7.8
16	8.3	24.4	17.4	18.3	19.8	14.8	8.6	76.6	27.9	6.3
17	6.2	15.7	13.3	12.9	16.0	14.2	7.1	39.6	14.7	4.4
18	4.5	11.4	11.4	11.8	11.5	8.5	3.7	26.0	12.8	4.3

[a] Therapeutic index calculated for CCRF-CEM line vs both fibroblasts.

7, **11**, **15**, **19**, **22** blocked or slowed down the cell cycle progression through G0/G1 or S-phase. Dihydrobetulinic acid (**4**) and 2,2-dibromodihydrobetulonic acid (**22**) were prepared during our previous work [16] and they had high cytotoxic activity. It was interesting to study how the cell cycle and DNA or RNA synthesis would be influenced by replacing hydrogen atoms in the position 2 by isosteric fluorine or bromine atoms. We found that both compounds **4** and **22** had similar influence on the cell cycle and DNA or RNA synthesis, however, 2,2-difluorodihydrobetulinic acid (**11**) was inhibiting RNA synthesis in 5× concentration. This is in concordance with the accumulation of the cells in the S phase of the cell cycle. Compounds **11**, **15**, **19**, and **22** in general decreased the DNA synthesis rate of CCRF-CEM cells. All 2,2-difluoroderivatives of betulinic acid were highly cytotoxic, which supports our hypothesis, that electronegative substituents such as fluorine or bromine in the position 2 of betulinic acid (with free carboxyl) enhance the cytotoxic activity.

2.2.3. Structure-property relationships

The solubility of both, betulinic acid and allobetulin derivatives in water based media is low but it can be significantly enhanced by esterification of the 3-OH group with a hemiester and using cyclodextrine formulas.

When we put our results of this simplified structure-activity relationship study into the context with the literature precedents, we get some general trends. It should be mentioned, however, that those assumption may be ambiguous because researchers worldwide often use different cell lines and their protocols vary in details. The trends we found are:

Table 3
Summary of conventional cell cycle, apoptosis, RNA/DNA — BrU/BrDU analysis of CEM leukemia cell line treated with the most potent compounds **4**, **7**, **11**, **15**, **19** and **22**. Data are expressed as a percentage of positive cells in the total cell population.

Derivatives	Cell cycle phases (%)					
	IC_{50}	Apoptosis	G$_{0/1}$	S	G$_2$/M	BrDU+	BrU+
control	0	2.20	43.00	45.00	12.00	62.50	47.80
4	1×	5.30	34.40	51.40	14.20	64.50	46.70
	2×	5.50	33.10	49.60	17.30	64.71	37.14
	5×	5.30	28.80	62.30	9.00	55.60	33.00
7	1×	2.00	38.30	50.00	11.70	61.90	53.60
	2×	1.90	36.20	49.60	14.20	63.38	50.89
	5×	2.00	32.40	56.40	11.20	61.30	40.00
11	1×	2.50	39.70	50.20	10.20	61.40	35.60
	2×	2.70	46.80	42.60	10.60	62.96	37.16
	5×	8.50	31.60	57.50	11.00	34.80	1.70
15	1×	3.00	45.60	43.90	10.50	60.00	39.40
	2×	3.60	48.60	40.00	11.40	60.87	42.91
	5×	2.30	44.20	39.40	16.40	41.30	30.13
19	1×	3.10	42.00	45.60	12.40	57.50	48.00
	2×	9.10	48.20	41.50	10.30	52.46	46.29
	5×	16.50	41.70	43.26	15.03	36.73	30.02
22	1×	4.80	37.60	51.00	11.40	64.40	52.50
	2×	18.10	43.60	48.30	8.10	65.88	55.26
	5×	26.20	33.20	52.90	13.90	45.10	39.60

1. The lowest IC_{50} can be found among the derivatives of betulinic acid while the activities of betulin and allobetulin analogs are generally worse [13,16,25]. In addition, in betulinic acid derivatives, the carboxylic function should be free [11,12,26].
2. Electronegative substituent at C-2 lowers the IC_{50} (improves the activity). It has previously been found in 2-carbonitrile derivatives [27], diosphenols [11], 2-halogenoderivatives [16,27], enamines [28], and here we report it in 2-fluoroderivatives.
3. 3-oxoderivatives are often more cytotoxic than 3-hydroxyderivatives, we saw it in our previous work [11,14,29] and we report it here. Dihydrobetulinic derivatives are slightly more active than the same analogs of betulinic acid (containing double bond 20(29)) [16,29].

Our recent book chapter [26] summarizes information from all papers about the influence of various prodrug-like substituents at 28-COOH and 3-OH in triterpenes on their biological activity and properties.

3. Conclusion

We prepared a small library of 21 compounds (11 of them new), derivatives of lupane and 18α-oleanane. The main aim was to investigate cytotoxicity of 2,2-difluoroderivatives because based on the data from analogs previously investigated; an electronegative substituent (EWG) on C-2 can enhance the biological activity. Starting from betulin (**1**), we prepared several derivatives with two fluorine atoms on C-2 and from the hydroxyanalogues, small sets of various hemiesters. The tests of cytotoxicity showed that the introduction of fluorine atoms to position 2 of triterpenic skeleton increased the cytotoxicity significantly (2.25× in lupane derivatives). The activity was selective against six cancer cell lines with rather low therapeutic indexes of 2—8. Hemiesters prepared from the active lupane derivatives had similar cytotoxicity to the parent compounds and there was almost no difference between various types of hemiesters, however, in allobetulin derivatives, the presence of the hemiester enhanced the activity >10×. We expect that they will show better pharmacological properties and bioavailability in *in vivo* experiments to follow than the parent hydroxyderivatives. Selectivity against p53 knock-out cancer line HCT116p53−/− was found in comparison to non-mutated line. From the cell cycle analysis we know that compounds **4**, **7**, **11**, **15**, **19**, **22** blocked or slowed down cell cycle progression through G0/G1 or S-phase which is in concordance with transcription inhibition by an unknown mechanism of action. From the comparison of dihydrobetulinic acid (**4**) to its 2,2-difluoro and 2,2-dibromoderivatives **9**, **11** and **22** it is clear that the introduction of two fluorine or bromine atoms enhanced the cytotoxicity. It seems that the mechanism of action is dependent on the halogen atom, however, along with an enhancement in activity, the selectivity decreases.

4. Experimental part

4.1. General experimental procedures

4.1.1. Materials and instruments

Melting points were determined using a Büchi B-545 apparatus and are uncorrected. Optical rotations were measured on an Autopol III (Rudolph Research, Flanders, USA) polarimeter in MeOH at 25 °C unless otherwise stated and are in [10^{-1} deg cm^2 g^{-1}]. ^{1}H, ^{19}F, and ^{13}C NMR spectra were recorded on Jeol (500 MHz for ^{1}H) instrument, using CDCl$_3$ or CD$_3$OD as a solvent (25 °C). Chemical shifts are expressed in ppm either with tetramethylsilane as an internal standard for ^{1}H spectra (CDCl$_3$) or were referenced to the residual signal of the solvent (CD$_3$OD). ^{13}C NMR spectra were referenced to CDCl$_3$ (77.00 ppm) or CD$_3$OD (49.15 ppm). EI MS spectra were recorded on an INCOS 50 (Finigan MAT) spectrometer at 70 eV and an ion source temperature of 150 °C. The samples were introduced from a direct exposure probe at a heating rate of 10 mA/s. Relative abundances stated are related to the most abundant ion in the region of $m/z > 180$. MS-ESI and MS-APCI spectra of prepared compounds were recorded on a Micromass Platform LC (Waters), samples were introduced as methanolic solutions. The concentrations and time of data collections were chosen to get optimal spectra, only [M + H]$^+$ or [M + Na]$^+$ ions are given. IR spectra were recorded on a Nicolet Avatar 370 FTIR. DRIFT stands for Diffuse Reflectance Infrared Fourier Transform. Elemental analyses were recorded at the Institute of Organic Chemistry Academy of Sciences of the Czech Republic on the PE 2400 Series II CHNS/O Analyzer (Perkin Elmer, USA).

TLC was carried out on Kieselgel 60 F$_{254}$ plates (Merck) detected by spraying with 10% aqueous H$_2$SO$_4$ and heating to 150–200 °C. Column chromatography was performed using silica gel 60 (Merck 7734). The HPLC system consisted of a high-pressure pump (Gilson model 361), a Rheodyne injection valve, and a preparative column (25 × 250 mm) filled with silica gel (Biospher 7 μm), the differential refractometer detector (Laboratorni Pristroje, Praha, CZ) was connected with a PC (software Chromulan) and an automatic fraction collector (Gilson model 246). A mixture of EtOAc and hexane was used as the mobile phase, its composition specified in each experiment. Work-up refers to pouring the reaction mixture into water, extracting the product into organic solvent, washing the organic layer successively in this order with water, diluted aqueous HCl, water, saturated aqueous sodium hydrogencarbonate, and again water. Then the organic phase was dried over magnesium sulfate, filtered, and the solvents evaporated under reduced pressure. Analytical samples were dried over P$_2$O$_5$ under diminished pressure. Bulk syntheses of the starting compounds were carried out in 30 L duplicated glass reaction vessel with shaft stirrer. Betulin (**1**) and hydroxyketone **12** were obtained from company Betulinines (www.betulinines.com). DAST and dimethylsuccinic anhydride were purchased from Acros Organics. All other chemicals and solvents were obtained from Sigma–Aldrich.

4.1.2. General procedure for deprotection of benzyl esters

Palladium on charcoal (0.12–3 g; 10%) was added to each benzyl ester (1.7–3.4 g; 10%) in mixture THF (10–25 mL) and methanol (10–25 mL), the solution was placed into a cylinder and pressurized with H$_2$ (0.5 MPa) while vigorously stirred at r.t. The reaction progress was monitored using TLC in toluene/Et$_2$O 6:1. Upon completion, the catalyst was filtered off using cellite column, then solvents were evaporated under vacuo and the crude acid was purified on silica gel (100 g, eluted with EtOAc, unless otherwise stated at the experiment). The solvents were evaporated under vacuo and pure acid was precipitated/crystallized using cyclohexane and dried under vacuo.

4.1.3. General procedure for acylation of hydroxyderivatives

DMAP (0.4 mmol) was added to a solution of each hydroxyderivative (1.0–1.5 mmol) followed by addition of each anhydride (5.0–6.1 mmol) in sym-collidine (15–20 mL) under argon. The mixture was heated under reflux and monitored by TLC in CHCl$_3$/EtOAc/AcOH 100:20:1. After the completion (30–50 h), the mixture was cooled to r.t. and then worked up by pouring into HCl (3%, 200 mL). The product was extracted to EtOAc (3×). Organic phase was washed with HCl (8%, twice) and with water, then dried and solvents were removed under vacuo. Crude product was purified by chromatography on silica gel (100 g) eluted with gradient from hexane/EtOAc 10%–100% EtOAc. Mobile phase was evaporated and the oily product was precipitated by heating with 2,2,4-trimethylpentane (or cyclohexane), filtered off and dried under reduced pressure.

4.2. Synthetic procedures

4.2.1. Benzyl dihydrobetulonate (**6**)

Betulin (**1**) was converted to dihydrobetulin-3β-acetate (**2**) by a standard procedure [21,22] with yield of 54% over three steps. All spectral data were identical to those in lit [22].

Benzyl dihydrobetulinate (**5**) was prepared by multistep procedure where some steps were different from the literature [23] however, all intermediates are well known compounds and their spectral data were identical to the authentic samples. Therefore we describe the procedures but we publish the spectral data only for the final product. Solution of sodium periodate (650 g, 2 mol) in water (3.8 L) was slowly added to a solution of **2** (150.0 g; 0.31 mol) in EtOAc (8 L), MeCN (0.5 L) and water (2.1 L) while the mixture was vigorously stirred. Ruthenium (IV) oxide was added and the mixture was heated to 55 °C while still vigorously stirred for 140 min. The reaction was monitored using TLC toluene/Et$_2$O 6/1. The reaction was quenched by adding isopropyl alcohol (100 mL). After another 15 min, ruthenium (IV) oxide was filtered off and water phase was removed. The organic phase was washed with water solution of sodium sulfite and sodium metabisulfite and solid precipitate was filtered off and discarded. Organic phase was filtered over a pad of silica gel (200 g) and the pad was washed with EtOAc. The solvents were removed under vacuo and the product was crystallized from isopropyl alcohol to give white crystals of 3β-acetyldihydrobetulinic acid (**3**) (125 g; 81%) which was immediately deacetylated by standard procedure (reflux with abundant KOH in mixture toluene and ethanol). Isolated dihydrobetulinic acid (**4**) was arylated with benzyl bromide (1.2 equiv.) and K$_2$CO$_3$ in a mixture of DMF (1 L) and MeCN (200 mL) to give crude benzyl-dihydrobetulinate (**5**). Benzyl-dihydrobetulinate (**5**) (120.0 g; 0.22 mol) and sodium acetate (120.0 g; 0.88 mol) was dissolved in a mixture of acetic acid (1.2 L), toluene (1 L) a acetic anhydride (72 mL) and sodium dichromate (60.0 g; 0.20 mol) was added. The reaction mixture was stirred 22 h at r.t. and the progress was monitored on TLC in toluene/Et$_2$O (6:1). After the completion, the reaction mixture was poured into water (12 L) and crude product was extracted to toluene. Organic phase was washed with solution of sodium bicarbonate (3×), water and the solvents were removed under vacuo. Crude benzylester **6** was chromatographed on silica gel in toluene and crystallized from methanol to give white crystals (102.8 g; 64% over all 4 steps). Benzyl dihydrobetulonate (**6**).

Yield 102.8 g (64% over 4 steps); mp 151–153 °C (Lit.^{23} 148–150 °C); [α]$_D$ +13.7 (c 0.35) {Lit [23]. [α]$_D$ +14.3 (c 0.70)}. IR (DRIFT): 1701 (C=O), 1717 (C=O) cm^{-1}. ^{1}H NMR and ^{13}C NMR are identical to the spectra in lit [23]. MS (ESI$^+$): m/z (%) = 569 (12, [M + Na]$^+$). Anal. Calcd for C$_{37}$H$_{54}$O$_3$: C, 81.27; H, 9.95; O, 8.78. Found: C, 81.30; H, 9.95; O, 8.77.

4.2.2. Benzyl 2α-hydroxydihydrobetulonate (7)

Benzyl dihydrobetulonate (6) (87.4 g; 0.16 mol) was dissolved in dichloromethane (1.4 L) and 0.1% (vol.) solution of H_2SO_4 in MeOH (2.8 L), then 3-chloroperoxybenzoic acid (75%; 108.6 g; 0.44 mol) was slowly added in several portions within 17 h while the mixture was vigorously stirred. The reaction was monitored on TLC in toluene/Et_2O 6:1. The reaction was diluted with water (8 L, twice), the organic phase was separated, washed with a concentrated solution of sodium sulfite ($2\times$) and then with a mixture of solution of potassium iodide (10%) and 25% solution of sodium thiosulfate in water. The last washing was performed using concentrated water solution of $NaHCO_3$. Organic phase was separated, dried over calcium chloride and the solvents were removed under vacuo. Crude benzylester 7 was purified by chromatography on silica gel (2.5 kg) in toluene/Et_2O 10:1. Product was crystallized from MeOH// acetone. Yield 32.4 g (36%); mp 157–159 °C; $[\alpha]_D$ +8.9 (c 0.45). IR (DRIFT): 1708 (C=O), 1753 (C=O), 3481 (O–H) cm^{-1}. ^{1}H NMR: δ = 0.74 (d, 3H, J = 8.8 Hz), 0.78 (s, 3H), 0.85 (d, 3H, J = 9.2 Hz), 0.89 (s, 3H), 1.09 (s, 3H), 1.13 (s, 3H), 1.15 (s, 3H), 2.15–2.35 (m, 4H, H-1α, H-13, H-16, H-19), 2.47 (dd, 1H, J = 12.6, 6.9 Hz, H-1β), 4.53 (dd, 1H, J = 12.3, 6.6 Hz, H-2β), 5.08 (d, 1H, J = 12.4 Hz, H-31a), 5.13 (d, 1H, J = 12.4 Hz, H-31b), 7.32 (m, 5H, Ph). ^{13}C NMR: δ = 14.5, 14.6, 16.0, 16.6, 19.1, 21.2, 21.4, 22.7, 23.0, 24.5, 26.7, 29.5, 29.7, 32.0, 34.1, 37.2, 37.9, 37.9, 40.76, 42.6, 44.2, 47.7, 48.9, 49.9, 49.9, 56.9, 57.8, 65.6, 69.3, 128.0, 128.2, 128.3, 128.4, 128.4, 136.5, 175.9, 216.7. MS (ESI$^+$): m/z (%) = 585 (5, [M + Na]$^+$). Anal. Calcd for $C_{37}H_{54}O_4$: C, 78.96; H, 9.67; O, 11.37. Found: C, 78.98; H, 9.66; O, 11.40.

4.2.3. Benzyl 2,2-difluorodihydrobetulonate (8)

DAST (20 mL; 0.15 mol) was added to a solution of benzyl ester 7 (13.3 g; 23.7 mmol) v $CHCl_3$ (250 mL) and immediately after was added pyridine (13.5 mL; 0.17 mol) and the mixture was stirred 11 h at r.t. while monitored on TLC toluene/hexane 1:1. After the completion, the reaction was quenched with isopropyl alcohol (20 mL) that was added slowly while the mixture was cooled in ice bath. Then ice was added (30 g) and the mixture was carefully neutralized by a solution of NaOH (10%, 30 mL), then more water (1 L) was added and the product was extracted to $CHCl_3$ ($3\times$). Organic phase was washed twice with diluted HCl (1:4), water ($3\times$), NaOH (1% in water) and water. Crude 8 (11.7 g) was chromatographed on silica gel in mixture of toluene/hexane 1:1 to give difluoroketone 8 (9.4 g; 68%); mp 143–145 °C (isopropyl alcohol); $[\alpha]_D$ +52.5 (c 0.40). IR (DRIFT): 1725 (C=O), 1740 (C=O) cm^{-1}. ^{1}H NMR; ^{13}C NMR; ^{19}F NMR with the full assignment of all signals are in the Supplementary Information. MS (ESI$^+$): m/z (%) = 605 (12, [M + Na]$^+$). Anal. Calcd for $C_{37}H_{52}F_2O_3$: C, 76.25; H, 8.99; F, 6.52; O, 8.24. Found: C, 76.27; H, 9.00; F, 6.52; O, 8.24.

4.2.4. 2,2-Difluorodihydrobetulonic acid (9)

Benzyl ester 7 (1.0 g; 1.7 mmol) was deprotected according to the general procedure (except $CHCl_3$ was used as a mobile phase for the chromatography) to give acid 7a (720 mg; 85%); mp 265–267 °C (cyclohexane); $[\alpha]_D$ +65.0 (c 0.40). IR (DRIFT): 1688 (C=O), 1741 (C=O), 2400–3350 (COOH) cm^{-1}. ^{1}H NMR: δ = 0.78 (d, 3H, J = 6.8 Hz), 0.87 (d, 3H, J = 6.8 Hz), 0.88 (s, 3H), 0.95 (s, 3H), 1.00 (s, 3H), 1.15 (s, 3H), 1.23 (d, 3H, J = 1.2 Hz), 1.71 (dd, 1H, J = 12.6 Hz, J_2 = 3.4 Hz), 1.79 (m, 2H), 1.91 (dd, 1H, J_1 = 13.0 Hz, J_2 = 7.5 Hz), 2.05 (m, 1H, H-1a), 2.15–2.35 (m, 4H, H-1b, H-13, H-16, H-19). ^{13}C NMR: δ = 14.5, 14.6, 15.4, 18.2, 19.6, 21.0, 21.8, 22.7, 23.0 26.7, 28.0, 29.6, 29.7, 31.9, 32.8, 37.0 (q, J = 3.3 Hz), 37.3, 38.3, 40.6, 42.7, 44.1, 46.0, 48.6, 49.4, 50.9, 51.5 (m, ΣJ = 50.3 Hz), 56.8, 181.4. ^{19}F NMR: δ = –99.96 (ddd, J = 262.4, 20.0, 6.8 Hz), -88.00 (ddd, J = 262.2, 29.3, 20.0 Hz). MS (ESI$^+$): m/z (%) = 515 (30, [M + Na]$^+$). Anal. Calcd for $C_{30}H_{46}F_2O_3$: C, 73.13; H, 9.41; F, 7.71; O, 9.74. Found: C, 73.17; H, 9.40; F, 7.70; O, 9.74.

4.2.5. Benzyl-2,2-difluorodihydrobetulinate (10)

$NaBH_4$ (700 mg; 3.7 mmol) was slowly added to a vigorously stirred solution of benzyl ester 8 (5.0 g; 8.6 mmol) in methanol (60 mL) and THF (70 mL) at 0 °C. The mixture was allowed to heat up to r.t. and stirred another 16 h while monitored on TLC toluene/Et_2O 6:1. The reaction was quenched by adding diluted HCl (1:5, 150 mL) and the product was extracted to EtOAc. Organic phase was collected, washed with water ($3\times$) and the solvents were removed in vacuo. Crude product was crystallized from isopropyl alcohol to give benzyl ester 10 (4.9 g; 98%); mp 175–176 °C; $[\alpha]_D$ +0.0 (c 0.40). IR (DRIFT): 1683 (C=O), 3496 (O–H) cm^{-1}. ^{1}H NMR (300 MHz; CDCl$_3$): δ = 0.75 (d, 3H, J = 6.9 Hz), 0.74 (s, 3H), 0.85 (d, 3H, J = 6.9 Hz), 0.88 (s, 3H), 0.93 (s, 3H), 0.97 (s, 3H), 1.08 (s, 3H), 2.20 (m, 1H, H-1a), 2.21–2.47 (m, 4H, H-1b, H-13, H-16, H-19), 3.34 (dd, 1H, J = 22.3, 6.9 Hz, H - 3α), 5.09 (d, 1H, J = 13.1 Hz, H - 31a), 5.13 (d, 1H, J = 11.0 Hz, H – 31b), 7.31 (m, 5H, ΣJ = 28.5 Hz, Ph). ^{13}C NMR (75.45 MHz): δ = 14.5, 14.6, 15.4 (d), 15.5 (d), 15.8, 18.0, 21.15, 22.7, 23.0, 26.7, 29.1, 29.4, 29.7, 32.0, 34.0, 37.3, 37.9, 38.2 (d), 39.6 (d), 40.8, 42.7, 44.2, 46.1 (t), 48.9, 50.7, 54.9, 56.9, 65.6, 78.5 m, 128.0, 128.3, 128.3, 128.5, 128.5, 136.5, 175.9. ^{19}F NMR: δ = –90.26 (d, 2 F, J = 244.7 Hz). MS (APCI$^-$): m/z (%) = 493 (100, [M-Bn]$^-$). MS (APCI$^+$): m/z (%) = 607 (15, [M + Na]$^+$). Anal. Calcd for $C_{37}H_{54}F_2O_3$: C, 76.06; H, 9.28; F, 6.48; O, 8.18. Found: C, 75.99; H, 9.31; F, 6.50; O, 8.21.

4.2.6. 2,2-Difluorodihydrobetulinic acid (11)

Benzyl ester 10 (2.0 g; 3.4 mmol) was deprotected using the general procedure to give difluorodihydrobetulinic acid (11) (1.6 g; 95%); mp 260 - 201 °C (cyclohexane); $[\alpha]_D$ –8.6 (c 0.35). IR (DRIFT): 1685 (C=O), 2300–3610 (COOH) cm^{-1}. ^{1}H NMR (300 MHz; CDCl$_3$): δ = 0.77 (d, 3H, J = 6.9 Hz), 0.87 (d, 3H, J = 7.2 Hz), 0.89 (s, 3H), 0.95 (s, 3H), 0.96 (s, 3H), 0.99 (s, 3H), 1.09 (s, 3H), 1.89 (m, 1H, H-1a), 2.28–2.55 (m, 4H, H-1b, H-13, H-16, H-19), 3.35 (dd, 1H, J = 12.3 Hz, 6.9 Hz, H – 3α). ^{13}C NMR (75.45 MHz; CDCl$_3$): δ = 14.5, 14.6, 15.3 (d), 15.5 (d), 16.0, 18.0, 21.13, 22.7, 23.0, 26.7, 29.1, 29.5, 29.7, 32.0, 34.0, 37.4, 38.1, 38.3 (d), 39.6 (d), 40.8, 42.7, 44.2, 46.1 (t), 48.7, 50.6, 54.9, 56.8, 78.5 (m), 182.4. ^{19}F NMR δ = –110.31 (dd, J = 242.5, 76.14 Hz), -90.88 (dd, J = 248.2 Hz, 5.6 Hz). MS (APCI$^-$): m/z (%) = 493 (6, [M–H]$^-$). MS (APCI$^+$): m/z (%) = 517 (13, [M + Na]$^+$). Anal. Calcd for $C_{30}H_{48}F_2O_3$: C, 72.90; H, 9.76; F, 7.66; O, 9.68. Found: C, 72.84; H, 9.78; F, 7.68; O, 9.70.

4.2.7. Difluoroallobetulone 13

Difluoroketone 13 was prepared using a original procedure (without pyridine) from lit [17] DAST (3.5 mL; 26.50 mmol) was added to a solution of known[17] hydroxyketone 12 (3.50 g; 8.0 mmol) in $CHCl_3$ (20 mL) and the mixture was stirred at r.t. for 4 days. The reaction progress was monitored on TLC in toluene/Et_2O 15:1. Then, water was added followed with solid $NaHCO_3$ until CO_2 was developing. The organic phase was separated, washed with water and the solvents were removed in vacuo. Crude compound was chromatographed on silica gel (100 g) in mixture of toluene/hexane 1:1 to give difluoroketone 13 (1.5 g; 41%), mp. 247–249 °C (MeOH), $[\alpha]_D$ +119 (c 0.52) (lit [17]. mp. 243–245 °C, $[\alpha]_D$ +123. ^{1}H NMR spectrum was identical to a spectrum in literature [17].

4.2.8. Difluoroallobetulin 14

Difluoroalcohol 14 was prepared using a modified procedure from lit.[17] $NaBH_4$ (200 mg, 5.3 mmol) was slowly added to a cooled (0 °C) solution of difluorketone 13 (1.5 g; 3.1 mmol) in a mixture of THF (145 mL) and MeOH (135 mL) and the mixture stirred for 3 h and then poured into diluted HCl (1:5, 500 mL), extracted to CHCl$_3$, collected organic phase was washed with water and the solvents were removed in vacuo. The crude product was chromatographed on silica gel (150 g) in toluene to give compound 14. Since the

purity wasn't sufficient yet, the sample was chromatographed on preparative HPLC in hexane/EtOAc 9:1 to give difluoroallobetulin **14** (850 mg; 57%); mp. 297–300 °C (MeCN), $[\alpha]_D$ +46 (c 0.39) (lit [17]. mp. 299–301 °C, $[\alpha]_D$ +48).

^{1}H NMR was identical to the spectrum in lit [17].

4.2.9. 3β-O-hemiglutaryl-2,2-difluorodihydrobetulinic acid (15)

Difluorodihydrobetulinic acid (**11**) (500 mg; 1.01 mmol) and glutaric anhydride (580 mg; 5.08 mmol) reacted according to the general procedure to give ester **15** (445 mg; 72%); mp 219–220 °C (2,2,4-trimethylpentane). IR (DRIFT): 1694 (C=O), 1729 (C=O), 2500–3300 (COOH) cm^{-1}. ^{1}H NMR (500 MHz; CDCl$_3$): δ = 0.75 (d, 3H, J = 6.9 Hz), 0.86 (d, 3H, J = 6.9 Hz), 0.90 (s, 3H), 0.92 (s, 3H), 0.93 (s, 3H), 0.95 (s, 3H), 1.02 (s, 3H), 1.68 (bd, 1H, J = 13.2 Hz), 1.73–1.83 (m, 1H), 1.87 (dd, 1H, J = 12.6 Hz, 7.5 Hz), 1.95–2.06 (m, 2H, HOOCCH$_2$**CH$_2$**CH$_2$COO), 2.13–2.35 (m, 4H, HOOC**CH$_2$**CH$_2$**CH$_2$**COO), 2.40–2.60 (m, 4H, H-1b, H-13, H-16, H-19), 4.86 (dd, 1H, J = 22.9 Hz, 5.7 Hz, H - 3α). ^{13}C NMR (125.77 MHz; CDCl$_3$) δ = 14.5, 14.6, 15.6, 15.6, 16.2, 16.5, 18.0, 19.9, 21.1, 22.7, 23.0, 26.6, 28.8, 29.5, 29.7, 30.1, 32.0, 32.9, 33.2, 34.0, 37.3, 38.1, 38.4 (d, J = 9.6 Hz), 39.4 (d, J = 4.8 Hz), 40.8, 42.7, 44.2, 46.4 (t, J = 19.2 Hz), 48.7, 50.5, 54.8, 56.8, 172.3, 179.0, 183.0. ^{19}F NMR δ = −105.59 (dm, J = 251.7 Hz), −90.04 (d, J = 251.9 Hz). MS (ESI$^+$): m/z (%) = 631 (100, [M + Na]$^+$). MS (ESI$^-$): m/z (%) = 607 (100, [M − H]$^-$). Anal. Calcd for C$_{36}$H$_{54}$F$_2$O$_6$: C, 69.05; H, 8.94; F 6.24; O, 15.77. Found: C, 69.11; H, 8.95; F 6.12; O, 15.70.

4.2.10. 3β-O-hemisuccinyl-2,2-difluorodihydrobetulinic acid (16)

Difluorodihydrobetulinic acid (**11**) (500 mg; 1.0 mmol) and succinic anhydride (500 mg; 5.0 mmol) reacted according to the general procedure to give ester **16** (344 mg; 57%); mp 256–257 °C (2,2,4-trimethylpentane); $[\alpha]_D$ −10.0 (c 0.40). IR (DRIFT): 1706 (C=O), 1761 (C=O), 2350–3300 (COOH) cm^{-1}. ^{1}H NMR (300 MHz; CDCl$_3$) δ = 0.76 (d, 3H, J = 6.0 Hz), 0.86 (d, 3H, J = 6.0 Hz), 0.90 (d, 3H, J = 6.0 Hz), 0.94 (s, 3H) 0.95 (s 3H) 0.96 (s, 3H), 1.02 (s, 3H), 1.79 (m, 1H), 1.88 (m, 1H), 2.10–2.45 (m, 4H, H-1b, H-13, H-16, H-19), 2.78 (m, 4H, ΣJ = 51 Hz, 2× CH$_2$), 4.89 (dd, 1H, J = 12.9 Hz, 5.2 Hz, H − 3α). ^{13}C NMR (75.45 MHz; CDCl$_3$) δ = 14.5, 14.7, 15.6 (d), 16.0, 16.4, 18.0, 21.3, 22.8, 23.0, 26.8, 28.8, 29.75, 29.8, 32.2, 34.1, 37.5, 38.1, 38.4 (d), 39.6 (d), 40.9, 42.8, 44.3, 44.3, 44.3, 46.5 (t), 48.7, 50.0, 50.7, 54.9, 56.7, 77.2, 171.7, 178.4, 183.2. ^{19}F NMR δ = −105.54 (dm, J = 251.9 Hz), −90.01 (d, J = 251.9 Hz). MS (ESI$^-$): m/z (%) = 593 (100, [M−H]$^-$). MS (ESI$^+$): m/z (%) = 617 (75, [M + Na]$^+$). Anal. Calcd for C$_{34}$H$_{52}$F$_2$O$_6$: C, 68.69; H, 8.80; F, 6.37; O, 16.14. Found: C, 68.66; H, 8.81; F, 6.39; O, 16.14.

4.2.11. 3β-O-3′,3′-dimethylhemiglutaryl-2,2-difluorodihydrobetulinic acid (17)

Difluorodihydrobetulinic acid (**11**) (500 mg; 1.0 mmol) and 3,3-dimethylglutaric anhydride (700 mg; 4.9 mmol) reacted according to the general procedure to given ester **17** (516 mg; 80%); mp 204–205 °C (2,2,4-trimethylpentan); $[\alpha]_D$ −14.3 (c 0.35). IR (DRIFT): 1702 (C=O), 1736 (C=O), 2500–3300 (COOH) cm^{-1}. ^{1}H NMR (300 MHz; CDCl$_3$): 0.76 (d, 3H, J = 6.0 Hz), 0.86 (d, 3H, J = 6.0 Hz), 0.89 (s, 3H), 0.92 (d, 3H, J = 3.0 Hz), 0.94 (s, 3H), 0.97 (s, 3H), 1.03 (s, 3H), 1.10 (s, 3H), 1.18 (s, 3H), 1.88 (m, 1H), 2.10–2.50 (m, 7H, H-1a, H-1b, H-13, H-16, H-19, 2× H-hemiester), 2.83 (d, 1H, J = 16.3 Hz, 1× H-hemiester), 3.80 (d, 1H, J = 16.3 Hz, 1× H-hemiester), 4.86 (dd, 1H, J = 22.9.0, 6.2 Hz, H - 3α). ^{13}C NMR (75.45 MHz; CDCl$_3$): δ = 14.1, 14.4, 15.7 (d), 16.5 (d), 18.1, 21.1, 22.8, 23.0, 25.4, 26.3, 28.4, 28.5, 29.6, 30.1, 32.2, 33.7, 37.2, 38.1, 38.4 (d), 39.5 (d), 40.6, 42.5, 43.2, 44.3, 44.5, 48.9, 49.9, 53.1, 54.5, 56.9, 171.4, 178.3, 183.1. ^{19}F NMR δ = −102.52 (dm, J = 244.7 Hz), −88.54 (d, J = 251.9 Hz). MS (ESI$^-$): m/z (%) = 635 (45, [M − H]$^-$). MS (ESI$^+$): m/z (%) = 659 (80, [M + Na]$^+$). Anal. Calcd for C$_{37}$H$_{58}$F$_2$O$_6$: C, 69.79; H, 9.17; F, 5.96; O, 15.08. Found: C, 69.78; H, 9.18; F, 5.97; O, 15.07.

4.2.12. 3β-O-3′,3′-dimethylhemisuccinyl-2,2-difluorodihydrobetulinic acid (18)

Difluorodihydrobetulinic acid (**11**) (760 mg; 1.5 mmol) and dimethylsuccinic anhydride (650 mg; 5.1 mmol) reacted according to the general procedure to give ester **18** (264 mg; 28%); mp 203–205 °C (2,2,4-trimethylpentane); $[\alpha]_D$ −22.9 (c 0.35). IR (DRIFT): 1682 (C=O), 1706 (C=O), 1742 (C=O), 2400–3400 (COOH) cm^{-1}. ^{1}H NMR (300 MHz; CDCl$_3$): δ = 0.76 (d, 3H, J = 9.0 Hz), 0.86 (d, 3H, J = 6.0 Hz), 0.89 (s, 3H), 0.92 (s, 3H), 0.94 (d, 3H, J = 9.0 Hz), 0.95 (s, 3H), 1.01 (s, 3H), 1.33 (s, 6H, 2× CH$_3$), 1.88 (m, 1H), 2.10–2.50 (m, 5H, H-1a, H-1b, H-13, H-16, H-19), 2.65 (d, 1H, J = 16.0 Hz, 1× H-hemiester), 3.80 (d, 1H, J = 16.0 Hz, 1× H-hemiester), 4.86 (bd, 1H, J = 22.0, Hz, H − 3α). ^{13}C NMR (75.45 MHz; CDCl$_3$): δ = 14.6, 14.8, 15.8, 16.3, 16.6, 18.2, 21.3, 22.9, 23.1, 25.3, 25.7, 26.8, 28.8, 29.8, 30.2, 32.2, 34.2, 37.6, 38.2, 38.5, 39.6, 40.5, 41.0, 42.9, 44.3, 44.3, 44.3, 48.8, 50.0, 50.7, 55.0, 56.8, 77.2, 171.2, 180.6, 180.6. ^{19}F NMR δ = −103.59 (dm, J = 244.7 Hz). MS (ESI$^-$): m/z (%) = 621 (75, [M − H]$^-$). MS (ESI$^+$): m/z (%) = 645 (100, [M + Na]$^+$). Anal. Calcd for C$_{36}$H$_{56}$F$_2$O$_6$: C, 69.44; H, 9.06; F, 6.09; O, 15.41. Found: C, 69.42; H, 9.06; F, 6.10; O, 15.41.

4.2.13. 2,2-Difluoro-19β,28-epoxy-18α-oleanane-3β-yl hemiglutarate (19)

Hemiglutarate **19** was prepared by the general procedure from **14** (200 mg; 0.40 mmol). Crude product was chromatographed on silica gel (40 g) in gradient from 40% EtOAc in hexane to 100% EtOAc to give **19** (110 mg; 44%); mp. 230.0 °C (lyophilized from t-BuOH); $[\alpha]_D$ +41.5 (c 0.24). IR (DRIFT): 1710 (C=O), 1744 (C=O), 2866 (COOH), 2946 (COOH) cm^{-1}. ^{1}H NMR (400 MHz; CDCl$_3$): δ = 0.80 (s, 3H), 0.90 (s, 3H), 0.93 (d, 3H, J = 0.9 Hz), 0.93 (s, 3H), 1.00 (s, 3H), 1.04 (s, 3H), 1.97–2.10 (m, 2H, HOOCCH$_2$**CH$_2$**CH$_2$COO), 2.31 (td, 1H, J = 13.7, 4.9 Hz, H-1α), 2.40–2.60 (m, 4H, HOOC**CH$_2$**CH$_2$**CH$_2$**COO), 3.46 (d, 1H, J = 7.8 Hz, H-28a), 3.54 (s, 1H, H-19α), 3.78 (d, 1H, J = 7.6 Hz, H-28b), 4.87 (dd, 1H, J = 23.3, 5.8, H-3α). ^{13}C NMR (125 MHz; CDCl$_3$): δ = 13.42, 15.67, 15.94 (d, J = 6 Hz), 16.48 (d, J = 3 Hz), 17.95, 19.96, 21.28, 24.51, 26.17, 26.22, 26.29, 28.75, 28.75, 32.60, 32.66, 33.16, 33.56, 33.99, 36.23, 36.68, 38.43 (d, J = 9 Hz), 39.37 (d, J = 6 Hz), 40.77, 40.88, 41.44, 46.66 (t, J = 19 Hz), 46.74, 51.42, 55.04, 71.16, 77.20, 87.92, 121.54 (J = 248, 240 Hz), 172.41, 177.69. ^{19}F NMR: δ = −90.06 (d, 2 F, J = 244.7 Hz). MS (EI): m/z (%) = 591 (M$^+$–H, 100), 544 (5), 425 (13), 361 (13), 32 (13), 265 (8). Anal. Calcd for C$_{35}$H$_{54}$F$_2$O$_5$: C 70.91; H 9.18; F 6.41. Found: C 70.89; H 9.17; F 6.44.

4.2.14. 2,2-Difluoro-19β,28-epoxy-18α-oleanane-3β-yl hemisuccinate (20)

Hemisuccinate **20** was prepared by the general procedure from **14** (200 mg; 0.40 mmol). Crude product was chromatographed on silica gel (40 g) in gradient from 40% EtOAc in hexane to 100% EtOAc to give **20** (100 mg; 41%); mp. 109.3 °C (acetonitrile); $[\alpha]_D$ +48,1 (c 0.26). IR (DRIFT): 1731 (C=O), 1751 (C=O), 2736 (COOH), 2851 (COOH), 2957 (COOH), 3407 (O—H) cm^{-1}. ^{1}H NMR (400 MHz; CDCl$_3$): δ = 0.80 (s, 3H), 0.89 (s, 3H), 0.92 (s, 3H), 0.93 (s, 3H), 0.94 (d, 3H, J = 0.9 Hz), 1.00 (s, 3H), 1.04 (s, 3H), 2.32 (td, 1H, J = 13.8, 4.8 Hz, H-1α), 2.67–2.81 (m, 4H, HOOC**CH$_2$**CH$_2$COO), 3.46 (d, 1H, J = 7.8 Hz, H-28a), 3.54 (s, 1H, H-19α), 3.78 (d, 1H, J = 7.5 Hz, H-28b), 4.88 (dd, 1H, J = 23.1, 5.7 Hz, H-3α). ^{13}C NMR (125 MHz; CDCl$_3$): δ = 13.42, 15.67, 15.93 (d, J = 6 Hz), 16.41 (d, J = 3 Hz), 17.93, 21.30, 24.51, 26.18, 26.22, 26.29, 28.57, 28.76, 28.80, 28.90, 32.66, 33.56, 34.00, 36.23, 36.68, 38.42 (d, J = 9 Hz), 39.44 (d, J = 6 Hz), 40.77, 40.88, 41.44, 46.68 (t, J = 19 Hz), 46.75, 51.41, 55.09, 71.17, 77.65 (t, J = 19 Hz), 87.93, 121.47 (dd, J = 242, 250 Hz), 171.64, 177.00. ^{19}F NMR spectrum: −90.60 (dd, J = 248, 4.8 Hz), −106.32 (dddd, J = 249.2, 34.7, 22.9, 14.1). MS (EI): m/z (%) = 577 (M$^+$ − H, 90), 478 (56), 458 (61), 407 (93), 342 (22), 323 (19), 297 (7), 269 (10), 236

(25), 205 (73), 191 (100). Anal. Calcd for $C_{34}H_{52}F_2O_5$: C 70.56; H 9.06; F 6.57. Found: C 70.61; H 9.07; F 6.55.

4.2.15. 2,2-Difluoro-19β,28-epoxy-18α-oleanane-3β-yl 3',3'-dimethylhemiglutarate (21)

Dimethylhemiglutarate **21** was prepared by the general procedure from **14** (200 mg; 0.40 mmol). Crude product was chromatographed on silica gel (40 g) in gradient from 40% EtOAc in hexane to 100% EtOAc to give **21** (190 mg; 73%); mp. 111.4 °C (lyophilized from t-BuOH); $[\alpha]_D$ +20.8 (c 0.39). IR (DRIFT): 1689 (C=O), 2700 (COOH), 2964 (COOH) cm^{-1}. ^{1}H NMR (400 MHz; CDCl$_3$): δ = 0.81 (s, 3H), 0.91 (s, 3H), 0.92 (s, 3H), 0.93 (s, 3H), 0.93 (s, 3H), 1.00 (s, 3H), 1.03 (s, 3H), 1.17 (s, 3H), 1.18 (s, 6H), 2.31 (td, 1H *J* = 13.7, 4.8 Hz, H-1α), 2.52 (s, 2H), 2.53 (d, 1H, *J* = 14.8 Hz), 2.67 (d, 1H, *J* = 14.8 Hz, HOOC**CH₂**C**CH₂**COO), 3.47 (d, 1H, *J* = 7.7 Hz, H-28a), 3.59 (s, 1H, H-19α), 3.81 (d, 1H, *J* = 7.8 Hz, H-28b), 4.88 (dd, 1H, *J* = 23.4, 5.9 Hz, H-3α). ^{13}C NMR (125 MHz; CDCl$_3$): δ = 13.42, 15.66, 15.89 (d, *J* = 6 Hz), 16.48 (d, *J* = 3 Hz), 17.95, 21.28, 24.50, 26.13, 26.20, 26.29, 27.77, 27.77, 28.72, 28.72, 32.52, 32.64, 33.57, 33.94, 36.18, 36.63, 38.41 (d, *J* = 9 Hz), 39.32 (d, *J* = 6 Hz), 40.77, 40.87, 41.44, 44.67, 45.07, 46.65 (t, *J* = 19 Hz), 46.71, 51.40, 55.06, 71.05, 77.12, 87.99, 121.52 (dd, *J* = 249, 240 Hz), 171.56, 178.03. ^{19}F NMR: δ = −89.29 (d, 2 F, *J* = 251.9 Hz). MS (EI): *m/z* (%) = 619 (M$^+$ − H, 100), 508 (3), 465 (3), 385 (4), 325 (5), 265 (4), 181 (3). Anal. Calcd for $C_{37}H_{58}F_2O_5$: C 71.58; H 9.42; F 6.12. Found: C 71.55; H 9.41; F 12.95.

4.3. MTT assay

Cell culture and cytotoxic MTT assay were performed as described in Refs. [30,31]. All cells were purchased from the American Tissue Culture Collection (ATCC), unless otherwise indicated: the CCRF-CEM line are highly chemosensitive T-lymphoblastic leukemia cells, K562 cells were derived from patient with acute myeloid leukemia with bcr-abl translocation, A549 line is lung adenocarcinoma, HCT116 is colorectal tumor cell line and its p53 gene knock-down counterpart (HCT116p53−/−, Horizon Discovery, UK) is a model of human cancers with p53 mutation frequently associated with poor prognosis. The daunorubicin resistant subline of CCRF-CEM cells (CEM-DNR bulk) and paclitaxel resistant subline K562-Tax were selected in our laboratory by the cultivation of maternal cell lines in increasing concentrations of daunorubicine or paclitaxel, respectively. The CEM-DNR bulk cells overexpress MRP-1 protein, while K562-Tax cells overexpress P-glycoprotein, both proteins belong to family of ABC transporters and are involved in primary and/or acquired multidrug resistance phenomenon [32,33]. MRC-5 and BJ are non-tumor human fibroblasts. The cells were maintained in Nunc/Corning 80 cm^2 plastic tissue culture flasks and cultured in cell culture medium (DMEM/RPMI 1640 with 5 g/L glucose, 2 mM glutamine, 100 U/mL penicillin, 100 μg/mL streptomycin, 10% fetal calf serum, and NaHCO₃). Cell suspensions were prepared and diluted according to the particular cell type and the expected target cell density (25,000–30,000 cells/well based on cell growth characteristics). Cells were added by pipette (80 μL) into 96-well microtiter plates. Inoculates were allowed a pre-incubation period of 24 h at 37 °C and 5% CO₂ for stabilization. Four-fold dilutions, in 20-μL aliquots, of the intended test concentration were added to the microtiter plate wals at time zero. All test compound concentrations were examined in duplicate. Incubation of the cells with the test compounds lasted for 72 h at 37 °C, in a 5% CO₂ atmosphere at 100% humidity. At the end of the incubation period, the cells were assayed using MTT. Aliquots (10 μL) of the MTT stock solution were pipetted into each well and incubated for further 1–4 h. After this incubation period the formazan produced was dissolved by the addition of 100 μL/well of 10% aq SDS (pH 5.5), followed by a further incubation at 37 °C overnight. The optical density (OD) was measured at 540 nm with a Labsystem iEMS Reader MF. Tumour cell survival (IC₅₀) was calculated using the following equation: IC = (ODdrug-exposed well/mean ODcontrol wells) x 100%. The IC₅₀ value, the drug concentration lethal to 50% of the tumour cells, was calculated from appropriate dose–response curves.

4.4. Cell cycle and apoptosis analysis

Apoptosis and cell cycle analysis by FACS, BrdU/BrU incorporation and flow cytometric analysis of DNA/RNA synthesis were performed according our previous publication [33]. Subconfluent CCRF-CEM cells (ATCC), seeded at the density of 5.10^5 cells/ml in 6-well panels, were cultivated with the 1 or 5× IC₅₀ of tested compound in a humidified CO₂ incubator at 37 °C in RPMI 1640 cell culture medium containing 10% fetal calf serum, 10 mM glutamine, 100 U/mL penicillin, and 100 μg/mL streptomycin. Control containing vehicle was harvested at the same time point (24 h). Cells were washed with cold PBS and fixed in 70% ethanol overnight at 20 °C. The next day, the cells were washed in hypotonic citrate buffer, treated with RNase (50 μg/mL), stained with propidium iodide, and analyzed by flow cytometry using a 488 nm single beam laser (Becton Dickinson). Cell cycle was analyzed in the program ModFitLT (Verity), and apoptosis was measured in logarithmic model as a percentage of the particles with propidium content lower than cells in G0/G1 phase (<G1) of the cell cycle.

4.5. BrDU incorporation analysis

Cells were cultured and treated as for cell cycle analysis. Before harvesting, they were pulse-labeled with 10 μM 5-bromo-2-deoxyuridine (BrDU) for 30 min. The cells were trypsinized, fixed with ice-cold 70% ethanol, incubated on ice for 30 min, washed with PBS, and resuspended in 2 M HCl for 30 min at room temperature to denature their DNA. Following neutralization with 0.1 M Na₂B₄O₇, the cells were washed with PBS containing 0.5% Tween-20 and 1% BSA. They were then stained with primary anti-BrdU antibody (Exbio) for 30 min at room temperature in the dark. Cells were than washed with PBS and stained with secondary antimouse-FITC antibody (Sigma). The cells were then washed with PBS and incubated with propidium iodide (0.1 mg/mL) and RNase A (0.5 mg/mL) for 1 h at room temperature in the dark and finally analyzed by flow cytometry using a 488 nm single beam laser (FACSCalibur, Becton Dickinson).

4.6. BrU incorporation analysis

Cells were cultured and treated as for cell cycle analysis. Before harvesting, they were pulse-labeled with 1 mM 5-bromouridine (BrU) for 30 min. The cells were fixed in 1% buffered para-formaldehyde with 0.05% of NP-40 in room temperature for 15 min, and then in the refrigerator overnight. They were then washed in 1% glycin in PBS, washed in PBS, and stained with primary anti-BrdU antibody crossreacting to BrU (Exbio) for 30 min at room temperature inthe dark. Cells were than washed with PBS and stained with secondary antimouse-FITC antibody (Sigma). Following the staining, the cells were washed with PBS and fixed with 1% PBS buffered paraformaldehyde with 0.05% of NP-40. The cells were then washed with PBS, incubated with propidium iodide (0.1 mg/mL) and RNase A (0.5 mg/mL) for 1 h at room temperature in the dark, and finally analyzed by flow cytometry using a 488 nm single beam laser (FACSCalibur, Becton Dickinson).

Acknowledgment

Appendix A. Supplementary data

Supplementary data associated with this article can be found in the online version, at http://dx.doi.org/10.1016/j.ejmech.2015.03.068. These data include MOL files and InChiKeys of the most important compounds described in this article.

References

[1] J.D. Connolly, R.A. Hill, Nat. Prod. Rep. 24 (2007) 465.
[2] P. Dzubak, M. Hajduch, D. Vydra, A. Hustova, M. Kvasnica, D. Biedermann, L. Markova, M. Urban, J. Sarek, Nat. Prod. Rep. 23 (2006) 394.
[3] W.N. Setzer, M.C. Setzer, Mini Rev. Med. Chem. 3 (2003) 540.
[4] S. Prasad, N. Kalra, Y. Shukla, Mol. Nutr. Food Res. 51 (2007) 352.
[5] S. Bani, A. Kaul, B. Khan, S.F. Ahmad, K.A. Suri, B.D. Gupta, N.K. Satti, G.N. Qazi, Phytother. Res. 20 (2006) 279.
[6] R.H. Cichewicz, S.A. Kouzi, Med. Res. Rev. 24 (2004) 90.
[7] Y. Kashiwada, F. Hashimoto, L.M. Cosentino, C.H. Chen, P.E. Garrett, K.H. Lee, J. Med. Chem. 39 (1996) 1016.
[8] P.F. Smith, A. Ogundele, A. Forrest, J. Wilton, K. Salzwedel, J. Doto, G.P. Allaway, D.E. Martin, Antimicrob. Agents Chemother. 51 (2007) 3574.
[9] S. Hoet, L. Pieters, G.G. Muccioli, J.L. Habib-Jiwan, F.R. Opperdoes, J. Quetin-Leclercq, J. Nat. Prod. 70 (2007) 1360.
[10] J. Sarek, J. Klinot, P. Dzubak, E. Klinotova, V. Noskova, V. Krecek, G. Korinkova, J.P. Thomson, A. Janost'akova, S.D. Wang, S. Parsons, P.M. Fischer, N.Z. Zhelev, M. Hajduch, J. Med. Chem. 46 (2003) 5402.
[11] M. Urban, J. Sarek, J. Klinot, G. Korinkova, M. Hajduch, J. Nat. Prod. 67 (2004) 1100.
[12] J. Sarek, M. Kvasnica, M. Urban, J. Klinot, M. Hajduch, Bioorg. Med. Chem. Lett. 15 (2005) 4196.
[13] M. Urban, J. Sarek, M. Kvasnica, I. Tislerova, M. Hajduch, J. Nat. Prod. 70 (2007) 526.
[14] M. Urban, J. Sarek, I. Tislerova, P. Dzubak, M. Hajduch, Bioorg. Med. Chem. 13 (2005) 5527.
[15] J. Sarek, M. Kvasnica, M. Vlk, M. Urban, P. Dzubak, M. Hajduch, The potential of triterpenoids in the treatment of melanoma, in: M. Murph (Ed.), Research on Melanoma — a Glimpse into Current Directions and Future Trends, InTech, Rijeka Croatia, 2011, ISBN 978-953-307-293-7, pp. 125—157. Chapter 7.
[16] M. Urban, M. Vlk, P. Dzubak, M. Hajduch, J. Sarek, Bioorg. Med. Chem. 20 (2012) 3666.
[17] D. Biedermann, J. Sarek, J. Klinot, M. Hajduch, P. Dzubak, Synthesis (2005) 1157.
[18] A.V. Symon, N.N. Veselova, A.P. Kaplun, N.K. Vlasenkova, G.A. Fedorova, A.I. Lyutik, G.K. Gerasimova, V.I. Shvets, Russ. J. Bioorg. Chem. 31 (2005) 286.
[19] D. Biedermann, M. Urban, M. Budesinsky, M. Kvasnica, J. Sarek, J. Fluor. Chem. 148 (2013) 30.
[20] A.T. Nguyen, C.L. Feasley, K.W. Jackson, T.J. Nitz, K. Salzwedel, G.M. Air, M. Sakalian, Retrovirology 8 (2011) 101.
[21] J. Protiva, F. Turecek, A. Vystrcil, Collect. Czech Chem. Commun. 42 (1977) 140.
[22] A. Wahhab, M. Ottosen, F.W. Bachelor, Can. J. Chem. 69 (1990) 570.
[23] K. Yuan-Ling, R. Venkateswara, C. Chung-Hsiung, W. Chi, G. Jih-Hwa, L. Shoei-Sheng, Helv. Chim. Acta 86 (2003) 697.
[24] J.N. Pezzuto, J.W. Kosmeder, Xu, Ze-Qi, N.E. Zhou, M.E. Goldsmith, (2007). Method of preparing and use of prodrugs of betulinic acid derivatives, US 2007072835, pub.date 2007-03-29.
[25] T.D. Ngoc, N. Moons, Y. Kim, W.D. Borggraeve, A. Mashentseva, G. Andrei, R. Snoeck, J. Balzarini, W. Dehaen, Bioorg. Med. Chem. 22 (2014) 3292.
[26] M. Urban, M. Kvasnica, N.J. Dickinson, J. Sarek, Biologically active terpenoids usable as prodrugs, in: A.R. Bates (Ed.), Terpenoids and Squalene: Biosynthesis, Function and Health Implications, Nova Science Publishers, Hauppauge NY USA, 2015, ISBN 978-1-63463-656-8, pp. 25—50. Chapter 2.
[27] Y.-J. You, Y. Kim, N.-H. Nam, B.-Z. Ahn, Bioorg. Med. Chem. Lett. 13 (2003) 3137.
[28] G.R. Pettit, N. Melody, F. Hempenstall, J.C. Chapuis, T.L. Groy, L. Williams, J. Nat. Prod. 77 (2014) 863.
[29] R. Mukherjee, M. Jaggi, M.J.A. Siddiqui, S.K. Srivastava, P. Rajendran, A. Vardhan, A.C. Burman, Bioorg. Med. Chem. 14 (2004) 4087.
[30] M. Hajduch, V. Mihal, J. Minarik, E. Faber, M. Safarova, E. Weigl, P. Antalek, Cytotechnology 19 (1996) 243.
[31] P. Naus, O. Caletkova, P. Konecny, P. Dzubak, K. Bogdanova, M. Kolar, J. Vrbkova, L. Slavetinska, E. Tloustova, P. Perlikova, M. Hajduch, M. Hocek, J. Med. Chem. 57 (2014) 1097.
[32] V. Noskova, P. Dzubak, G. Kuzmina, A. Ludkova, D. Stehlik, R. Trojanec, A. Janostakova, G. Korinkova, V. Mihal, M. Hajduch, Neoplasma 49 (2002) 418.
[33] L. Brulikova, P. Dzubak, M. Hajduch, L. Lachnitova, M. Kollareddy, M. Kolar, K. Bogdanova, J. Hlavac, Eur. J. Med. Chem. 45I (2010) 3588.

Synthesis and cytotoxic activity of triterpenoid thiazoles derived from allobetulin, methyl betulonate, methyl oleanonate, and oleanonic acid

FULL PAPER

Synthesis and Cytotoxic Activity of Triterpenoid Thiazoles Derived from Allobetulin, Methyl Betulonate, Methyl Oleanonate, and Oleanonic Acid

Lucie Borkova,[b] Richard Adamek,[b] Petr Kalina,[c] Pavel Drašar,[c] Petr Dzubak,[a] Sona Gurska,[a] Jiri Rehulka,[a] Marian Hajduch,[a] Milan Urban,[a]* and Jan Sarek[a]*

[a]   Dr. Petr Dzubak, Dr. Sona Gurska, Jiri Rehulka, Assoc. Prof. Marian Hajduch, Assoc. Prof. Milan Urban, ORCID: C-9611-2010, Dr. Jan Sarek
        Institute of Molecular and Translational Medicine
        Faculty of Medicine and Dentistry, Palacky University in Olomouc
        Hnevotinska 5, 779 00 Olomouc, Czech Republic.
        e-mail: urban@upol.cz
                jan.sarek@gmail.com

[b]   Lucie Borkova, Richard Adamek
        Department of Organic Chemistry
        Faculty of Science, Palacky University in Olomouc
        17. listopadu 1192/12, 771 46 Olomouc, Czech Republic

[c]   Petr Kalina, Prof. Pavel Drašar
        Department of Chemistry of Natural Compounds
        Faculty of Science, University of Chemistry and Technology
   Technicka 5, 166 28 Prague, Czech Republic

        Supporting information for this article is given via a link at the end of the document. It contains experimental data for methyl betulonate derivatives **3b – 3l**, methyl oleanonate derivatives **4b – 4l**, and oleanonic acid derivatives **5b – 5l**, and pictures of ^{1}H and ^{13}C NMR spectra of all new compounds.

Abstract: 41 New triterpenoids were prepared from allobetulon, methyl betulonate, methyl oleanonate, and oleanonic acid to study their influence on cancer cells. Each 3-oxo triterpene was brominated at C-2, substituted with thiocyanate; following cyclization with appropriate ammonium salts gave N-substituted thiazoles. All compounds were tested for their in vitro cytotoxic activity on eight cancer cell lines and two non-cancer fibroblasts. 2-Bromoallobetulon (**2b**) methyl 2-bromobetulonate (**3b**), 2-bromooleanonic acid (**5b**), and 2-thiocyanooleanonic acid (**5c**) were best with $IC_{50} < 10$ μM to CCRF-CEM cells (e.g. **3b**, IC_{50} =2.9 μM) as well as 2'-(diethylamino)olean-12(13)-eno[2,3-*d*]thiazole-28-oic acid (**5f**, IC_{50} 9.7 μM) and 2'-(N-methylpiperazino)olean-12(13)-eno[2,3-*d*]thiazole-28-oic acid (**5k**, IC_{50} 11.4 μM). Compound **5c** leads to accumulation of cells in the G2 phase of the cell cycle and inhibits RNA/DNA synthesis significantly at $1 \times IC_{50}$. The G2/M cell cycle arrest probably corresponds to the DNA/RNA synthesis inhibition, similarly to actinomycin D. Compound **5c** is new, active, non-toxic, therefore it is the most promising for future drug development. Methyl 2-bromobetulonate (**3b**) and methyl 2-thiocyanometulonate (**3c**) inhibited nucleic acid synthesis only at $5 \times IC_{50}$. We assume that in **3b** and **3c** (unlike in **5c**) DNA/RNA inhibition is a non-specific event and unknown primary cytotoxic target is activated at $1 \times IC_{50}$ or lower concentration.

Introduction

Pentacyclic triterpenes are natural compounds that may be found in almost all living organisms, they are particularly common in plants. They often have many interesting biological activities such as anti-inflammatory,[1,2] antibacterial,[3,4] antiviral,[5,6] antiprotozoal,[7,8] cytotoxic,[9,10] and anti-hypoglycemic.[11,12] However, in many cases the effective concentrations of most of the natural triterpenoids are not low enough for their therapeutic use. In addition, their solubility in water is low, which causes insufficient bioavailability. As a result, it is necessary to focus on the preparation of triterpenoid derivatives with higher activity, improved pharmacological properties, and more favorable therapeutic index.[13]
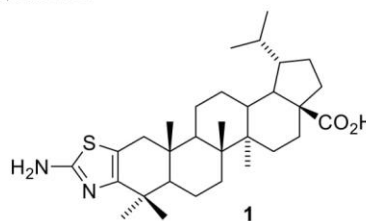
Recently, many cytotoxic derivatives were found among triterpenes that contain a heterocycle fused to the A-ring of the triterpenoid skeleton. The most active compounds were indoles,[14,15] pyrazoles,[14,16-22] isoxazoles,[23,24] triazoles,[25] pyrazines,[14,20,26-30] quinoxalines,[14] pyrimidines,[23] and triazines.[31,32] Previously, we synthesised a set of triterpenes modified with five membered heterocycles and among them aminothiazole derivative **1** was the most active on multiple cancer cell lines,[19] which sparked our interest in such compounds.

FULL PAPER

We also reported the synthesis of cytotoxic triterpenoids conjugated to biotin which would allow us to search for their molecular targets which may afford more information about the mechanism of action.[33] Consequently, we have seen hints in ongoing pull down assays that many of the potential targets are enzymes dealing with lipophilic substrates or membrane proteins that contain significant lipophilic surface areas. In order to improve the ligand-target binding, we decided to add a variety of rather lipophilic substituent(s) onto the polar amino group in triterpenoid aminothiazoles similar to **1**. To further explore the structure-activity relationships (SARs) among substituted triterpenoid aminothiazoles, we choose to add substituents of various size and shape to the NH₂ group. In order to get more data about the influence of the terpenic part of the molecule on the cytotoxic activity, we prepared four analogous sets of *N*-substituted aminothiazoles from four different commercially available triterpenes, allobetulon (**2a**), methyl betulonate (**3a**), methyl

oleanonate (**4a**), and oleanonic acid (**5a**). Compounds **2a**, **3a**, **4a**, and **5a** are derivatives of triterpenes betulinic acid, oleanolic acid, and 18α-oleanane, derivatives of which are commonly studied for their high cytotoxic activities.[34-37] Comparing activities in derivatives prepared from methyl oleanonate (**4a**) and from free oleanonic acid (**5a**) would allow us to estimate, if methyl esters are less active than free acids, as it is usual in triterpenoids.[20,27,38] The classical Hantzsch synthesis of aminothiazoles does not give good yields in the case of triterpenoids and steroids because of harsh reaction conditions[39,40] and the reaction does not allow to simply obtain N-substituted compounds. Therefore, we used an alternative approach[41-43] involving the reaction of 3-oxo-2-thiocyanotriterpenoids with various alkyl ammonium acetates. This method allowed us to obtain a variety of *N*-substituted triterpenoid aminothiazoles and was used the first time to prepare terpenoid aminothiazoles.
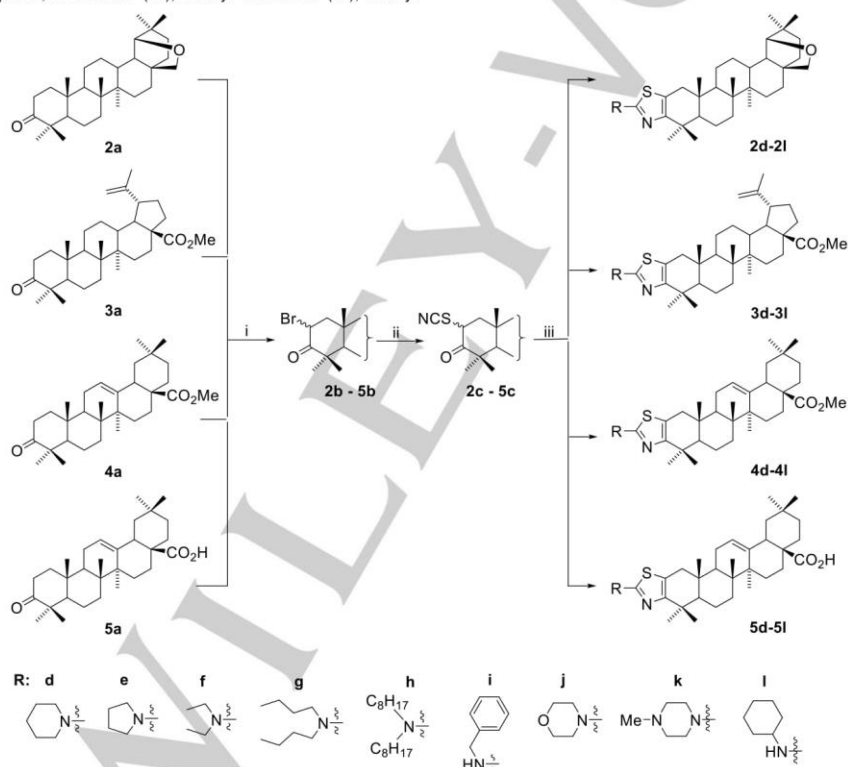
Scheme 1. Reagents and conditions: (i) CuBr₂, CHCl₃, EtOAc, MeOH, r.t., 18 h; (ii) NH₄SCN, N-methylpyrrolidone, 50 °C, 4 h; (iii) piperidinium acetate (for **d**), pyrrolidinium acetate (for **e**), diethylammonium acetate (for **f**), dibutylammonium acetate (for **g**), dioctylammonium acetate (for **h**), benzylammonium acetate (for **i**), morpholinium acetate (for **j**), N-methylpiperazinium acetate (for **k**), or cyclohexylammonium acetate (for **l**), CHCl₃, r.t., 24 h.

Results and Discussion

Chemistry

In our work,[19] the aminothiazole derivative **1** was obtained in rather low yield which was probably caused by a presence of the

2

FULL PAPER

free 28-carboxyl group which is lowering the solubility and causes problems during purification. Allobetulon (**2a**), methyl betulonate (**3a**), and methyl oleanonate (**4a**) do not contain carboxyl group, therefore we expected simple purification and higher yields. The starting 3-oxotriterpenoids **2a**, **3a**, **4a**, and **5a** were brominated by CuBr$_2$ in a mixture of CHCl$_3$, EtOAc, and MeOH at r.t. according to the known procedure.[23,44-48] The crude 2-bromo-3-oxoderivatives **2b**, **3b**, **4b**, and **5b** were used without further purification for the synthesis of 3-oxo-2-thiocyano derivatives **2c**, **3c**, **4c**, and **5c** by the nucleophilic substitution of bromide by the ammonium thiocyanate in *N*-methylpyrrolidone at 50 °C. 2-Thiocyano-3-oxo derivatives **2c**, **3c**, **4c**, and **5c** were obtained as mixtures of 2α/2β epimers, which were not separated because the final cyclization and aromatization of each epimer leads to the same flat, aromatic system (Scheme 1). Thiazoles **2d – 2l**, **3d – 3l**, **4d – 4l** and **5d – 5l** were prepared by a procedure[23] in which each thiocyanate was stirred with five equivalents of the corresponding alkyl ammonium acetate at r.t. for various periods

of time. The yields of cyclization were usually moderate to high depending on the solubility of the starting terpene in organic solvents, which influenced the work-up procedures and chromatography.

Biological assays - cytotoxicity

The cytotoxic activity of all synthesized compounds was investigated in vitro against eight human cancer cell lines and two non-tumor fibroblasts by using the standard MTS test (Table 1). The cancer cell lines were derived from T-lymphoblastic leukemia CCRF-CEM, leukemia K562 and their multiresistant counterparts (CEM-DNR, K562-TAX), solid tumors including lung (A549) and colon (HCT116, HCT116p53-/-) carcinomas, osteosarcoma cell line (U2OS), and for comparison, on two human non-cancer fibroblast lines (BJ, MRC-5). In general, the CCRF-CEM line was the most sensitive cancer cell line to the prepared compounds with only a few exceptions. Therefore SARs assumption were mostly based on the activities in CCRF-CEM cells.

Table 1. Cytotoxic activities of selected compounds on eight tumor (including resistant) and two normal fibroblast cell lines.[a]

Comp.	IC$_{50}$ (μM)[b]										
	CCRF-CEM	CEM-DNR	HCT116	HCT116 p53-/-	K562	K562-TAX	A549	U2OS	BJ	MRC-5	TI[c]
1	3.5	11.2	5.1	4.3	4.8	6.9	7.0	-	24.9	15.7	5.8
2a[d]	>50.0	>50.0	>50.0	>50.0	>50.0	>50.0	>50.0	>50.0	>50.0	-	-
3a[d]	>50.0	>50.0	>50.0	>50.0	>50.0	>50.0	>50.0	>50.0	>50.0	-	-
4a[d]	>50.0	>50.0	>50.0	>50.0	>50.0	>50.0	>50.0	>50.0	>50.0	-	-
5a[d]	15.1	17.4	45.1	>50.0	>50.0	21.5	49.5	48.5	>50.0	>50.0	5.3
2b	**5.2**	>50.0	21.5	22.8	11.7	**7.5**	>50.0	47.5	>50.0	>50.0	>9.6
2c	43.0	>50.0	35.6	>50.0	41.1	>50.0	>50.0	>50.0	>50.0	>50.0	>1.2
2l	42.8	>50.0	>50.0	>50.0	>50.0	>50.0	>50.0	>50.0	>50.0	>50.0	>1.2
3b	**2.9**	15.0	14.9	12.4	**9.0**	11.0	>50.0	13.5	22.9	26.3	8.5
3c	10.8	>50.0	34.6	29.9	15.5	>50.0	46.2	>50.0	32.3	36.1	3.2
4b	14.0	22.2	>50.0	>50.0	19.9	**7.2**	>50.0	>50.0	>50.0	48.2	>3.5
4c	29.0	48.5	>50.0	38.5	46.9	>50.0	>50.0	47.8	>50.0	45.7	>1.7
4f	41.8	42.6	44.9	43.6	42.6	42.3	44.2	43.2	>50.0	42.4	>1.1
5b	**4.5**	14.8	**4.1**	**8.2**	**2.1**	13.5	15.8	29.3	27.7	20.0	5.0
5c	**6.4**	31.1	23.6	16.3	28.6	>50.0	21.7	46.1	>50.0	48.0	>7.7
5f	**9.7**	>50.0	>50.0	48.7	>50.0	>50.0	>50.0	>50.0	>50.0	>50.0	>5.2
5i	23.5	>50.0	>50.0	>50.0	>50.0	>50.0	>50.0	>50.0	>50.0	>50.0	>2.1
5j	25.6	48.5	>50.0	21.1	46.1	>50.0	>50.0	48.7	>50.0	>50.0	>2.0
5k	11.4	31.1	>50.0	>50.0	>50.0	14.4	>50.0	>50.0	>50.0	>50.0	>4.4
5l	42.8	>50.0	>50.0	>50.0	>50.0	14.3	>50.0	>50.0	>50.0	>50.0	>1.2

[a]All other compounds prepared in this work were also tested but their activities on these 10 cell lines were higher than 50 μM and may be found in Supporting data file. [b]The lowest concentration that kills 50 % of cells. The standard deviation in cytotoxicity assays is typically up to 15 % of the average value. [c]Therapeutic index is calculated for IC$_{50}$ of CCRF-CEM line vs average of both fibroblasts (BJ and MRC-5). [d]Parent compounds used as standards. Compounds with IC$_{50}$ > 50 μM are considered inactive.

3

FULL PAPER

Among the starting material and intermediates, 2-bromo-3-oxoderivatives **2b**, **3b**, and **5b** were cytotoxic against the CCRF-CEM line in a low micromolar range of 3-5 µM. This is surprising because compound **2b** is derivative of allobetulon **2a**, analogues

of which are often inactive.[27,33] In addition, the active compound **3b** is a methyl ester and triterpenic methyl esters are also usually not active.[27,33] Even bromo derivative **4b**, also a methyl ester, had a moderate IC$_{50}$ of 14 µM. 2-Thiocyano derivatives **3c** and **5c** had

Table 2. Influence of **2b**, **3b**, **3c**, **5b**, **5c**, and **5f** on cell cycle and DNA and RNA synthesis inhibition at 1 × and 5 × IC$_{50}$.

	Used conc. (µM)	Sub G1 (%)	G0/G1 (%)	S (%)	G2/M (%)	pH3^{Ser10} (%)	DNA synthesis	RNA synthesis
Control		3.38	41.63	44.18	14.19	1.62	58.76	48.80
2b	5.2[a]	5.84	44.78	40.95	14.27	0.99	52.18	41.37
2b	21.2[b]	43.57	44.30	37.92	17.77	1.74	37.24	31.77
3b	2.9[a]	7.76	40.23	38.24	21.53	2.79	25.98	49.31
3b	14.5[b]	32.49	45.58	31.06	23.35	2.44	**13.34**	**1.37**
3c	10.8[a]	3.42	36.14	47.92	15.93	2.09	41.05	47.46
3c	54.0[b]	58.50	30.90	41.29	27.81	1.02	**13.82**	**0.97**
5b	4.5[a]	5.96	42.73	42.51	14.77	1.11	61.70	53.54
5b	22.5[b]	57.69	45.40	39.88	14.71	1.55	36.20	24.60
5c	6.4[a]	41.55	56.86	22.77	**20.37**	1.11	**10.52**	**5.44**
5c	32.0[b]	83.11	34.90	25.32	**39.78**	0.26	**2.86**	**0.64**
5f	9.7[a]	4.27	36.59	48.14	15.27	1.18	40.16	67.11
5f	48.5[b]	7.79	40.35	49.43	10.22	1.87	32.95	58.95

[a]The values were obtained at 1 × IC$_{50}$. [b]The values were obtained at 5 × IC$_{50}$. Control are cells treated with vehicle.
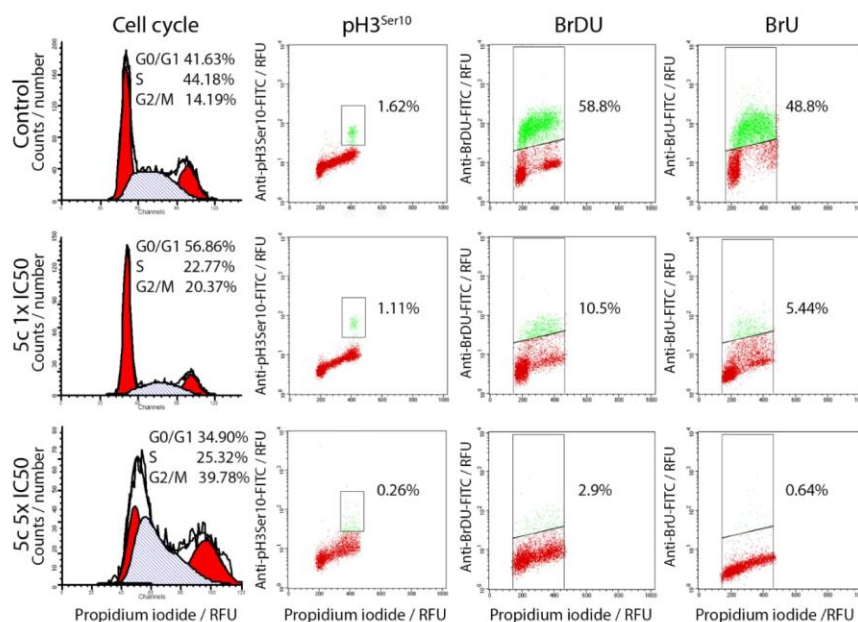
4

Figure 1. Graphs and dot plots of flow cytometry analysis are showing the cell cycle inhibition in G2/M phase and almost complete DNA, RNA synthesis inhibition by the best compound **5c**, monitored by incorporation of BrDU/BrU into the DNA.

IC$_{50}$ values of 6 – 10 μM. In contrast, compounds **2c** and **4c** had IC$_{50}$ values in higher micromolar ranges (Table 1). The cytotoxicity of most of the substituted aminothiazoles was below the detection limit with two exceptions, **5f** and **5k** with cytotoxicity of 9.7 and 11.3 μM (CCRF-CEM), respectively, which we consider enough active to be interesting for further studies towards the mechanism of action. The activity of **2l**, **4f**, **5i**, **5j** and **5l** was higher than the detection limit, however, not sufficient for more tests. The activity of almost all derivatives with IC$_{50}$ < 50 μM on the resistant cell lines CEM-DNR and K562-TAX is worse in comparison to parental cell lines CCRF-CEM and K562 and indicates the possible mechanism of resistance by MDR transporter proteins.

To sum up, within this study, 8 compounds (**2b**, **3b**, **3c**, **4b**, **5b**, **5c**, **5f**, **5k**) had higher cytotoxic activity than their parent compounds **2a**, **3a**, **4a**, and **5a**. This is significant improvement. Six compounds (**2b**, **3b**, **3c**, **5b**, **5c**, **5f**) with IC$_{50}$ < 10 μM were further investigated for their mechanisms of action and therefore the analysis of apoptosis, cell cycle, DNA and RNA synthesis in CCRF-CEM cells was done.

Biological assays – analysis of apoptosis, cell cycle, and DNA/RNA synthesis

All of those promising compounds with an IC$_{50}$ below or around 10 μM in CCRF-CEM cell line (**2b**, **3b**, **3c**, **5b**, **5c**, **5f**) were further investigated for their mechanisms of action and therefore the analysis of apoptosis, cell cycle, DNA and RNA synthesis in CCRF-CEM cells at 1 × or 5 × IC$_{50}$ was done (Table 2). These concentrations were used in concordance with our previous publications.[49-51] Interestingly, highly active compound **5c** led to the accumulation of cells in G2 phase of the cell cycle and had no toxicity in non-cancer fibroblasts. Nucleic acid synthesis monitored by BrU/BrDU incorporation was almost completely inhibited by **5c** at both tested concentrations, pointing to a possible mechanism of action (Figure 1) somewhere within the regulatory mechanisms of cell cycle proliferation. Therefore, **5c** is the most promising candidate for further cell biology studies and drug development. Similar phenomenon (inhibition of DNA/RNA synthesis) but at higher concentrations (5 × IC$_{50}$) was detected for compounds **3b** and **3c**. However, in this case the interpretation of why the DNA/RNA synthesis is inhibited at higher concentration

5

FULL PAPER

than the IC$_{50}$ is more difficult. It can, for example, be simply a secondary effect of the cytotoxicity in general or a result of other processes in dying cells. Other tested derivatives had no significant effect on the cell cycle and DNA/RNA synthesis.

Conclusions

We have described the synthesis and biological activities of 41 new triterpenoid derivatives. From known 3-oxocompounds **2a**, **3a**, **4a**, and **5a**, we prepared 2-bromo-3-oxocompounds, then 2-thiocyano-3-oxocompounds and finally, the cyclization with alkyl ammonium acetates afforded N-substituted aminothiazoles. We used nine different types of substituents at the amino group to be able to evaluate their influence on cytotoxicity. Substituents were chosen rather lipophilic, because we expected to improve interactions of the terpenes with lipophilic areas on potential protein targets. Although the majority of the aminothiazoles were active in high micromolar ranges, there were two exceptions, **5f** and **5k**, with cytotoxicity around 10 μM. Cells treated with **5f** and **5k** were used for cell cycle and DNA/RNA synthesis analysis. However, no significant effect on the cell cycle and nucleic acid synthesis was detected. Both compounds are derivatives of oleanonic acid with free 28-carboxy groups. This suggests that future research on aminothiazoles should be more oriented towards free terpenic acids but such studies should also take problems with isolation of the products, yields, and solubility into account. Of the substituents at the thiazole part, diethylamino and N-methylpiperazino substituents were the best. Within this study, however, the most active compounds were the intermediate 2-bromo-3-oxo derivatives **2b**, **3b**, **5b**, and thiocyanates **3c**, and **5c** and studies to better understand the mechanism of action were also performed with them. Thiocyanates **3c** and **5c** were identified to modulate the cell cycle and it is highly possible that observed S phase alteration and G2/M cell cycle arrest is a response to the DNA/RNA inhibition which in the case of compound **5c** is significant already at 1 × IC$_{50}$. Similar response of the cells was observed when cancer cells were treated with low doses of actinomycin D which is commonly used antineoplastic drug and well-know inhibitor of RNA/DNA synthesis.[52] We can speculate if such mechanism is due to the direct interference with some specific targets like cyclin-dependent kinases, RNA/DNA polymerases[53] or in general it is a dose dependent effect of the drug which is atenuating nucleic acid synthesis and therefore abrogates check point signaling. Further biological studies will be needed to answer such questions. Since **5c** has also no toxicity on non-cancer fibroblasts, it is the most promising candidate for further drug development.

Experimental Section

General experimental procedures
Materials and instruments
Melting points were determined using a Büchi B-545 apparatus and are uncorrected. Optical rotations were measured on an Autopol III (Rudolph Research, Flanders, USA) polarimeter in MeOH at 25 °C and are in [10^{-1} deg cm^2 g^{-1}]. IR spectra were recorded on a Nicolet Avatar 370 FTIR. DRIFT stands for Diffuse Reflectance Infrared Fourier Transform. ^{1}H and ^{13}C NMR spectra

were recorded on Varian^{UNITY} Inova 400 (400 MHz for ^{1}H) or Varian^{UNITY} Inova 300 (300 MHz for ^{1}H) or Jeol ECX-500SS (500 MHz for ^{1}H) instruments, using CDCl$_3$, D$_6$-DMSO or CD$_3$OD as solvents (25°C). Chemical shifts were eider referenced to the residual signal of the solvent (CDCl$_3$, D$_6$-DMSO) or to TMS added as an internal standard. ^{13}C NMR spectra were eider referenced to CDCl$_3$ (77.00 ppm) or D$_6$-DMSO (39.51 ppm) or to TMS added as an internal standard. EI-MS spectra were recorded on an INCOS 50 (Finnigan MAT) spectrometer at 70 eV and an ion source temperature of 150 °C. The samples were introduced from a direct exposure probe at a heating rate of 10 mA/s. Relative abundances stated are related to the most abundant ion in the region of $m/z > 180$. HRMS analysis was performed using LC-MS an Orbitrap high-resolution mass spectrometer (Dionex Ultimate 3000, Thermo Exactive plus, MA, USA) operating at positive full scan mode in the range of 100–1000 m/z. The settings for electrospray ionization were as follows: oven temperature of 150 °C, source voltage of 3.6 kV. The acquired data were internally calibrated with phthalate as a contaminant in methanol (m/z 297.15909). Samples were diluted to a final concentration of 0.1 mg/mL in methanol. The samples were injected to mass spectrometer over autosampler after HPLC separation: precolumn phenomenex 2.6μm C18. Mobile phase isokrat MeCN/IPA/ammonium acetate 0.01 M 80/10/10, flow 0,3 mL/min and MeCN/IPA/water/HCOOH 80/10/10/0.1 for compounds **3g**, **3h**, **4g**, and **4h**. TLC was carried out on Kieselgel 60 F$_{254}$ plates (Merck) detected by spraying with 10% aqueous H$_2$SO$_4$ and heating to 150 – 200 °C. Column chromatography was performed using silica gel 60 (Merck 7734). Work-up refers to pouring the reaction mixture into water, extracting the product into organic solvent, washing the organic layer successively in this order with water, diluted aqueous HCl, water, saturated aqueous sodium hydrogencarbonate, and again water. Then the organic phase was dried over magnesium sulfate, filtered, and the solvents evaporated under reduced pressure. Analytical samples were dried over P$_2$O$_5$ under diminished pressure. Allobetulon (**2a**), methyl betulonate (**3a**), methyl oleanonate (**4a**) and oleanonic acid (**5a**) were obtained from company Betulinines (www.betulinines.com), which manufactures them from betulin, betulinic acid and oleanolic acid in bulk scale. Scheme and references about their preparation were added to the supporting data file. All other chemicals and solvents were obtained from Sigma-Aldrich.

Synthetic procedures
General procedure for synthesis of 2-bromoderivatives
Each starting oxoderivative **2a**, **3a**, **4a**, and **5a** (23 mmol) was dissolved in a mixture of solvents (chloroform, ethylacetate and methanol, ratio is at each experiment). Anhydrous CuBr$_2$ (50 mmol) was added, and reaction mixture was stirred for 18 hours at r.t. until the starting material was fully consumed, (controlled by TLC in toluene/diethylether 5:1 v/v). Then, the precipitate of copper(I) bromide was filtered off, organic solvents were washed with water, dried over MgSO$_4$, and crude product was purified by chromatography on silica gel (mobile phase at each experiment). Evaporation of solvents gave each 2-bromoderivative as a mixture of 2α/2β epimeres.

General procedure for synthesis of 2-thiocyano derivatives
Each bromo derivative **2b**, **3b**, **4b**, and **5b** (19 mmol) was dissolved in N-methylpyrrolidone (100 mL). Ammonium

6

FULL PAPER

thiocyanate (96 mmol) was added, and reaction mixture was stirred for 4 hours at 50 °C until the reaction was finished (controlled by TLC, mobile phase at each experiment). Then, water was added, resulting solid precipitate was filtered off and organic phase was washed with water. Crude product was purified by chromatography on silica gel (mobile phase at each experiment), which provided each 2-thiocyano derivative as a mixture of 2α/2β epimeres.

General procedure for synthesis of triterpenoid thiazole-derivatives

Alkylammonium acetate of each corresponding amine (5 mmol) was added to the solution of 2-thiocyano derivative (1 mmol) in chloroform (20 mL). Reaction mixture was left for 24 hours at r.t., monitored by TLC (mobile phase at each experiment). Reaction mixture was then washed with water several times, organic phase was dried with MgSO$_4$ and the solvents were removed under vacuo. Crude product was purified by chromatography on silica gel (mobile phase at each experiment) unless otherwise stated at the experiment. Collected fractions were evaporated to give respective thiazole-derivatives.

2α/β-bromoallobetulone (2b)

Epimeric mixture of 2-bromoallobetulons **2b** was prepared according to the general procedure from allobetulon **2a** (10 g, 22.7 mmol) and CuBr$_2$ (11.2 g, 50 mmol) in mixture of chloroform (50 mL), ethyl acetate (150 mL) and methanol (20 mL). After standard work up without further purification compound **2b** was obtained as white crystals (11.3 g, 96%): R_f=0.50 (toluene/diethylether 20:1); mp: 222–224 °C (hexane/MeOH); [α]$_D^{20}$=+68 (c=0.55 in CHCl$_3$); (lit.[44,51] mp: 216–225 °C; [α]$_D^{20}$=+74).

2α/β-thiocyanoallobetulone (2c)

Epimeric mixture of **2c** was prepared according to the general procedure from compound **2b** (10 g; 19.2 mmol) and ammonium thiocyanate (7.3 g; 96 mmol) in N-methylpyrrolidone (100 mL) after 4 hours at 50 °C, controlled by TLC (mobile phase toluene/diethylether 5:1). After standard work up and purification (gradient elution: toluene → toluene/diethylether 5:1) compound **2c** was obtained as a mixture of epimers in the ratio 0.3:0.7 determined by the intensity of signals in NMR, white microcrystals (7.3 g; 76%): R_f=0.20 (toluene/diethylether 5:1); mp: 150–156 °C (toluene/diethylether); [α]$_D^{20}$=+5 (c=1.5 in CHCl$_3$); ^{1}H NMR (500 MHz, CDCl$_3$): δ=0.81, 0.82, 0.91, 0.95, 0.96, 0.97, 1.05, 1.12, 1.13, 1.15, 1.17, 1.20 (all s, 21H, 7×CH$_3$ from both epimers), 2.02 (dd, J_1 = 13.5 Hz, J_2 = 8.3 Hz, 0.7H, H-1a from one epimer), 2.52 (t, J = 12.9 Hz, 0.7H, H-1b from one epimer), 2.75 (dd, J_1 = 12.9 Hz, J_2 = 6.0 Hz, 0.3H, H-1b from the other epimer), 3.46 (d, J = 7.7 Hz, 1H, H-28a from both epimers), 3.54 (s, 1H, H-19 from both epimers), 3.78 (d, J = 7.5 Hz, 1H, H-28b from both epimers), 4.71 – 4.76 ppm (m, 1H, H-2 from both epimers); ^{13}C NMR (75 MHz, CDCl$_3$): δ=13.39, 15.02, 15.85, 16.43, 18.81, 18.98, 19.56, 19.85, 21.22, 21.31, 22.07, 24.50, 24.52, 24.76, 26.08, 26.14, 26.17, 26.26, 26.36, 26.38, 28.74, 29.14, 32.24, 32.66, 33.46, 34.02, 34.36, 36.24, 36.68, 38.53, 39.16, 40.45, 40.79, 40.82, 40.92, 41.40, 41.43, 46.67, 46.72, 47.34, 49.51, 49.53, 50.24, 50.68, 51.05, 52.23, 52.35, 53.98, 57.41, 71.18, 71.20, 87.87, 87.88, 112.21, 112.46, 209.35, 211.62 ppm; IR (film): ν=2930, 2860, 2152 (SCN), 1700 (C=O), 1457(-O-), 1033 cm^{-1}; MS (ESI) m/z (%): 498.4 (100) [M+H]$^+$; Anal. calcd for C$_{31}$H$_{47}$NO$_2$S: C 74.80, H 9.52, S 6.44, N 2.81; found C 74.80, H 9.64, S 6.02, N 2.57.

Thiazole derivative 2d

Compound **2d** was prepared according to the general procedure from 2α/β-thiocyano allobetulone (**2c**) (500 mg; 1.0 mmol) and piperidinium acetate (732 mg; 5.0 mmol) in chloroform (20 mL) after 24 hours controlled by TLC (mobile phase toluene/diethylether 5:1). Dissolved crude product was filtred through a short pad of silica gel. Evaporation of solvent furnished **2d** (536 mg; 95 %); R_f=0.35 (toluene/diethylether 5:1); mp: 152–155 °C (toluene/diethylether); [α]$_D^{20}$=+50 (c=0.79 in CHCl$_3$); ^{1}H NMR (300 MHz, CDCl$_3$): δ=0.81 (s, 3H), 0.91 (s, 3H), 0.94 (s, 6H), 1.03 (s, 3H), 1.13 (s, 3H), 1.23 (s, 3H, 7×CH$_3$), 1.58 – 1.73 (m, 6H, H-piperidine), 2.15 (d, J = 15.2 Hz, 1H, H-1a), 2.61 (d, J = 14.9 Hz, 1H, H-1b), 3.30 – 3.43 (m, 4H, H-piperidine), 3.46 (d, J = 7.9 Hz, 1H, H-28a), 3.55 (s, 1H, H-19), 3.80 ppm (d, J = 7.6 Hz, 1H, H-28b); ^{13}C NMR (75 MHz, CDCl$_3$): δ=13.49, 15.41, 16.51, 19.51, 21.45, 21.91, 24.25, 24.55, 25.15, 26.22, 26.45, 28.79, 29.68, 30.24, 32.68, 33.03, 34.25, 36.25, 36.70, 37.13, 38.56, 39.28, 40.59, 40.70, 41.48, 46.75, 49.41, 49.66, 52.92, 71.25, 87.88, 112.25, 143.65, 153.22, 166.55 ppm; IR (film): ν=2935, 2858, 1553 (thiazole), 1524 (thiazole), 1415 (thiazole), 1035 cm^{-1}; MS (ESI) m/z (%): 565.4 (100) [M+H]$^+$; Anal. calcd for C$_{36}$H$_{56}$N$_2$OS: C 76.54, H 9.99, N 4.96, S 5.68; found C 76.70, H 9.81, N 4.42, S 5.44.

Thiazole derivative 2e

Compound **2e** was prepared according to the general procedure from 2α/β-thiocyano allobetulone (**2c**) (500 mg; 1.0 mmol) and pyrrolidinium acetate (655 mg; 5.0 mmol) in chloroform (20 mL) after 24 hours controlled by TLC (mobile phase toluene/diethylether 5:1). Dissolved crude product was filtred through a short pad of silica gel. Evaporation of solvent furnished **2e** (501 mg; 91 %): R_f=0.20 (toluene/diethylether 5:1); mp: 151–155 °C (toluene/diethylether); [α]$_D^{20}$=+58 (c=1.26 in CHCl$_3$); ^{1}H NMR (300 MHz, CDCl$_3$): δ=0.82 (s, 3H), 0.92 (s, 3H), 0.95 (s, 6H), 1.03 (s, 3H), 1.17 (s, 3H), 1.27 (s, 3H, 7×CH$_3$), 1.96 – 2.04 (m, 4H, H-pyrrolidine), 2.16 (d, J = 15.2 Hz, 1H, H-1a), 2.61 (d, J = 15.3 Hz, 1H, H-1b), 3.36 – 3.51 (m, 5H, H-28a, H-pyrrolidine), 3.56 (s, 1H, H-19), 3.81 ppm (d, J = 7.9 Hz, H-28b); ^{13}C NMR (75 MHz, CDCl$_3$): δ=13.50, 15.42, 16.49, 19.52, 21.45, 21.84, 24.55, 25.65, 26.22, 26.46, 28.80, 30.22, 32.69, 33.03, 34.26, 36.26, 36.71, 37.22, 38.57, 39.41, 40.59, 40.70, 41.48, 46.75, 49.66, 53.00, 71.25, 87. 89, 113.01, 143.31, 153.14, 164.67; IR (film): ν=2944, 2865, 1546 (thiazole), 1453 (thiazole), 1034 cm^{-1}; MS (ESI) m/z (%) = 551.4 (100) [M+H]$^+$; Anal. calcd for C$_{35}$H$_{54}$N$_2$OS: C 76.31, H 9.88, N 5.09, S 5.82; found C 76.53, H 9.91, N 4.12, S 5.64.

Thiazole derivative 2f

Compound **2f** was prepared according to the general procedure from 2α/β-thiocyano allobetulone (**2c**) (500 mg; 1.0 mmol) and diethylammonium acetate (665 mg; 5.0 mmol) in chloroform (20 mL) after 24 hours controlled by TLC (mobile phase toluene/diethylether 5:1). Dissolved crude product was filtred through a short pad of silica gel. Evaporation of solvent furnished **2f** (520 mg; 94 %): R_f=0.35 (toluene/diethylether 5:1); mp: 152–156 °C (toluene/diethylether); [α]$_D^{20}$=+57 (c=0.43 in CHCl$_3$); ^{1}H NMR (300 MHz, CDCl$_3$): δ=0.81 (s, 3H), 0.93 (s, 3H), 0.94 (s, 6H), 1.03 (s, 3H), 1.12 (s, 3H), 1.23 (s, 3H, 7×CH$_3$), 1.20 (t, J = 7.0 Hz, 6H, (CH$_3$CH$_2$)$_2$N), 2.14 (d, J = 15.3 Hz, 1H, H-1a), 2.59 (d, J = 15.0 Hz, 1H, H-1b), 3.35 – 3.47 (m, 5H, H-28a, (CH$_3$CH$_2$)$_2$N), 3.56 (s, 1H, H-19), 3.81 ppm (d, J = 7.6 Hz, 1H, H-28b); ^{13}C NMR (75

7

MHz, CDCl$_3$): δ=12.72, 13.51, 15.44, 16.56, 19.55, 21.44, 21.92, 24.55, 26.23, 26.47, 28.80, 30.25, 32.70, 33.96, 34.26, 36.26, 36.72, 37.14, 38.61, 39.31, 40.60, 40.70, 41.48, 44.98, 46.77, 49.69, 52.93, 71.27, 87.90, 112.48, 143.17, 153.11, 166.19 ppm; IR (film): v=2925, 2865, 1535 (thiazole), 1468 (thiazole), 1035 cm^{-1}; MS (ESI) m/z (%): 553.4 (100) [M+H]$^+$; Anal. calcd for C$_{35}$H$_{56}$N$_2$OS: C 76.03, H 10.21, N 5.07, S 5.80; found C 75.54, H 10.36, N 4.64, S 5.57.

Thiazole derivative 2g

Compound **2g** was prepared according to the general procedure from 2α/β-thiocyano allobetulone (**2c**) (500 mg; 1.0 mmol) and dibutylammonium acetate (947 mg; 5.0 mmol) in chloroform (20 mL) after 24 hours controlled by TLC (mobile phase toluene/diethylether 5:1). Dissolved crude product was filtered through a short pad of silica gel. Evaporation of solvent furnished **2g** (463 mg; 76 %): R_f=0.40 (toluene/diethylether 5:1); mp: 148–152 °C (toluene/diethylether); [α]$_D^{20}$=+55 (c=0.51 in CHCl$_3$); ^{1}H NMR (300 MHz, CDCl$_3$): δ=0.81 (s, 3H), 0.92 – 0.97 (m, 15 H), 1.03 (s, 3H), 1.11 (s, 3H), 1.21 (s, 3H, 7×CH$_3$, (CH$_3$CH$_2$CH$_2$CH$_2$)$_2$N), 1.28 -1.40 (m, 8H, (CH$_3$CH$_2$CH$_2$CH$_2$)$_2$N), 2.13 (d, J = 15.2 Hz, 1H, H-1a), 2.58 (d, J = 15.0 Hz, 1H, H-1b), 3.24 – 3.43 (m, 4H, (CH$_3$CH$_2$CH$_2$CH$_2$)$_2$N), 3.46 (d, J = 7.6 Hz, 1H, H-28a), 3.55 (s, 1H, H-19), 3.80 ppm (d, J = 7.6 Hz, 1H, H-28b); ^{13}C NMR (75 MHz, CDCl$_3$): δ=13.51, 13.92, 15.44, 16.58, 19.55, 20.16, 21.42, 21.92, 24.55, 26.23, 26.48, 27.41, 28.80, 29.62, 30.23, 32.70, 33.07, 34.26, 36.26, 36.72, 37.14, 38.61, 39.31, 40.60, 40.70, 41.48, 46.77, 49.69, 50.81, 52.89, 71.28, 87.90, 112.27, 143.78, 153.01, 166.74 ppm; IR (film): v=2925, 2864, 1538 (thiazole), 1465 (thiazole), 1035 cm^{-1}; MS (ESI) m/z (%): 609.4 (100) [M+H]$^+$; Anal. calcd for C$_{39}$H$_{64}$N$_2$OS: C 76.92, H 10.59, N 4.60, S 5.27; found C 76.92, H 10.61, N 4.33, S 5.24.

Thiazole derivative 2h

Compound **2h** was prepared according to the general procedure from 2α/β-thiocyano allobetulone (**2c**) (500 mg; 1.0 mmol) and dioctylammonium acetate (1.50 g; 5.0 mmol) in chloroform (20 mL) after 24 hours controlled by TLC (mobile phase toluene/diethylether 5:1). Dissolved crude product was filtered through a short pad of silica gel. Evaporation of solvent furnished **2h** (562 mg; 78 %): R_f=0.45 (toluene/diethylether 5:1); mp: 146–152 °C (toluene/diethylether); [α]$_D^{20}$=+51 (c=1.18 in CHCl$_3$); ^{1}H NMR (300 MHz, CDCl$_3$): δ=0.81 (s, 3H), 0.86 – 0.91 (m, 6H, H-dioctyl), 0.93 (s, 3H), 0.95 (s, 6H), 1.03 (s, 3H), 1.11 (s, 3H), 1.22 (s, 3H, 7×CH$_3$), 1.25 – 1.33 (m, 24H, (CH$_3$(CH$_2$)$_6$CH$_2$)$_2$N), 2.14 (d, J = 15.2 Hz, 1H, H-1a), 2.59 (d, J = 14.9 Hz, 1H, H-1b), 3.23 – 3.41 (m, 4H, (CH$_3$(CH$_2$)$_6$CH$_2$)$_2$N), 3.46 (d, J = 7.9 Hz, 1H, H-28a), 3.56 (s, 1H, H-19), 3.81 ppm (d, J = 7.9 Hz, 1H, H-28b); ^{13}C NMR (75 MHz, CDCl$_3$): δ=13.52, 14.11, 15.44, 16.58, 19.57, 21.43, 21.93, 22.65, 24.55, 26.24, 26.49, 26.98, 27.42, 27.46, 28.80, 29.24, 29.34, 30.25, 31.82, 32.70, 33.08, 34.27, 36.27, 36.73, 37.15, 38.62, 39.33, 40.61, 40.71, 41.49, 46.78, 49.70, 51.19, 52.90, 71.28, 87.91, 112.27, 143.09, 153.02, 166.72 ppm; IR (film): v=2925, 2856, 1539 (thiazole), 1453 (thiazole), 1036 cm^{-1}; MS (ESI) m/z (%): 721.6 (100) [M+H]$^+$; Anal. calcd for C$_{47}$H$_{80}$N$_2$OS: C 78.27, H 11.18, N 3.88, S 4.45; found C 77.65, H 11.09, N 3.53, S 4.43.

Thiazole derivative 2i

Compound **2i** was prepared according to the general procedure from 2α/β-thiocyano allobetulone (**2c**) (500 mg; 1.0 mmol) and

benzylammonium acetate (836 mg; 5.0 mmol) in chloroform (20 mL) after 24 hours controlled by TLC (mobile phase toluene/diethylether 5:1). Dissolved crude product was filtered through a short pad of silica gel. Evaporation of solvent furnished **2i** (522 mg; 89 %): R_f=0.10 (toluene/diethylether 5:1); mp: 148–154 °C (toluene/diethylether); [α]$_D^{20}$=+56 (c=0.61 in CHCl$_3$); ^{1}H NMR (300 MHz, CDCl$_3$): δ=0.81 (s, 3H), 0.92 (s, 3H), 0.95 (s, 6H), 1.03 (s, 3H), 1.14 (s, 3H), 1.24 (s, 3H, 7×CH$_3$), 2.15 (d, J = 15.5 Hz, 1H, H-1a), 2.59 (d, J = 15.2 Hz, 1h, H-1b), 3.46 (d, J = 7.9 Hz, 1H, H-28a), 3.55 (s, 1H, H-19), 3.80 (d, J = 7.9 Hz, 1H, H-28b), 4.39 (s, 2H, PhCH$_2$), 5.59 (bs, 1H, NH), 7.29 – 7.44 ppm (m, 5H, Ph); ^{13}C NMR (75 MHz, CDCl$_3$): δ=13.49, 15.43, 16.51, 19.45, 21.45, 21.99, 24.55, 26.22, 26.43, 26.47, 28.80, 30.23, 32.69, 33.00, 34.25, 36.26, 36.71, 37.00, 38.66, 39.28, 40.60, 40.71, 41.48, 46.75, 49.68, 50.13, 52.80, 71.25, 87.89, 114.31, 127.63, 127.72, 128.62, 137.71, 142.82, 151.94, 166.77 ppm; IR (film): v=3520 (NH), 2934, 2865, 1542 (thiazole), 1463 (thiazole), 1035 cm^{-1}; MS (ESI) m/z (%): 587.4 (100) [M+H]$^+$; Anal. calcd for C$_{38}$H$_{54}$N$_2$OS: C 77.76, H 9.27, N 4.77, S 5.46; found C 77.69, H 9.28, N 4.55, S 4.93.

Thiazole derivative 2j

Compound **2j** was prepared according to the general procedure from 2α/β-thiocyano allobetulone (**2c**) (500 mg; 1.0 mmol) and morpholinium acetate (736 mg; 5.0 mmol) in chloroform (20 mL) after 24 hours controlled by TLC (mobile phase toluene/diethylether 5:1). Dissolved crude product was filtered through a short pad of silica gel. Evaporation of solvent furnished **2j** (510 mg; 90 %): R_f=0.20 (toluene/diethylether5:1); mp: 151–155 °C (toluene/diethylether); [α]$_D^{20}$=+65 (c=0.95 in CHCl$_3$); ^{1}H NMR (500 MHz, CDCl$_3$): δ=0.81 (s, 3H), 0.91 (s, 3H), 0.95 (s, 6H), 1.03 (s, 3H), 1.12 (s, 3H), 1.22 (s, 3H, 7×CH$_3$), 2.17 (d, J = 15.2 Hz, 1H, H-1a), 2.63 (d, J = 15.2 Hz, 1H, H-1b), 3.39 (t, J = 4.9 Hz, 4H, O(CH$_2$CH$_2$)$_2$N), 3.46 (d, J = 8.1 Hz, 1H, H-28a), 3.55 (s, 1H, H-19), 3.79 – 3.81 ppm (m, 5H, H-28b, O(CH$_2$CH$_2$)$_2$N); ^{13}C NMR (75 MHz, CDCl$_3$): δ=13.49, 15.43, 16.49, 19.52, 21.47, 21.98, 24.55, 26.23, 26.45, 26.47, 28.79, 30.29, 32.71, 33.04, 34.27, 36.27, 36.73, 37.22, 38.63, 39.30, 40.62, 40.72, 41.49, 46.78, 48.57, 49.69, 52.89, 66.28, 71.27, 87.90, 115.21, 153.34, 168.39 ppm; IR (film): v=2924, 2856, 1529 (thiazole), 1452 (thiazole), 1036 cm^{-1}; MS (ESI) m/z (%): 567.4 (100) [M+H]$^+$; Anal. calcd for C$_{35}$H$_{54}$N$_2$O$_2$S: C 74.16, H 9.60, N 4.94, S 5.66; found C 73.43, H 9.63, N 4.59, S 6.03.

Thiazole derivative 2k

Compound **2k** was prepared according to the general procedure from 2α/β-thiocyano allobetulone (**2c**) (500 mg; 1.0 mmol) and N-methylpiperazinium acetate (802 mg; 5.0 mmol) in chloroform (20 mL) after 24 hours controlled by TLC (mobile phase toluene/diethylether 5:1). Dissolved crude product was filtered through a short pad of silica gel. Evaporation of solvent furnished **2k** (557 mg; 96 %): R_f=0.15 (toluene/diethylether 5:1); mp: 147–154 °C (toluene/diethylether); [α]$_D^{20}$=+61 (c=0.99, CHCl$_3$); ^{1}H NMR (300 MHz, CDCl$_3$): δ=0.80 (s, 3H), 0.90 (s, 3H), 0.94 (s, 6H), 1.02 (s, 3H), 1.11 (s, 3H), 1.21 (s, 3H, 7×CH$_3$), 2.15 (d, J = 15.2 Hz, 1H, H-1a), 2.35 (s, 3H, N-CH$_3$), 2.52 – 2.55 (m, 4H, CH$_3$N(CH$_2$CH$_2$)$_2$N), 2.61 (d, J = 15.2 Hz, 1H, H-1b), 3.40 – 3.48 (m, 5H, H-28a, CH$_3$N(CH$_2$CH$_2$)$_2$N), 3.54 (s, 1H, H-19), 3.79 ppm (d, J = 7.6 Hz, 1H, H-28b); ^{13}C NMR (75 MHz, CDCl$_3$): δ=13.50, 15.42, 16.51, 19.51, 21.45, 21.98, 24.55, 26.22, 26.44, 28.79, 30.28, 32.69, 33.03, 34.25, 36.26, 36.71, 37.19, 38.59, 39.28,

8

143

40.60, 40.71, 41.48, 46.12, 46.75, 48.07, 49.66, 52.87, 54.27, 71.25, 87.88, 114.97, 147.97, 153.28, 168.03 ppm; IR (film): ν=2940, 2865, 1529 (thiazole), 1453 (thiazole), 1035 cm^{-1}; MS (ESI) m/z (%): 580.4 (100) [M+H]$^+$; Anal. calcd for $C_{36}H_{57}N_3OS$: C 74.56, H 9.91, N 7.25, S 5.53; found C 73.13, H 9.44, N 6.58, S 5.23.

Thiazole derivative 2l

Compound 2l was prepared according to the general procedure from 2α/β-thiocyano allobetulone (2c) (500 mg; 1.0 mmol) and cyclohexylammonium acetate (797 mg; 5.0 mmol) in chloroform (20 mL) after 24 hours controlled by TLC (mobile phase toluene/diethylether 5:1). Dissolved crude product was filtered through a short pad of silica gel. Evaporation of solvent furnished 2l (504 mg; 87 %): R_f=0.10 (toluene/diethylether 5:1); mp: 14–151 °C (toluene/diethylether); $[\alpha]_D^{20}$=+60 (c=0.92 in CHCl$_3$); ^{1}H NMR (300 MHz, CDCl$_3$): δ=0.81 (s, 3H), 0.92 (s, 3H), 0.94 (s, 6H), 1.03 (s, 3H), 1.12 (s, 3H), 1.22 (s, 3H, 7×CH$_3$), 2.14 (d, J = 15.2 Hz, 1H, H-1a), 2.58 (d, J = 15.3 Hz, 1H, H-1b), 3.08 – 3.20 (m, 1H, H-cyclohexyl), 3.46 (d, J = 7.9 Hz, 1H, H-28a), 3.55 (s, 1H, H-19), 3.80 (d, J = 7.6 Hz, 1H, H-28b), 5.30 ppm (bs, 1H, NH); ^{13}C NMR (75 MHz, CDCl$_3$): δ=13.49, 15.42, 16.50, 19.44, 21.45, 21.94, 24.54, 24.64, 25.52, 26.21, 26.44, 26.46, 28.80, 30.20, 32.68, 33.00, 33.04, 33.08, 34.24, 36.26, 36.70, 36.89, 38.64, 39.30, 40.59, 40.71, 41.48, 46.75, 49.68, 52.81, 55.25, 71.25, 87.89, 113.27, 145.26, 151.93, 166.25 ppm; IR (film): ν=3500 (NH), 2927, 2856, 1538 (thiazole), 1452 (thiazole), 1032 cm^{-1}; MS (ESI) m/z (%): 578.4 (100) [M+H]$^+$; Anal. calcd for $C_{37}H_{58}N_2OS$: C 76.76, H 10.10, N 4.84, S 5.54; found C 76.23, H 10.06, N 4.87, S 5.40.

Cell lines

Cell lines were chosen and used the same way as in our previous work.[49,51,54] All cells (if not indicated otherwise) were purchased from the American Tissue Culture Collection (ATCC). The CCRF-CEM line is derived from T lymphoblastic leukemia, evincing high chemosensitivity, K562 represent cells from an acute myeloid leukemia patient sample with bcr-abl translocation, U2OS line is derived from osteosarcoma, HCT116 is colorectal tumor cell line and its p53 gene knock-down counterpart (HCT116p53-/-, Horizon Discovery Ltd, UK) is a model of human cancers with p53 mutation frequently associated with poor prognosis, A549 line is lung adenocarcinoma. The daunorubicin resistant subline of CCRF-CEM cells (CEM-DNR bulk) and paclitaxel resistant subline K562-TAX were selected in our laboratory by the cultivation of maternal cell lines in increasing concentrations of daunorubicine or paclitaxel, respectively. The CEM-DNR bulk cells overexpress MRP-1 and P-glycoprotein, while K562-TAX cells overexpress P-glycoprotein only. Both proteins belong to the family of ABC transporters and are involved in the primary and/or acquired multidrug resistance phenomenon.[49] MRC-5 and BJ cell lines were used as a non-tumor control and represent human fibroblasts. The cells were maintained in nunc/corning 80 cm^2 plastic tissue culture flasks and cultured in cell culture medium according to ATCC or Horizon recommendations (DMEM/RPMI 1640 with 5 g/L glucose, 2 mM glutamine, 100 U/mL penicillin, 100 mg/mL streptomycin, 10% fetal calf serum, and NaHCO$_3$).

Cytotoxic MTS assay

MTS assays were performed as described earlier[49-51,54] The assays were carried out at the Institute of Molecular and Translational Medicine by robotic platform (HighResBiosolutions). Cell suspensions were prepared and diluted according to the particular cell type and the expected target cell density (25000 – 35000 cells/mL based on cell growth characteristics). Cells were added by automatic pipetor (30 µL) into 384 well microtiter plates. All tested compounds were dissolved in 100% DMSO and four-fold dilutions of the intended test concentration were added in 0.15 µL aliquots at time zero to the microtiter plate wells by the echoacustic non-contact liquid handler Echo550 (Labcyte). The experiments were performed in technical duplicates and three biological replicates at least. The cells were incubated with the tested compounds for 72 h at 37 °C, in a 5% CO$_2$ atmosphere at 100% humidity. At the end of the incubation period, the cells were assayed by using the MTS test. Aliquots (5 µL) of the MTS stock solution were pipetted into each well and incubated for additional 1–4 h. After this incubation period, the optical density (OD) was measured at 490 nm with an Envision reader (Perkin Elmer). Tumor cell survival (TCS) was calculated by using the following equation: TCS = (OD$_{drug-exposed\ well}$/mean OD$_{control\ wells}$) × 100%. The IC$_{50}$ value, the drug concentration that is lethal to 50% of the tumor cells, was calculated from the appropriate dose-response curves in Dotmatics software.

Cell Cycle and Apoptosis Analysis

Analysis of the cell cycle and apoptosis was done in concordance with our previus research.[50,51,54] Suspension of CCRF-CEM cells, seeded at a density of 1.10^6 cells/mL in 6-well panels, were cultivated with the 1 or 5 × IC$_{50}$ of tested compound in a humidified CO$_2$ incubator at 37 °C in RPMI 1640 cell culture medium containing 10% fetal calf serum, 10 mM glutamine, 100 U/mL penicillin, and 100 µg/mL streptomycin. Together with the treated cells, control sample containing vehicle was harvested at the same time point after 24 h. After another 24 hours, cells were then washed with cold PBS and fixed in 70% ethanol added dropwise and stored overnight at -20 °C. Afterwards, cells were washed in hypotonic citrate buffer, treated with RNAse (50 µg/mL) and stained with propidium iodide. Flow cytometer using a 488 nm single beam laser (Becton Dickinson) was used for measurement. Cell cycle was analyzed in the program ModFitLT (Verity), and apoptosis was measured in logarithmic model expressing percentage of the particles with propidium content lower than cells in G0/G1 phase (<G1) of the cell cycle. Half of the sample was used for pH3^{Ser10} antibody (Sigma) labeling and subsequent flow cytometry analysis of mitotic cells.[50]

BrDU Incorporation Analysis (DNA synthesis)

For this analysis, the same procedure of cultivation as previously[50,51,54] was used. Before harvesting, 10 µM 5-bromo-2-deoxyuridine (BrDU), was added to the cells for puls-labeling for 30 min. Cells were fixed with ice-cold 70% ethanol and stored overnight. Before the analysis, cells were washed with PBS, and resuspended in 2 M HCl for 30 min at room temperature to denature their DNA. Following neutralization with 0.1 M Na$_2$B$_4$O$_7$ (Borax), cells were washed with PBS containing 0.5% Tween-20 and 1% BSA. Staining with primary anti-BrDU antibody (Exbio) for 30 min at room temperature in the dark followed. Cells were then washed with PBS and stained with secondary antimouse-FITC antibody (Sigma). Cells were then washed with PBS again and incubated with propidium iodide (0.1 mg/mL) and RNAse A (0.5

9

FULL PAPER

mg/mL) for 1 h at room temperature in the dark and afterwards analyzed by flow cytometry using a 488 nm single beam laser (FACSCalibur, Becton Dickinson).[50]

BrU Incorporation Analysis (RNA synthesis)

For this analysis, the same procedure of cultivation as previously[50,51,54] was used. Cells were cultured and treated as above. Before harvesting, pulse-labeling with 1 mM 5-bromouridine (BrU) for 30 min followed. The cells were then fixed in 1% buffered paraformaldehyde with 0.05 % of NP-40 in room temperature for 15 min, and then stored in 4°C overnight. Before measurement, they werewashed in PBS with 1% glycin, washed in PBS again, and stained by primary anti-BrDU antibody crossreacting to BrU (Exbio) for 30 min at room temperature in the dark. After another washing step in PBS cells were stained by secondary antimouse-FITC antibody (Sigma). Following the staining, cells were washed with PBS and fixed with 1% PBS buffered paraformaldehyde with 0.05% of NP-40 for 1 hour. Cells were washed by PBS, incubated with propidium iodide (0.1 mg/mL) and RNAse A (0.5 mg/mL) for 1 h at room temperature in the dark, and finally analyzed by flow cytometry using a 488 nm single beam laser (FACS Calibur, Becton Dickinson).[50]

Acknowledgements

**Keywords:** thiazoles • cytotoxicity • cell cycle • triterpene • heterocycles

References:

[1] Y. Zhang, J. Li, J. Zhao, S. Wang, Y. Pan, K. Tanaka, S. Kadota, *Bioorg. Med. Chem. Lett.* **2005**, *15*, 1629-1632.

[2] R. Martín, J. Carvalho-Tavares, M. Hernández, M. Arnés, V. Ruiz-Gutiérrez, M.L. Nieto, *Biochem. Pharm.* **2010**, *79*, 198-208.

[3] S. Fontanay, M. Grare, J. Mayer, C. Finance, R.E. Duval, *Ethnopharmacol.* **2008**, *120*, 272-276.

[4] O. Salin, S. Alakurtti, L. Pohjala, A. Siiskonen, V. Maass, M. Maass, J. Yli-Kauhaluoma, P. Vuorela, *Biochem. Pharm.* **2010**, *80*, 1141-1151.

[5] Y.M. Zhu, J.K. Shen, H.K. Wang, L.M. Cosentino, K.H. Lee, *Bioorg. Med. Chem. Lett.* **2001**, *11*, 3115-3118.

[6] M.S. Yu, J. Lee, J.M. Lee, Y Kim, Y.W. Chin, J.G. Jee, J.S. Keum, Y.J. Jeong, *Bioorg. Med. Chem. Lett.* **2012**, *22*, 4049-4054.

[7] N. Singh, B.B. Mishra, S. Bajpai, R.K. Singh, V.K. Tiwari, *Bioorg. Med. Chem.* **2014**, *22*, 18-45.

[8] B.D. Domínguez-Carmona, F. Escalante-Erosa, K. García-Sosa, G. Ruiz-Pinell, D. Gutierrez-Yapu, M.J. Chan-Bacab, A. Giménez-Turba, L.M. Peña-Rodríguez, *Phytomedicine.* **2010**, *17*, 379-382.

[9] J.J. Ramírez-Espinosa, M.Y. Rios, P. Paoli, V. Flores-Morales, G. Camici, V. Rosa-Lugo, S. Hidalgo-Figueroa, G. Navarrete-Vázquez, S. Estrada-Soto, *Eur. J. Med. Chem.* **2014**, *87*, 316-327.

[10] Z. Lin, Y. Zhang, Y. Zhang, H. Shen, L. Hu, H. Jiang, X. Shen, *Biochem. Pharm.* **2008**, *76*, 1251-1262.

[11] R. Csuk, B. Siewert, C. Dressel, R. Schäfer, *Eur. J. Med. Chem.* **2012**, *56*, 237-245.

[12] R. Csuk, S. Schwarz, B. Siewert, R. Kluge, D. Ströhl, *Eur. J. Med. Chem.* **2011**, *46*, 5356-5369.

[13] J. Sarek, M. Kvasnica, M. Vlk, D. Biedermann in: *Pentacyclic Triterpenes as Promising Agents in Cancer* (Ed.: J.A.R. Salvador), Nova Science Publishers, Hauppauge NY USA, **2010**, pp. 159-189. Chapter 7.

[14] W.-W. Qiu, Q. Shen, S.F. Yang, B. Wang, H. Zou, J.-Y. Li, J. Li, J. Tang, *Bioorg. Med. Chem. Lett.* **2009**, *19*, 6618-6622.

[15] V. Kumar, N. Rani, P. Aggarwal, V.K. Sanna, A.T. Singh, M. Jaggi, N. Joshi, P.K. Sharma, R. Irchhaiya, A.C. Burman, *Bioorg. Med. Chem. Lett.* **2008**, *18*, 5058-5062.

[16] J. Chen, Y. Gong, J. Liu, W. Hua, L. Zhang, H. Sun, *Chem. Biodiversity* **2008**, *5*, 1304-1312.

[17] J. Chen, Y. Gong, J. Liu, L. Zhang, W. Hua, H. Sun, *Drug Discov. Ther.* **2008**, *2*, 115-121.

[18] H. Li, H. Zou, L. Gao, T. Liu, F. Yang, J. Li, J. Li, W.-W. Qiu, J. Tang, *Heterocycles* **2012**, *85*, 1117-1139.

[19] M. Urban, M. Vlk, P. Dzubak, M. Hajduch, J. Sarek, *Bioorg. Med. Chem.* **2012**, *20*, 3666-3674.

[20] J. Xu, Z. Li, J. Luo, F. Yang, T. Liu, M. Liu, W.-W. Qiu, J. Tang, *J. Med. Chem.* **2012**, *55*, 3122-3134.

[21] M. Laavola, R. Haavikko, M. Hämäläinen, T. Leppänen, R. Nieminen, S. Alakurtti, V.M. Moreira, J. Yli-Kauhaluoma, E. Moilanen, *J. Nat. Prod.* **2016**, *79*, 274-280.

[22] C. Gao, F.-J. Dai, H.-W. Cui, S.-H. Peng, Y. He, X. Wang, F.-Z. Yi, W.-W. Qiu, *Chem. Biol. Drug. Des.* **2014**, *84*, 223-233.

[23] X. Kang, J. Hu, Z. Gao, Y. Ju, C. Xu, *Med. Chem. Commun.* **2012**, *3*, 1245-1249.

[24] Y.-J. You, Y. Kim, N.-H. Nam, B.-Z. Ahn, *Bioorg. Med. Chem. Lett.* **2003**, *13*, 3137-3140.

[25] N.V. Galaiko, A.V. Nazarov, I.A. Tolmacheva, P.A. Slepukhin, Y.B. Vikharev, O.A. Maiorova, V.V. Grishko, *Chem. Het. Comp.* **2014**, *50*, 65-75.

[26] R. Haavikko, A. Nasereddin, N. Sacerdoti-Sierra, D. Kopelyanskiy, S. Alakurtti, M. Tikka, C.L. Jaffe, J. Yli-Kauhaluoma, *Med. Chem. Commun.* **2014**, *5*, 445-451.

[27] M. Urban, J. Sarek, M. Kvasnica, I. Tislerova, M. Hajduch, *J. Nat. Prod.* **2007**, *70*, 526-532.

[28] P. Ghosh, A. Mandal, *Green Chem. Lett. Rev.* **2012**, *5*, 127-134.

[29] P. Ghosh, M.G. Rasual, M. Chakraborty, A. Mandal, A. Saha, *Indian. J. Chem. B.* **2011**, *50*, 1519-1523.

[30] M. Vlk, P. Micolova, M. Urban, M. Kvasnica, D. Saman, J. Sarek, *J. Radioanal. Nucl. Chem.* **2016**, *308*, 733-739.

[31] T.D. Ngoc, M. Moons, Y. Kim, DeBorggraeve, A. Mashentseva, G. Andrei R. Snoeck, J. Balzarini, W. Dehaen, *Bioorg. Med. Chem.* **2014**, *22*, 3292-3300.

[32] M. Kvasnica, M. Urban, N.J. Dickinson, J. Sarek, *Nat. Prod. Rep.* **2015**, *32*, 1303-1330.

[33] M. Soural, J. Hodon, N.J. Dickinson, V. Sidova, S. Gurska, P. Dzubak, M. Hajduch, J. Sarek, M. Urban, *Bioconjugate Chem.* **2015**, *26*, 2563-2570.

[34] K. Challa, M.V. Bhargavi, G.L. Krupadanam, *J. Asian. Nat. Prod. Res.* **2016**, *18*, 1158-1168.

[35] M. Drąg-Zalesińska, T. Wysocka, S. Borska, M.Drąg, M. Poręba, A. Choromańska, J. Kulbacka, J. Saczko, *Biomed. Pharmacother.* **2016**, *72*, 91-97.

[36] L. Heller, A. Knorrscheidt, F. Flemming, J. Wiemann, S. Sommerwerk, I.Z. Pavel, A. Al-Harrasi, R. Csuk, *Bioorg. Chem.,* **2016**, *68*, 137-151.

[37] L. Heller, A. Obernauer, R. Csuk, *Bioorg. Med. Chem.,* **2015**, *23*, 3002-3012.

[38] M. Urban, M. Kvasnica, N.J. Dickinson, J. Sarek in *Terpenoids and Squalene: Biosynthesis, Functions and Health Implications* (Ed.: A. R. Bates), Nova Science Publishers, Hauppauge NY USA, **2015**, pp 25-50. Chapter 2.

[39] L.C. King, K.G. Ostrum, *J. Org. Chem.* **1964**, *29*, 3459-3461.

10

FULL PAPER

[40] B.L. Zhang, E. Zhang, L.P. Pang, L.X. Song, Y.F. Li, B. Yu, H.M. Liu, *Steroids*, **2013**, *78*, 1200-1208.

[41] J. Teller, H. Dehne, T. Zimmermann, G.W. Fischer, B. Olk, *J. Prakt. Chem.* **1990**, *332*, 453-460.

[42] J. Teller, H. Dehne, T. Zimmermann, G.W. Fischer, B. Olk, *J. Prakt. Chem.* **1990**, *332*, 723-730.

[43] K. Takeda, T. Komeno, T. *Chem. Pharm. Bull.* **1960**, *8*, 468-474.

[44] J. Klinot, A. Vystrcil, *Collect. Czech. Chem. Commun.* **1966**, *31*, 1079-1092.

[45] J.M. Lehn, S. Ourisson, *Bull. Soc. Chim. Fr.* **1963**, *5*, 1113-1121.

[46] S. Sommerwerk, L. Heller, I. Serbian, R. Csuk, *Tetrahedron* **2015**, *71*, 8528-8534.

[47] S. Sommerwerk, R. Csuk, *Tetrahedron Lett.* **2014**, *55*, 5156-5158.

[48] L. Heller, S. Schwarz, P. Vincent A. Koewitsch, B. Siewert, R. Csuk, *Eur. J. Med. Chem.* **2015**, *101*, 391-399.

[49] V. Noskova, P. Dzubak, G. Kuzmina, A. Ludkova, D. Stehlik, R. Trojanec, A. Janostakova, G. Korinkova, V. Mihal, M. Hajduch, *Neoplasma* **2002**, *49*, 418-425.

[50] A. Bourderioux, P. Nauš, P. Perlikova, R. Pohl, I. Pichova, I. Votruba, P. Dzubak, P. Konecny, M. Hajduch, K.M. Stray, T. Wang, A.S. Ray, J.Y. Feng, G. Birkus, T. Cihlar, M. Hocek, *J. Med. Chem.* **2011**, *54*, 5498-5507.

[51] L. Borkova, S. Gurska, P. Dzubak, R. Burianova, M. Hajduch, J. Sarek, I. Popa, M. Urban, *Eur. J. Med. Chem.* **2016**, *121*, 120-131.

[52] H. Xu, G.W. Krystal, *Clin. Cancer Res.* **2010**, *16*, 4392-4400.

[53] J. N. Patro, M. Urban, R.D. Kuchta, *Biochemistry* **2009**, *48*, 8271-8278.

[54] L. Borkova, L. Jasikova, J. Rehulka, K. Frisonsova, M. Urban, I. Frydrych, I. Popa, M. Hajduch, N. J. Dickinson, M. Vlk, P. Dzubak, J. Sarek, *Eur. J. Med. Chem.* **2015**, *96*, 482-490.

11

WILEY-VCH

Entry for the Table of Contents
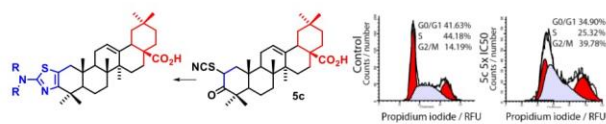
Cytotoxic triterpenes (SAR & MOA): Aminothiazoles were prepared from four triterpenic scaffolds. Diethylamino- and N-methylpiperidinothiazoles of oleanonic acid were best, however, much better candidate is intermediate thiocyanate **5c** as it is new, active, non-toxic, inducing apoptosis selectively in cancer cells via cell cycle arrest in G2/M phase and inhibits DNA/RNA synthesis.

147